AD-A073 553 NORTHROP RESEARCH AND TECHNOLOGY CENTER PALOS VERDES --ETC F/G 1/3
INVESTIGATION OF ADVANCED PROGNOSTIC ANALYSI S TECHNIQUES.(U)
JUN 79 R C GROVE DAAJ02-77-C-0054

UNCLASSIFIED NRTC78-47R USARTL-TR-79-10 NL

1 OF 3
AD A073553

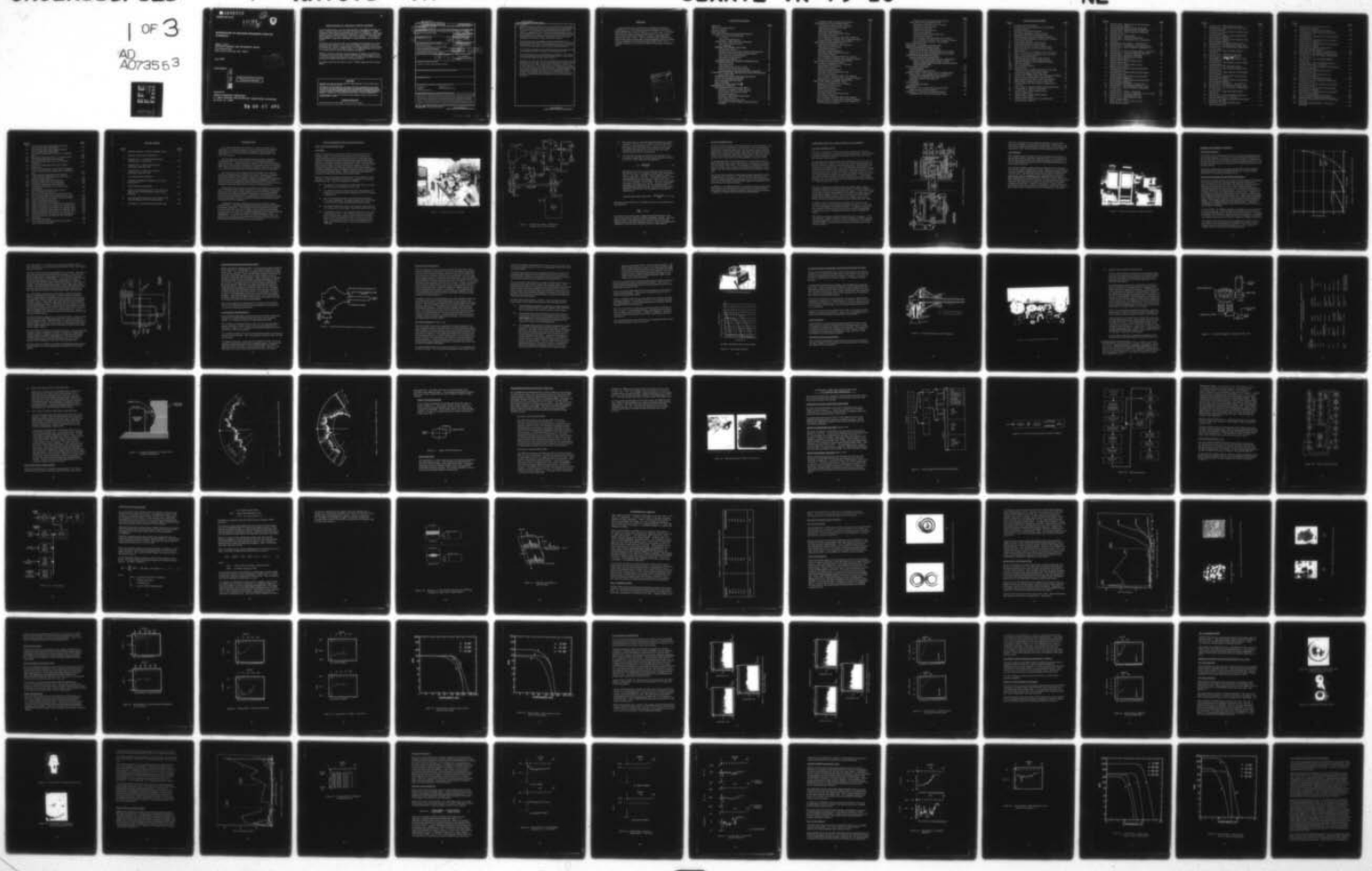

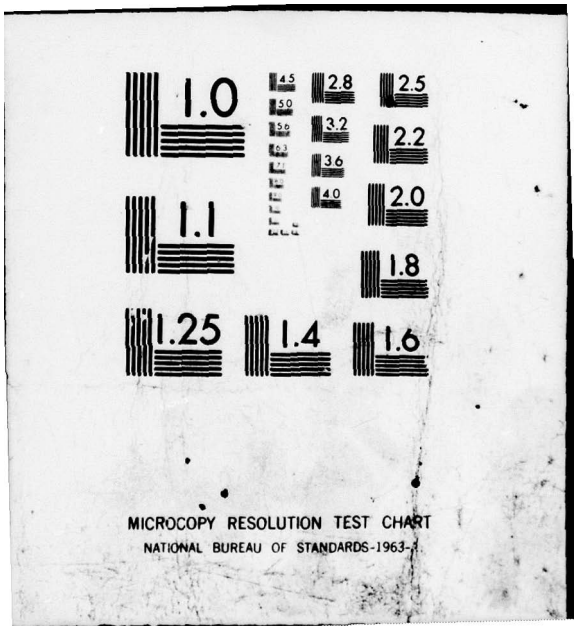
1.0
1.1
1.25
1.4
1.6
1.8
2.0
2.2
2.5
2.8
3.2
3.6
4.0
4.5
5.0
5.6
MICROCOPY RESOLUTION TEST CHART
NATIONAL BUREAU OF STANDARDS-1963-A

AD A073553

USARTL-TR-79-10

LEVEL II

INVESTIGATION OF ADVANCED PROGNOSTIC ANALYSIS TECHNIQUES

Ralph C. Grove
NORTHROP RESEARCH AND TECHNOLOGY CENTER
One Research Park
Palos Verdes Peninsula, Calif. 90274

June 1979

Final Report

Approved for public release; distribution unlimited.

Prepared for

APPLIED TECHNOLOGY LABORATORY
U. S. ARMY RESEARCH AND TECHNOLOGY LABORATORIES (AVRADCOM)
Fort Eustis, Va. 23604

APPLIED TECHNOLOGY LABORATORY POSITION STATEMENT

The work reported herein is part of a continuing effort of the Applied Technology Laboratory, US Army Research and Technology Laboratories (AVRADCOM), to conduct investigations directed toward advancing the state of the art of diagnostics. Technological advances continue to afford the Army the opportunity to improve the maintenance and support requirements for Army helicopter power train components. It is the intent of this organization to apply these technologies in a timely, productive, and cost-effective manner.

The objective of this particular effort was to investigate analysis techniques that would provide prognostic information on the mechanical condition of helicopter power train components. The contractor instrumented six UH-1 90-degree gearboxes and tested them for over 4700 hours under controlled conditions. The analysis techniques which proved to be productive will be used for future prognostic investigations.

Although no immediate additional contractual prognostic investigations are planned by our organization, an in-house effort has been initiated using the test equipment of this contract where additional gearboxes will be tested. Vibration and oil condition data will be acquired for analysis and correlation to mechanical condition.

The technical monitor for this contract was Mr. G. William Hogg, Aeronautical Systems Division.

UNCLASSIFIED

SECURITY CLASSIFICATION OF THIS PAGE (When Data Entered)

REPORT DOCUMENTATION PAGE	READ INSTRUCTIONS BEFORE COMPLETING FORM
1. REPORT NUMBER: USARTL-TR-79-10	2. GOVT ACCESSION NO. / 3. RECIPIENT'S CATALOG NUMBER
4. TITLE (and Subtitle): INVESTIGATION OF ADVANCED PROGNOSTIC ANALYSIS TECHNIQUES.	5. TYPE OF REPORT & PERIOD COVERED: FINAL REPORT.
	6. PERFORMING ORG. REPORT NUMBER: NRTC 78-47R
7. AUTHOR(s): Ralph C. Grove	8. CONTRACT OR GRANT NUMBER(s): DAAJ02-77-C-0054
9. PERFORMING ORGANIZATION NAME AND ADDRESS: Northrop Research and Technology Center, One Research Park, Palos Verdes Peninsula, California 90274	10. PROGRAM ELEMENT, PROJECT, TASK AREA & WORK UNIT NUMBERS: 62209A 1L262209AH76 00 212 EK
11. CONTROLLING OFFICE NAME AND ADDRESS: Applied Technology Laboratory, U.S. Army Research & Technology Laboratories (AVRADCOM), Fort Eustis, Virginia	12. REPORT DATE: June 1979 / 13. NUMBER OF PAGES: 260
14. MONITORING AGENCY NAME & ADDRESS (if different from Controlling Office)	15. SECURITY CLASS. (of this report): UNCLASSIFIED / 15a. DECLASSIFICATION/DOWNGRADING SCHEDULE

16. DISTRIBUTION STATEMENT (of this Report)

Approved for public release; distribution unlimited.

17. DISTRIBUTION STATEMENT (of the abstract entered in Block 20, if different from Report)

18. SUPPLEMENTARY NOTES

19. KEY WORDS (Continue on reverse side if necessary and identify by block number)

Prognostics
Trending
Vibration Data Base
Diagnostics
Machinery Monitoring

20. ABSTRACT (Continue on reverse side if necessary and identify by block number)

This report presents the results of an experimental program with the following objectives: to collect and process test data from six different UH-1 helicopter 90° gearboxes, tested for a total of 4712 hours under controlled conditions, and to perform a theoretical investigation and data analysis to develop and optimize trend detection and prediction algorithms for application to the processed test cell data in order to establish valid predictions of gearbox failure time. A variety of sensors were used to monitor the wear occurring in the

DD FORM 1 JAN 73 1473 EDITION OF 1 NOV 65 IS OBSOLETE

UNCLASSIFIED

SECURITY CLASSIFICATION OF THIS PAGE (When Data Entered)

407 696

20. (continued)

gearboxes including oil debris monitors, accelerometers, a shock pulse analyzer, and temperature sensors. Spectrometric oil analyses (SOA) of the gearbox oil were performed on daily samples from the gearbox oil reservoir. The gearboxes were disassembled and inspected for wear prior to and following each test. Wear measurement techniques included visual inspection by an expert, measurements of ball and ball track wear, dynamic noise testing of bearings, and scanning electron microscope photographs of the surface of one ball from each bearing.

During the theoretical investigation twelve trend paramenters were examined to determine their ability to indicate the current wear condition of the gearbox. One of these, the matched filter parameter, proved to be superior to the others and was used in failure prediction modeling.

A trend detection algorithm was developed that proved extremely sensitive to the detection of trends, requiring a low computational burden.

Three mathematical wear trend models were investigated. One of these, an upward-constrained second order exponential model, proved superior to the others in ability to predict onset of failure.

Application of the test cell data to the trend detection and failure prediction algorithms was successful. Of the six gearboxes that were tested, three of them failed at 273, 488, and 1301 hours, respectively. Failure predictions made at 2/3 or less of the life-span of the gearboxes were within 62, 31, and 137 hours of the actual failure time. A fourth gearbox failed after 88 hours of testing, and a wear trend was detected immediately. The remaining two gearboxes were tested for 1519 and 588 hours with no failures. The algorithms detected unsustained wear trends in these two gearboxes and made failure time predictions in excess of the respective test times.

PREFACE

This program was carried out for the Applied Technology Laboratory, U. S. Army Research and Technology Laboratories (AVRADCOM) under Contract DAAJ02-77-C-0054. Mr. G. William Hogg served as the principal technical monitor for this program. His continued enthusiastic support is hereby acknowledged and appreciated. Mr. James J. Reis of Northrop, who conducted the initial investigation of helicopter gearbox prognosis under preceding contracts DAAJ02-72-C-0118 and DAAJ02-75-C-0019, was of valuable assistance in an advisory capacity during this investigative effort.

TABLE OF CONTENTS

	Page
PREFACE	3
LIST OF ILLUSTRATIONS	8
LIST OF TABLES	13
INTRODUCTION	14
TEST INSTRUMENTATION AND PROCEDURES	15
TEST CELL AND CONTROLLER	15
Test Stand	15
Torque and RPM Sensing	19
COMPUTER - TEST CELL I/O CONTROL	20
Test Cell Controller (TCC)	20
I/O Controller	22
SENSORS AND SENSOR LOCATIONS	24
Temperature Sensors	24
Spectrometric Oil Analysis and Other Oil Analyses)	24
Capacitive Discharge Chip Detection System	28
Low Frequency Accelerometers	28
Ultrasonic Accelerometers	30
Shock Pulse Analyzer	30
DETERMINATION OF BEARING CONDITION AND SURFACE WEAR	34
Visual Inspection	34
Ball Bearing Wear Measurements	34
Roller Bearing Wear Measurements	40
Scanning Electron Microscope Surface Inspection	45
AUTOMATIC COMPUTER-CONTROLLED DATA COLLECTION AND REDUCTION	48
OVERVIEW OF MAIN COMPUTER SOFTWARE	48
START-UP SEQUENCE ROUTINE	48
DATA COLLECTION ROUTINE	48
EXIT ROUTINES	52
VIBRATION DATA REDUCTION	55
EXPERIMENTAL RESULTS	60
BAD BEARING FOUR GEARBOX TESTS	60
Mechanical Condition of BB-4 Gearbox	62
Spectrometric Oil Analysis (SOA)	64
Temperature Sensors	68
Ultrasonic RMS Accelerometer Data	68
Shock Pulse Analyzer	68
Low Frequency Vibration Data	74
Correlation of Sensor Outputs with Mechanical Condition	78

Page

Summary of BB-4 Gearbox Test Results 78
BAD BEARING FIVE GEARBOX TESTS 80
Mechanical Condition of BB-5 Gearbox 80
Spectrometric Oil Analysis (SOA) 83
Temperature Sensors 86
RPM and Torque Indicators 86
Ultrasonic RMS Accelerometer Data 90
Shock Pulse Analyzer 90
Low Frequency Vibration Data Time Analysis 95
Low Frequency Vibration Data Frequency Analysis . . 98
Summary of BB-5 Gearbox Test Results 101
HIGH TIME FIVE GEARBOX TESTS 103
Mechanical Condition of HT-5 Gearbox 103
Spectrometric Oil Analysis 104
Temperature Sensors 104
RPM and Torque Indicators 104
Ultrasonic RMS Accelerometer Data 104
Shock Pulse Analyzer 111
Low Frequency Vibration Data Time Analysis 111
Low Frequency Vibration Data Frequency Analysis . . 117
Summary of HT-5 Gearbox Test Results 117
HIGH TIME TWO GEARBOX TESTS 120
Mechanical Condition of HT-2 Gearbox 120
Spectrometric Oil Analysis 121
Temperature Sensors 121
RPM and Torque Indicators 121
Ultrasonic RMS Accelerometer Data 126
Shock Pulse Analyzer 126
Low Frequency Vibration Data Time Analysis 126
Low Frequency Vibration Data Frequency Analysis . . 134
Summary of HT-2 Gearbox Test Results 134
HIGH TIME THREE GEARBOX TESTS 139
Mechanical Condition of HT-3 Gearbox 139
Spectrometric Oil Analysis 140
Temperature Sensors 140
RPM and Torque Indicators 140
Tedeco Chip Detector 149
Ultrasonic RMS Accelerometer Data 149
Shock Pulse Analyzer 153
Low Frequency Vibration Data Time Analysis 156
Low Frequency Vibration Data Frequency Analysis . . 162
Results of B & K Accelerometer Data Applied to Shaker Envelope Detector 162

Page

Summary of HT-3 Gearbox Tests Results 166
HIGH TIME FOUR GEARBOX TESTS 167
Mechanical Condition of HT-4 Gearbox 167
Spectrometric Oil Analysis 168
Temperature Sensors 168
RPM and Torque Indicators 172
Tedeco Chip Detector 172
Ultrasonic RMS Accelerometer Data 172
Shock Pulse Analyzer 175
Low Frequency Vibration Data Time Analysis 179
Low Frequency Vibration Data Frequency Analysis . . 183
Summary of HT-4 Gearbox Test Results 183
DATA BASE ANALYSIS 186
FREQUENCY ANALYSIS METHODOLOGY 187
TREND PARAMETER INVESTIGATION 190
TREND PARAMETER DESCRIPTION 190
RESULTS OF CLASS I PARAMETER EVALUATION. . . . 197
RESULTS OF CLASS II PARAMETER EVALUATION . . . 200
TREND DETECTION INVESTIGATION. 210
TREND DETECTION ALGORITHM 217
EVALUATION OF MATCHED-FILTER, GEOMETRIC MEAN, AND ARITHMETIC MEAN TREND PARAMETERS USING REVERSE-ARRANGEMENTS TREND DETECTION 221
WEAR TREND MODELING 227
METHODOLOGY 227
MATH MODEL EVALUATION 227
APPLICATION OF TEST CELL DATA TO SMOOTHING, DETECTION, AND PREDICTION ALGORITHMS 236
CRITERIA FOR SENSOR DATA SELECTION 236
FAILURE PREDICTION RESULTS 238
SUMMARY 247
CONCLUSIONS 249
RECOMMENDATIONS 254
REFERENCES 255
APPENDIX A. SOFTWARE DATA-COLLECTION SUBROUTINE FLOW DIAGRAMS 256
APPENDIX B. THEORY OF LEAST-SQUARES EXPONENTIAL CURVE-FITTING OF DATA 260

LIST OF ILLUSTRATIONS

Figure		Page
1	Overall View of Test Stand	16
2	Gearbox Test Stand-Mechanical and Hydraulic Circuit Diagram	17
3	Computer-Test Cell I/O Control	21
4	Interactive Computer Graphics System	23
5	Example of SOA Data for Defective Gear	25
6	Block Diagram of Direct-Reading Ferrograph	27
7	Gearbox Profile Showing Accelerometer Locations	29
8	Shock Pulse Analysis	33
9	Cross-Sectional View of 90° Gearbox	35
10	Partial Disassembly of 90° Gearbox	36
11	Schematic Diagram of Dynamic Noise Test	38
12	Schematic Diagram of Cross-Groove Profile Measurement	41
13	BBT-3 Cross-Groove Profile at Zero Test Hours	42
14	BBT-3 Cross-Groove Profile at 1022 Test Hours	43
15	Roller Crown Parameters	44
16	SEM Micrographs of BBT-2 (407 Hours)	47
17	Timing Diagram for Data Collection Effort	49
18	Test Cell-Computer Data Collection Program	50
19A	Start-Up Sequence	51
19B	Data Collection Routine	53
19C	Exit Routines	54
20	Reduction of DFT Sidelobe Structure by Hamming Weighting an Input Time Domain Signal	58
21	Ensemble Averaging of PSD Functions	59
22	Gearbox BB-4 Output Duplex Pair Bearing Assemblies	63
23	Spectrometric Oil Analysis - Gearbox BB-4	65
24	Optical Microscopic View of BB-4 Metal Chips	66
25	SEM Photomicrographs of BB-4 Metal Chips	67
26	Gearbox BB-4; Oil and Ambient Temperature vs. Test Time	69
27	Gearbox BB-4; Ultrasonic RMS Accelerometer Data	70
28	Gearbox BB-4; RPM vs. Test Time	71
29	Gearbox BB-4; Shock Profile Curves, Input Accelerometer	72
30	Gearbox BB-4; Shock Profile Curves, Output Accelerometer	73
31	Gearbox BB-4; Input Lateral Accelerometer Power Spectral Density	75

Figure		Page
32	Gearbox BB-4; Output Lateral Accelerometer Power Spectral Density	76
33	Geometric Mean and Arithmetic Mean Data	77
34	Gearbox BB-4: Matched Filter and RMS Data	79
35	Gearbox BB-5; Pinion Teeth Cold-Welded to Ring Gear Teeth	81
36	Gearbox BB-5; Input Coupler	81
37	Gearbox BB-5: Toothless Pinion Gear	82
38	Gearbox BB-5: Housing with Gear Assemblies Removed	82
39	Spectrometric Oil Analysis - Gearbox BB-5	84
40	Gearbox BB-5; Oil Samples and Change Times	85
41	Gearbox BB-5; Oil and Ambient Temperature vs. Test Time	87
42	Gearbox BB-5; Input and Output RPM vs. Test Time	88
43	Gearbox BB-5; Torque and Gearbox Efficiency	89
44	Gearbox BB-5; Ultrasonic RMS Data	91
45	Gearbox BB-5; SKF Peak Shock Value, Output Accelerometer	92
46	Gearbox BB-5; Shock Profile Curves, Input Accelerometer	93
47	Gearbox BB-5; Shock Profile Curves, Output Accelerometer	94
48	Gearbox BB-5; Input Lateral Accelerometer Trend Parameters	96
49	Gearbox BB-5; Output Lateral Accelerometer Trend Parameters	97
50	Gearbox BB-5; Input Lateral Accelerometer Power Spectral Densities	99
51	Gearbox BB-5; Output Lateral Accelerometer Power Spectral Densities	100
52	Spectrometric Oil Analysis-Gearbox HT-5	105
53	Gearbox HT-5; Oil Sample and Change Times	106
54	Gearbox HT-5; Oil and Ambient Temperature vs.Test Time	107
55	Gearbox HT-5; RPM vs. Test Time	108
56	Gearbox HT-5; Torque and Efficiency vs.Test Time	109
57	Gearbox HT-5; Ultrasonic RMS Data	110
58	Gearbox HT-5; Shock Profile Curves, Input Accelerometer	112
59	Gearbox HT-5: Shock Profile Curves, Output Accelerometer	113

Figure		Page
60	Gearbox HT-5; SKF Peak Shock Value	114
61	Gearbox HT-5; Input Lateral Accelerometer Trend Parameters	115
62	Gearbox HT-5; Output Lateral Accelerometer Trend Parameters	116
63	Gearbox HT-5; Input Lateral Accelerometer Power Spectral Density	118
64	Gearbox HT-5; Output Lateral Accelerometer Power Spectral Density	119
65	Spectrometric Oil Analysis-Gearbox HT-2	122
66	Gearbox HT-2; Oil Sample and Change Times	123
67	Gearbox HT-2; Oil and Ambient Temperature vs. Test Time	124
68	Gearbox HT-2; Input and Output RPM vs. Test Time	125
69	Gearbox HT-2: Torque vs. Test Time	127
70	Gearbox HT-2; Ultrasonic RMS Data	128
71	Gearbox HT-2; [redacted] Profile Curves, Input Accelerometer	129
72	Gearbox HT-2; Shock Profile Curves, Output Accelerometer	130
73	Gearbox HT-2; SKF Peak Shock Value	131
74	Gearbox HT-2; Input Lateral Accelerometer Time Histories	132
75	Gearbox HT-2; Output Lateral Accelerometer Time Histories	135
76	Gearbox HT-2; Input Lateral Accelerometer Power Spectral Density	137
77	Gearbox HT-2; Output Lateral Accelerometer Power Spectral Density	138
78	Spectrometric Oil Analysis - Gearbox HT-3	141
79	Gearbox HT-3; Oil Sample and Change Times	142
80	Gearbox HT-3; Oil and Ambient Temperature vs. Test Time	143
81	Gearbox HT-3; Input and Output RPM vs. Test Time	145
82	Gearbox HT-3: Input and Output Torque and Gearbox Efficiency vs. Test Time	147
83	Gearbox HT-3; Input and Output Accelerometer Ultrasonic RMS Data	151
84	Gearbox HT-3: Shock Profile Curve, Input Accelerometer	154

Figure		Page
85	Gearbox HT-3; Shock Profile Curve, Output Accelerometer	155
86	Gearbox HT-3; SKF Peak Shock Value	157
87	Gearbox HT-3 ; Input Lateral Accelerometer Time Histories	158
88	Gearbox HT-3; Output Lateral Accelerometer Time Histories	160
89	Gearbox HT-3; Input Lateral Accelerometer Power Spectral Density	163
90	Gearbox HT-3; Output Lateral Accelerometer Power Spectral Density	164
91	Gearbox HT-3; Output Accelerometer Ultrasonic Envelope Detector	165
92	Spectrometric Oil Analysis - Gearbox HT-4	169
93	Gearbox HT-4; Oil Sample and Change Times	170
94	Gearbox HT-4; Oil and Ambient Temperature vs. Test Time	171
95	Gearbox HT-4; Input and Output RPM vs. Test Times	173
96	Gearbox HT-4; Input and Output Torque and Gearbox Efficiency vs. Test Time	174
97	Gearbox HT-4; Input and Output Accelerometer Ultrasonic RMS Data	176
98	Gearbox HT-4; Shock Profile Curves, Input Accelerometer	177
99	Gearbox HT-4; Shock Profile Curve, Output Accelerometer	178
100	Gearbox HT-4; SKF Peak Shock Value	180
101	Gearbox HT-4; Input Lateral Accelerometer Trend Parameters	181
102	Gearbox HT-4; Output Lateral Accelerometer Trend Parameters	182
103	Gearbox HT-4; Input Lateral Accelerometer Power Spectral Density	184
104	Gearbox HT-4; Output Lateral Accelerometer Power Spectral Density	185
105	Class I Trend Parameter Comparison	198
106	Cepstral Ratio vs. Number of Coefficients	199
107	Gear-Mesh Mean-Squared Ratio vs. Gear-Mesh Bandwidth	202
108	Noise Mean-Squared Ratio vs. Gear-Mesh Bandwidth	203

Figure		Page
109	Noise Energy/Gear-Mesh Energy Ratio for Various Gear-Mesh Bandwidths	205
110	Total Energy/Gear-Mesh Energy Ratio for Various Gear-Mesh Bandwidths	206
111	Gear-Mesh Mean-Squared Ratio vs. Frequency Band	207
112	Noise Mean-Squared Ratio vs. Frequency Band	208
113	Data Editing Algorithm Flow Diagram	211
114	Reverse-Arrangements Scores for Various Waveforms	214
115	Reverse-Arrangements Scores for Various Waveforms	215
116	Reverse-Arrangements Trend Detector Applied to HT-3 Matched Filter Output Raw and Smoothed Data	216
117	Trend Detection Algorithm Flow Diagram	218
118	Trend Detection 99% Confidence Threshold vs. Number of Data Samples	220
119	Matched-Filter Data Trend Detection	222
120	Geometric Mean Data Trend Detection	223
121	Arithmetic Mean Data Trend Detection	224
122	Computational Algorithms for Three Trend Parameters	225
123	Smoothed Matched-Filter Data for HT-3, HT-4, and BB-5 Gearboxes	228
124	Failure Predictions and Trend Detection Using HT-3 Output Accelerometer Matched-Filter Data	230
125	Graphical Depiction of Failure Prediction Model	233
126	Failure Prediction Algorithm	234
127	Sensor Data Selection Flowchart	237
128	Failure Prediction Time History for Gearbox HT-3	239
129	Failure Prediction Time History for Gearbox HT-4	240
130	Failure Prediction Time History for Gearbox BB-5	241
131	Failure Prediction Time History for Gearbox BB-4	242
132	Failure Prediction Time History for Gearbox HT-5	243
133	Failure Prediction Time History for Gearbox HT-2	244
A-1	A-D Converted and Averaged DC Data Collection Subroutine	257
A-2	Sorted FFT Subroutine	258
A-3	A-D Converted, Hamming-Weighted Vibration Data Collection Subroutine	259

LIST OF TABLES

Table		Page
1	Dynamic Analysis: Bearing Condition Levels	39
2	Summary of Gearbox Testing Time	61
3	Gearbox HT-3; Average Oil and Ambient Temperature vs. Test Time	149
4	Gearbox HT-3; Tedeco Chip Detector Cumulative Chip Burn-offs	153
5	Gearbox HT-4; Tedeco Chip Detector Cumulative Chip Burn-offs	175
6	Trend Parameter Candidates	191
7	Reverse-Arrangements Statistics for Various Sample Sizes	217
8	Trend Parameter Evaluation	226
9	Failure Time Predictions for Three Gearboxes Made at 100, 150 and 200 Hours After Trend Detection	235
10	Gearbox Failure Prediction Times Made at 100, 150 and 200 Hours After Trend Detection	245
11	Predicted vs. Actual Remaining Gearbox Life	248

INTRODUCTION

This report describes the results of a research program whose objective is to develop techniques for failure prognosis with general applicability to rotating machinery components, and with specific application to a U. S. Army UH-1 helicopter component part: a 90° tail-rotor gearbox.

Northrop Research and Technology Center has been engaged in an on-going effort since 1972 in the area of helicopter component failure prognosis. During this period, nearly 10,000 hours of sampled data from accelerometers mounted on 90° gearboxes have been collected and computer-processed to determine and detect symptoms of component wear and to make predictions of useful remaining life in the gearbox.

The data base used for failure prediction analysis was collected on the preceding program: DAAJ02-75-C-0119, "Program for Experimental Investigation of Helicopter Component Failure Prognosis". A special test cell used for component testing was designed and constructed in the initial failure prognosis work on Contract DAAJ02-72-C-0118. This test cell was modified for the present data base collection to permit loading each gearbox with 70 HP on a 24-hour continuous basis.

Signal processing techniques and results are presented in this report, which encompass three areas of interest: (a) development of sensitive parameters that indicate subtle departures from the normal vibrations associated with rotating machinery components containing gears and bearings; (b) early detection of the beginning of a wear trend in the component; (c) generation of failure prediction models that will predict useful remaining life in the component.

In addition to the data compilation and failure prediction results presented here, considerable supplementary data is on file at the Applied Technology Laboratory. This includes: (a) all documentation obtained on the pre- and post-test wear condition of the mechanical components in each gearbox; (b) detailed oil analysis supplied by the Army Oil Analysis section at the U. S. Army Aeronautical Depot Maintenance Center (ARADMAC), Corpus Christi, Texas; (c) software listings of key data collection and processing algorithms; (d) trend detection and failure prediction hourly tabulations for the six tested gearboxes.

TEST INSTRUMENTATION AND PROCEDURES

TEST CELL AND CONTROLLER

Test Stand

Figure 1 illustrates an overall view of the test stand used for 90° gearbox testing. The test stand is inclined 42° to simulate the actual mounting position of the gearbox in the UH-1 helicopter and to guarantee proper operation of its splash-type internal lubrication system. Previously, this test cell was used to collect sensor data from 90° gearboxes on Contract DAAJ02-72-C-0118. For the present data collection effort, the test cell has been modified to increase loading on each gearbox from 40 hp to 70 hp, and to allow testing on a 24-hour continuous basis. In addition, torque sensors were mounted on both input and output shafts. These sensors provided capability of torque and shaft rpm measurement on both shafts.

Figure 2 shows the mechanical and hydraulic circuit diagrams of the test stand. Torque loading of the gearbox is supplied by a hydraulic feedback process. The circuit operates as follows:

(1) The electric motor operates on 440V three-phase AC power and rotates at a fixed speed of 1750 rpm.

(2) To obtain the 4150 rpm required to drive the gearbox, the output of the electric motor is stepped up 2.37:1 by a pulley arrangement.

(3) Due to its internal gearing, the gearbox itself provides a 2.6:1 speed reduction. Its output rotation rate of 1596 rpm is used to drive a fixed-displacement hydraulic pump.

(4) The fixed-displacement inner-vane hydraulic pump delivers 76.6 gallons per minute (gpm) of hydraulic fluid at 1596 rpm.

(5) The hydraulic motor is mechanically connected to the shaft of the electric motor. Since the primary source of power in the test cell is the electric motor, and since its rpm is fixed at 1750, the hydraulic motor must also turn at 1750 rpm. This hydraulic motor is also a fixed-displacement design and will accept only 56.4 gpm of hydraulic fluid at 1750 rpm.

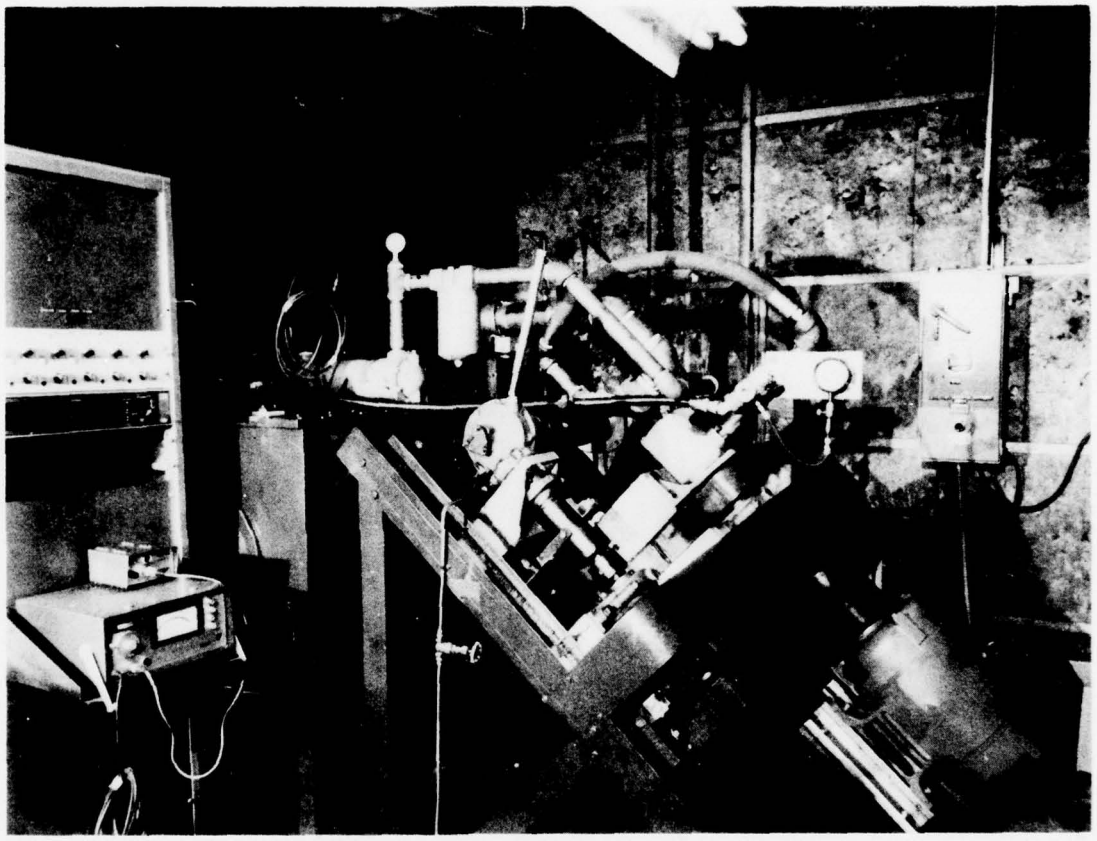

Figure 1. Overall View of Test Stand.

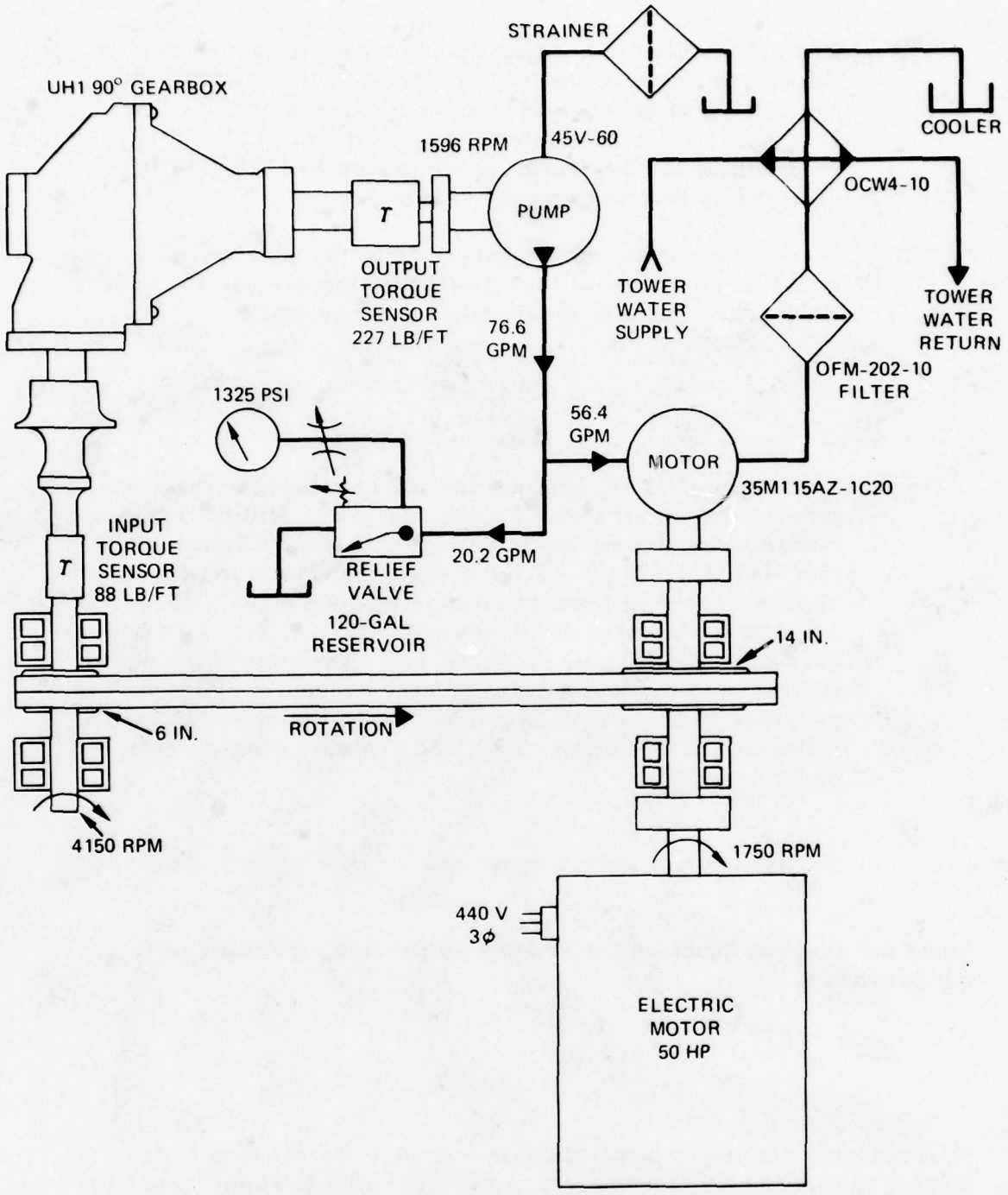

Figure 2. Gearbox Test Stand - Mechanical and Hydraulic Circuit Diagram.

(6) The relief valve is a manually adjustable pressure-regulating device that serves to maintain a constant operating pressure into the hydraulic motor. Excess oil flow (about 20.2 gpm in this case) above the maximum of 56.4 gpm required by the hydraulic motor to turn at 1750 rpm is directed by this valve to the reservoir.

(7) To determine the input horsepower to the gearbox, it is necessary to calculate the power flowing through the hydraulic circuit. This is given in horsepower by

$$hp = \frac{gpm \times psi}{1714} \qquad (1)$$

Since the relief valve is set for 1325 psi and the flow rate through the motor is 56.4 gpm, the power into the hydraulic motor = 56.4 gpm, the power into the hydraulic motor = (56.4) (1325)/1714 = 43.6 hp. The hydraulic motor, being approximately 85 percent efficient, returns .85 x 43.6 = 37 hp to the input of the gearbox. The relief valve passes 20.2 gpm at 1325 psi, or 15.62 hp. The sum of the power delivered to the relief valve and the hydraulic motor is provided by the hydraulic pump. Since the hydraulic pump efficiency is 88 percent, the load applied to the gearbox under test is

$$\text{Gearbox output shaft torque load} = \frac{15.62 + 43.6}{.88} = 67.3 \text{ hp.}$$

Since the gearbox efficiency is roughly 96 percent, the input power to the gearbox is

$$\frac{67.3}{.96} = 70 \text{ hp.}$$

In summary, the output power supplied through the gearbox is fed back to the input by a closed mechanical-hydraulic system. Since the electric motor must make up for all frictional losses, hydraulic leakage losses, and bypass hydraulic power, it need only supply power sufficient to start the test cell and to overcome these losses.

Torque and RPM Sensing

In order to insure accurate and constant loading of the gearboxes, two torque sensors were utilized on this program. One was mounted in series with the gearbox input shaft and the other in series with the output shaft. These torque sensors have full-scale 2000 inch-lb and 5000 inch-lb measuring capability, approximately double the requirements for the input and output shaft, respectively. These torque sensors may be observed in mounting position in Figures 1 and 2.

A second output from each torque sensor is a sinusoidal electrical signal from the sensor rotary transformer whose period is the time for one rotation of the shaft. These signals are shaped into square waves and sent to rpm counters in the Test Cell Controller, where digital rpm data is generated and collected by the computer on mag tape.

The torque sensor utilizes a strain gage bridge configuration on the rotating portion of the sensor. The electrical torque signals are coupled to signal conditioner modules in the test cell instrumentation rack which provide the required analog signals for digitization and collection by the computer system.

In addition to recording this data, the computer calculates both input and output horsepower from these torque and rpm measurements and provides test cell shutdown signals if either gearbox horsepower or efficiency deviates from 5 percent of nominal values.

COMPUTER-TEST CELL INPUT/OUTPUT (I/O) CONTROL

Test Cell Controller (TCC)

The TCC is composed of all the electronics required for automatic command and control of all phases of test cell operation. The controller provides the interface between the computer and the test cell control and data digitization system.

Considerable improvements have been introduced to the TCC since the previous contract. Figure 3 illustrates an overview block diagram of the TCC and I/O controller (to be described next). All data sent to the computer is in digital format. The 14-bit DATEL analog-digital converter (ADC) is located at the test cell and digitizes the data at a 20 KHz rate under control of a crystal oscillator. The digitized data is sent to the computer upon request over a 500-foot digital transmission cable. The cable contains 20 double-shielded twisted pairs. Bidirectional balanced line driver/receivers at both ends of the cable allow duplex operation over the cable and assure that information is only transmitted in a single direction at a time.

All sensor signals are multiplexed into the DATEL ADC with the exception of outputs from the two rpm sensors. These are digital in nature, and counts are accumulated in two counters. The counter results are stored in a buffer and updated every minute to provide a measure of each shaft rotation in rpm. These rpm signals are then multiplexed with the ADC output and sent to the computer upon request. Parity checks are made on all data sent from either end of the cable.

In addition, fault detection logic is provided in the TCC as in the previous contract to automatically shut down the test cell in the event of a test cell problem or computer problem. In addition, interlocks are provided to shut down the test cell in the event of cooling water becoming too warm or loading on the electric motor becoming too heavy.

The TCC also accepts commands directly from the computer. In the event that the computer senses a severe malfunction in either the test stand or the gearbox, or when the current test interval is completed, an AUTO STOP command is sent to the fault detection logic to shut down the testing.

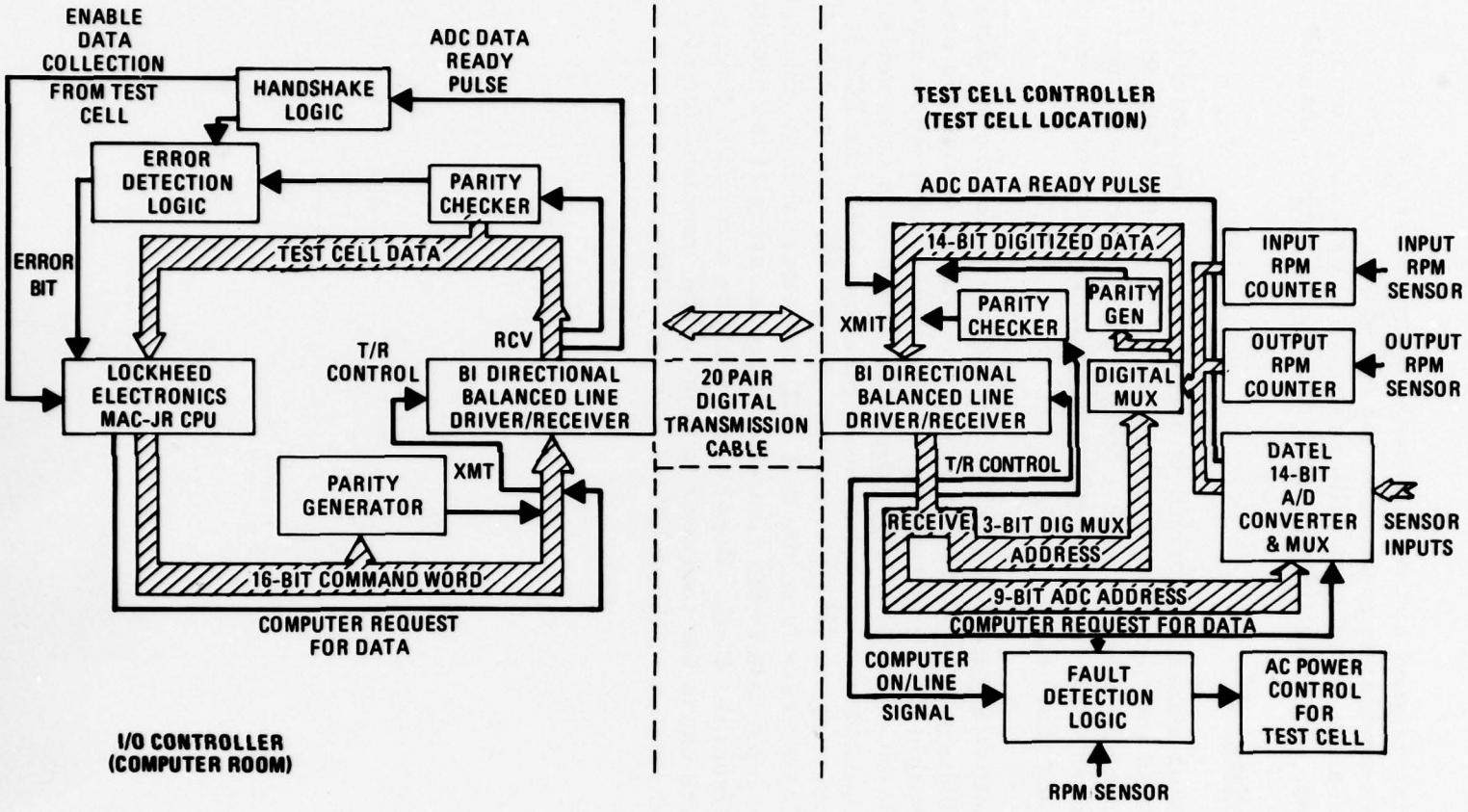

Figure 3. Computer-Test Cell I/O Control.

The TCC is designed so that unattended operation is not possible unless the computer is monitoring the operation. Furthermore, the test stand cannot be automatically restarted after a stop command has been issued. The start-up sequence must be performed manually.

I/O Controller

The computer shown in Figure 4 is used to monitor the activities of the test stand and to collect the prognostics data. It is located some 500 feet from the test cell area. Special precautions were taken to insure that reliable communications are maintained between the computer and the test cell.

The left half of Figure 3 shows the block diagram for the computer-test cell I/O signal conditioning circuitry. Digital commands originating from within the computer are sent via the external output channel to a data latch. The data latch stores the computer's commands, allowing the CPU to accomplish other functions while the TCC is busy interpreting the latest command. Similarly, upon receipt of a DATA READY pulse from the test cell, the external input channel will proceed to input data to the computer for processing at the proper command from the CPU. Errors occurring as a result of timing or parity check cause the computer to reissue the command for data for a prescribed number of times before test cell operation is shut down.

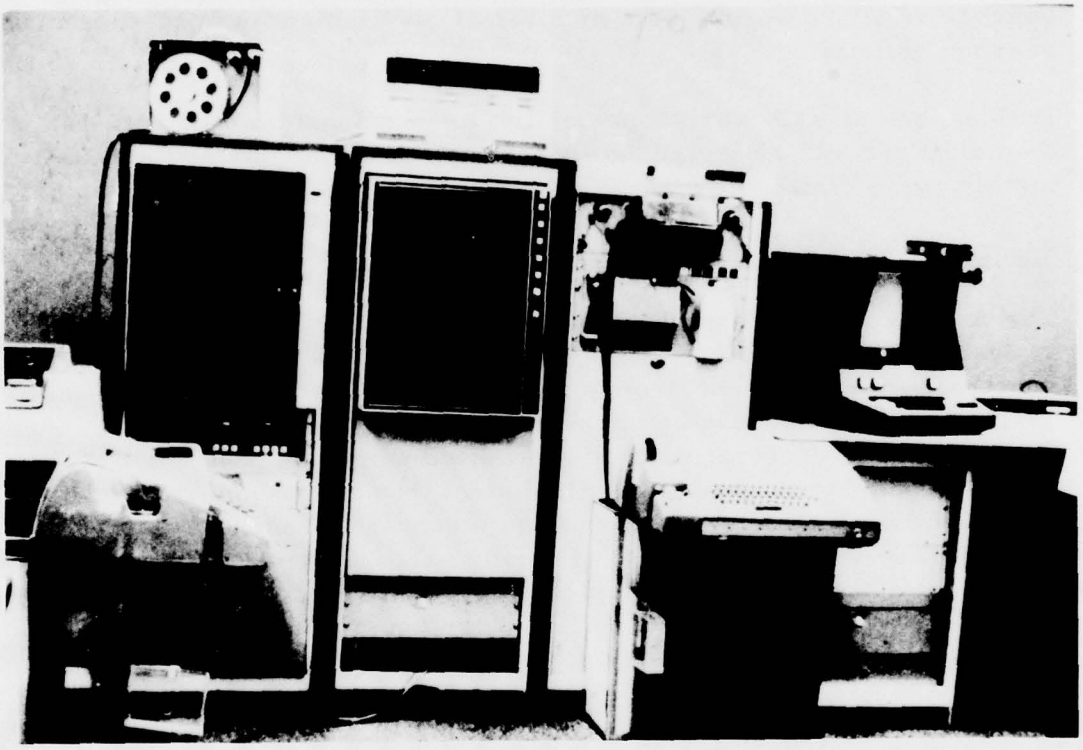

Figure 4. Interactive Computer Graphics System.

SENSORS AND SENSOR LOCATIONS

Temperature Sensors

Two platinum-type temperature sensors in a probe configuration were used on this program. One probe was inserted through a tapped hole in the gearbox case into the oil sump to measure gearbox oil temperature. The second probe was secured by a clamp in a position proximate to the gearbox case and served as a monitor of the ambient temperature in the gearbox vicinity.

Both sensor signals were converted to proportional voltage outputs, then digitized and collected as digital data by the computer approximately every 10 minutes during the test run.

Spectrometric Oil Analysis (and Other Oil Analyses)

The Army currently samples the oil from UH-1 helicopter 90° gearboxes at 25-30-hour intervals. These samples are then subjected to a spectrochemical, or spectrometric, oil analysis at a remote location. This type of oil analysis has proven to be a useful technique for determining mechanical wear of oil-wetted components in helicopter engines, gearboxes, and transmissions. Iron is the contaminant in the oil which is of most use in diagnosing mechanical wear. Figure 5 is an example of the type of upward trend in iron content one would expect from a defective gear with accelerating wear. Since the oil is changed every 100 hours in this example, the iron content decreases after each change. The sharply increasing slope between oil changes indicates that the gear is deteriorating at an accelerating rate. A good gear would have no significant change in the rate of increase of the iron content between oil changes.

In this program, 20 milliliter samples were taken once every 24 hours, except on weekends. These samples were shipped to Corpus Christi Army Depot (CCAD),Texas, for spectrometric oil analysis. In addition, the drained oil at 100-hour change intervals was shipped to the Applied Technology Laboratory at Fort Eustis, Virginia, for additional analysis.

The density of 20 elements in each oil sample is recorded in parts-per-million on the spectrometric oil analysis data record. By scanning any column for a particular element (e.g., Fe), trends and relative element content may be readily discerned.

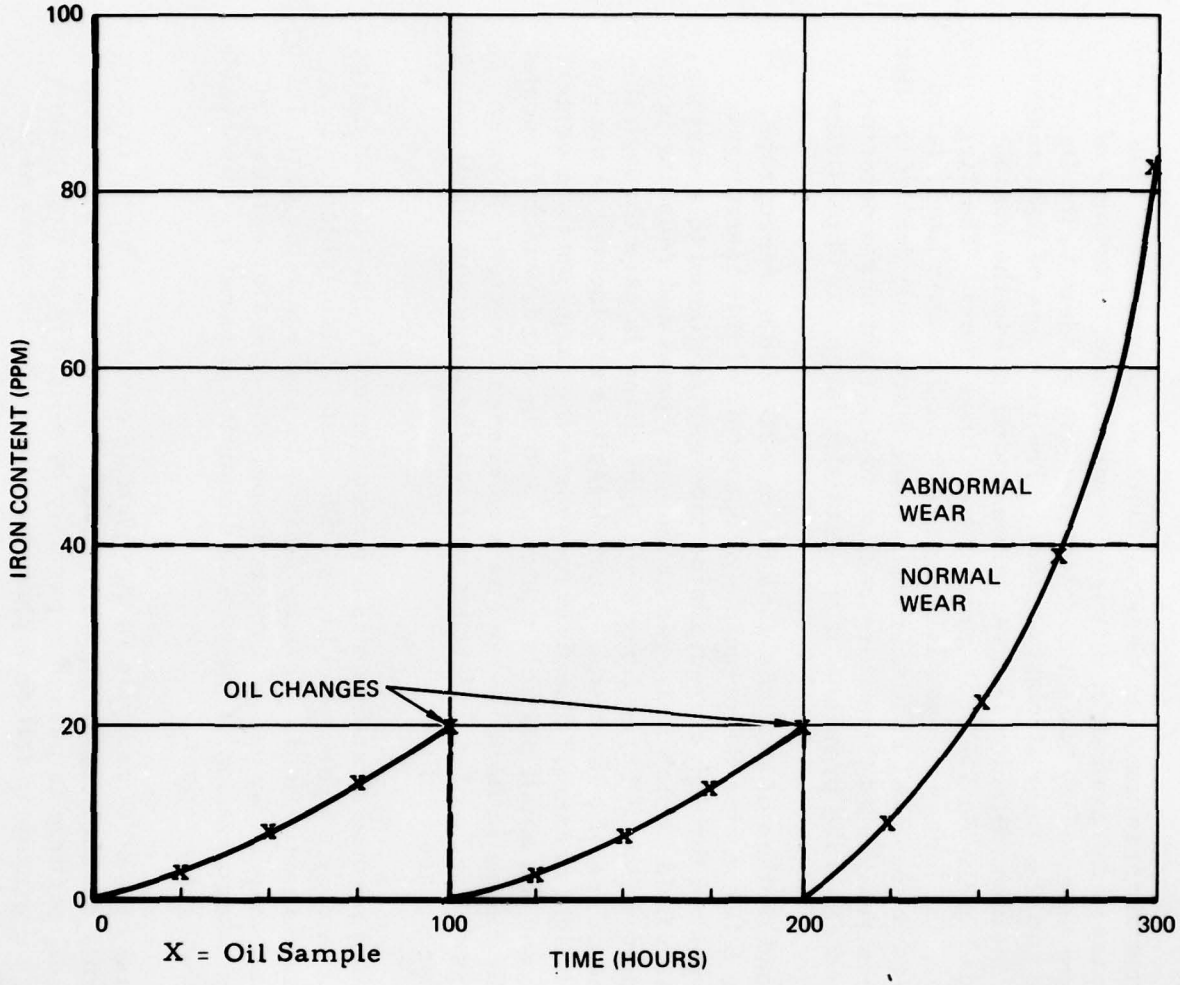

Figure 5. Example of SOA Data for Defective Gear

Four other types of oil analysis are performed at CCAD. Each of these analyses covers pertinent information about the particle content of the oil samples.

The first of these uses the General Electric oil monitor. This instrument passes infrared light through the oil sample. Portions of the light are detected by two photodetectors: one incident to the light source and the other at right angles. The measure of light received by the incident detector is inversely proportional to the number recorded in the ATTEN column of the analysis sheet. The larger the number, the higher the particle density. On the other hand, large numbers in the SCATTER column indicate that a good deal of the light has been redirected through refraction to the right angle detector. This indicates the presence of substantially large-sized particles.

A second method of analysis uses the direct-reading ferrograph. Figure 6 illustrates the principle of operation of this instrument. Oil is passed through a precipitator tube and subjected to a varying magnetic field which is larger at the entry point and reducing in the direction of flow. Three fiber optic light channels pass through the oil tube at specific locations. Photodetectors are located at the end of each light channel. The first measures the large particle content, the second the small particle content, and the third, which is located past the magnetic field, serves as a reference detector. A wear index is defined as the difference between the large and small particle detector squared values.

The third method of analysis is a ferrogram analysis. In this method, oil is run over a prescribed glass slide, that is also subjected to a varying magnetic field. This field tends to segregate the particles by size and shape. By use of a microscope, the operator enters a subjective categorization of the type and quantity of particles observable on the analysis report.

The last method of analysis is the particle counter. The oil is pumped through a channel containing an orifice. Because of the dynamics, every oil particle is passed separately by a light beam that passes through a window to fall on a photodetector. The intensity of the received light gives an indication of the particle size, so that a particle size distribution is recorded on the analysis sheet.

All these analysis methods are helpful in attributing the mode of wear in the gearbox and in correlating with trend data derived by other means.

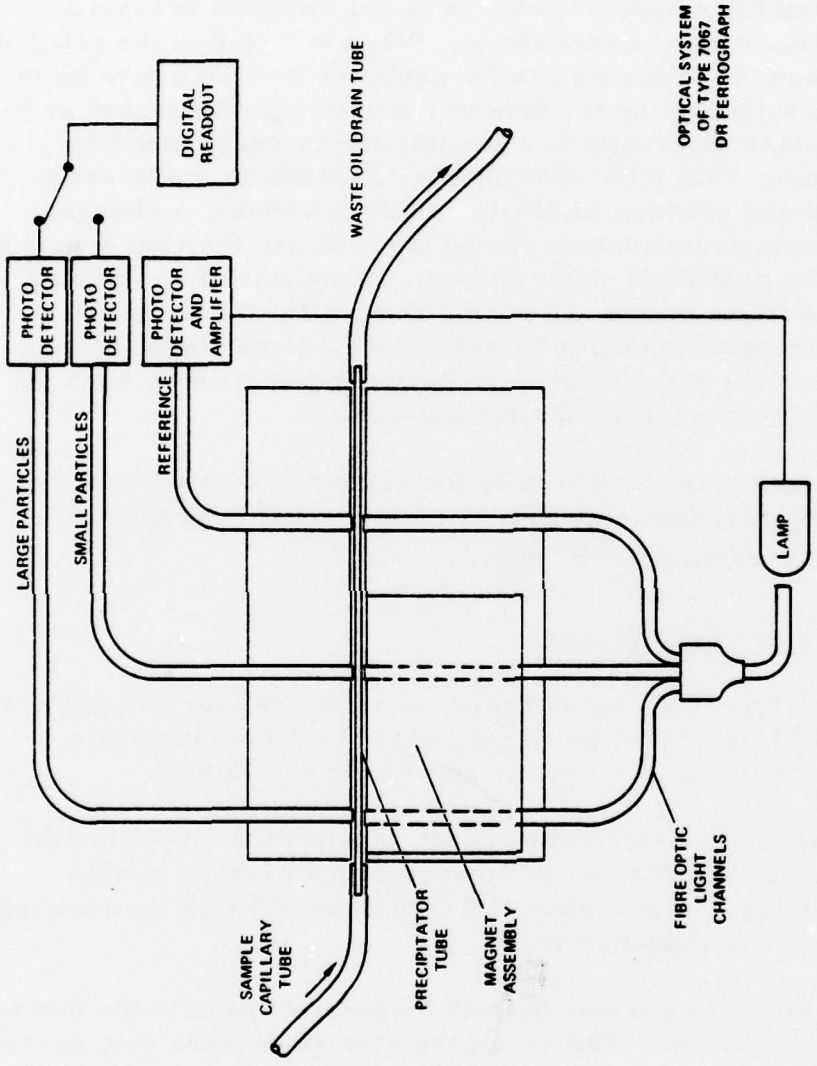

Figure 6. Block Diagram of Direct-Reading Ferrograph.

Capacitive Discharge Chip Detection System

Midway through the testing program, a chip detection system produced by the Tedeco Co. of Glenolden, Pa., was made available for evaluation by ATL. This system uses a magnetic particle detector inserted in the oil drain passage which also provides automatic closing of the oil passage when the magnetic probe is either retained in the oil passage or withdrawn for examination. When inserted in the gearbox oil drain passage, it collects metallic particles that happen to be in the vicinity. Two points on the face of the detector (separated by a gap) are connected externally to a capacitive discharge and chip recording system. When the chip debris collection is sufficient to bridge this gap and produce an electrical short circuit, a charged capacitor in the instrumentation dumps current into the chip debris to "burn off" the electrical short circuit. If successful, a count is recorded. With light debris collection, burn-offs will occur infrequently. As the gearbox begins to wear more, more counts will be recorded. When the size of the chips becomes too large to burn off, a red light is turned on at the instrumentation.

The counter output was monitored by the computer data collection system, and the test data pertinent to each gearbox is presented in the section on Experimental Results.

Low Frequency Accelerometers

Briel and Kjaer type 4344 accelerometers were used for sensing low frequency (< 10 kHz) vibration signals and also some ultrasonic energy. The frequency response is approximately 45 kHz.

Two of these accelerometers were used: one to sense input (shaft) lateral vibrations and the second to sense output (shaft) lateral vibrations. Figure 7 is a profile of the gearbox showing the location of the two B & K accelerometers.

The mounting method used was to weld magnesium pads to the desired locations on the gearbox. The accelerometer studs were then screwed into the pads.

To separate ultrasonic energy from low frequency energy, the accelerometer signals were filtered in two parallel paths. In one path the signal was passed through a 10 kHz cutoff low-pass filter before digitizing; in the other path, it was passed through a 20 kHz cut-off high-pass filter before processing described in the next section.

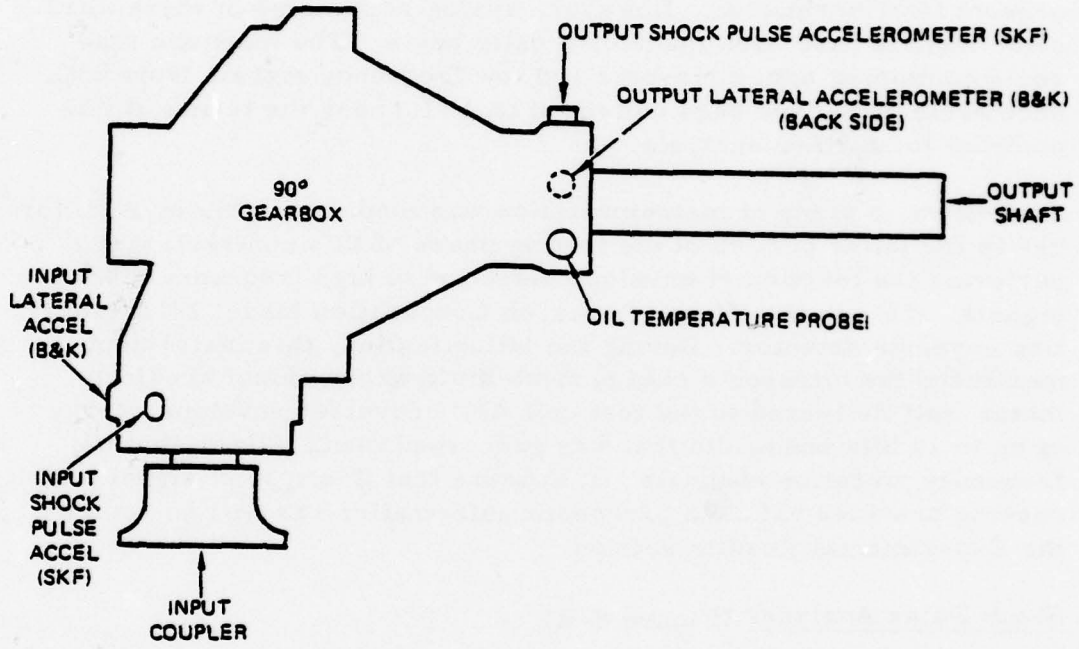

Figure 7. Gearbox Profile Showing Accelerometer Locations.

Ultrasonic Accelerometers

Much has appeared in the literature regarding the diagnostic usefulness of ultrasonic emissions (> 20 kHz) from mechanical components. Because of the broader frequency response of the B & K model 4344 accelerometers, data was collected on a regular basis from the ultrasonic energy in these accelerometers during testing. The Root Mean Square (RMS) ultrasonic level from each of the accelerometers has been collected by the computer approximately every 10 minutes. Because the data digitization sampling rate was set at 20 kHz, a frequency analysis of the spectral content of this energy has not been possible with our present instrumentation. However, analog recordings of these ultrasonic signals have been made on a daily basis. The magnetic tape reels containing both ultrasonic and low frequency signals from both accelerometers have been delivered to ATL under the terms of this contract for further analysis.

In addition, a piece of instrumentation was made available by ATL for use in the latter portion of the testing phase of this contract, that performs the function of envelope detection of high frequency vibration signals. This is the Shaker Research Corporation Model 223A vibration envelope detector. During the latter testing, this instrument monitored the ultrasonic energy from the gearbox output accelerometer and delivered to the test cell A/D converter envelope energy of up to 10 kHz bandwidth that was processed identically to the low frequency vibration channels. It appears that this type of signal processing provides valuable prognostic information, as will be seen in the Experimental Results section.

Shock Pulse Analyzer (Figure 8-A)

The shock pulse monitor was manufactured by SKF Industries, Inc. This instrument uses an accelerometer to sense the ultrasonic shock pulses emitted by bearing defects in order to determine bearing health. The locations of the input and output shock pulse accelerometers are observabie in Figure 7. The interaction between the rolling element and discontinuities in the contact ellipse gives rise to mechanical impacts, which in turn release discrete emissions of energy within the bearing elements. These mechanical impacts create two different kinds of shock pulses within the bearing: a transient shock pulse and an elastic resonance shock pulse.

A transient shock pulse of very short rise time ($< 1\ \mu s$) radiates from the point of impact. The rise time and amplitude of this initial shock

wave are essentially determined by the impact velocity and the speed of sound through the material and are independent of the mass of the interacting bodies.

The initial shock pulse sets up a multitude of different transients of relatively high frequencies in the different parts of the machinery. The amplitude, frequency, and damping of these transients are determined by the material and the design of the machine parts.

The second type of shock pulse, the elastic resonance shock pulse, is generated by the total kinetic energy of the original impact. The amplitude and frequency of this wave will be determined by the impact velocity and the mass and rigidity of the bodies involved. These types of pulses are associated with the mechanical resonances of the bearing. Most current bearing diagnostic techniques model the bearing physical and operational characteristics to predict the frequency of these elastic shock pulses.

The SKF shock pulse analyzer, however, uses the transient shock pulse instead of the elastic shock pulse for the following reasons:

(1) The transient shock pulse is a sharp-rise, short-duration pulse of energy which is directly related to the severity of the discontinuity in the bearing element contact ellipse.

(2) The transient shock pulse depends only upon the speed of sound in the structure for its propagation velocity and is independent of the spring/mass characteristics of the structure. Therefore, it is not dependent on modeling of the mechanical system for data interpretation.

(3) The transient shock pulse is markedly attenuated at mechanical interfaces (empirical data indicates about 14 dB per interface). Because of this, with careful sensor placement the shock pulse analyzer can discriminate between a faulty bearing and a good bearing when the two bearings are in close proximity to each other. The electronic signal processing used in the shock pulse analyzer is somewhat involved, and the interested reader is referred to the user's manual for these details. The new effect of the electronic signal processing is to provide a means for obtaining the cumulative amplitude distribution function of the shock pulses (integrated over sufficient time to ensure proper

statistics) which SKF calls a "shock emission profile." The shock emission profile is a plot of the total cumulative rate of shock pulse emissions above a given amplitude level (for a given unit of time) against the given amplitude level (potentiometer level). Figure 8-B shows the three basic curve shapes (shock emission profiles) obtained by SKF in their testing of mechanical systems.

Curve A is a typical shock emission profile obtained when foreign particulate matter is present in the bearing lubricant. This curve is characterized by having high rates of very small shock levels but no shocks above a level of 3 to 5.

Curve B is typical data obtained from dry bearings or when there is rolling element damage. This curve is characterized by very low rates of very high shock levels.

Curve C, characterized by high shock rates at high levels, indicates a damaged bearing. The spread in shock level is caused by the specific characteristics of each rolling element as it interacts with the damaged portions of the bearing.

Curve C' is an example of the shock emission profile one would expect to observe as the damaged bearing, represented by the data in Curve C taken at an earlier time, continues to degrade. The shock emission profile should reflect an increase in both shock rate and shock level.

All of the shock pulse data collected on this program had shock emission profiles similar to Curves C and C'.

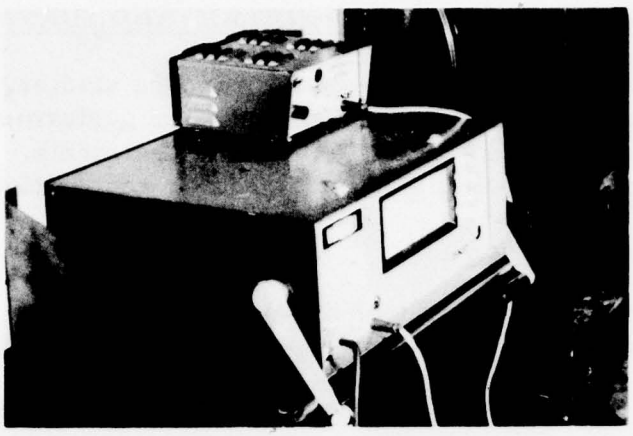

(A) SKF Shock Pulse Analyzer.

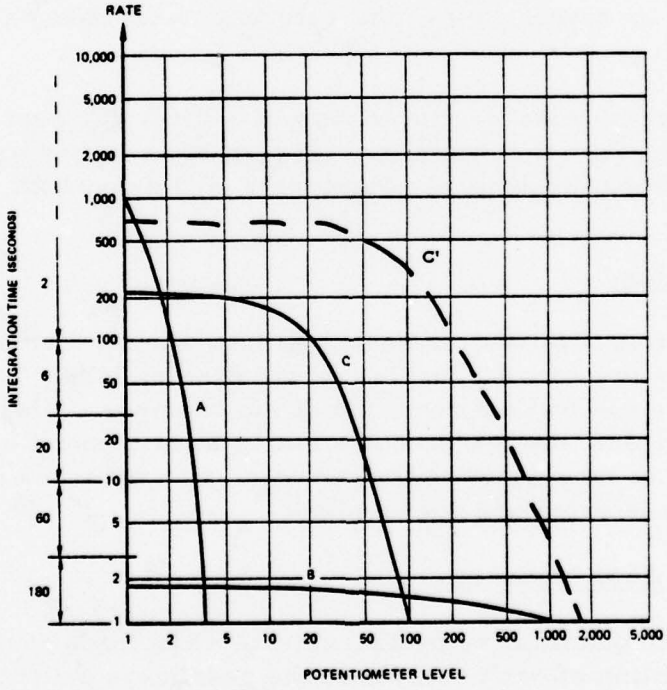

(B) Shock Emission Profile Curve Types

Figure 8. Shock Pulse Analysis

DETERMINATION OF BEARING CONDITION AND SURFACE WEAR

Except for the scanning and electron microscope studies, the tests for mechanical wear discussed in this section were performed by Bearing Inspection Incorporated of Santa Fe Springs, California. Bearing Inspection is authorized by the FAA to repair or recondition aircraft bearings.

No quantitative measurement technique was available for monitoring gear wear. Early in the previous program, it was requested that Bell Helicopter provide us with gear profiles, but they could not make profiles on spiral bevel gears. The condition of the gears was determined by a subjective assessment of their visual appearance, as discussed in the section on Experimental Results.

In all of the bearing wear measurements, the bearing condition after testing was compared to its condition prior to testing. Since all of the gearboxes were already in a worn condition and no measurement data was available on new bearings, the very important data point on zero wear is missing.

Figure 9 shows a cross-sectional view of a UH-1 90^{o} gearbox and the location of the gears and bearings. Figure 10 is a photograph which shows most of the mechanical components of the gearbox.

Visual Inspection

Visual inspection involves the complete disassembly of the bearing. The subjective opinion of a highly trained bearing inspector is used to evaluate the mechanical condition of the bearings. This test helps to identify reasons why the bearings are in their present condition. The presence of large-scale contaminants, pits, grooves, or other irregularities is noted and documented.

Ball Bearing Wear Measurements

Three separate quantitative measurements were made to determine the wear condition of each bearing in the gearboxes prior to and after each phase of the test program.

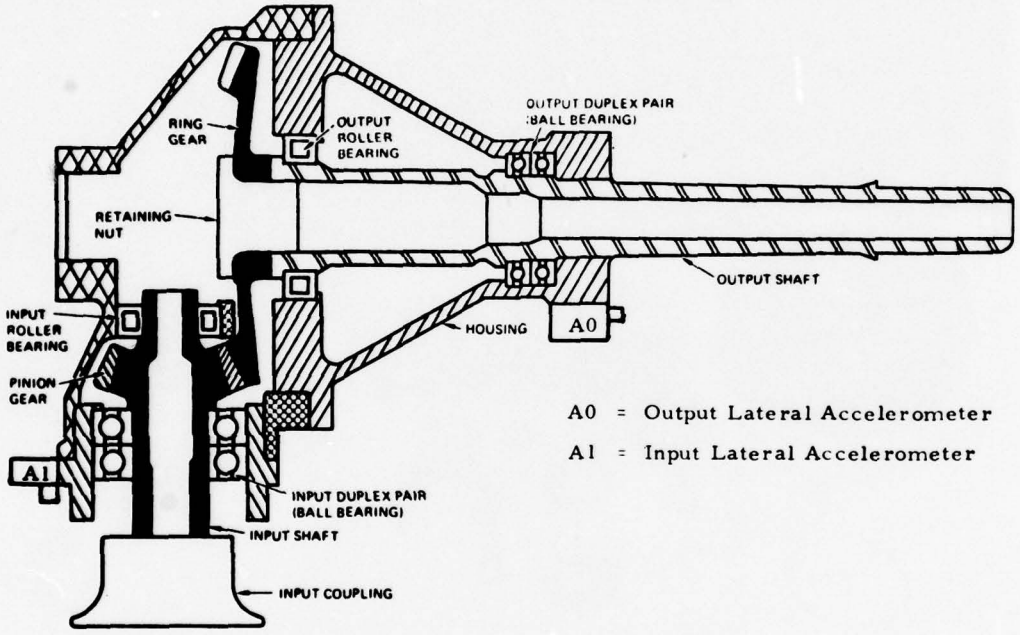

Figure 9. Cross-Sectional View of 90° Gearbox.

Figure 10. Partial Disassembly of 90° Gearbox.

(1) Dynamic Noise Testing of Ball Bearings

This test characterizes the bearing as an operational dynamic unit. The results of this test give an accurate picture of the overall health of the bearing and are found to correlate well with visual and microscopic inspections of the individual components.

The test bearing is mounted on a shaft and is caused to rotate at low speeds by the application of a rotating rubber wheel to the outer casing of the bearing. Vibrations set up in the bearing are transferred to the (stationary) shaft and are sensed by a piezoelectric crystal as shown in Figure 11. The shaft and its support mechanism have a mechanical resonance of about 800 Hz. After amplification, the bearing vibrations are low-pass filtered to 2 kHz and the RMS noise level is determined. The RMS noise level is an overall indication of degree of wear in the bearing. This level is compared with the vibration noise level of known good bearings and should not exceed 0 dB for a new bearing.

Table 1 is an excerpt from Bearing Inspection's "Product Specification" and gives a summary of how the (RMS) noise level compares with the physical condition of the bearing.

Another parameter derived from the noise test is the relationship between the peak-to-peak vibration noise level and the RMS noise level.[1] This relationship is called "peak rise" and is a measure of how uniformly the wear is distributed around the bearing. A peak rise of 0 dB is normally found in good bearings. A peak rise of -3 dB indicates an exceptionally uniform wear pattern, while a peak rise of +7 dB indicates considerable local damage.

In order that a bearing be considered acceptable as new, both the noise level and the peak rise must be below 0 dB.

---

1 This parameter is closely related to the so-called "crest factor" developed by the General Electric Company. See Houser, Donald R., et. al., VIBRATION SIGNAL ANALYSIS TECHNIQUE, Ohio State University Research Foundation; USAAMRDL Technical Report 73-101, Eustis Directorate, U.S. Army Air Mobility Research and Development Laboratory, Fort Eustis, Virginia, December 1973, AD776397, p. 78.

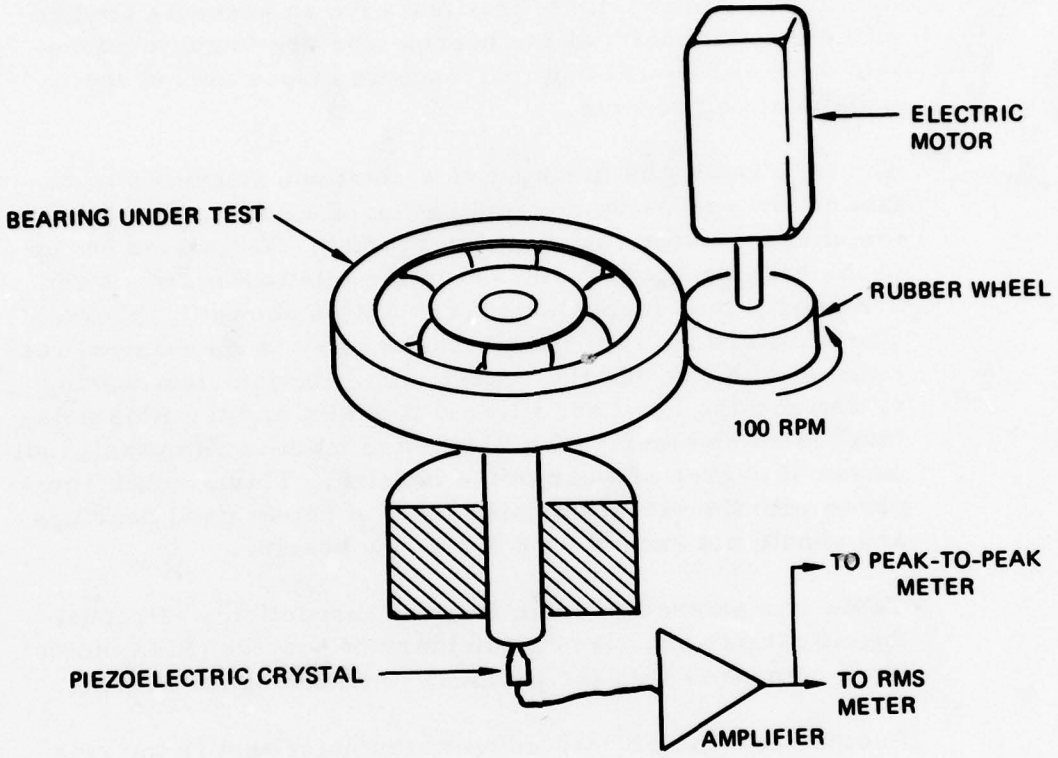

Figure 11. Schematic Diagram of Dynamic Noise Test.

TABLE 1. DYNAMIC ANALYSIS: BEARING CONDITION LEVELS
(Bearing Inspection, Inc.)

Bearing Noise Level Range (dB)	Condition	Visual	Microscopic	Common Conditions
Below -7	EXCELLENT	Like new	Smooth polish	N.A.
-7 to -5	GOOD	Like new	Polish	N.A.
-5 to -3	FAIR	Like new	Polish	N.A.
-3 to 0	ACCEPTABLE NEGLIGIBLE Wear	Like new	Slight pitting and denting	Slight wear
0 to 3	LIGHT Wear	Like new	Light pitting and denting	Light wear
3 to 7	MODERATE Wear	Well defined wear tracks	Pitting and denting	Moderate wear
7 to 12	HEAVY Wear	Wear tracks with pitting and denting	Heavy pitting and denting	Fatigue spalling
12 and above	EXTREME Wear	Very rough	Gross surface disturbance	Heavy electric current damage; extensive smearing and material transfer

(2) Radial Play Measurements of Ball Bearings

Radial play is defined as the maximum total clearance between the inner and outer races of the bearing. It is measured by first pushing the inner race as close to the outer race as possible (this ensures intimate contact between the inner race, the ball, and the outer race) and then by pushing the inner race radially in the opposite direction as far as possible. The total distance traveled is called radial play and is a measure of running clearances and overall material wear (race and balls) in the bearing.

(3) Cross-Groove Profile of Inner Race of Ball Bearings

This test measures the actual shape of the inner race of the bearing. A stylus with a very fine diamond tip is pressed lightly against the surface of the inner race. The other end of the stylus is connected to a linear displacement sensor. As the stylus is moved across the race, a profile of the bearing is plotted out. Figure 12 illustrates in principle how this measurement is performed.

A polar plot is usually made to show differences in curvatures across the inner race. As a bearing wears, the balls wear a groove (called a ball track) into the races. Typical polar plots are shown in Figures 13 and 14. These measurements were taken on the inner races of bearing number 3 of gearbox BBT. Figure 13 shows a cross-groove profile of BBT-3 prior to testing. The radius plot has a scale of 10 microinches per division. The "reference side" and "BBT-3 side" refer to the orientation of the bearing in the gearbox. The cone of interest is marked "ball path." This is where the changes are expected to occur as the bearing deteriorates. Due to the bearing design, the ball contacts only the inner race at this point. Figure 14 is a cross-groove profile plot of the same bearing at 1022 hours testing. Notice how the depth of the ball track has increased during testing. The cross-groove profile measurement is a very sensitive indicator of inner race wear.

Roller Bearing Wear Measurements

Only the ball bearings were completely disassembled. The output roller had only one roller removed in order to preserve its overall

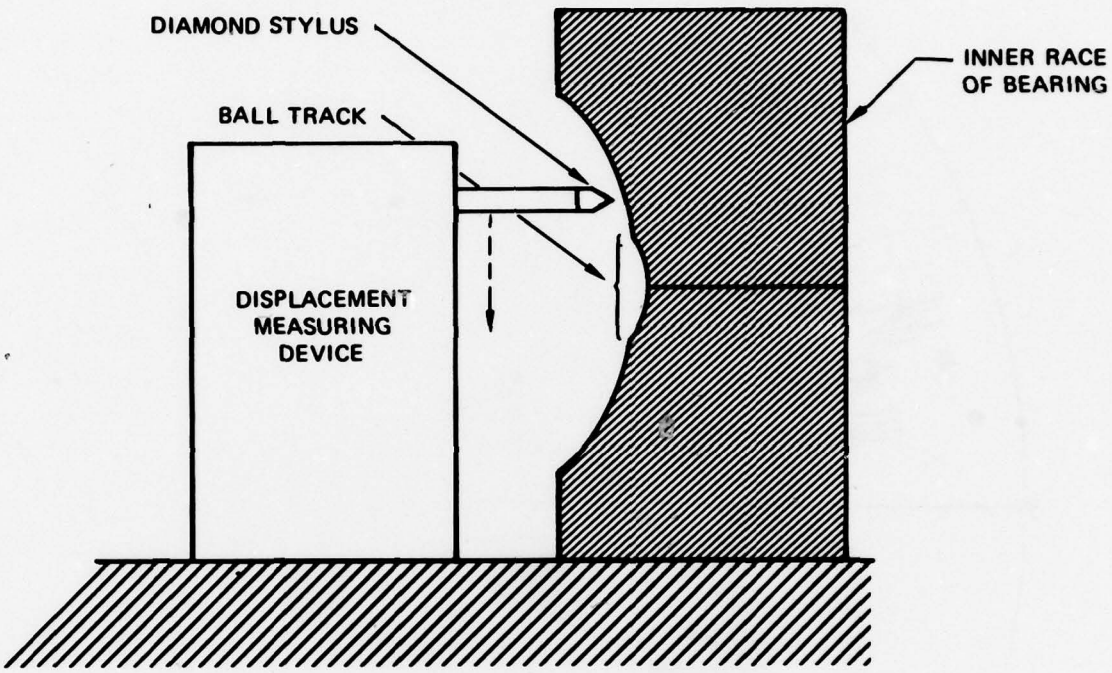

Figure 12. Schematic Diagram of Cross-Groove Profile Measurement.

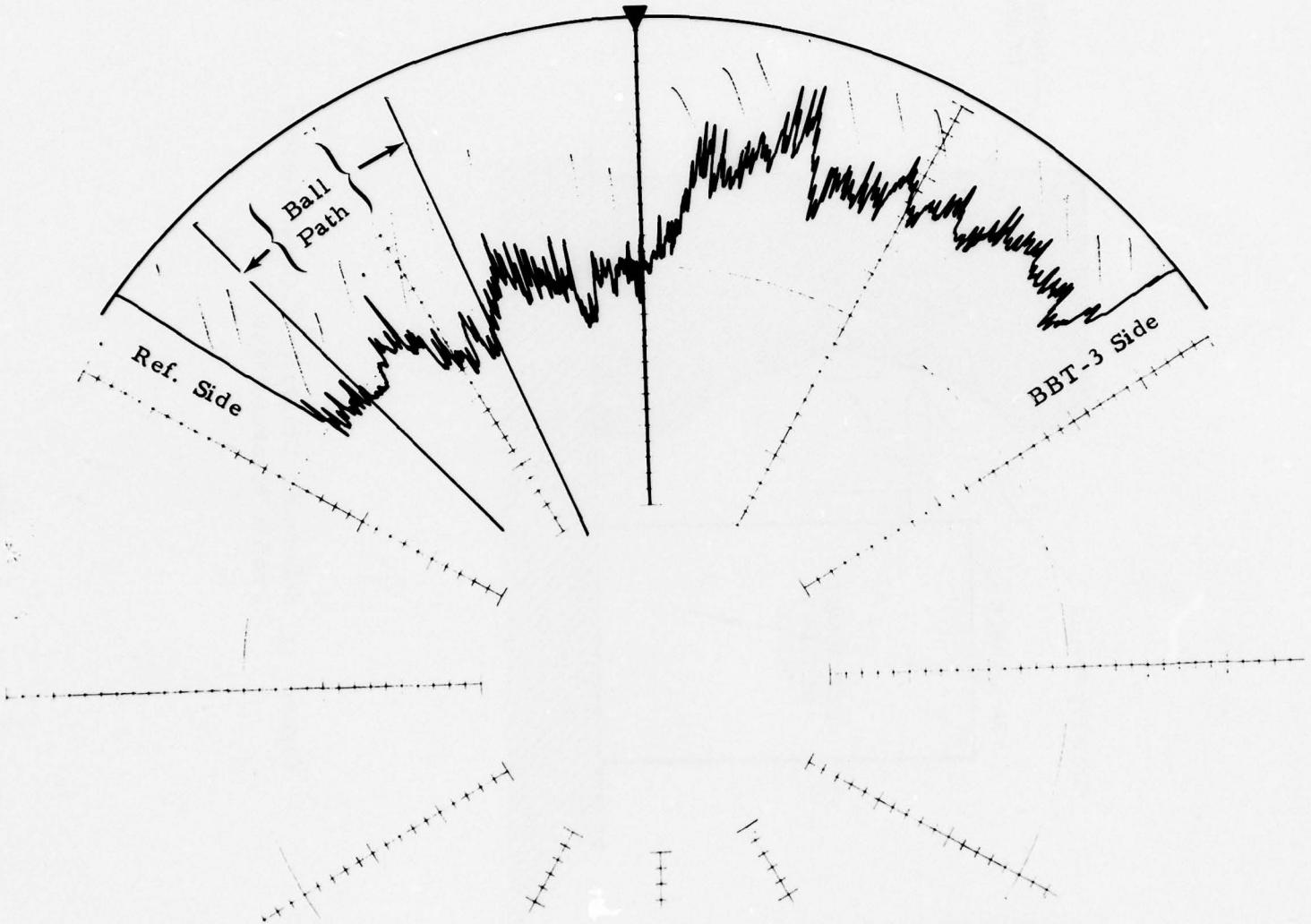

Figure 13. BBT-3 Cross-Groove Profile at Zero Test Hours.

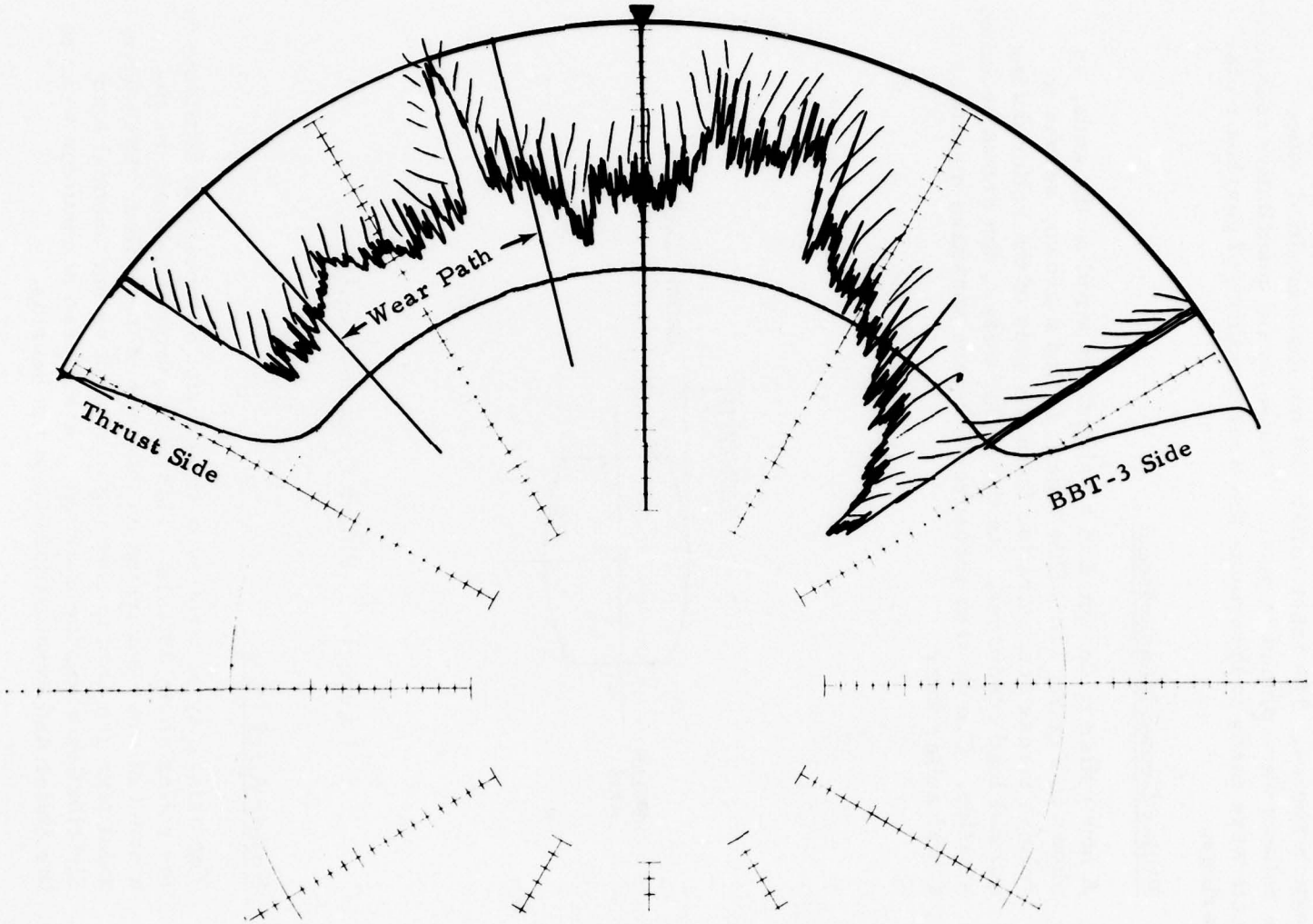

Figure 14. BBT-3 Cross-Groove Profile at 1022 Test Hours.

characteristics. The input roller was not disassembled since the rollers were pinned in place. Two separate quantitative measurements were made to determine the wear condition of gearbox roller bearings.

Roller Crown Measurement

A new roller is designed to be slightly tapered on the ends, as shown in Figure 15 . This taper, called a crown, serves to relieve stress concentration from the ends of the roller during normal load conditions. As the roller wears, the crown becomes smaller. Crown wear measurements are sensitive measures of actual roller wear.

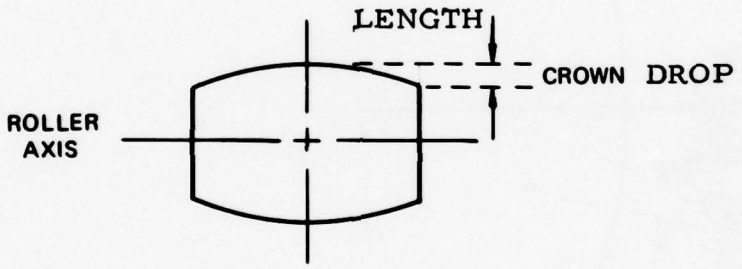

Figure 15 . Roller Crown Parameters.

Roller Axial Play

The axial play of a roller is the amount of movement available to the roller along its axis. This measurement determines the amount of wear occurring on the ends of the roller. Excessive axial play can lead to skewing of the roller and unequal load distribution along the bearing. This causes nonuniform wear of the roller and eventual failure of the bearing.

Scanning Electron Microscope Surface Inspection

For completeness in determining the overall condition of the bearings, one ball and one roller from each bearing (except for the pinned roller bearing number 6 which was not disassembled in any gearbox) were examined with the scanning electron microscope (SEM). Each part was thoroughly cleaned in acetone before examination to remove fingerprints, excess oil, and extraneous surface debris. The microscope has two modes of operation: the secondary emission mode (SEC) and the backscatter emission mode (BSE). The two modes produce different types of view of the same surface area because one mode (SEC) operates with low-energy electrons and the other (BSE) with high-energy electrons.

Secondary Emission Mode (SEC)

The SEC mode utilizes a low-energy (100 ev) electron beam to scan the surface of the specimen. The surface structure responds to the electron beam by emitting secondary electrons which, in turn, are collected for display purposes. Irregularities in the number of secondary electrons, in turn, give rise to the picture of the topography of localized portions of the surface. The SEC mode detects the structure of the first several angstroms (10^{-8} cm) of the specimen. The major advantage of the SEC mode is its ability to look around corners or into depressions and provide the viewer with a picture that appears to have three-dimensional characteristics. The SEC mode produces surface pictures that have no obscuring shadows around raised or depressed areas, making it somewhat difficult to differentiate between these two surface characteristics.

Backscatter Emission Mode (BSE)

The BSE mode utilizes a high-energy (10 kev) focused electron beam to scan the specimen. The high-energy electrons penetrate the specimen's surface to a depth of about 10-20 microns. Some of these electrons are scattered back out of the specimen, where they are collected for display purposes. These high-energy electrons travel in straight lines, which causes the BSE photo to be characterized by shadows around raised or depressed surfaces. The BSE mode is often the only way one can positively identify a raised or depressed surface. The BSE mode is most useful when surface films (e.g., oil stains) must be penetrated to view the surface underneath.

Examples of SEM pictures using the SEC and BSE modes are given in Figure 16. These were obtained from the surface of a ball from bearing number 2 in gearbox BBT. Both photographs are of the same surface area on the ball and both are taken at a magnification of 1000 to 1. Note the sharpness but lack of surface detail in the BSE picture.

For the gearbox bearing data given in this report, the SEM pictures were obtained using the SEC mode, unless specifically designated as BSE pictures. The SEC mode was selected for most of the data presented because, from our subjective viewpoint in determining surface abnormalities, the SEC mode produced the most useful pictures.

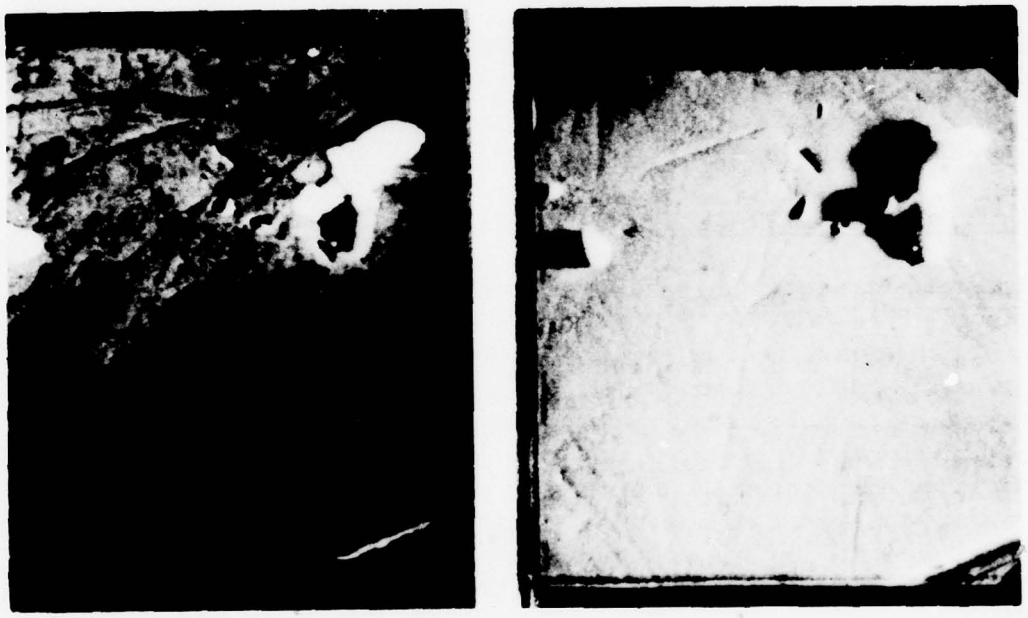

(A) Secondary Emission Mode (B) Backscatter Emission Mode

Figure 16. SEM Micrographs of BBT-2 (407 Hours).

AUTOMATIC COMPUTER-CONTROLLED DATA COLLECTION AND REDUCTION

This section describes the computer-controlled data collection system and the documentation procedures for the gathering and initial reduction of the real-time test cell data.

OVERVIEW OF MAIN COMPUTER SOFTWARE

The data collection program was written to implement the timing diagram shown in Figure 17 . Data was collected on a continuous round-the-clock basis and stored periodically on magnetic tape in the format of files containing three records each.

The fundamental flowchart of Figure 18 describes how this timing diagram was implemented in the data collection program. Actual detailed flow diagrams of software data-collection subroutines are presented in Appendix A.

START-UP SEQUENCE ROUTINE (Figure 19A)

The start-up sequence is followed every time the test cell must be started or restarted. In the event a shutdown had occurred previously, the mag-tape reel is backspaced to the start of the file, to maintain a uniform formatting. Input parameters are entered on the teletype in response to computer prompting. When finished, a command is printed to start the test cell. At this point, horsepower and efficiency are continually computed until both are within limits. They are then checked 1 minute later. If not stabilized, the 1-minute timer is reset and the process is repeated. When finally stabilized, date and time are printed on the teletype and data collection is begun.

DATA COLLECTION ROUTINE (Figure 19B)

Data is collected continuously by the computer from the test cell. This data is transferred periodically onto magnetic tape for later reduction and analysis. A record of data is transferred to tape every 10 minutes. The record consists of a high, low, and average value of data from 131,072 samples of each monitored DC channel; a 512-line power spectral density averaged over 128 FFT's computed from 128 groups of 1024 samples of vibration data from each vibration channel; and pertinent elapsed time data and RMS vibration channel data.

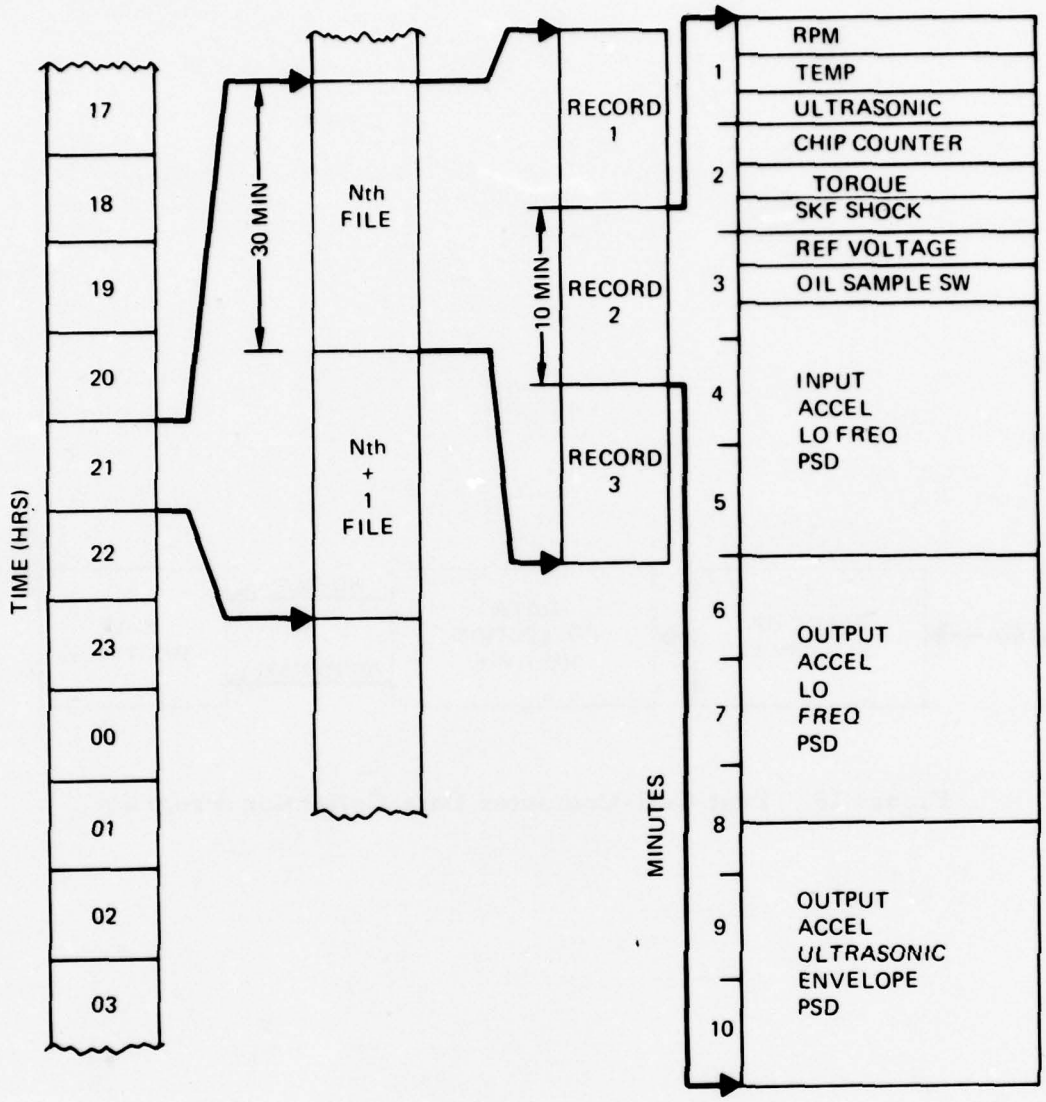

Figure 17. Timing Diagram for Data Collection Effort.

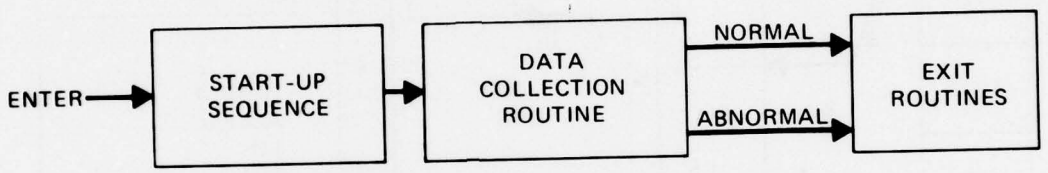

Figure 18. Test Cell-Computer Data Collection Program.

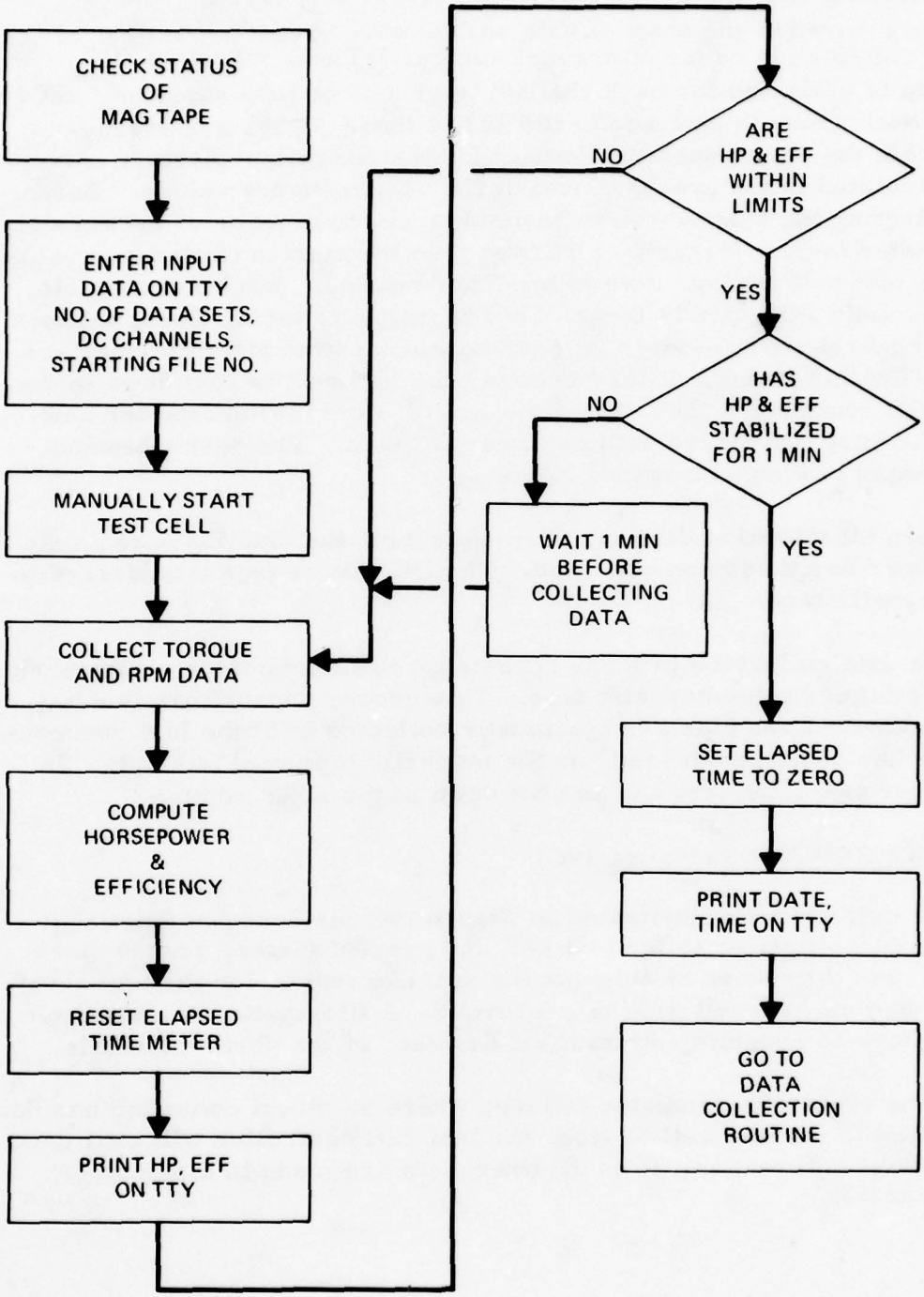

Figure 19A. Start-Up Sequence.

Referring to Figure 19B, all file, record, and channel counters are cleared at the start of data collection. Secondly DC data is collected in order of channel number. Then, vibration data is collected for each channel in groups of 1024 samples. An FFT of each group is computed, and 128 of these FFT's are averaged to obtain the power spectral density for that vibration channel. Also calculated is the average level of the 512 frequency values. Before selecting the next vibration channel, a check is made of the accelerometer level. If it is 26 dB lower than the start-up reference value, the test cell is shut down in the EXIT routine. But, if acceptable, this valid PSD data is transferred to magnetic tape. Then, a check is again made to verify that gearbox horsepower and efficiency are still within limits. If they are not, the test cell is shut down in the EXIT routine. If they are within limits, current horsepower and efficiency are stored with the other DC data. The next vibration channel is then addressed.

When all vibration data has been collected, the data for a complete record has then been collected. The DC data is then transferred to magnetic tape.

The data collection process repeats three times before a file-mark is written on the magnetic tape. This occurs approximately every 30 minutes. Data files are continually collected until the last requested file has been transferred or the magnetic tape reel is empty. In either case, the test cell is shut down in the EXIT routine.

EXIT ROUTINES (Figure 19C)

The exit routines illustrated in Figure 19C perform two functions: (a) shut off power to the test cell and prevent further gearbox testing and (b) record on teletype the specific reason for the test abort, as well as date and time of shutdown. A file-mark is also written on the tape to expedite retrieval, if desired, of the partial data file.

In the event of a computer failure, where no direct command has been issued to the test cell to stop, the test cell controller will shut down the test cell by itself if no data requests are made in a period of 8 minutes.

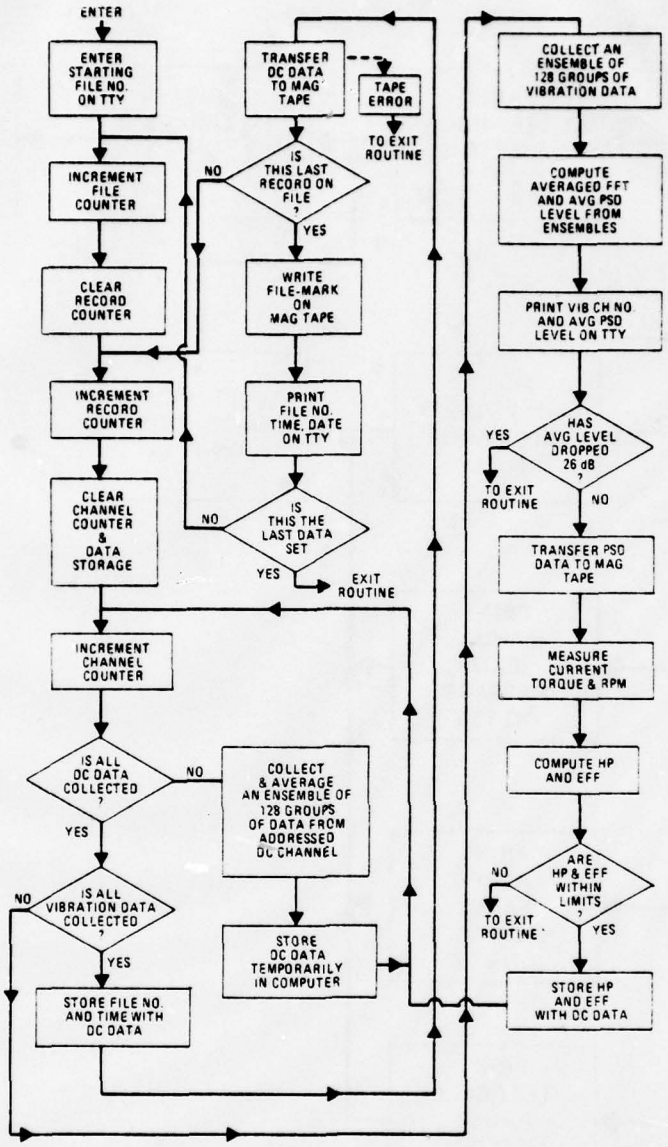

Figure 19B. Data Collection Routine.

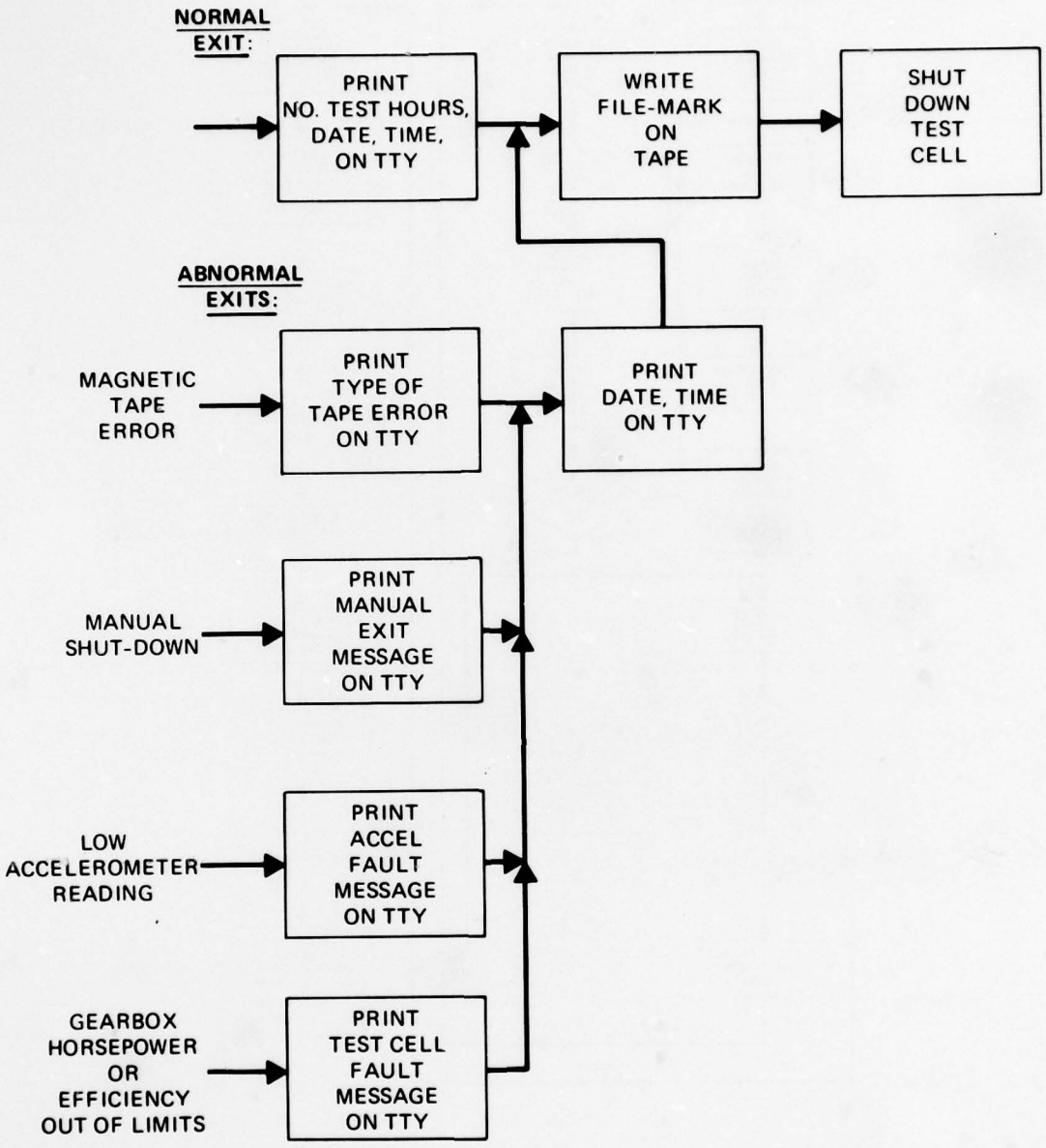

Figure 19C. Exit Routines.

VIBRATION DATA REDUCTION

This section describes the data reduction procedures used to analyze the data collected under this contract. Six different gearboxes were tested for a cumulative test period of over 4600 hours. Each sensor was sampled every 10 minutes. These samples were statistically reduced by the on-line computer via the procedures described below. The reduced samples were stored on magnetic tapes, which were later edited and placed in various formats for trend analysis.

Although the data base contains sensor samples taken every 10 minutes, only sensor data from every sixth record (1 hour) were used for the trending analysis discussed in the section on Trend Parameter Investigation.

Vibration measurements for this contract were taken from two low-frequency accelerometers located as shown in Figure 7. The frequency range of analysis was DC to 10 kHz. This range was divided into 512 frequency bins which were 19.531 Hz wide.

Each accelerometer signal was low-pass filtered to 10 kHz by a sixth-order Butterworth filter before being digitized by a 14-bit analog-to-digital converter. The resulting digital signals were preprocessed in the following manner.

First the discrete Fourier transform (DFT) of each signal was computed. The DFT converts time domain signals into frequency domain spectra. The DFT is defined as

$$F(k) = \sum_{i=0}^{N-1} [W(i) \cdot f(i)] \exp [-j (2\pi ik/N)], \quad k = 0, \ldots, N-1 \qquad (2)$$

where

$F(k)$ = k_{th} Fourier transform coefficient

k = frequency bin index

N = transform size

$f(i)$ = i_{th} time domain signal sample

i = time signal sample index

$W(i)$ = Hamming weighting function

$= 0.54 - 0.46 \cos [2\pi i/(N-1)]$

The DFT was computed using the "fast" Fourier transform (FFT) technique.

The purpose of Hamming weighting the time domain vibration signal prior to computing the DFT is to reduce the sidelobe structure of the transform caused by abrupt time domain transitions associated with transforming over a finite time interval. Without the Hamming weighting, the sidelobes would obscure low-amplitude transform coefficients.

Figure 20 shows a finite-length time domain sine wave without Hamming weighting and the magnitude of its DFT. Note the high sidelobe levels (down from the main lobe by only 13.2 dB). Figure 20 shows the same signal with Hamming weighting. Here the sidelobes have been reduced to 42 dB.

Next, the power spectral density (PSD) function of each signal was computed. The PSD is obtained from the DFT by the relation

$$P(k) = |F(k)|^2 = F(k) \cdot F(k)^*, \; k = 0, 1 \ldots, N/2 - 1 \qquad (3)$$

where

$P(k)$ = power spectral density in frequency bin k

$F(k)^*$ = complex conjugate of $F(k)$

The vibration signals were sampled at a 20-kHz rate, and the sample duration was 51.2 ms, which corresponds to a DFT size, N, of 1024. A short-term PSD was computed over this interval. The computation time by the computer was less than 1 second.

To increase the statistical accuracy and our confidence level that the true PSD values were being calculated, we ensemble averaged 128 short-term PSD's to form a statistically averaged PSD. The sample standard deviation of the ensembled PSD's approaches the true PSD value as the ensemble becomes larger. The selection of the ensemble size is a trade-off between the need for statistical accuracy and reasonable computation time. Since the relative statistical accuracy

increases in proportion to the square root of the sample size, a sample size of 128 yields a statistical accuracy of 0.5 dB and a computation time of approximately 2 minutes. Figure 21 shows how the 128 PSD's are ensemble averaged to obtain the statistically averaged PSD, which is then stored as reduced data on magnetic tape for off-line processing.

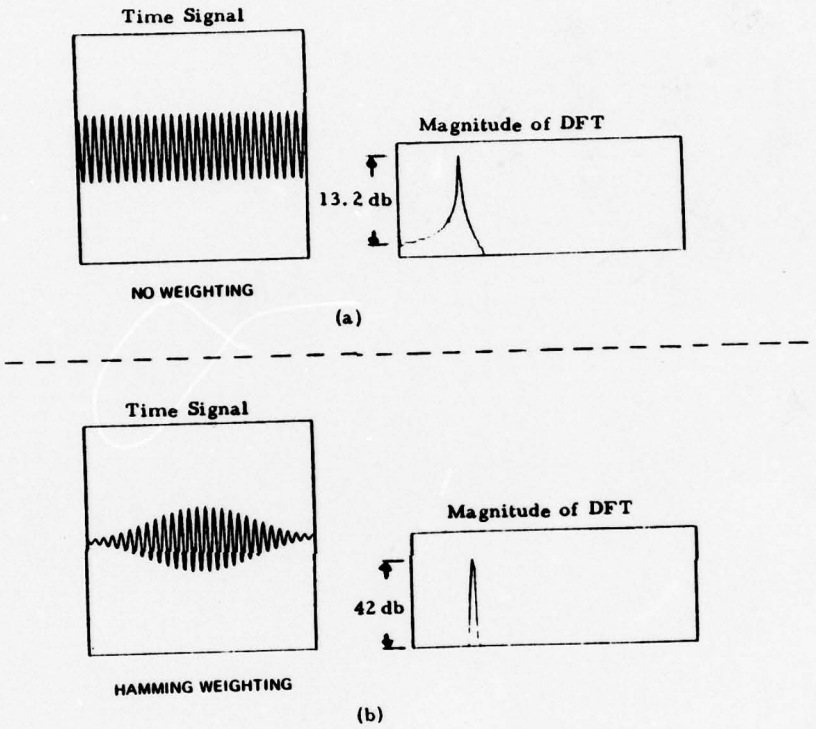

Figure 20. Reduction of DFT Sidelobe Structure by Hamming Weighting an Input Time Domain Signal.

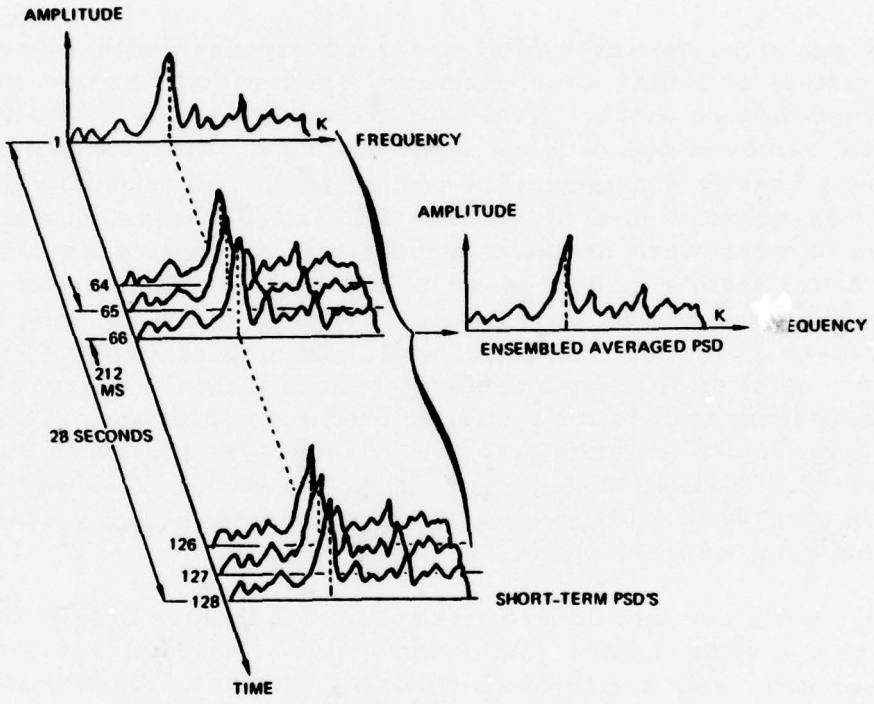

Figure 21. Ensemble Averaging of PSD Function.

EXPERIMENTAL RESULTS

This section presents a detailed description of the test runs on six UH-1 90° gearboxes. A total of 4712 hours of testing was accumulated on these gearboxes. Table 2 summarizes the number of hours each gearbox was tested, as well as lists that portion of the test hours that are useful for trending purposes. A very high ratio of the data, 96 percent, is considered usable for solving the prognosis problem.

This set of gearboxes exhibited a good "spread" with regard to (a) variety of initial wear condition, (b) longevity of test time, and (c) final failure mode. Two gearboxes, BB-4 and HT-4, were finally removed due to worn input bearings. Gearbox BB-5 suffered a heavily damaged input pinion gear. An unusually long test run was accomplished by gearbox HT-3 (1437 hours) during which signs of wear were detected by post-test processing as early as 300 hours from commencement of the test. This gearbox was finally removed due to worn output bearings. An unexpected occurrence was a test cell that failed while testing gearbox HT-5. A worn coupler on the output shaft disengaged from the gearbox and caused termination of the test after 596 hours of testing. This gearbox had given indication of an early wear trend developing when the mishap occurred. Finally, at the other extreme, gearbox HT-2 was run for 1519 hours with negligible wear indication from either sensor data, oil analysis, or mechanical inspection.

Test results covered in each test subsection include results of pre- and post-test mechanical inspection analysis, oil analyses, temperature sensor data, rpm and torque indicator data, accelerometer low frequency and ultrasonic data, and data from the SKF shock pulse analyzer and the Tedeco chip detector. Also, results of data trending using the following four trend parameters are given: RMS, matched filter, geometric mean, and arithmetic mean processing. In addition, power spectral densities processed from accelerometer data at representative test time periods are displayed and analyzed for each gearbox.

BB-4 GEARBOX TESTS

Gearbox BB-4 was the first gearbox selected for testing in the present contract. This gearbox had extremely bad bearings at the start of the test. The operation of the gearbox was monitored very closely from the beginning, knowing that it could fail at any time. Testing of BB-4 was

TABLE 2. SUMMARY OF GEARBOX TESTING TIME

GEARBOX	NO. TEST HOURS	TRENDABLE HOURS
BB-4	171	152
BB-5	437	330
HT-5	596	575
HT-2	1519	1519
HT-3	1437	1437
HT-4	552	510
TOTALS	4712	4521

finally terminated after 171 hours due to impending catastrophic failure. 152 hours of trendable data were available from this test. The remainder were absorbed in initial test cell checkout.

Mechanical Condition of BB-4 Gearbox

Pre-Test Inspection

Visual inspections of both ball and roller bearings before testing indicated considerable wear and damage. The inner and outer races of the two input bearings had a 1/8-in.-wide ball track along with electrical pitting and denting. The ball condition was poor, with bearing No. 1 having a prominent wear band on each ball.

Dynamic testing of the bearings verified the visual examination. The bearing noise level measurements were high, between 14.5 and 17 dB for both input and output bearings. As a comparison, gearbox BB from the previous program had a noise level of 18.5 to 20.5 dB on the output duplex pair prior to its testing, and it failed catastrophically after 166 test hours. The general wear condition of all ball bearing assemblies of BB-4 was classified as "extreme" prior to testing.

Post-Test Inspection

Visual examination after 171-hour testing and during the disassembly period revealed considerable metal observable in and on parts of the BB-4 gearbox. The output duplex pair on the output shaft was loose. It was noted that the outer bearing race was installed improperly prior to initial testing. Figure 22 (A) illustrates the two faces that were erroneously mounted flush to each other. These sides should have been mounted as in Figure 22 (B). It is quite possible that the bearings obtained insufficient splash lubrication due to this incorrect installation. Also, when installed properly, the inner races are held locked against each other, preventing these races from working loose. Although this error may have contributed to the early failure of this gearbox, we feel that the data is valuable and usable for trending purposes. An error of this type is possible in the field, and hopefully our data analysis will provide early warning indicators of similar assembly errors.

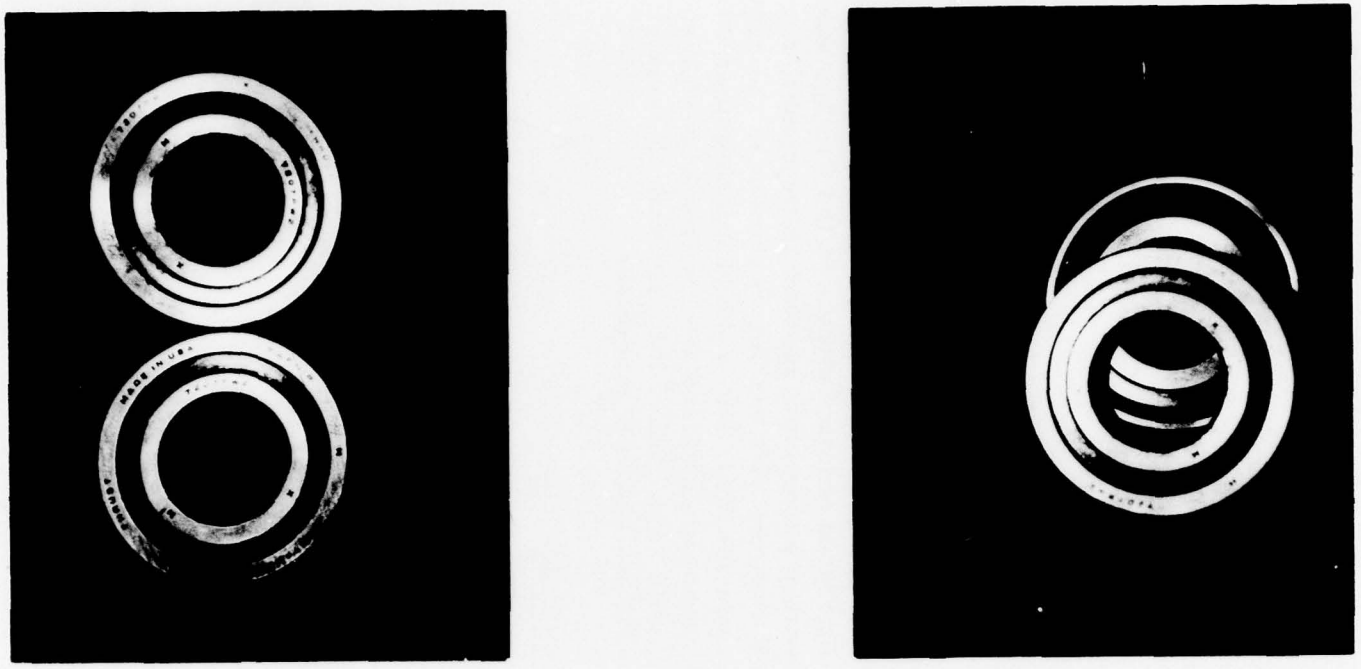

(A) (B)

Figure 22. Gearbox BB-4 Output Duplex Pair Bearing Assemblies.

The dynamic and mechanical measurements revealed little change in roller bearing play or wear. The major O-ring seal in the input ball bearing sleeve assembly was badly cut. This could possibly have caused a bad oil leak. The No. 1 outer ball-bearing assembly was pitted so badly that it fell apart when pressed out of the sleeve. Both inner and outer races of bearing No. 1 were considered in a failure mode due to fatigue and heavy wear. The balls also had failed. There was considerable fatigue damage on every ball. Observation of the SEM photographs of the No. 1 bearing before and after test revealed the extensive damage sustained by this bearing assembly. Dynamic noise tests on bearing No. 1 were also revealing. The already high noise level increased from 14 dB to 29 dB. Also, raceway wear depth increase was dramatic: from 133 microinches before test to 4600 microinches after test.

Both mechanical measurements and dynamic noise tests revealed a slight increase in wear on the other three bearing assemblies, but the gearbox failure could be attributed almost entirely to the damage sustained by the No. 1 ball bearing assembly. Insofar as its condition was roughly the same as the other three ball bearing assemblies, the exact cause of this failure cannot be verified, but because the ring gear wear pattern was excessive and razor sharp along the trailing edge of the teeth, the bearing failure could have caused the gear path to deviate significantly, resulting in significant chip generation.

Spectrometric Oil Analysis (SOA)

Eleven oil samples were taken from the BB-4 gearbox during the relatively short testing period. The SOA data is summarized in Figure 23. The data indicates the presence of a high concentration of iron in the oil at the start of testing. This condition persisted throughout the BB-4 test and is probably associated with gear wear. We also know from the mechanical measurements performed before and after testing that the wear in the input duplex bearing was in an advanced stage, and that the gearbox was in the initial phase leading to catastrophic failure.

Figures 24 and 25 illustrate the large metallic chips noticed in the oil sample at about the 170-hour point. Figure 24 (A) was taken with white filter paper and Figure 24 (B) with black filter paper. Preliminary elemental analysis on the scanning electron microscope (SEM) indicated a large iron content with traces of chromium and copper.

Figures 25(A) and (B) show more detail of the chips. These photographs were taken at 20 X and 50 X magnification, respectively.

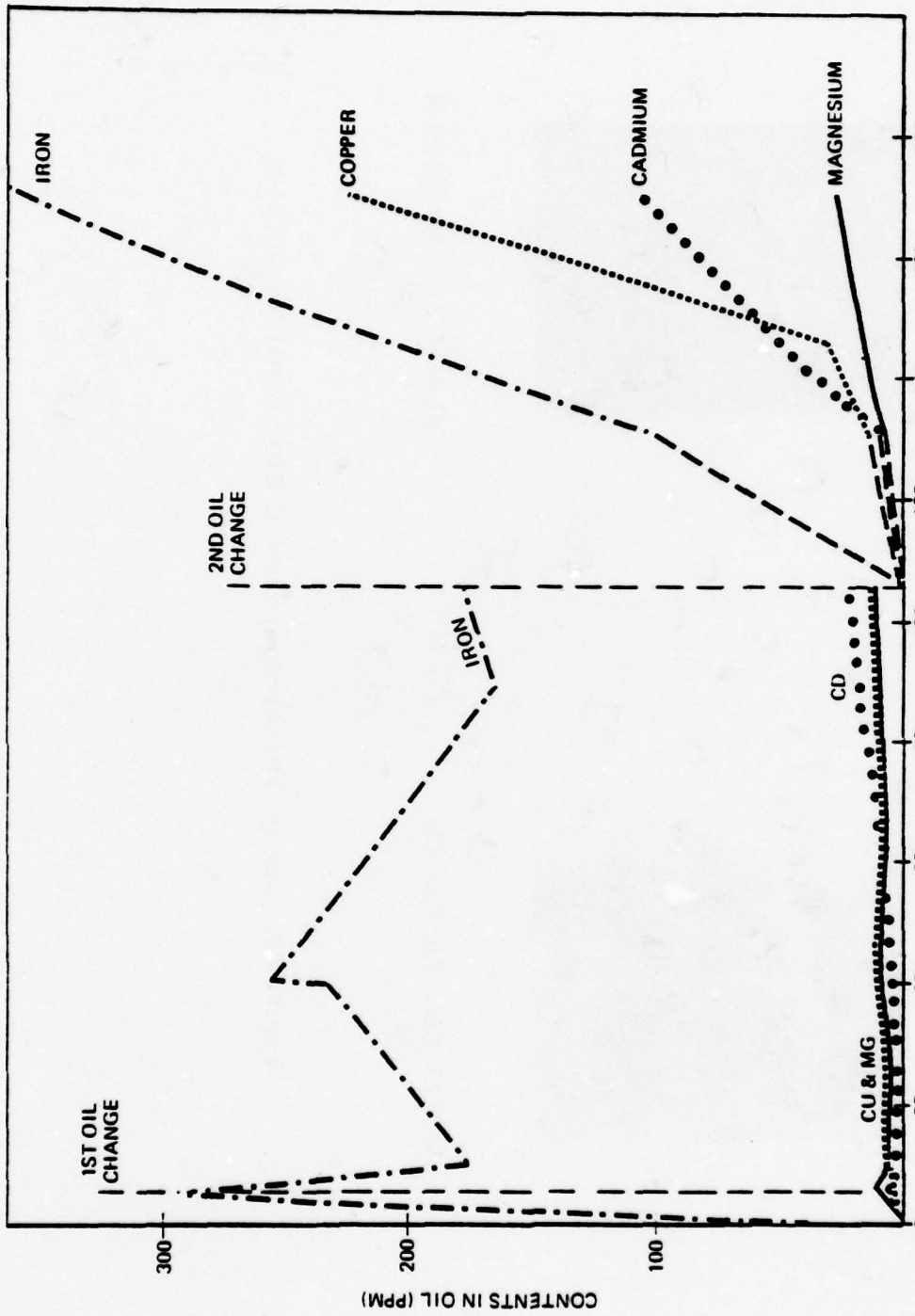

Figure 23. Spectrometric Oil Analysis - Gearbox BB-4.

WHITE FILTER PAPER
(A)

BLACK FILTER PAPER
(B)

Figure 24. Optical Microscopic View of BB-4 Metal Chips (X10).

20X
(A)

50X
(B)

Figure 25. SEM Photomicrographs of BB-4 Metal Chips.

Referring again to the SOA data in Figure 23, the increase in copper content to over 200 ppm near the end of the test indicates excessive wear of bearing cages as a result of the bearing failure. Also, the increase in cadmium indicates increasing bearing wear.

Temperature Sensors

Analysis of the gearbox temperature sensor outputs revealed no correlating data from either the ambient or the oil temperature sensors. From Figures 26 (A) and (B), it is seen that there is a 115° F ambient temperature, quite possibly too high for proper testing of the gearbox, inasmuch as the gearbox is exposed to the external air during actual flight.

Ultrasonic RMS Accelerometer Data

Since no broadband ultrasonic accelerometers were available, the ultrasonic data appearing in Figures 27 (A) and (B) represents the detected energy above 20 kHz from the input and output lateral accelerometers. Both plots indicate an increasing energy level near the end of the test. The energy from the input accelerometer becomes saturated at approximately the 100-hour level. The detector subsequently was adjusted to prevent limiting from occurring.

It is difficult to properly interpret the peaks and valleys exhibited by the output accelerometer data. They do not correlate with energy-vs-time indications that will be seen later from the lower 10 kHz of the same accelerometer data. Quite possibly, certain frequency bands of the spectrum are responsible for these perturbations.

Shock Pulse Analyzer

Shock emission profile data using the SKF shock pulse analyzer is plotted for both input and output accelerometers in Figures 29 and 30. These profiles indicate the rate of shock pulses exceeding successively greater threshold levels. The area under these profile curves could be considered an indication of the general mechanical condition of the gearbox. This area increases with gearbox testing time mainly because of higher rates of shock pulses at higher threshold values.

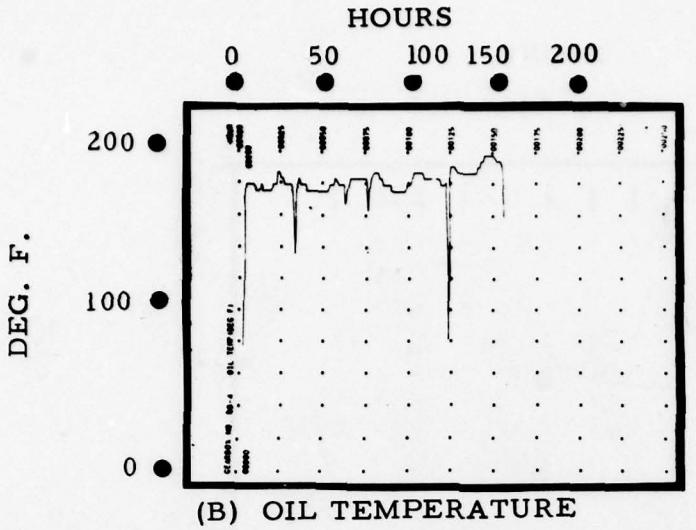

(B) OIL TEMPERATURE

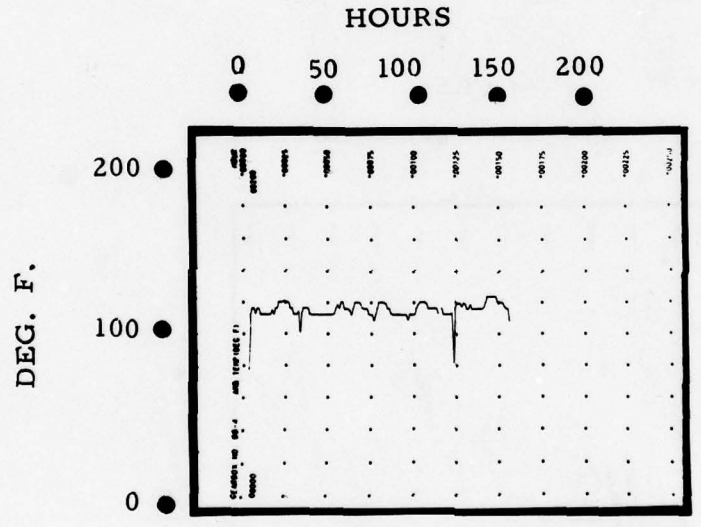

(A) AMBIENT TEMPERATURE

Figure 26. Gearbox BB-4; Oil and Ambient Temperature vs. Test Time.

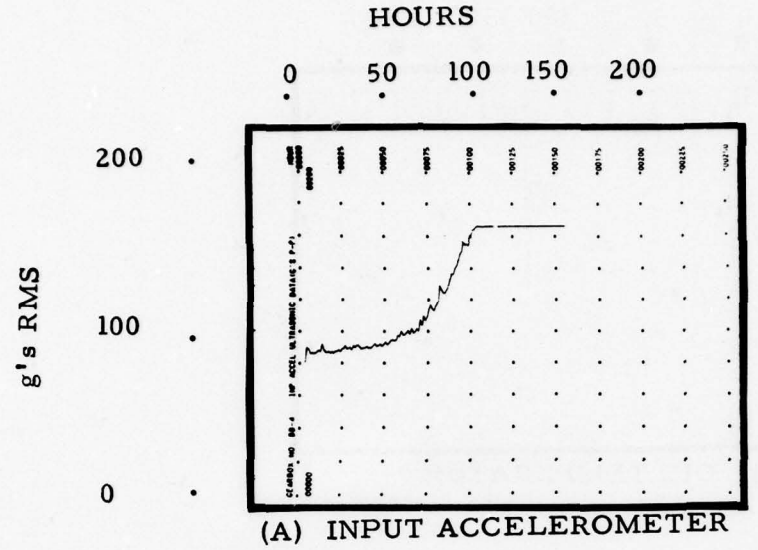

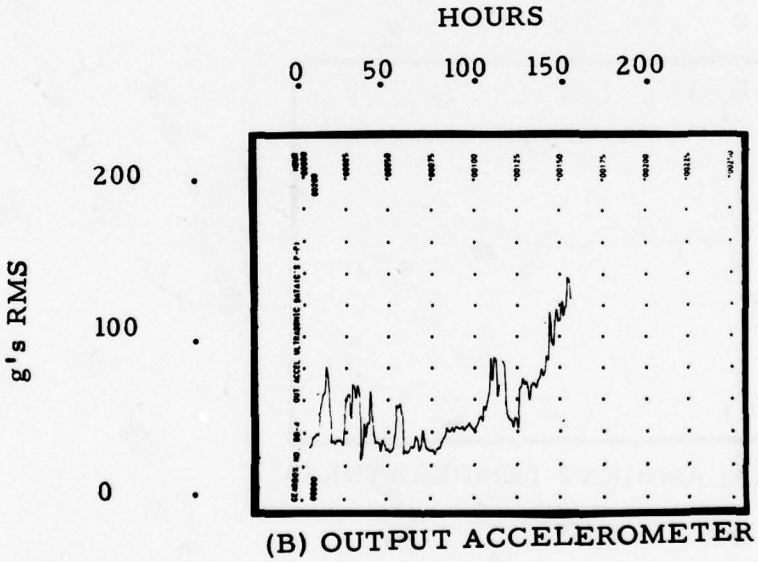

Figure 27. Gearbox BB-4; Ultrasonic RMS Data.

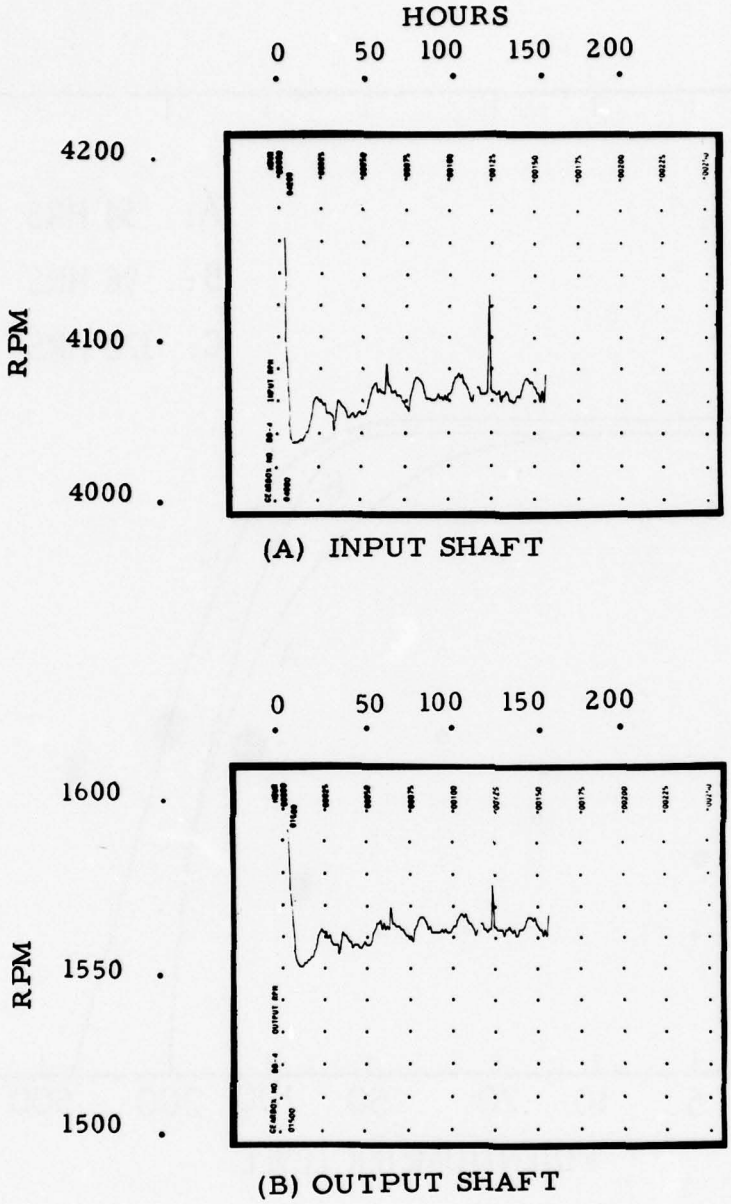

Figure 28. Gearbox BB-4; RPM vs. Test Time.

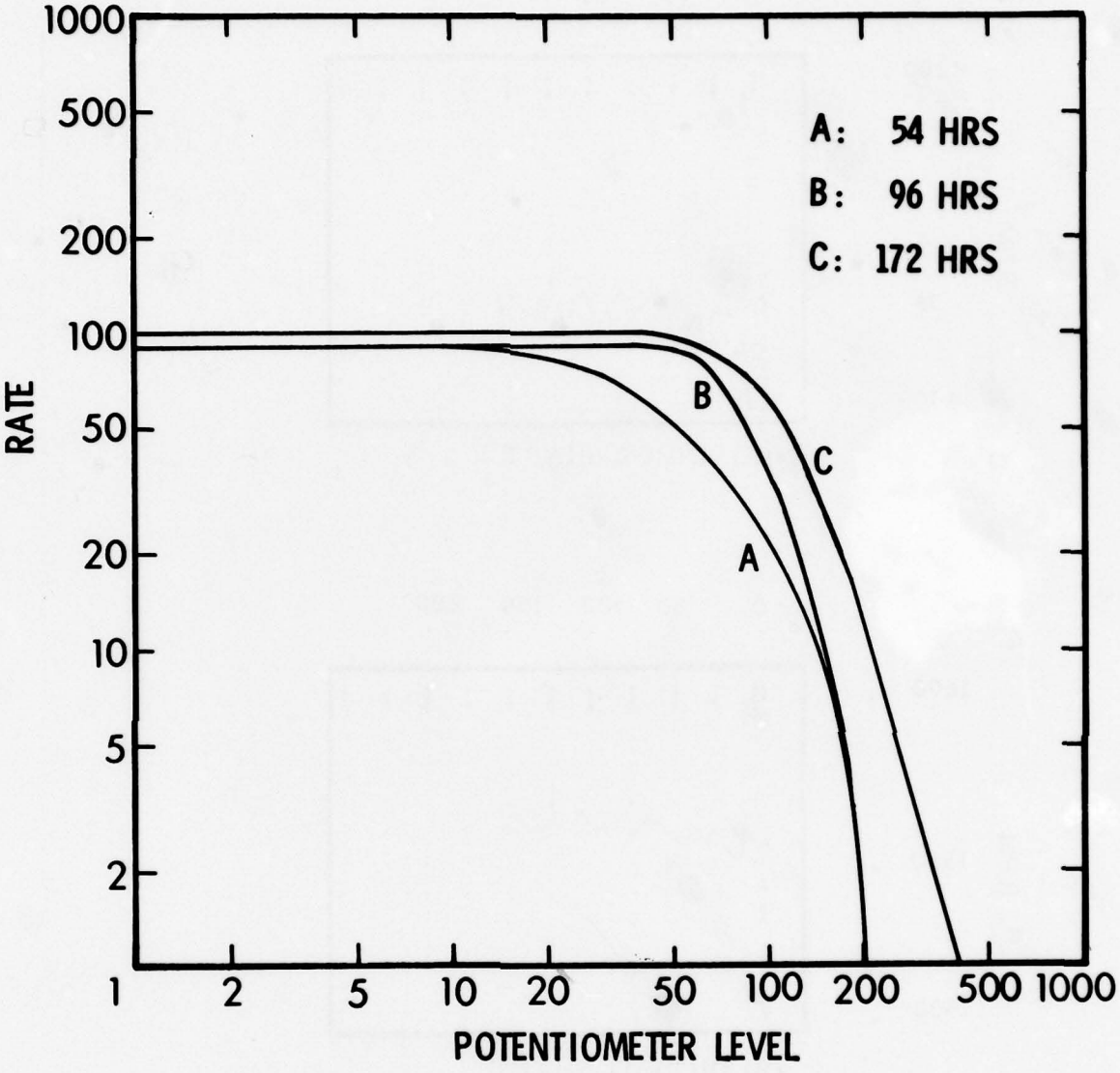

Figure 29. Gearbox BB-4; Shock Profile Curves, Input Accelerometer.

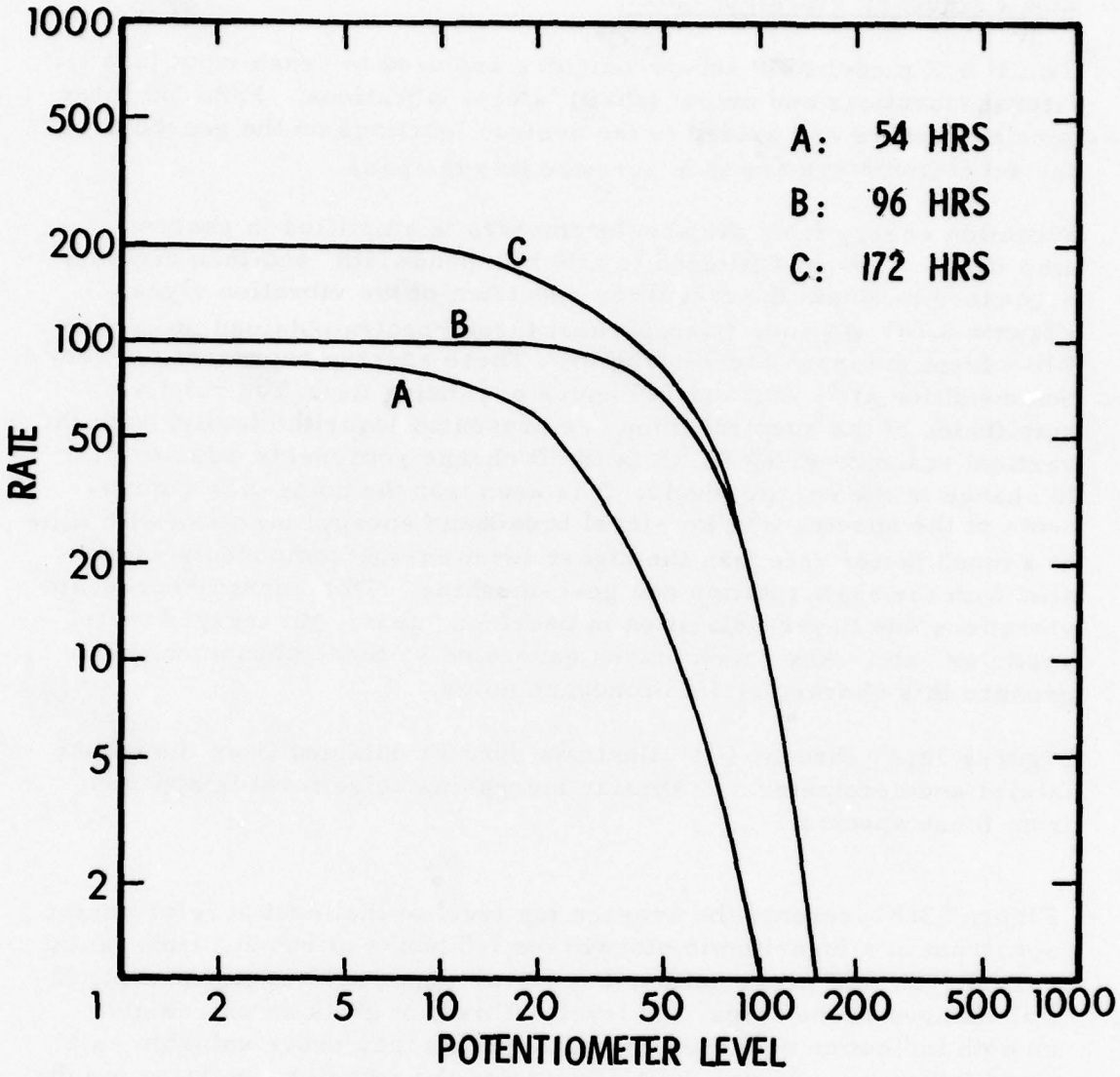

Figure 30. Gearbox BB-4; Shock Profile Curves, Output Accelerometer.

Low Frequency Vibration Data

Two B & K model 4300 accelerometers are used to sense input (shaft) lateral vibrations and output (shaft) lateral vibrations. Pads for these accelerometers are welded to the desired locations on the gearbox, and the accelerometers are then screwed into the pads.

Vibration energy from the accelerometers is amplified in charge amplifiers low-pass filtered to a 10 kHz bandwidth and then digitally processed to obtain the frequency spectrum of the vibration signal. Figures 31(A) through (C) represent three spectra obtained on gearbox BB-4 from the input accelerometer. These spectra represent the gearbox condition at 7, 40, and 140 hours of running time. The relative amplitudes of the spectral lines are presented logarithmically, with the vertical scale covering 80 dB (a 10-dB change represents a factor of 10 change in the energy level). It is seen that the noise-like components of the spectra (the low-level broadband energy) increase with time at a much faster rate than the higher level energy components associated with the shaft rotation and gear-meshing. This energy represents vibrations due to irregularities in bearings, gears, disengaged metal particles, etc. Any shock pulses generated by these phenomena will produce this characteristic broadband noise.

Figures 32(A) through (C) illustrate spectra obtained from the output lateral accelerometer. A similar increasing noise level is apparent from these spectra.

Figure 33(A) presents the average log level of the input accelerometer spectrum in a logarithmic plot versus 148 hours of running time (solid curve). On this presentation, any linear segments represent exponential changes in the actual "g" level. This plot gives an extremely smooth indication of increasing activity that may prove valuable as a trend indicator. Figure 33(B) illustrates the same presentation for the output accelerometer.

Figures 33(A) and (B) also present the average spectral level for both input and output accelerometers over 152 hours of running time (dashed curve). This is a possible trend indicator, as the energy level as well as the rate is increasing in a quasi-exponential fashion.

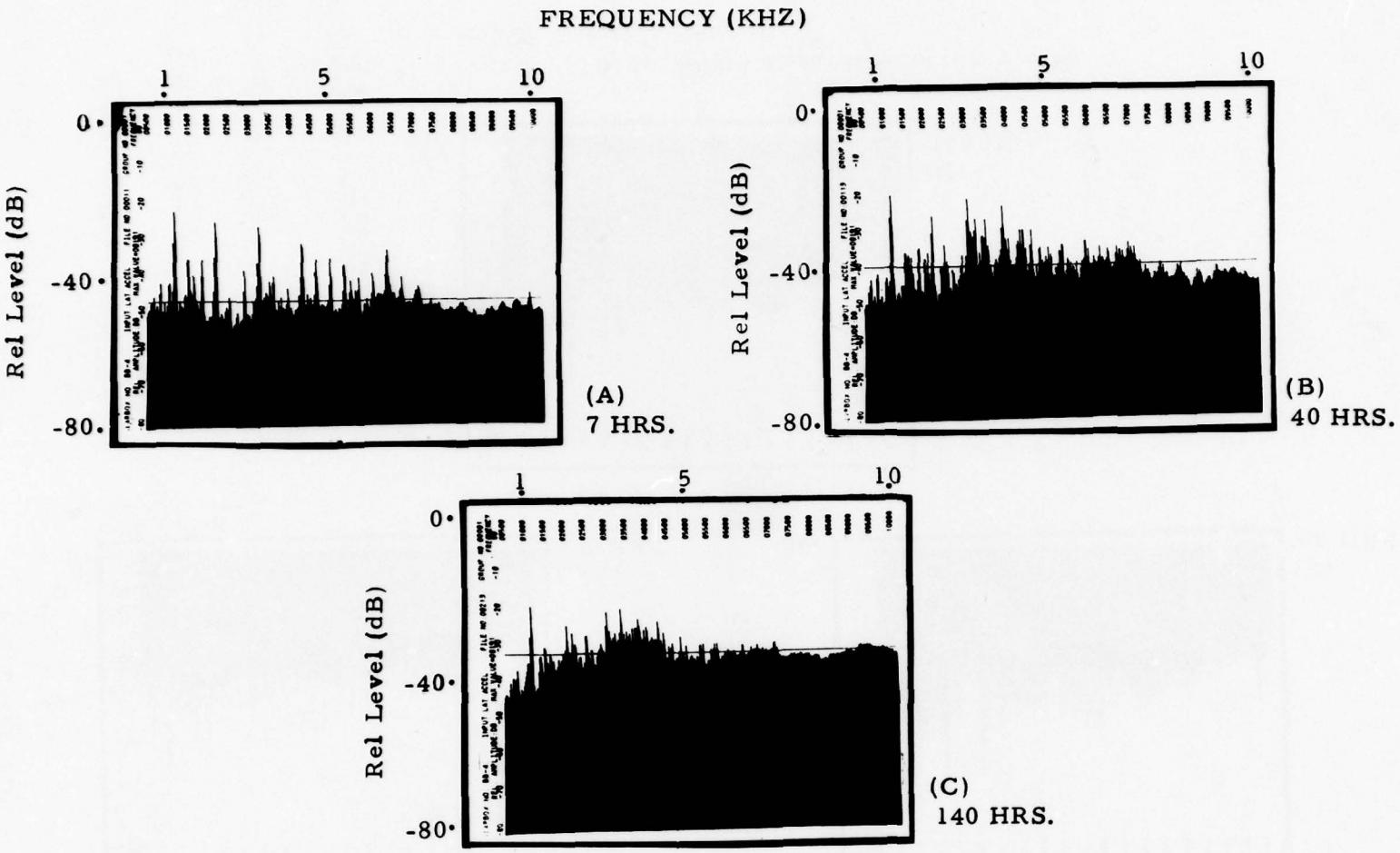

Figure 31. Gearbox BB-4; Input Lateral Accelerometer Power Spectral Density.

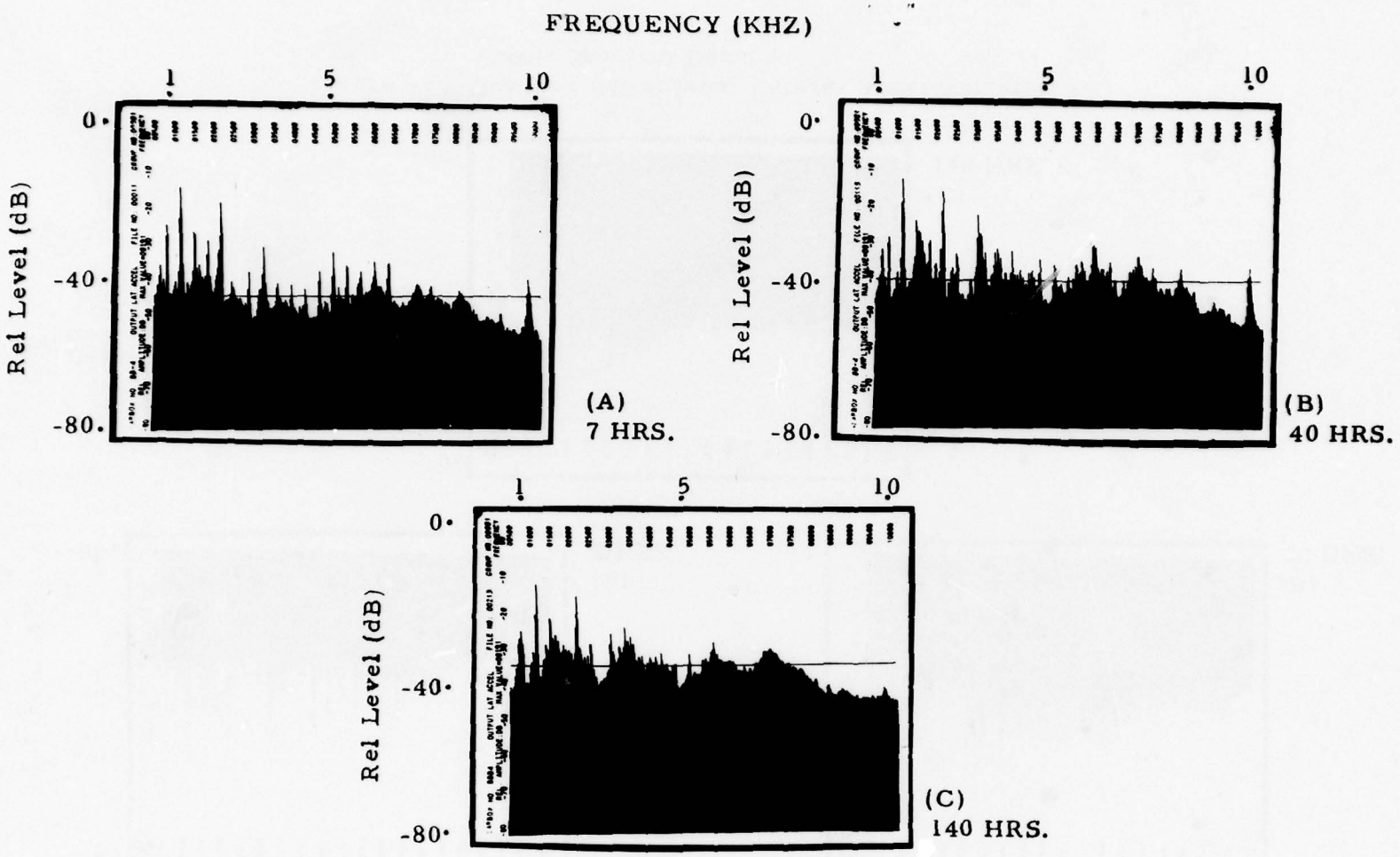

Figure 32. Gearbox BB-4; Output Lateral Accelerometer Power Spectral Density.

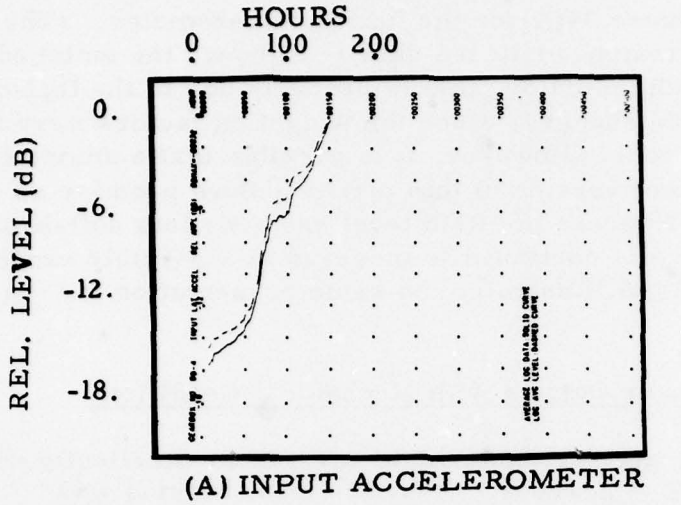

(A) INPUT ACCELEROMETER

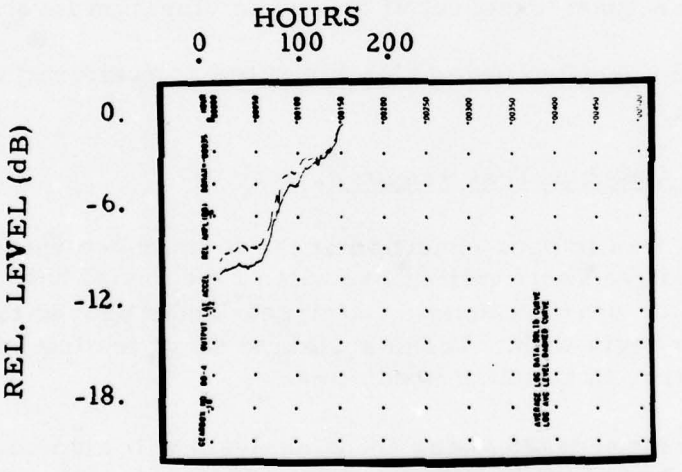

(B) OUTPUT ACCELEROMETER

Figure 33. Gearbox BB-4: Geometric Mean and Arithmetic Mean Data.

A comparison of the RMS levels with and without matched filtering is presented in Figure 34(A) for the input accelerometer. (The solid curve represents matched-filtered data.) Although the matched-filter plot is not a smooth indicator, this is probably due to the fact that it is sensitive to RPM changes, since the weighting factors were for initial RPM conditions. However, it is possible that a smoothed (or an RPM-normalized) version of this plot will show promise as a trend indicator. Whereas the RMS level has gone into soft-limiting, the matched-filter plot continues to increase in a possible exponential fashion. Figure 34(B) illustrates the same presentation for the output accelerometer.

Correlation of Sensor Outputs with Mechanical Condition

The low frequency accelerometer data correlated excellently with the condition of the BB-4 gearbox. Since the input bearing was causing the major failure condition, it would be expected that the input accelerometer data would indicate a more predominant trend. This was the case, as can be seen by reviewing the plots. Both accelerometers indicated a quasi-exponential growth in vibration level.

The shock emission profile curves also indicated a deteriorating gearbox condition.

Summary of BB-4 Gearbox Test Results

The BB-4 gearbox was in poor condition at the commencement of testing. Therefore, its relative short testing life will prove useful only when correlated with later gearbox tests. Later gearboxes proved to be in better condition to begin with. These sustained more testing hours and gave more credibility to trending predictions.

The four indicators discussed under trend analysis will also be applied to succeeding gearboxes in an attempt to establish correlation between any or all of these indicators and gearbox mechanical condition.

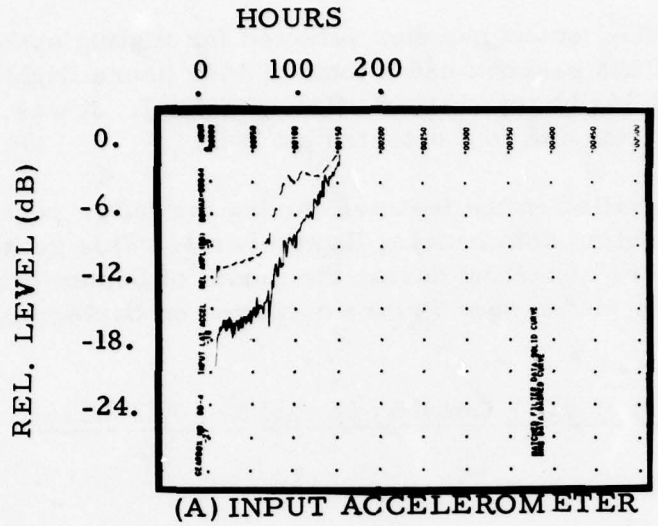

(A) INPUT ACCELEROMETER

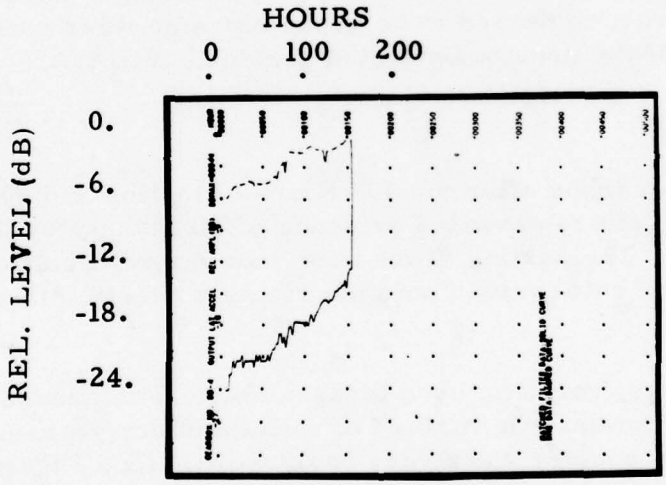

(B) OUTPUT ACCELEROMETER

Figure 34. Gearbox BB-4; Matched Filter and RMS Data.

BB-5 GEARBOX TESTS

Gearbox BB-5 was the second gearbox selected for testing under the present contract. This gearbox had a total of 1405 hours flight service since new and 342 hours since its first overhaul. It was removed from operation due to a detected oil leak.

The gearbox was installed in the test cell during the latter portion of August 1976, with testing commencing September 1. This gearbox accumulated 437 hours of testing during the month of September before a catastrophic pinion gear failure occurred on September 27, 1976.

Mechanical Condition of BB-5 Gearbox (Serial No. A13-2236)

Pre-Test Inspection

The preliminary bearing inspection revealed that the general condition of the reference bearings was poor. All bearings had sustained moderate to heavy wear and some electrical current damage. None of the bearings, however, appeared to be in the extreme wear condition exhibited by those of the previously tested gearbox, BB-4.

Post-Test Inspection

Examination of the gearbox after the 437 hours of testing and subsequent pinion gear failure revealed evidence of oil leakage at the input shaft oil seal. The parting of the case was very difficult because the pinion teeth were cold-welded onto the ring gear teeth. (See Figure 35.)

The input coupler was frozen up upon disassembly. The grease was dried and turned to powder - a mixture of metal and dry grease. The teeth in the sprocket coupler were very badly worn. (See Figure 36.)

When pulling the complete pinion assembly out of the case, the O-ring seal appeared to be vulcanized to the outer case. The No. 1 bearing fell apart due to bad balls. The No. 2 bearing did not fall apart, but everything was darkened and blue from heat. The nut on the end of the pinion shaft was loose, even though the safety washer was still intact. The pinion gear teeth were completely gone. (See Figure 37 showing pinion assembly removed and Figure 38 showing housing with gear assemblies removed.)

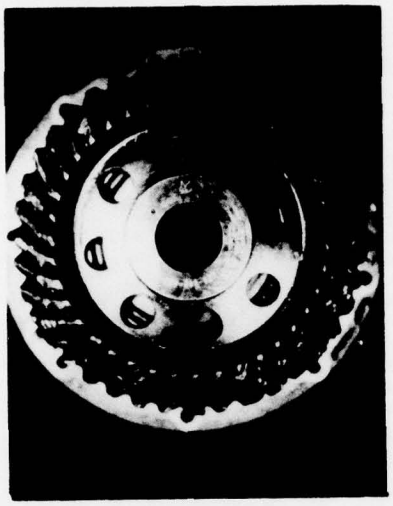

Figure 35. Gearbox BB-5; Pinion Teeth Cold-Welded to Ring Gear Teeth.

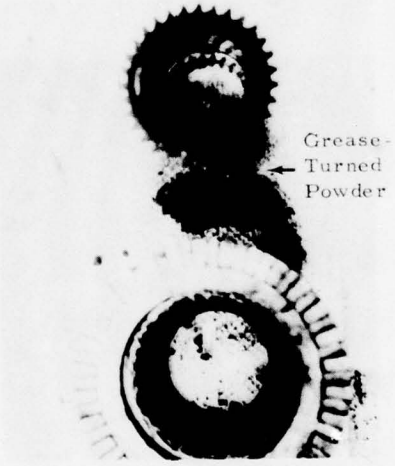

Figure 36. Gearbox BB-5; Input Coupler.

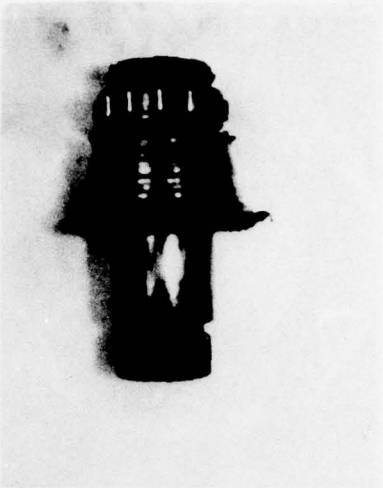

Figure 37. Gearbox BB-5; Toothless Pinion Gear.

Figure 38. Gearbox BB-5; Housing With Gear Assemblies Removed.

All the seals around the input shaft appeared good, but upon removal of the gearbox from the test fixture, signs of oil seepage were visible.

The output bearings and the remainder of the assembly, with the exception of the ring gear, looked good. The ring gear safety wire was missing.

The bearing inspection report indicated that the input shaft bearings were in an extreme wear condition. They had been listed in moderate wear condition prior to testing. At the end of testing, the noise level of the No. 1 bearing had risen from 6.5 to 27.5 dB. The No. 2 bearing noise level had risen from 5 to 13.5 dB. The inner raceway wear depth increase was especially noticeable on the No. 1 bearing. It increased from 35 to 9500 microinches during the testing period. Gearbox BB-4 had also exhibited this exaggerated racewear on bearing No. 1. The bearing No. 1 races were described as "failed".

The selected balls from bearings No. 2 and No. 4 actually appeared to be in better shape after test. The same may be said for the roller bearing selected from bearing assembly No. 5. Bearing No. 3 appeared to be damaged both before and after test. It must be kept in mind that the photographs display the condition of only one ball or roller from each bearing before and after test, and may not correlate exactly with the overall bearing condition data . In the post-test bearing inspection report, bearing No. 5 raceway was described as "failed" and the rollers described as "similar to raceways; very heavy wear and denting."

Spectrometric Oil Analysis (SOA)

Eighteen oil samples were taken from the BB-5 gearbox during the 437-hour testing period. The SOA data is summarized in Figure 39. This data, as in the case of gearbox BB-4, indicates the presence of a high concentration of iron in the oil before the first oil change. The rapid rise in iron content after 350 hours of testing is evidence of the pinion gear wear that eventually resulted in culmination of the testing. The increase in copper and cadmium content also indicates bearing and bearing cage wear. For reference, oil sample times are shown graphically in Figure 40.

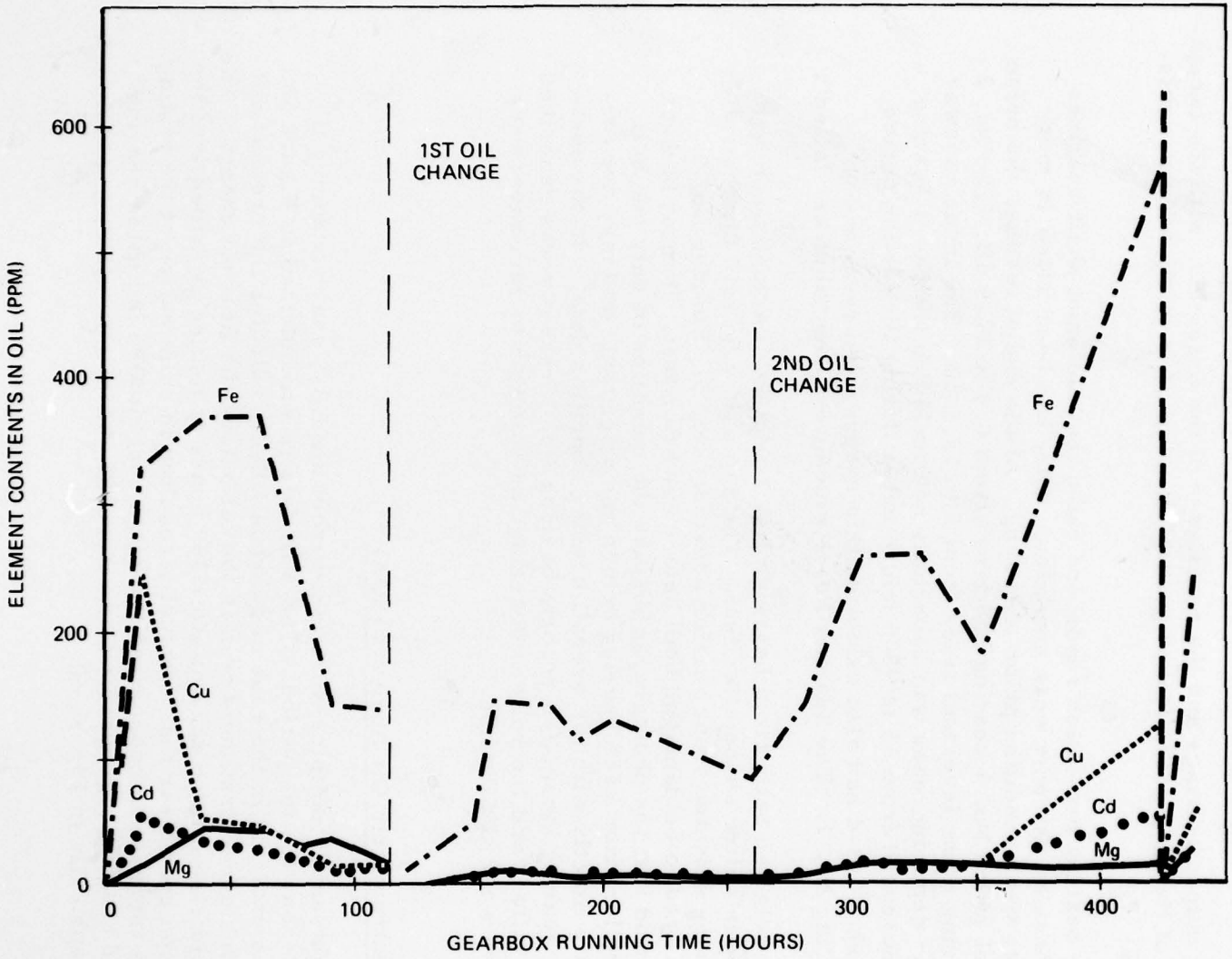

Figure 39. Spectrometric Oil Analysis - Gearbox BB-5.

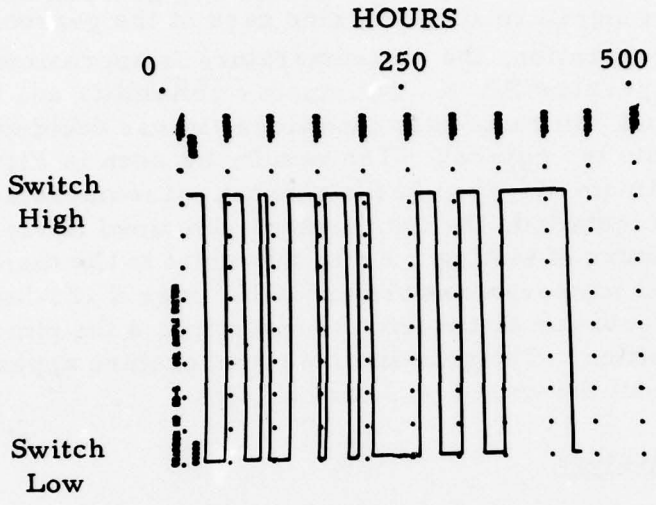

Figure 40. Gearbox BB-5; Oil Samples and Change Times.

Temperature Sensors

Figures 41 (A) and (B) present graphical displays of the temperature readings recorded from the two sensors monitoring gearbox oil temperature and ambient temperature at the outside case of the gearbox. During the first 50 hours of operation, the oil temperature is approximately the same as that for gearbox BB-4. To improve reliability and to more closely simulate actual environmental conditions, it was decided to direct an air blower onto the gearbox. The result, as seen in Figure 41 (A), was an approximate 30° drop in the gearbox oil temperature. After the blower was installed, the temperature remained fairly steady during the next 250 hours of testing. From this point to the termination of testing, the oil temperature rose about 10° over a 125-hour span. This was no doubt due to the friction mounting as the pinion gear began wearing and galling. The gearbox case temperature appeared fairly steady throughout the entire test period.

RPM and Torque Indicators

Figures 42(A) and (B) present input and output RPM data for the full 437 hours of testing of gearbox BB-5. As can be seen, RPM remained steady on both input and output shafts during the full test period. This implies that teeth engagement remained intact throughout this period, even though accelerated wear was taking place.

Figure 43 presents three displays: (A) input shaft torque, (B) output shaft torque, and (C) gearbox efficiency. The latter calculates the ratio of output horsepower to input horsepower based on the equation

$$\text{Efficiency} = \frac{(\text{Output RPM})}{(\text{Input RPM})} \times \frac{(\text{Output Torque})}{(\text{Input Torque})} \qquad (4)$$

Since the variations in RPM are minimal (see Figure 42), the efficiency is determined mainly by the torque ratios. The efficiency averages about 94 percent until the 190th hour of testing, and then rises abruptly to 97 percent and stays in that neighborhood for about 35 hours. A corresponding drop in input torque can be seen during this time. Possibly, a frictional loading on the input shaft of the gearbox was relieved at hour 190. At hour 225 the input torque again rose abruptly for another 35 hours. At hour 260 it dropped for approximately 50 hours. During this whole time, output torque remained fairly steady. At 310 hours, both input and output torque rose in synchronism, indicating an increased loading on the output shaft.

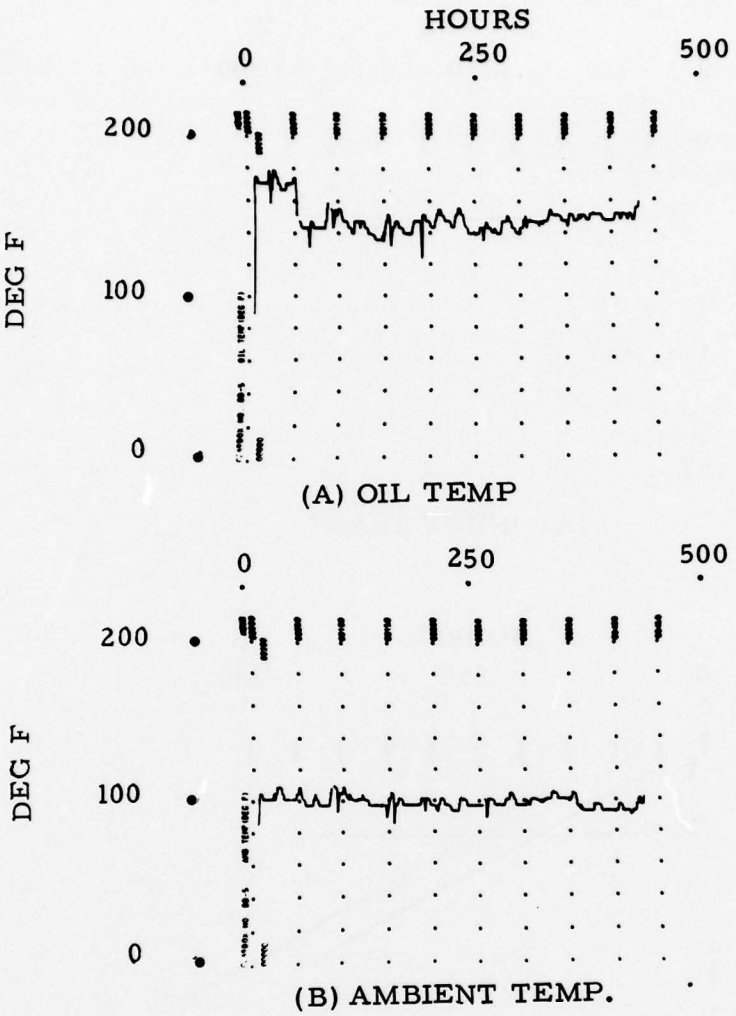

Figure 41. Gearbox BB-5; Oil and Ambient Temperature vs. Test Time.

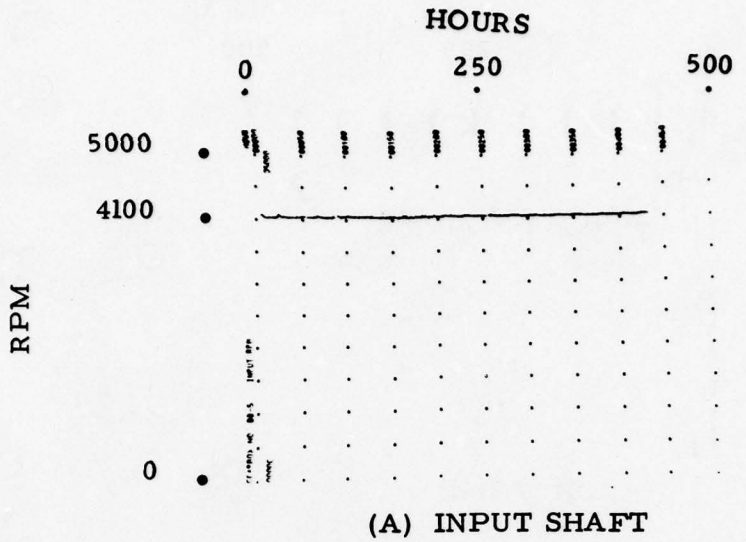

(A) INPUT SHAFT

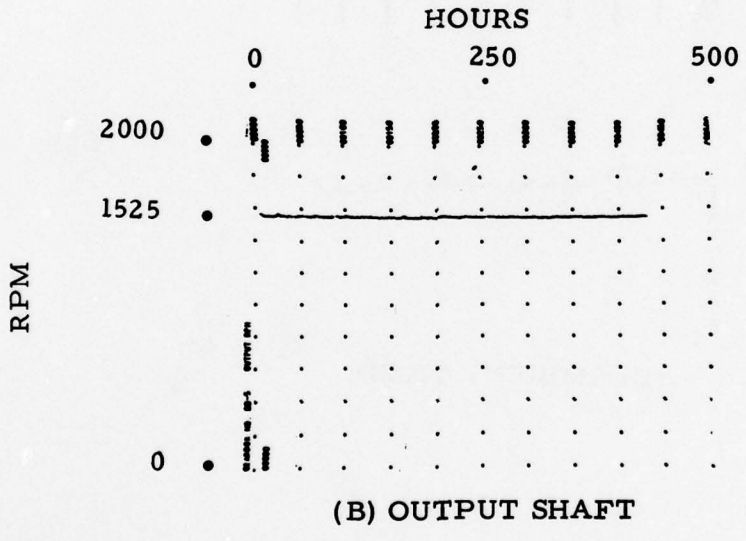

(B) OUTPUT SHAFT

Figure 42. Gearbox BB-5; Input and Output RPM vs. Test Time. .

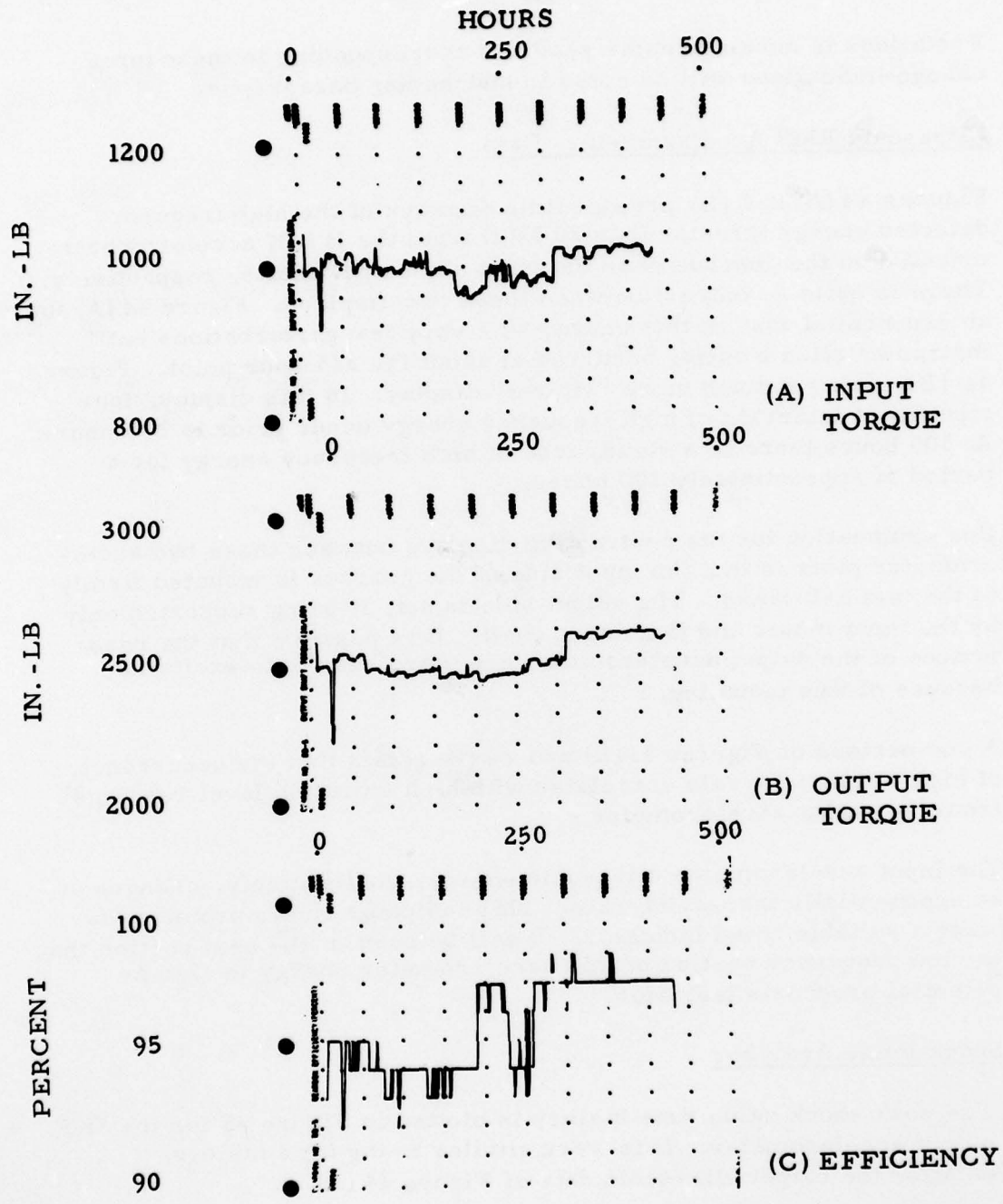

Figure 43. Gearbox BB-5; Torque and Gearbox Efficiency.

Variations in accelerometer readings corresponding to these torque-change indications will be noted in succeeding paragraphs.

Ultrasonic RMS Accelerometer Data

Figures 44 (A) and (B) present time displays of the high frequency detected energy (greater than 20 kHz) from the B & K accelerometers mounted on the gearbox near the input and output shafts, respectively. There is quite a contrast between these two displays. Figure 44 (A) shows an exponential rise in this energy with very few perturbations until instrumentation limiting occurred at about the 315-hour point. Figure 44 (B) shows a much more "violent" display. In this display, four significant intervals of high frequency energy occur prior to 300 hours. At 300 hours there is a steady rise of high frequency energy for a period of approximately 100 hours.

One explanation for the contrasting displays between these two accelerometer plots is that the input side of the gearbox is mounted firmly to the test cell stand. The output side is not, it being supported only by the input mount and the output shaft. It is possible that the resonances of the output accelerometer are more subject to excitation because of this mounting.

A comparison of Figures 43 (B) and 44 (B) shows that the occurrence of high torque intervals correlates with high vibration level readings from the output accelerometer.

The input accelerometer ultrasonic energy, contrastingly, changes at an exponentially increasing rate. This indicator shows promise of being a suitable trend indicator. It will be seen in the next section that the low frequency portion of this accelerometer energy is also a potential prognosis indicator.

Shock Pulse Analyzer

The peak shock value time history is plotted in Figure 45 for the SKF output accelerometer. It is very similar to the time history data for the output ultrasonic data of Figure 44 (B).

Shock profile curves for both input and output shock accelerometers are illustrated in Figures 46 and 47. The monotonic deteriorating condition is very evident from the input profiles of Figure 46. The output profiles in Figure 47 reflect the erratic nature of the other BB-5 output data.

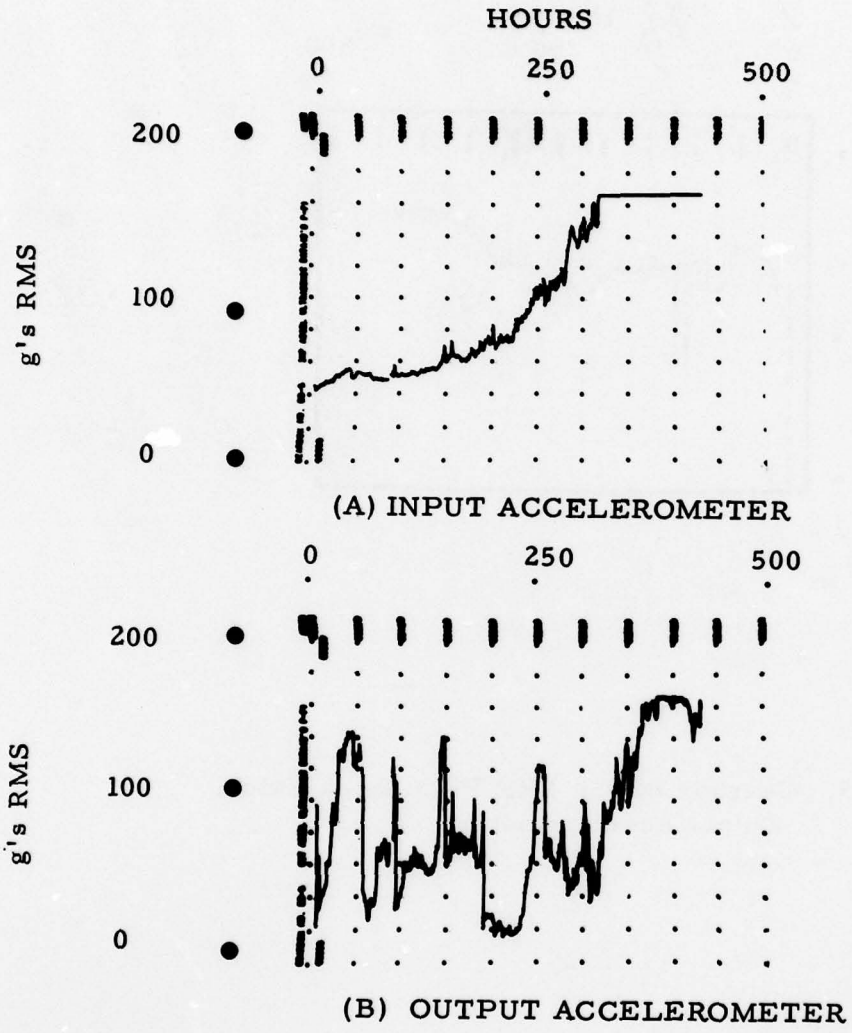

Figure 44. Gearbox BB-5; Ultrasonic RMS Data.

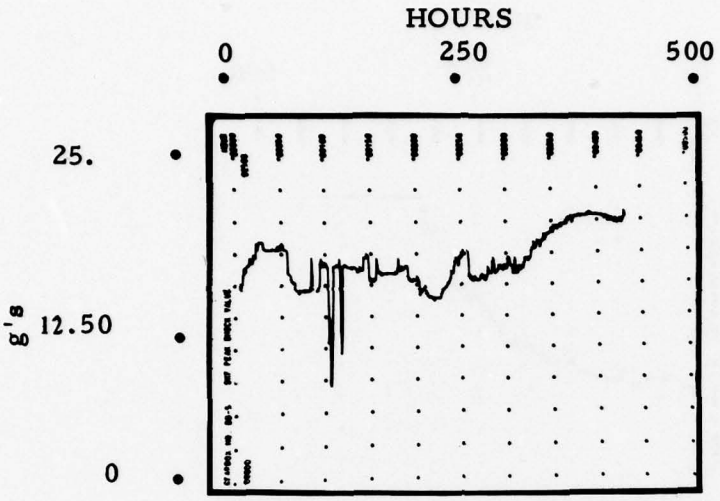

Figure 45. Gearbox BB-5; SKF Peak Shock Value, Output Accelerometer .

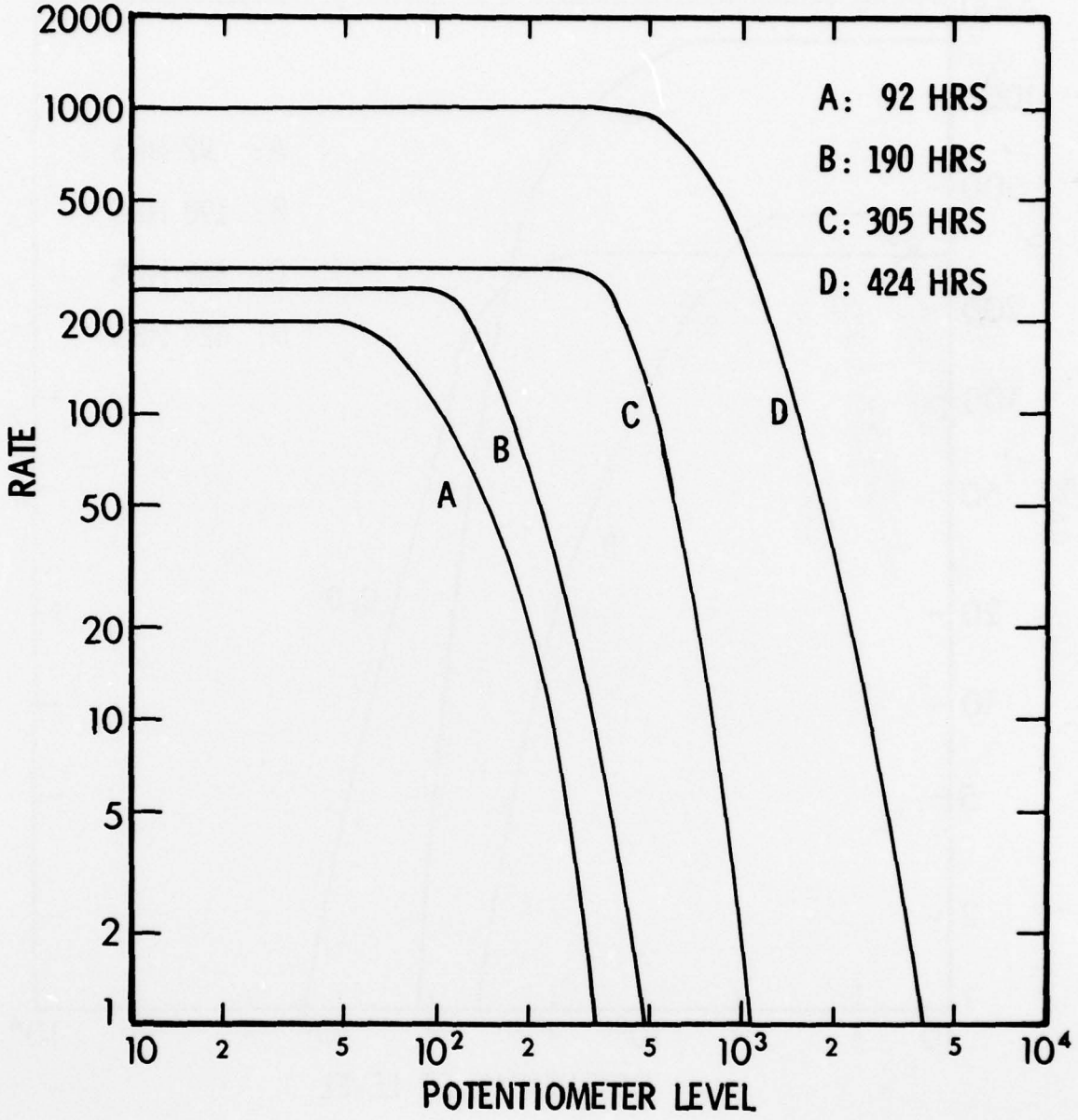

Figure 46. Gearbox BB-5; Shock Profile Curves, Input Accelerometer.

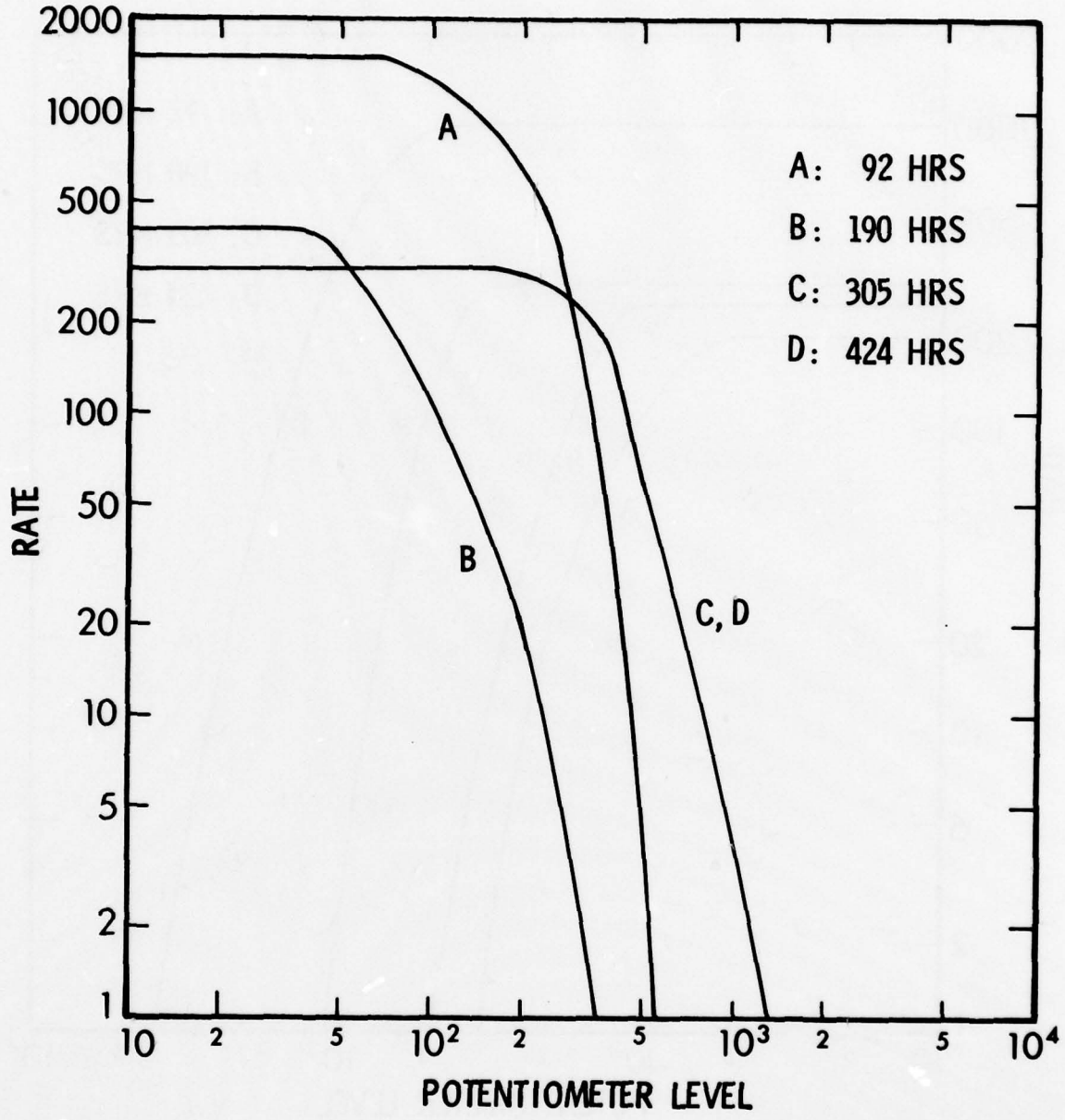

Figure 47. Gearbox BB-5; Shock Profile Curves, Output Accelerometer.

Low Frequency Vibration Data Time Analysis

Four unique representations of the data obtained from input and output accelerometers were presented in the section for gearbox BB-4. These will be presented in all gearbox test sections. In order to better compare the four representations, their relative levels are all displayed logarithmically versus time.

Figure 48 (A) presents the RMS level from the input lateral accelerometer as a dashed curve and the corresponding matched filter data as a solid curve. The vertical scale is 3 dB per division and the horizontal scale is 50 hours per division. Note that the total change in RMS level over 420 hours is approximately 10 dB. The dynamic range of the matched filter display is about 25 dB. At about 310 hours, both curves accelerate their amplitude rise until, at 330 hours, a reversal in the trend occurs. Referring to the input torque curve of Figure 43 (A) it is seen that the step change in torque loading occurred at 310 hours. Apparently at 330 hours, whatever was causing the extreme vibration freed itself. This reversal phenomenon had been observed during the previous contract, and the reversal point may be considered (for all practical purposes) the point of failure.

Figure 48 (B) presents two curves: (1) the solid curve represents the average of all the logarithmic values of the 512 spectral lines in the 10 kHz bandwidth (geometric mean); (2) the dashed curve represents the average of all the absolute values of the spectral lines (arithmetic mean) presented in a logarithmic display. Note that there are only small differences between these two plots. The dashed curve is slightly more influenced by the stronger vibration components corresponding to gear-mesh frequencies. Note the correlation between these curves and the matched filter curve of Figure 48 (A). The pedestal-type discontinuities appearing on the geometric and arithmetic mean curves of Figure 48 (A) appear to have a relationship to the input torque curve of Figure 43 (A). Note the dip in torque on the input shaft during this period. Also, as described in the section on torque, the output torque did not take a corresponding dip at the beginning of the period. These curves appear to be excellent detectors of abnormalities, as well as trend indicators. Observe that the RMS level does not give signs of the pedestal discontinuity at about 200 hours.

Figure 49 (A) presents RMS data (dashed curve) and matched filter data (solid curve) for the output accelerometer. Similarly, Figure 49 (B) presents geometric mean (solid curve) and arithmetic mean data (dashed curve) for the output accelerometer. After 250 hours of running time,

AD-A073 553 NORTHROP RESEARCH AND TECHNOLOGY CENTER PALOS VERDES --ETC F/G 1/3
INVESTIGATION OF ADVANCED PROGNOSTIC ANALYSI S TECHNIQUES.(U)
JUN 79 R C GROVE DAAJ02-77-C-0054
UNCLASSIFIED NRTC78-47R USARTL-TR-79-10 NL

2 OF 3
AD A073563

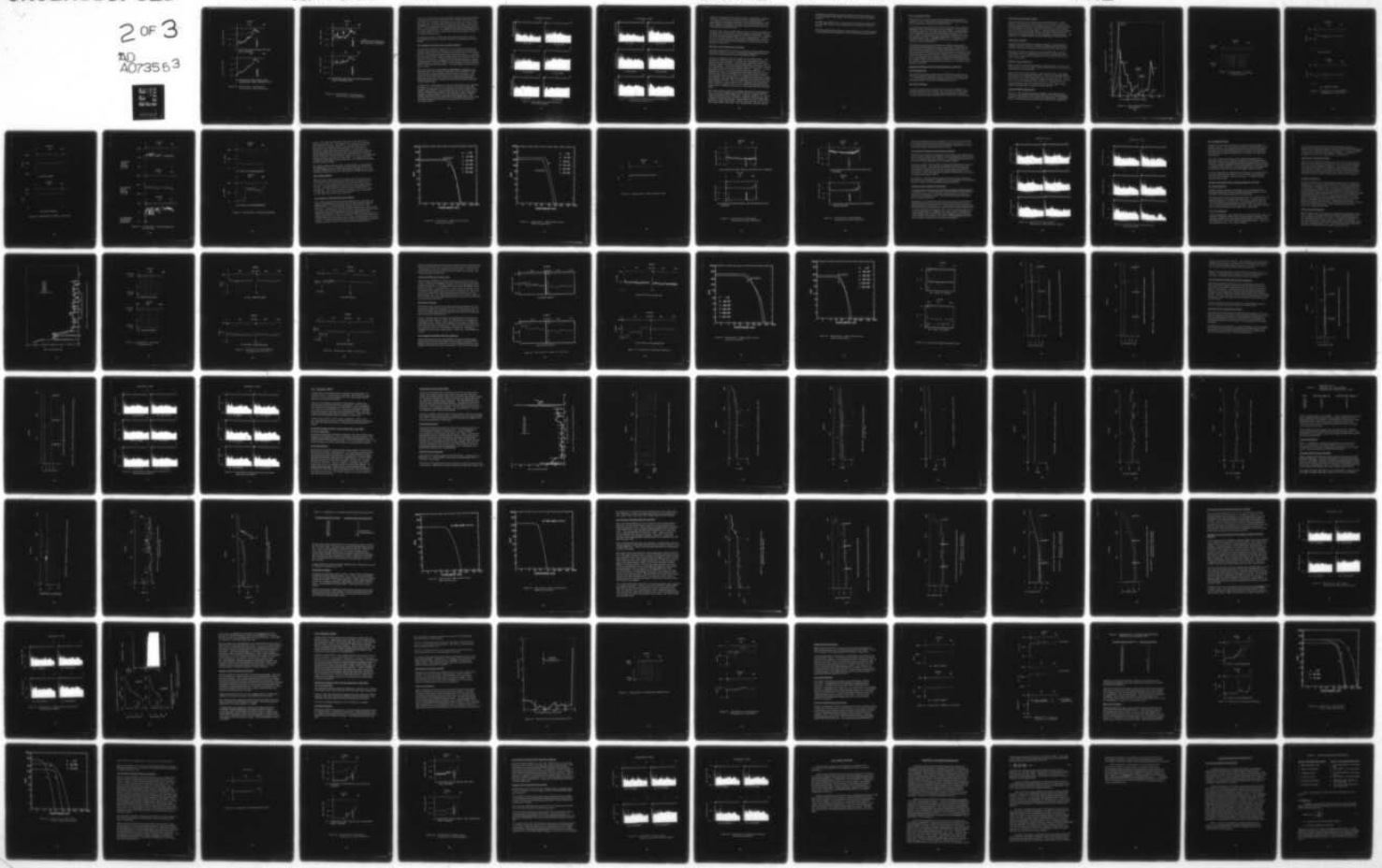

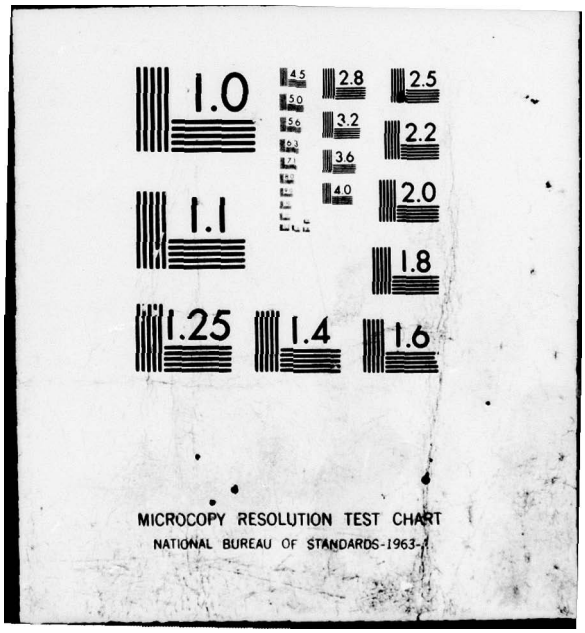
1.0
1.1
1.25
1.4
1.6
1.8
2.0
2.2
2.5
2.8
3.2
3.6
4.0
4.5
5.0
5.6
MICROCOPY RESOLUTION TEST CHART
NATIONAL BUREAU OF STANDARDS-1963-A

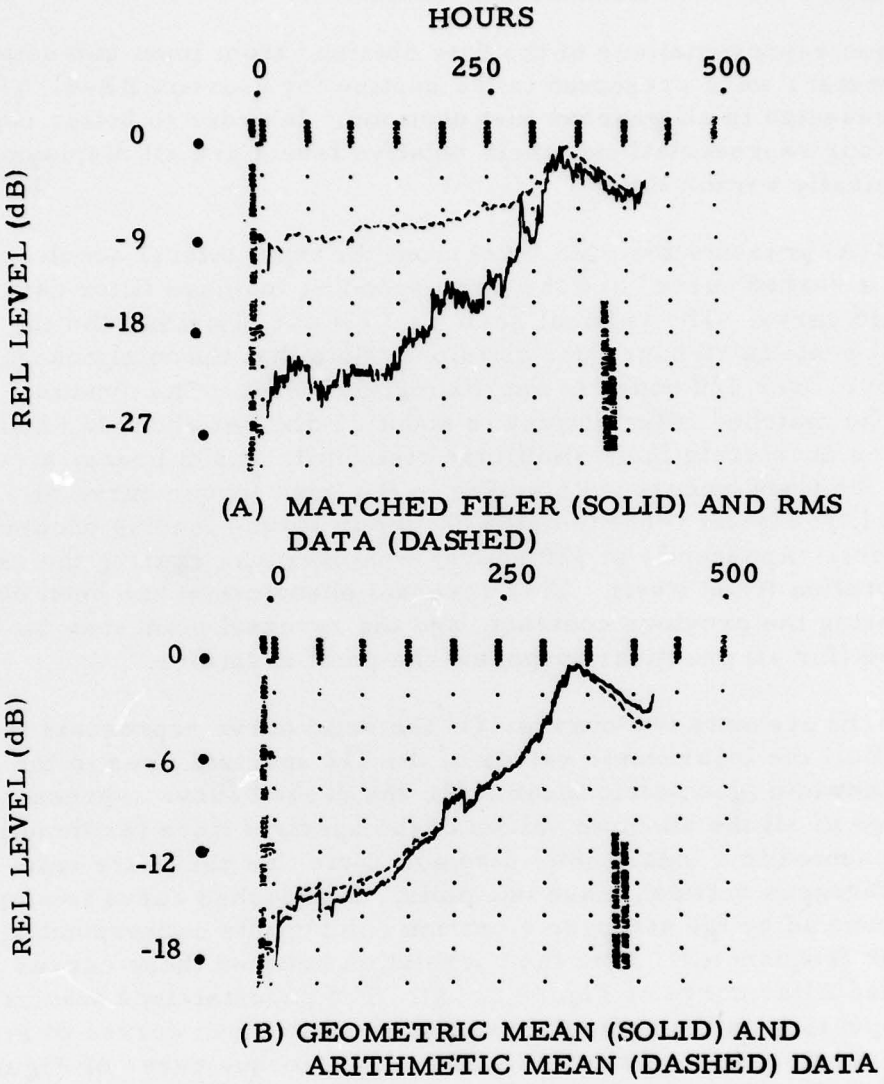

Figure 48. Gearbox BB-5; Input Lateral Accelerometer Trend Parameters.

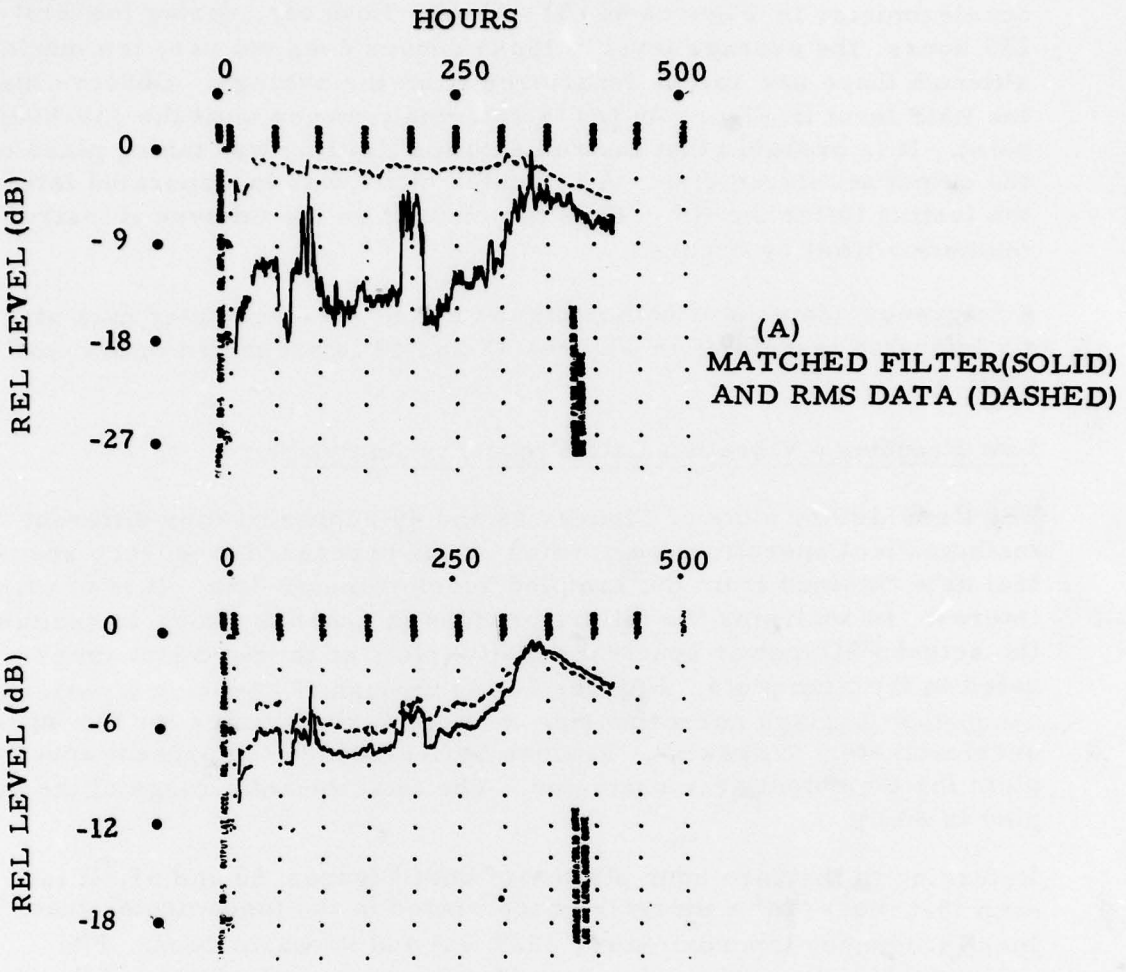

Figure 49. Gearbox BB-5; Output Lateral Accelerometer Trend Parameters.

these curves follow very closely the same trend as those for the input accelerometer in Figures 48 (A) and (B). However, during the first 250 hours the average level of these curves does not vary too much, although there are abrupt departures from the average. Observe that the RMS level in Figure 49 (A) is extremely steady until the 330-hour point. It is probable that instrumentation limiting was taking place on the output accelerometer. A computer check was incorporated later in the testing (after the HT-5 test) to print out on the teletype if instrumentation limiting occurs.

A frequency analysis of both input and output accelerometer data at six indicated test times in Figures 48 and 49 is presented in the next section.

Low Frequency Vibration Data Frequency Analysis

The time history plots of Figures 48 and 49 represent four different mathematical operations performed on the processed frequency spectral data obtained from the sampled accelerometer data. It is of prime interest in analyzing the failure process in gearbox BB-5 to examine the actual PSD (power spectral density) plots at the pertinent times indicated in the time plots. Figures 50 (A) through (F) present a series of frequency displays corresponding to these various times for the input accelerometer. Likewise, Figures 51 (A) through (F) present spectral plots for the output accelerometer. The total dynamic range of the display is 80 dB.

Referring to the zero hour plots (A) of both Figures 50 and 51, it is seen that most of the energy is concentrated in the fundamental gear-mesh frequency (approximately 1025 Hz) and its harmonics. The solid line across each of the plots is a computer calculation of the geometric mean of the 500 spectral lines comprising the display. Note that the geometric mean lies very close to the dense noise floor of each spectral plot.

At 250 hours, considerably more discrete spectral lines are observed on Figure 50 (C) as well as an increase in the dense noise-like energy around 5000 Hz. It is possible that an uneven rotation of the shafts is taking place, caused by bearing wear or gear tooth wear or damage. Uneven rotation will cause sidebands to form around the fundamental and harmonics of the gear-mesh frequencies. This frequency effect becomes exaggerated at the higher frequencies, since the absolute frequency deviation is proportional to the particular harmonic number.

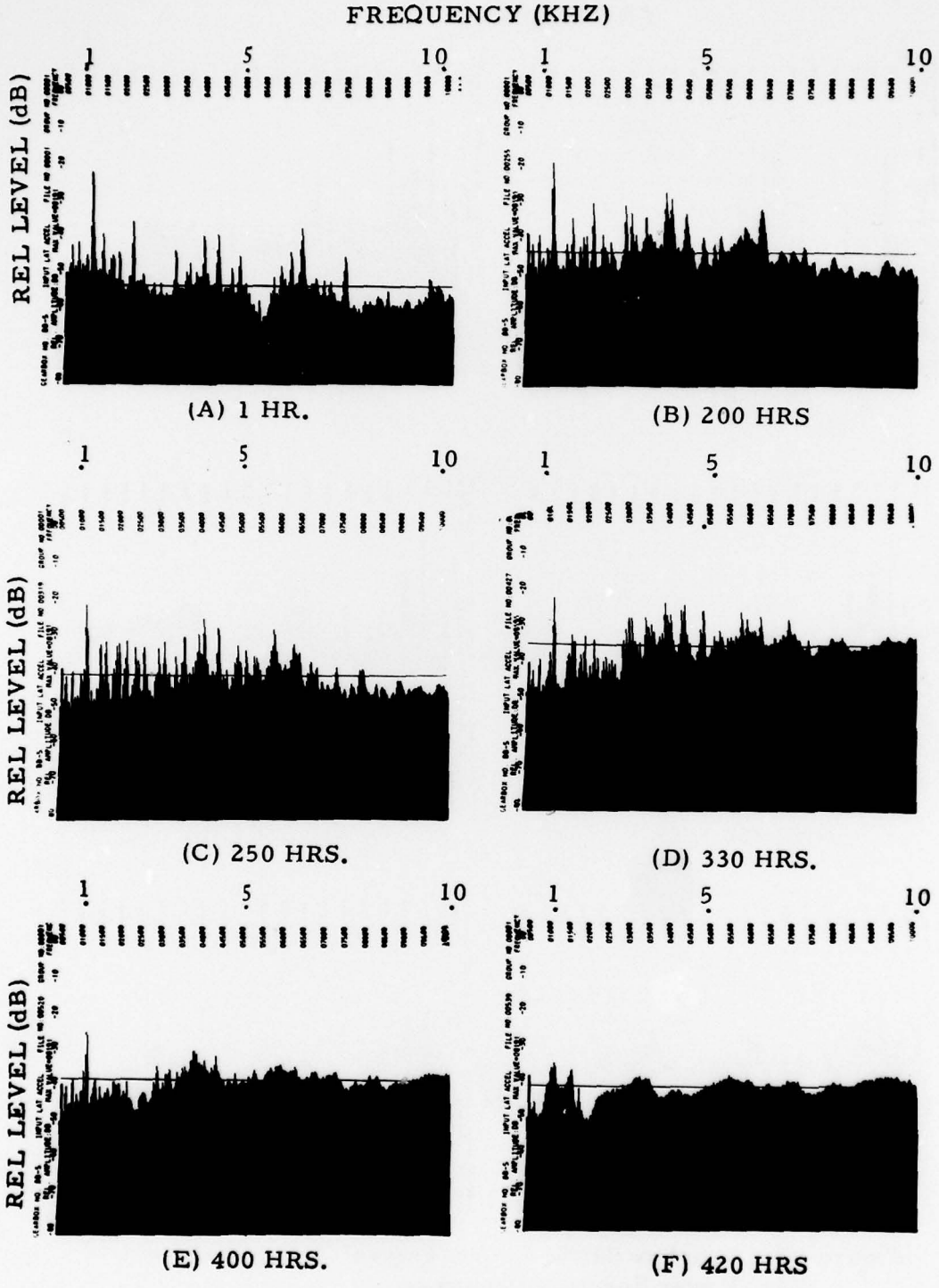

Figure 50. Gearbox BB-5; Input Lateral Accelerometer Power Spectral Densities.

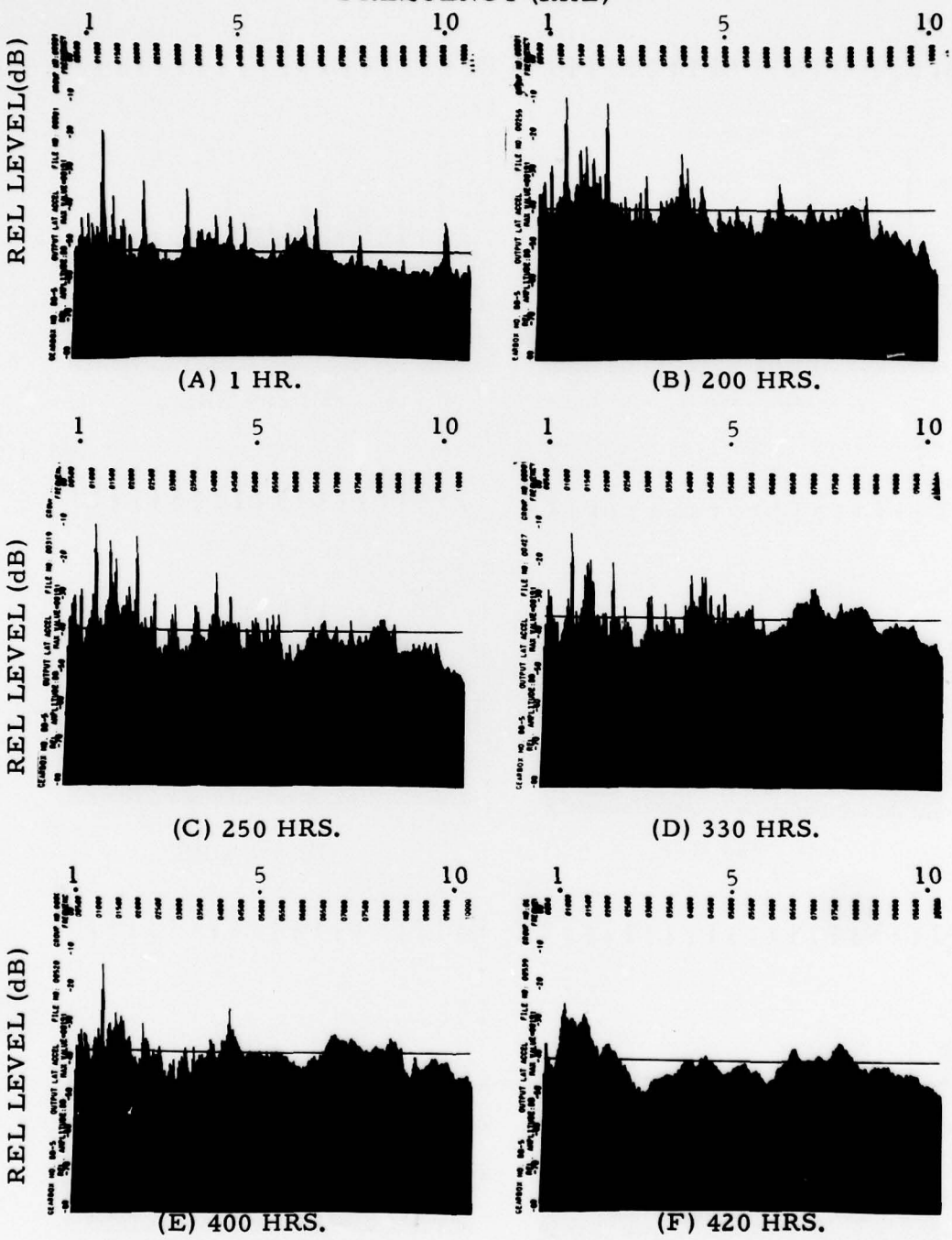

Figure 51. Gearbox BB-5; Output Lateral Accelerometer Power Spectral Densities.

Figures 51 (B) and (C) at 200 and 250 hours, respectively, indicate a very high second harmonic content, possibly indicating that an asymmetrical limiting is taking place in the instrumentation. Very little change is observable in the noise floor level between these two plots, although a modulation sideband component becomes very predominant at the 250-hour mark.

Plots (D), (E), and (F) of both Figures 50 and 51 show a gradual deterioration in the "discreteness" of the frequency components. Plot (D) at 330 hours represents the peak level of the geometric mean, arithmetic mean, and matched-filter data for both accelerometers. At 420 hours, no discrete gear-mesh engagement is taking place, since Figures 50 (F) and 51 (F) both show an absence of discrete high energy frequency components.

Summary of BB-5 Gearbox Test Results

The data collected from the 437-hour testing of the BB-5 gearbox was particularly useful, not only in developing a trending philosophy but as an aid in analyzing the causes of the gearbox failure.

There is no apparent clear-cut reason for the gearbox failure. The mechanical condition was poor to begin with; oil leakage and heavy bearing wear were detected. The post-test inspection revealed that the input coupler was frozen up after disassembly, and any grease was turned to powder. The best mechanical clue to cause of failure was the wear path formed on the inner raceway of the No. 1 bearing. This had increased from 35 to 9500 microinches during the testing period. Whether this was due to misalignment of the shaft caused by extreme bearing wear, downward loading of the shaft caused by the weight of the suspended in-line torque sensor, or gradual coupling wear has not been verified. This wearpath was observable also on the gearbox BB-4 input bearing assembly. These two gearboxes were the first two to be tested using the in-line torque sensors. Alignment checks have been made on the next gearbox, HT-5, and the post-test bearing inspection report will be carefully scrutinized for correlation with these two gearboxes.

Most of the sensors proved to be definite indicators of impending failure. The most trendable appeared to be the B & K lateral accelerometers mounted near the input shaft. A glance at Figure 48 shows a fairly smooth and linear increase in output for both geometric and arithmetic mean plots from the commencement of test. Gearbox BB-4 exhibited a similar time history, and its peak value differed from the BB-5 peak value by only 3 dB. The matched-filter indicator closely

parallels the geometric mean and arithmetic mean time histories on an average basis, while being a more sensitive indicator of spectral change.

The SKF shock profile curve areas showed a general correlation with the time plots of the B & K accelerometers over portions of the test period.

The torque and gearbox efficiency measurements were useful as guides to interpretation of discontinuities in the sensor data described above.

HT-5 GEARBOX TESTS

Gearbox HT-5 was the third gearbox selected for testing under the present contract. This gearbox had been pulled from service for its first overhaul after 1186 hours of flight service.

The gearbox was installed in the test cell during the latter portion of September 1976, with testing commencing October 1. This gearbox accumulated 596 hours of testing during the month of October before a test cell failure occurred over the weekend of October 30-31. A worn coupler located between the output shaft of gearbox HT-5 and the output torque sensor disengaged itself from the gearbox. The condition of this coupler had been noted and a new coupler was on order at the time of the failure.

The RMS measurements taken from the two B&K accelerometers monitoring the low frequency vibration signals (DC-10 kHz) near the gearbox input and output shafts exhibited extremely small variance from their mean values over most of the total HT-5 test period. This indicated that HT-5 would have been tested at least a few hundred more hours if the test cell had not failed. Because of nicking and scarring to the ring and pinion gears caused by the gearbox disengaging from the coupling shafts, it was decided not to test the HT-5 gearbox further As a result, only partial results and conclusions can be gathered from analysis of the data.

Mechanical Condition of HT-5 Gearbox (Serial No. ABL 606)

Pre-Test Inspection

The preliminary bearing inspection revealed that the general condition of the reference bearings was poor. Three of the bearings (Nos. 1, 3, and 4)were categorized as having heavy wear, but none of the bearing assemblies was listed as having extreme wear.

Post-Test Inspection

Very little change was noticed between the general condition of the bearings before and after testing. The cross-groove profile charts match up extremely well, and the largest change was a reduction in inner race wear depth of bearing No. 3 from 43 to 30 microinches.

Spectrometric Oil Analysis (SOA)

Twenty oil samples were collected for the testing period. A comparison of the metallic particle content in the oil of HT-5 with that of gearboxes BB-4 and BB-5 reveals that this gearbox oil stayed relatively clear throughout its testing. Its amount of iron was, on the average, only 10 to 20 percent of that of BB-5. An initial amount recorded during the "green" run was less than 100 ppm, and then reduced down (see Figure 52) to less than 50 ppm for the remainder of the test period. For reference, oil sample times are shown graphically in Figure 53 (B).

Temperature Sensors

Figures 54(A) and (B) present graphical displays of the temperature readings recorded from the two sensors monitoring gearbox oil temperature and ambient temperature at the outside case of the gearbox.

Other than an initial oil temperature perhaps 20°F higher than that throughout most of the testing period, no marked temperature effects can be seen. The negative transient at the 175-hour point was due to a test cell shutdown.

RPM and Torque Indicators

Figures 55 (A) and (B) present input and output RPM data for 550 of the 596 test hours. As can be seen, RPM remained steady on both input and output shafts during this period.

Figure 56 presents three displays: (A) input shaft torque, (B) output shaft torque, and (C) gearbox efficiency. The most noticeable effect in these plots is the erratic input torque from hour 45 to hour 170. There seems to be a 5 percent variation in torque during this period. The reason for this is not apparent at the present time, although there is a correlation between the end of this variation and the output accelerometer ultrasonic data, as noted in the next section.

Ultrasonic RMS Accelerometer

Figures 57 (A) and (B) present time displays of the high frequency detected energy (greater than 20 kHz) from the B & K accelerometers mounted on the gearbox near the input and output shafts, respectively. There is a steady response from the input channel over the full test

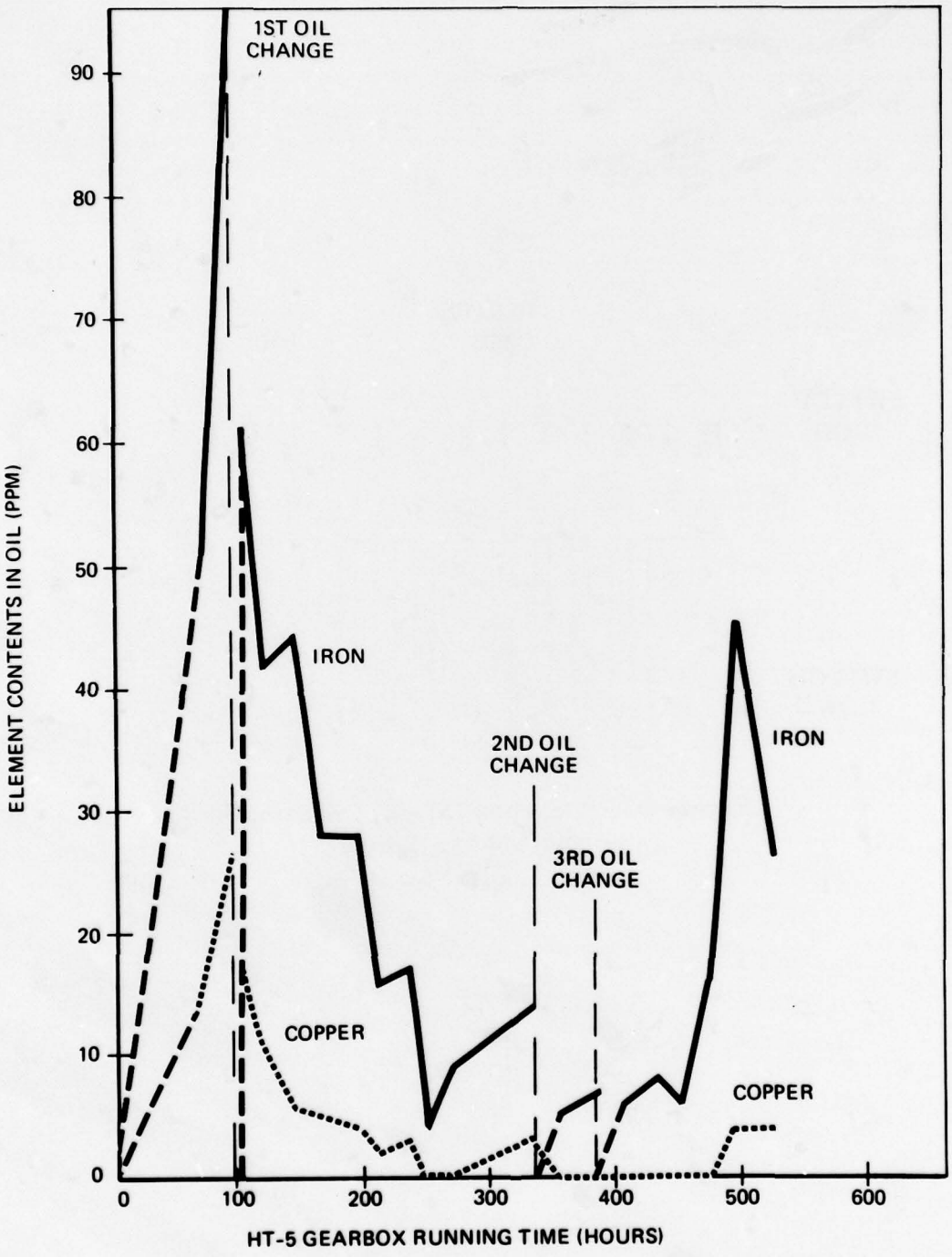

Figure 52. Spectrometric Oil Analysis - Gearbox HT-5.

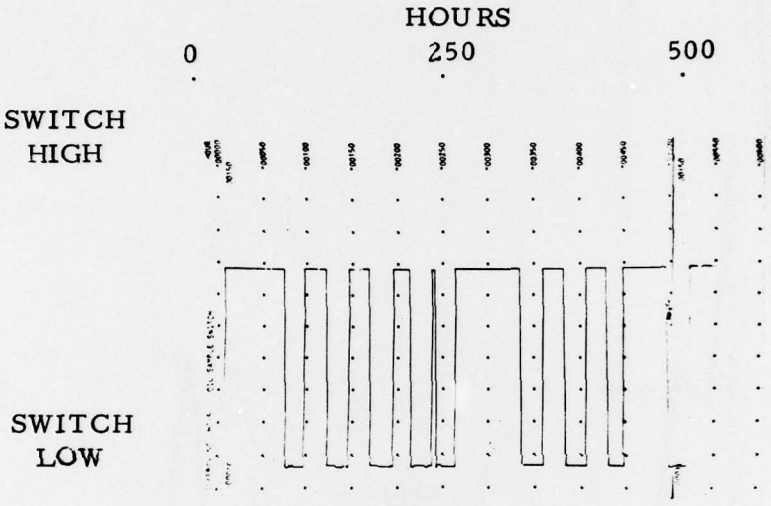

Figure 53. Gearbox HT-5; Oil Sample and Change Times.

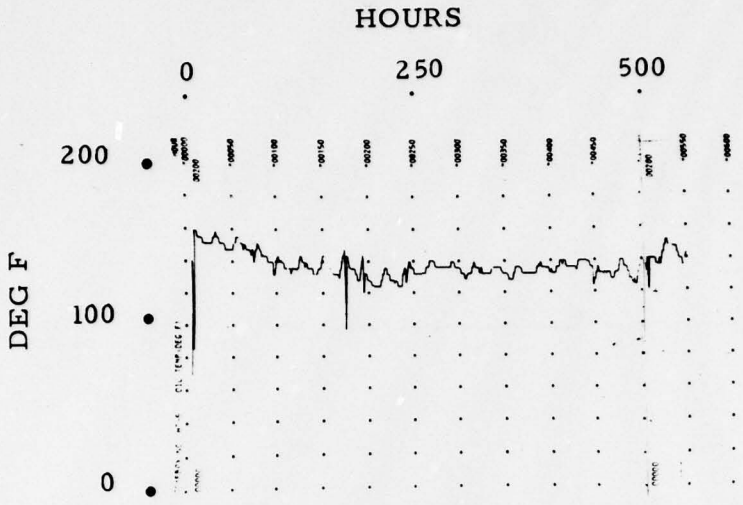

(A) OIL TEMP.

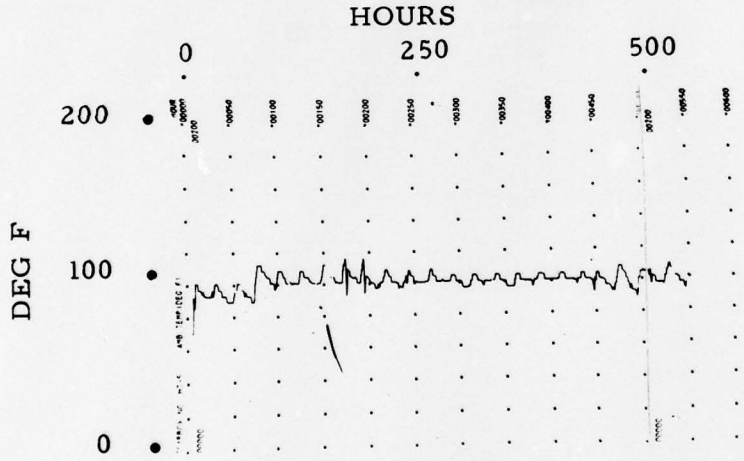

(B) AMBIENT TEMP.

Figure 54. Gearbox HT-5; Oil and Ambient Temperature vs. Test Time.

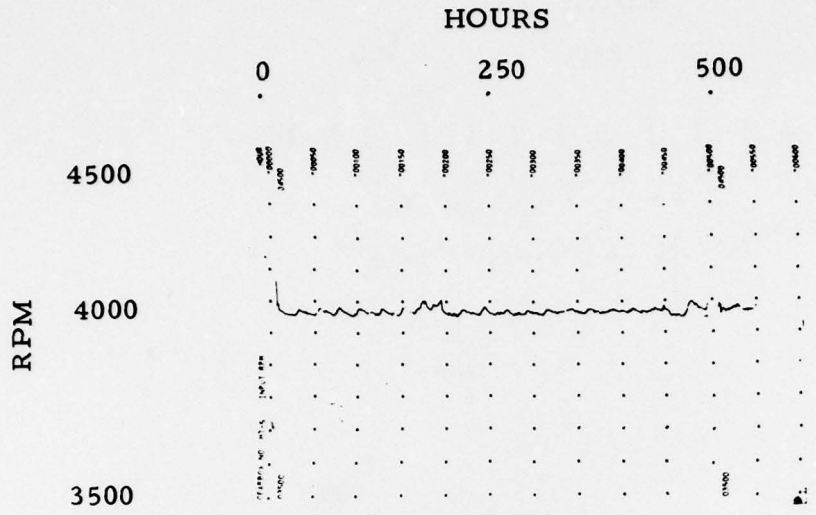

(A) INPUT SHAFT

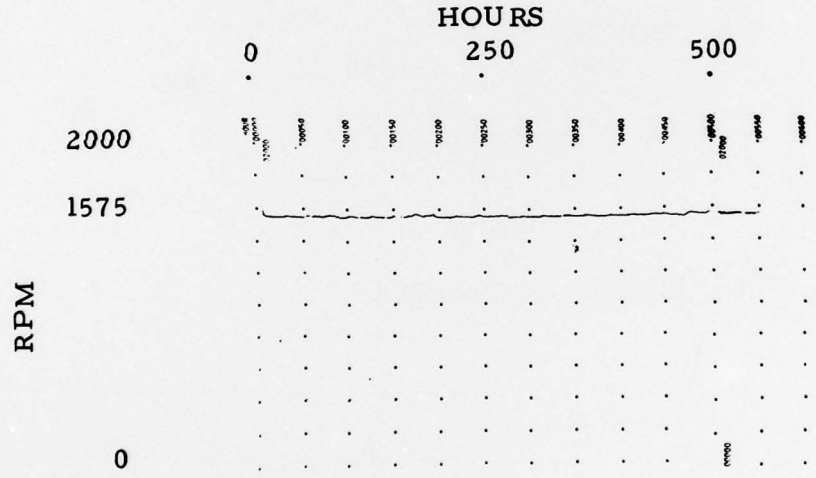

(B) OUTPUT SHAFT

Figure 55. Gearbox HT-5; RPM vs. Test Time.

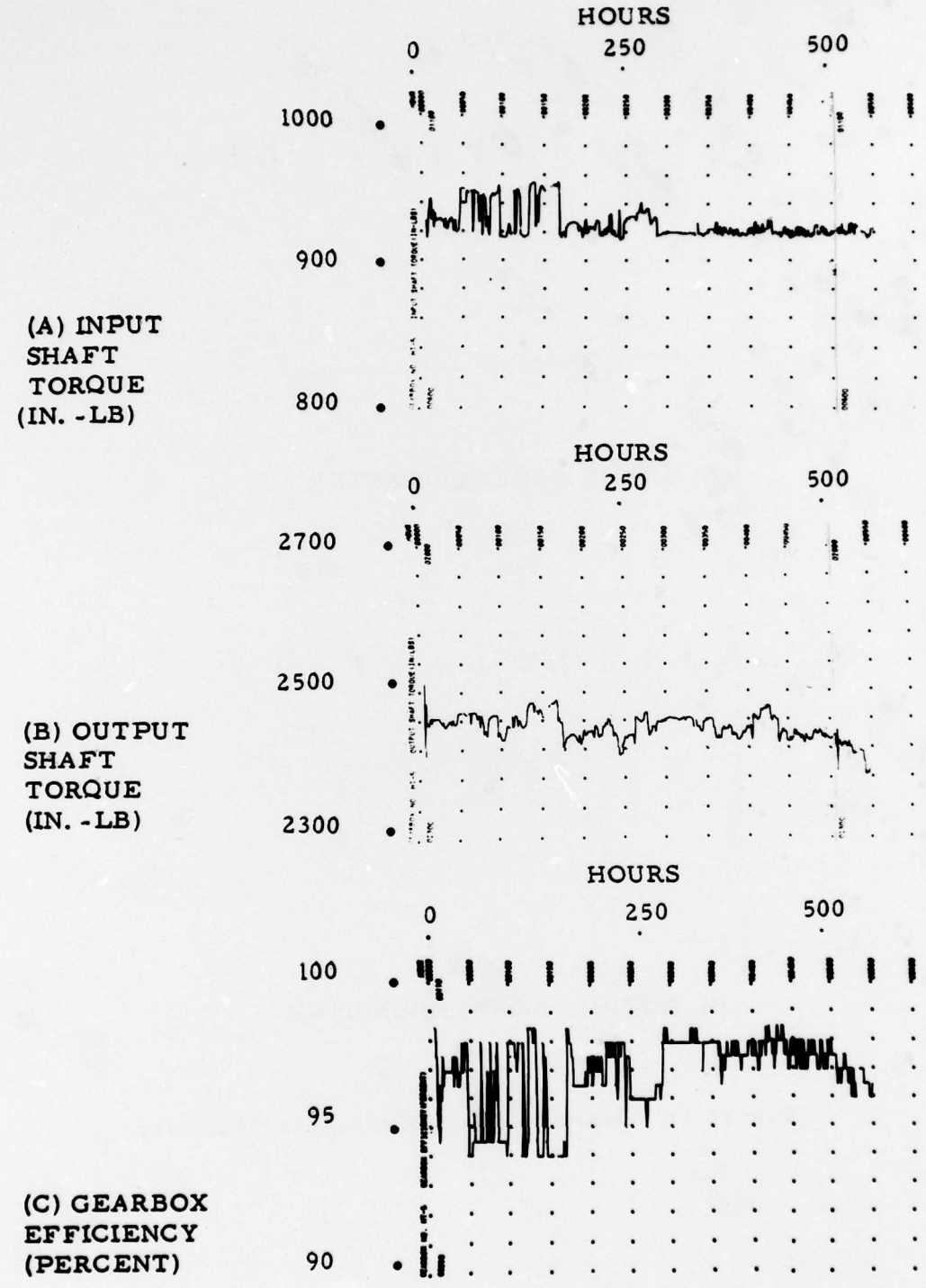

Figure 56. Gearbox HT-5; Torque and Efficiency vs. Test Time.

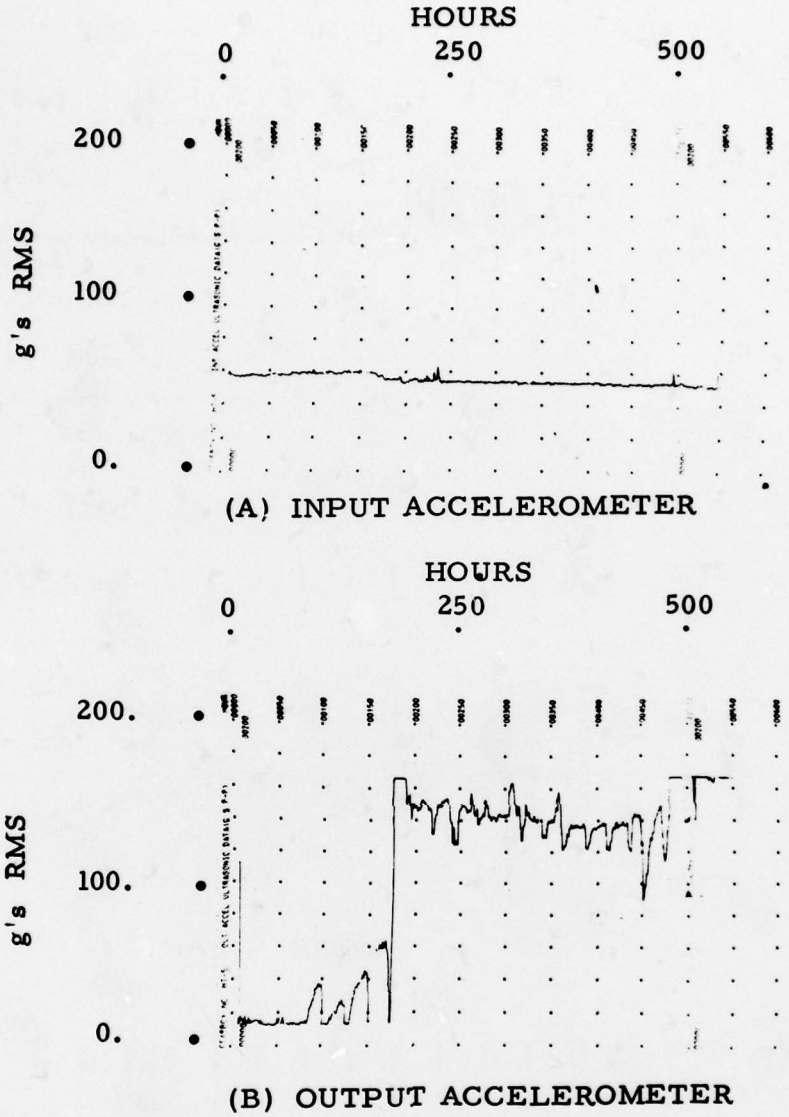

Figure 57. Gearbox HT-5; Ultrasonic RMS Data.

period. The output accelerometer shows a severe step rise at approximately hour 170. This happens very closely to the settling down of torque variations (Figure 56). It is possible that the output coupler wear effect is being observed by the high level of ultrasonic energy from this accelerometer. It was noted in the report on gearbox BB-5 (which also had contrasting data between the two accelerometers) that the input side of the gearbox is mounted firmly to the test cell stand while the output side is not. It is supported only by the input mount and the output shaft. It is possible that the resonances of the output accelerometer are more subject to excitation because of this mounting.

The input accelerometer ultrasonic energy appears to be the better trend indicator, since its steady level agrees with the steadiness of the data exhibited by most of the other gearbox monitors, i.e., low frequency energy from B & K accelerometers and SKF shock profiles.

Shock Pulse Analyzer

Shock emission profile data using the SKF shock pulse analyzer is plotted for both input and output accelerometers in Figures 58 and 59. There is some erratic behavior in the 100-200-hour period. However, the data during the latter 300-hour period appears fairly uniform and would indicate no cumulative deteriorating effect in the gearbox. This is also indicated in Figure 60, which is a plot of the SKF peak shock value for the input accelerometer. This data is essentially flat for the entire test period.

Low Frequency Vibration Data Time Analysis

Four unique representations of the data obtained from the input and output accelerometers are presented in the same format as that for gearbox BB-5. It is instructive to compare the data for the two gearboxes. Figures 61 (A) and (B) present matched filter, RMS, geometric mean, and arithmetic mean for the HT-5 input lateral accelerometer. Figures 62 (A) and (B) present the same time histories for the output accelerometer. It can be seen that a definite trend started to develop shortly after the 500th hour of testing. This was shortly before the weekend of the test cell failure, and no doubt was attributable to the worn coupler. During the first 500 hours of testing, all indications in Figures 61 and 62 are very constant and indicative of a healthy gearbox.

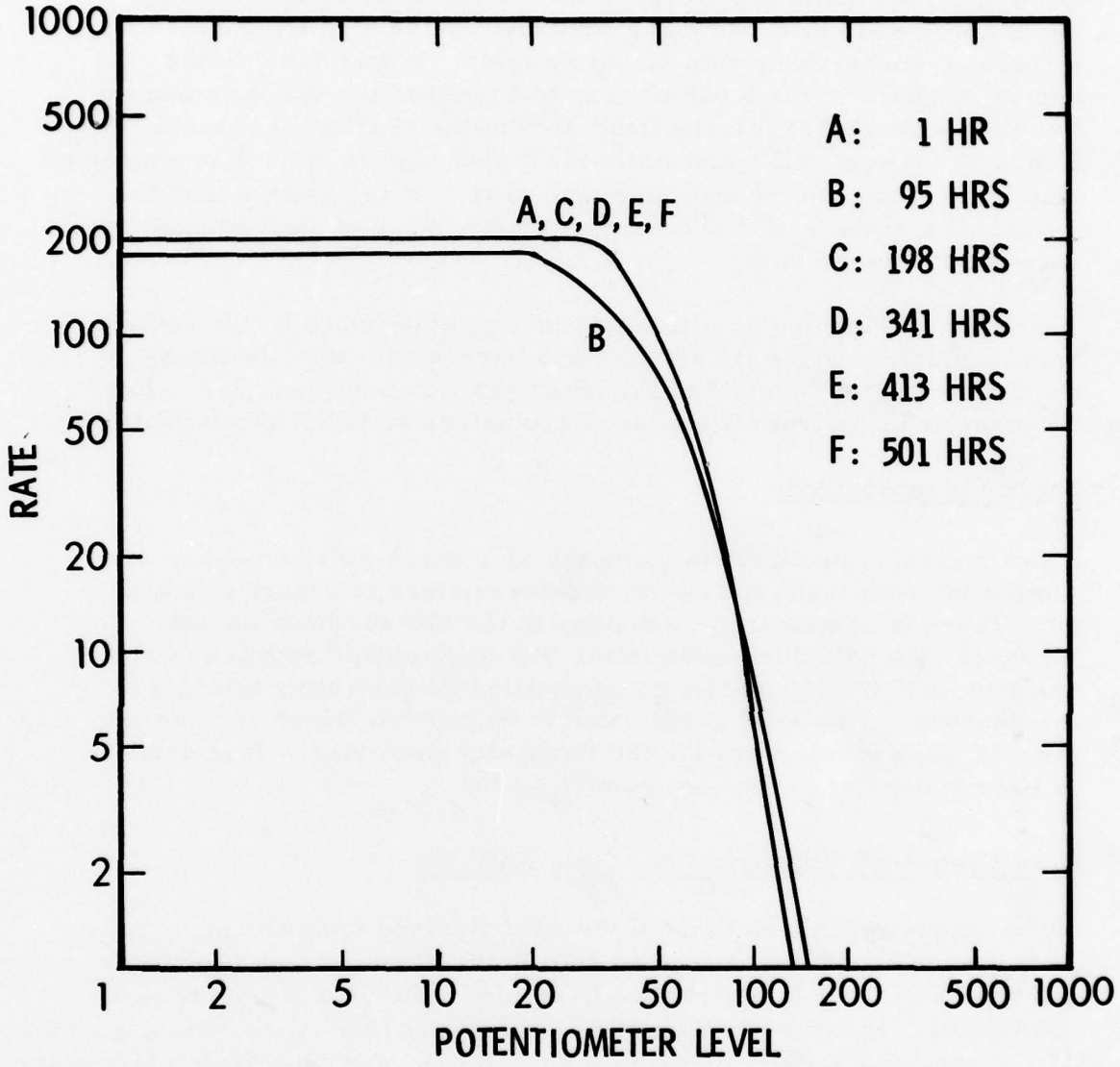

Figure 58. Gearbox HT-5; Shock Profile Curves, Input Accelerometer.

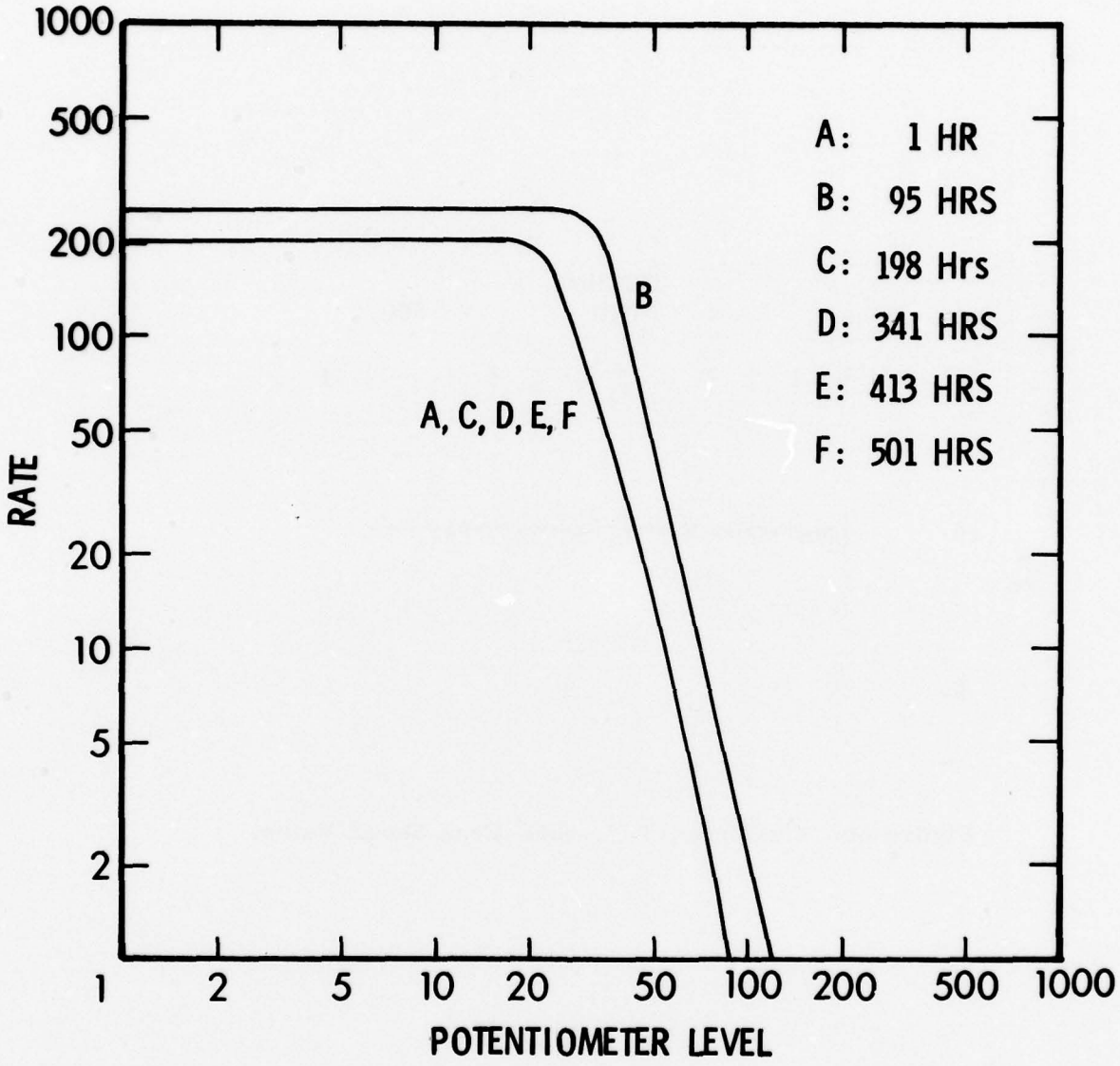

Figure 59. Gearbox HT-5; Shock Profile Curves, Output Accelerometer.

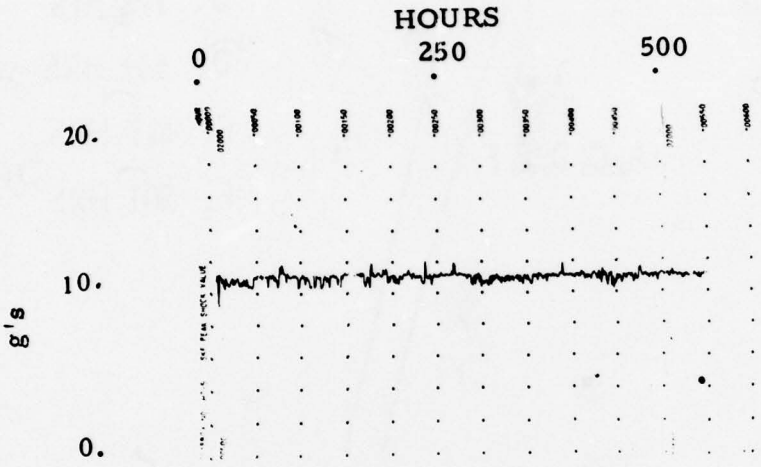

Figure 60. Gearbox HT-5; SKF Peak Shock Value.

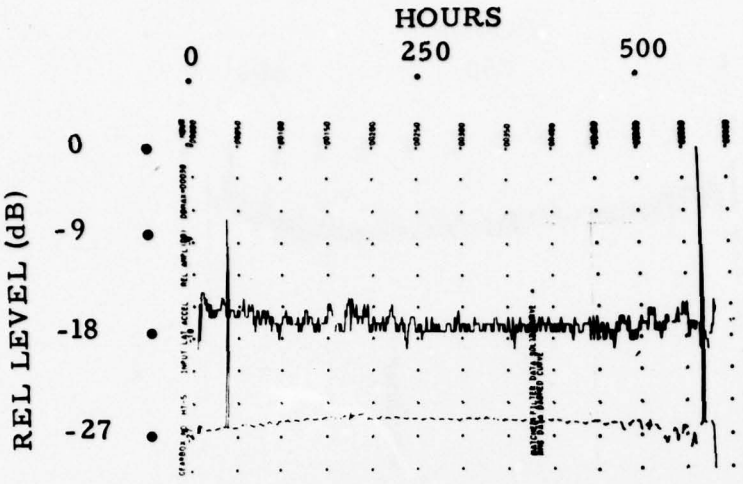

(A) MATCHED FILTER (SOLID) AND RMS DATA (DASHED)

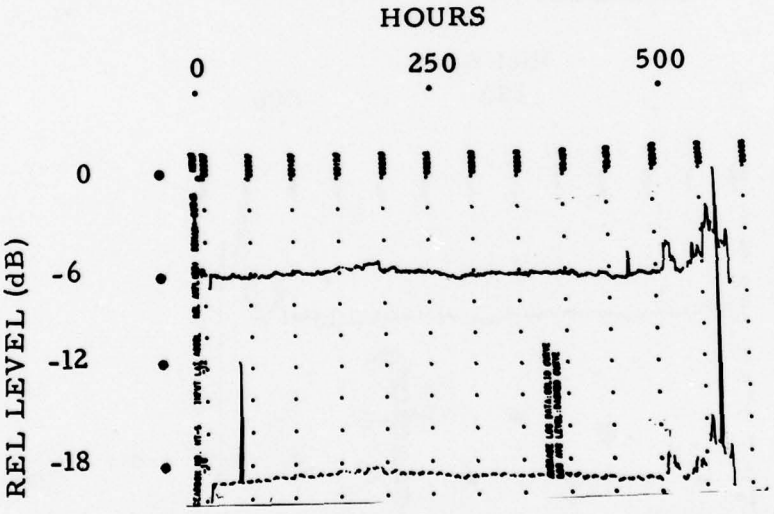

(B) GEOMETRIC MEAN (SOLID) AND ARITHMETIC MEAN (DASHED)

Figure 61. Gearbox HT-5; Input Lateral Accelerometer Trend Parameters.

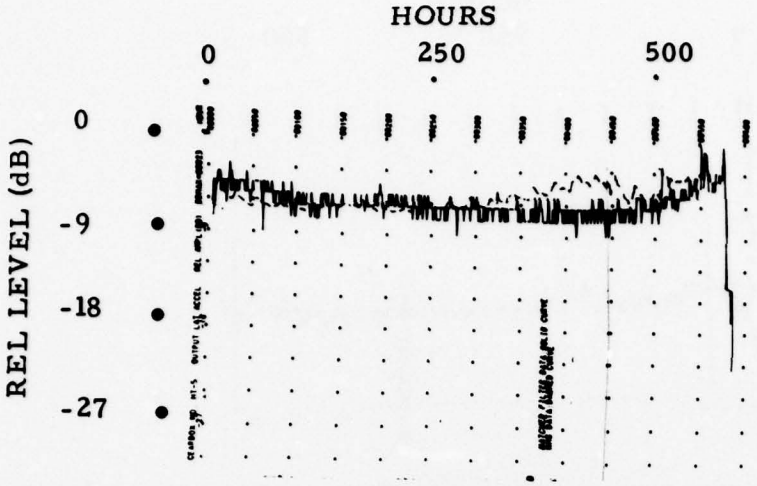

(A) MATCHED FILTER(SOLID) AND RMS DATA (DASHED)

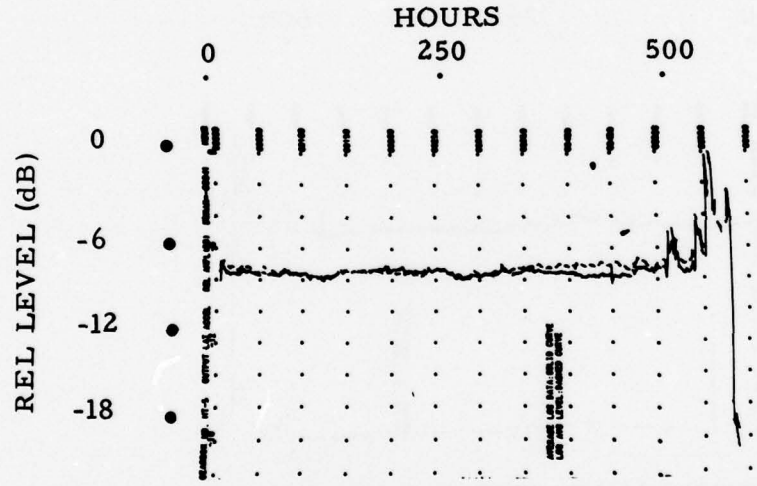

(B) GEOMETRIC MEAN(SOLID) AND ARITHMETIC MEAN (DASHED)

Figure 62. Gearbox HT-5; Output Lateral Accelerometer Trend Parameters.

The times indicated at the top of Figures 61 and 62 are the times that power spectral density plots are illustrated (see next section). It will be seen that fairly uniform spectra are obtained through 400 hours and very little change is evident even at 510 hours.

Low Frequency Vibration Data Frequency Analysis

Figures 63 (A) through (F) illustrate the DC-10 kHz power spectral density of the HT-5 input accelerometer. Note that frequency structure only starts to change at hour 510. At hour 573 the gearbox has been separated from the output shaft because of the coupler failure.

Similarly, Figures 64 (A) through (F) present the PSD plots for the output accelerometer. Note that the fundamental and second harmonic components of the gear-mesh rate are close to the same amplitude over 510 hours of test time, with each predominating slightly at specific times. Again, the sensings of Figures 64 (E) and (F) occur during the output shaft coupler failure.

In summary, no deterioration seems to have been evident during the first 500 hours of testing, as evidenced by an examination of the frequency structure of the two accelerometers during this period.

Summary of HT-5 Gearbox Test Results

It was unfortunate that the test cell failure prevented continued testing of gearbox HT-5. For the most part, the DC sensors and the trending parameters indicated no cumulative deterioration due to bearing or gear wear in the gearbox itself. The post-test bearing inspection appears to support this data.

Safeguards were installed after this failure to prevent a recurrence of the situation where the gearbox under test had to be withdrawn due to damage caused by external forces. These included more extensive soft-wear monitoring of both input and output RPM and torque measurements to assure that automatic shutdown will occur if torque loading falls out of prescribed limits. In addition, both torque sensors (on input and output shafts) were provided with shock mounting to ease the gravitational moment-arm loading on each shaft. Shaft alignment and inspection of coupler condition were given special attention.

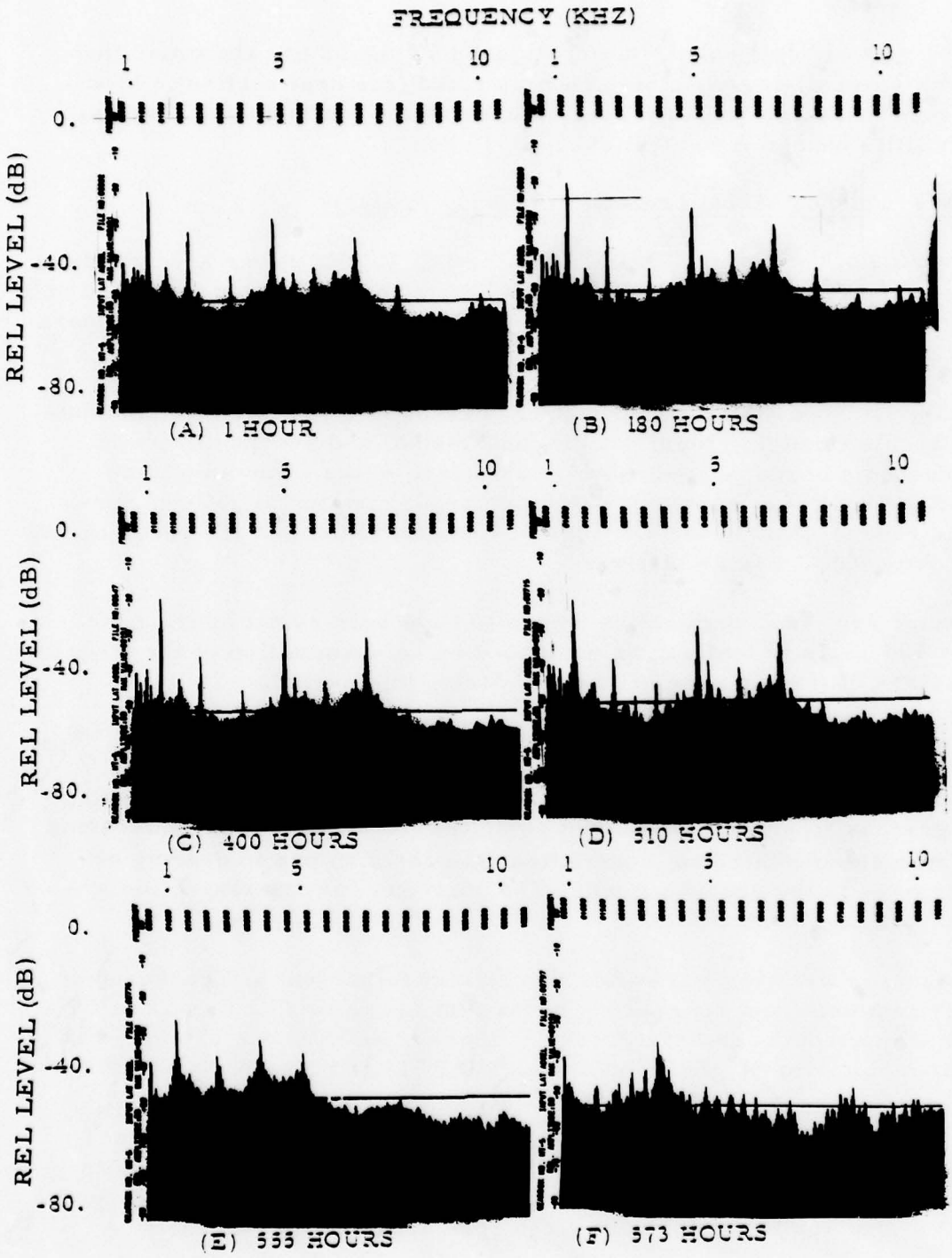

Figure 63. Gearbox HT-5; Input Lateral Accelerometer Power Spectral Density.

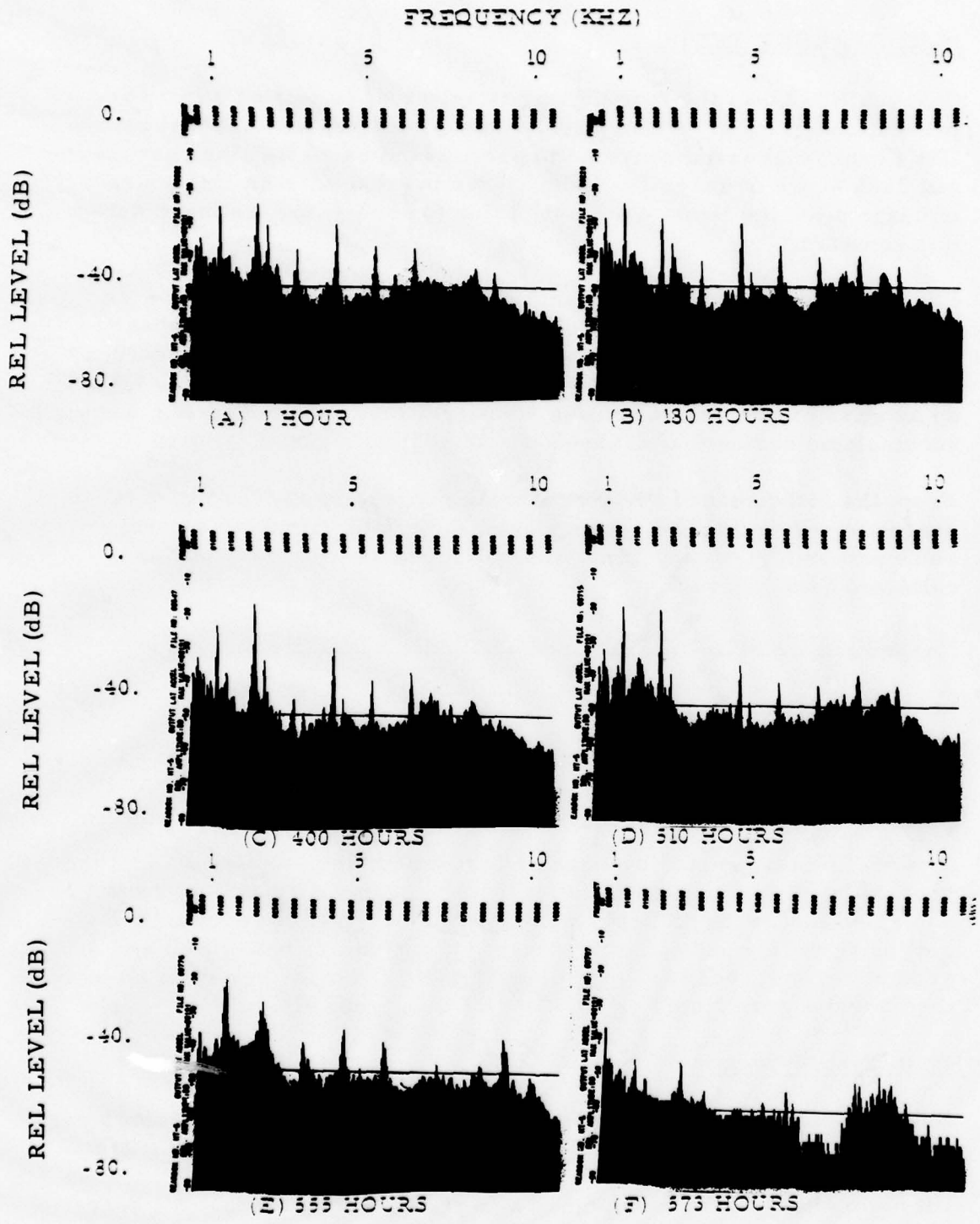

Figure 64. Gearbox HT-5; Output Lateral Accelerometer Power Spectral Density.

HT-2 GEARBOX TESTS

Gearbox HT-2 was the fourth gearbox selected for testing under the present contract. The component removal and repair/overhaul record (DA Form 2410) accompanying the gearbox indicated that the gearbox had 2685 hours of usage (including three overhauls, with 1241 hours of usage after the latest overhaul) prior to receipt for testing under this contract.

HT-2 ran a total of 1519 hours with no signs of impending failure indicated by either the computer-collected data or physically observable data. This was subsequently verified by using the HT-2 gearbox in a test evaluation of polymer-film accelerometers (a separate report; an addition to this contract). An additional 1460 hours of testing were accumulated during that evaluation with <u>still</u> no signs of failure!

From the standpoint of component wear prognosis, the testing of HT-2 served to verify that the sensors used were valid trend indicators, since extremely "steady" data was collected. A summary of this collected data follows.

Mechanical Condition of HT-2 Gearbox (Serial No. B13-875)

Pre-Test Inspection

During the initial teardown inspection, it was noted that the No. 1 bearing assembly did not turn smoothly when hand-rotated, but after assembly the bearings appeared to be satisfactory.

The preliminary report by Bearing Inspection, Inc. indicated that "the general condition of reference bearings is poor. All bearings have sustained moderate to heavy wear. Some bearings have sustained corrosive pitting and fatigue damage; in particular, bearings 3 and 4 are not recommended for further operation." The noise levels on bearings 3 and 4 were listed as 16.5 and 21 dB, respectively.

Post-Test Inspection

During disassembly, only a slight leak at the input and output seals was observed. Otherwise, there was no visible change or damage. The ring gear and pinion gear assembly showed slightly more contact wear but maintained a very smooth and acceptable wear pattern. All bearings appeared normal and rotated smoothly.

The bearing inspection report revealed that input bearing No. 2 appeared to have degraded slightly, with the noise level increasing from 0 dB to 4 dB. Output bearing No. 3 experienced a raceway wear depth increase of from 74 to 90 microinches. However, its noise level actually decreased 5 dB, indicating more uniform wear.

Spectrometric Oil Analysis (SOA)

Fifty one oil samples were collected for the 1519-hour testing period. Figure 65 is a graphical representation of the iron content in gearbox HT-2 oil over the complete test period. The maximum iron content recorded is only 26 parts per million, and this occurred during the early stages of testing. The actual iron content during the majority of the 1519 hours of testing was less than 5 parts per million. Other elements contained in the oil samples were of even lesser density.

Temperature Sensors

Figure 67 illustrates the oil and ambient temperature time history for gearbox HT-2. The first and last 500 hours of testing are displayed. The 500-hour intermediate test period did not vary substantially from the data shown. In Figure 67(A) the average oil temperature is seen to be approximately 140° F. The average ambient temperature displayed in Figure 67(B) is approximately 82° F. Note the slightly elevated temperatures during the first 50 hours of testing. During this time, intermittent problems with test cell pulley-belt slippage were experienced. The belts and associated shafts became very hot, this heat being transmitted to the rest of the components and equipment. A blower was mounted near the pillow block bearings to cool this area and lower the overall temperature. Later, pulley-belt tension was increased, stabilizing shaft rpm.

RPM and Torque Indicators

Input and output rpm are presented in Figures 68 (A) and (B), respectively. Again, the middle 500 hours of testing is omitted because of the non changing character of the data. The initial perturbations in rpm during the first 135 hours were due to pulley-belt slippage. It was discovered that the rpm analog signal from the input torque sensor was also intermittent at this time. This explains the perturbations in input rpm in Figure 68(A) occurring as late as hour 215.

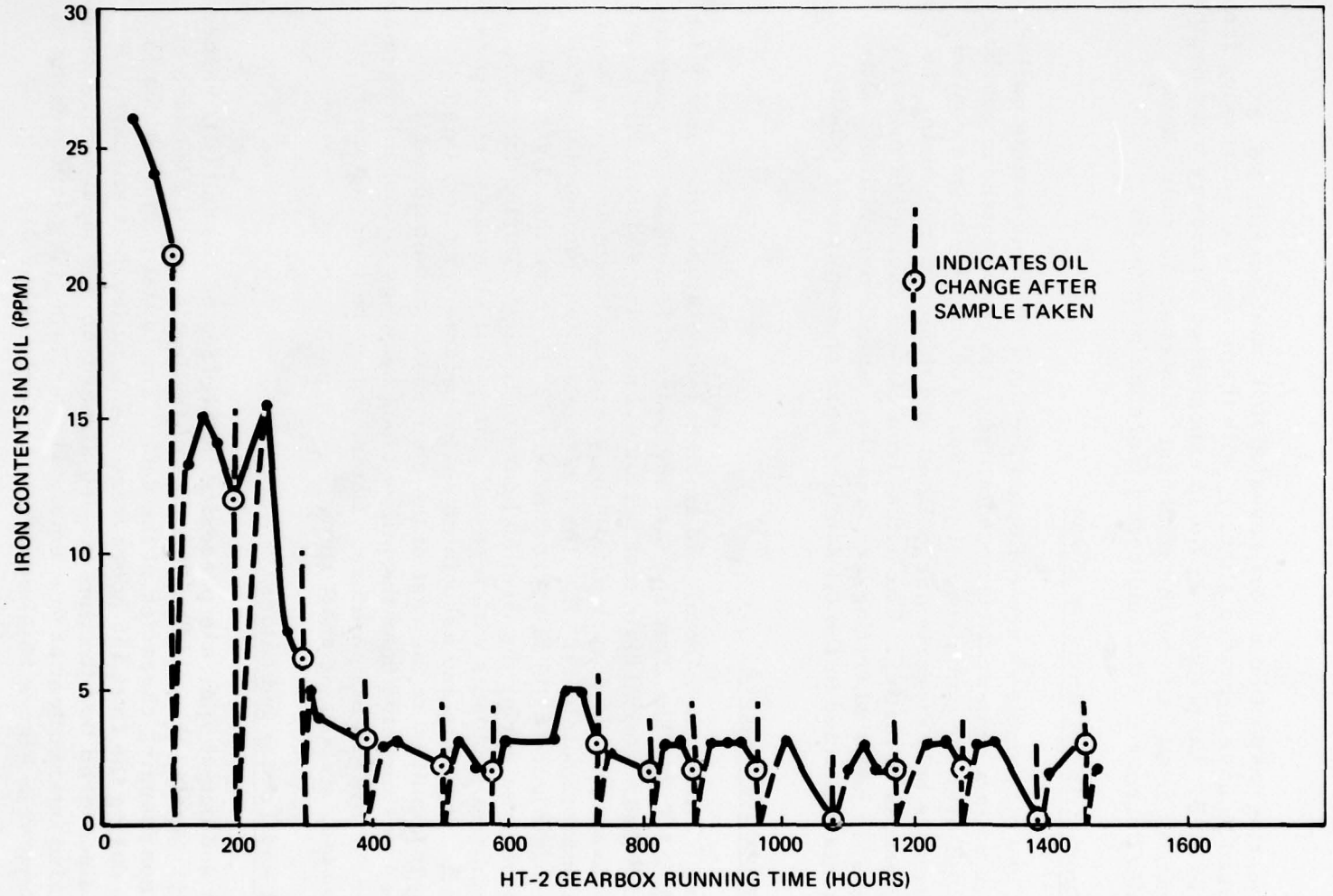

Figure 65. Spectrometric Oil Analysis-Gearbox HT-2.

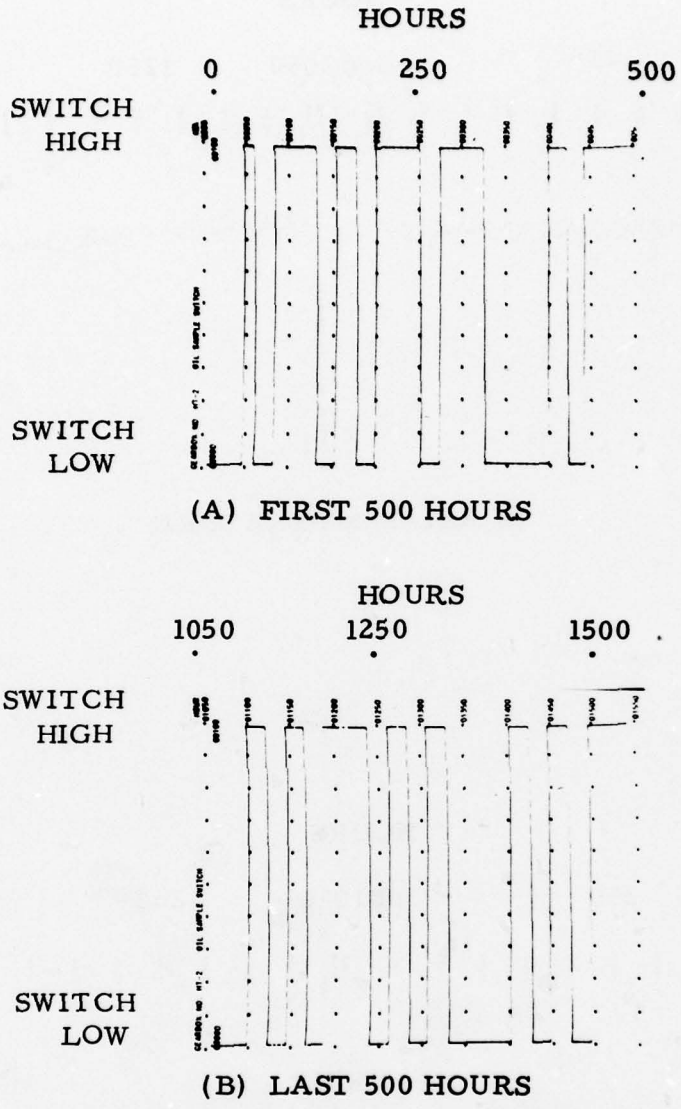

Figure 66. Gearbox HT-2: Oil Sample and Change Times.

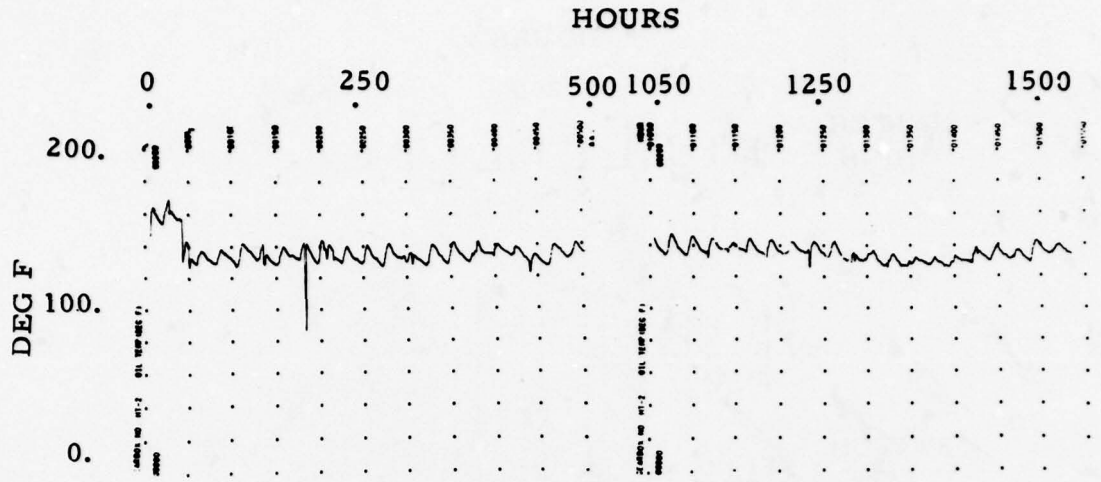

(A) OIL TEMPERATURE

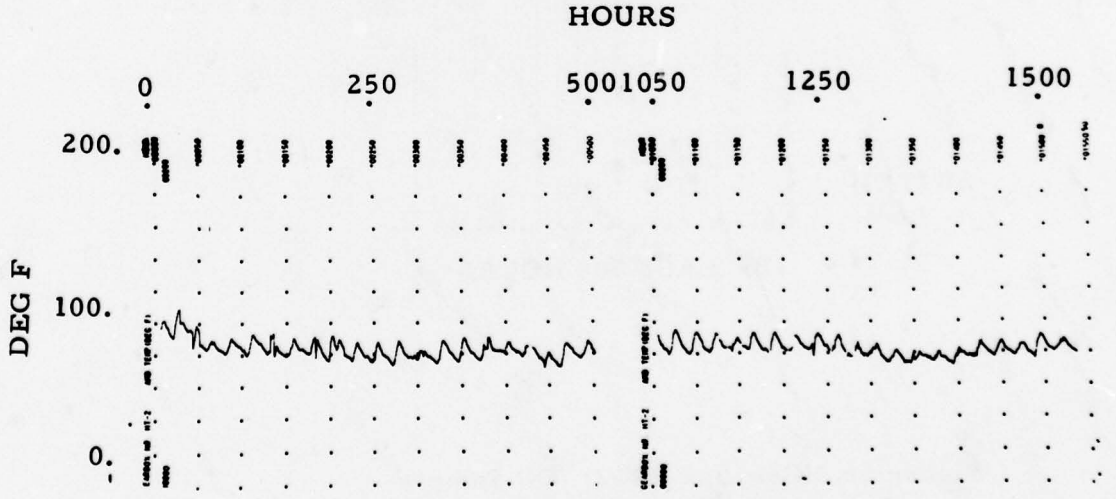

(B) AMBIENT TEMPERATURE

Figure 67. Gearbox HT-2; Oil and Ambient Temperature vs. Test Time.

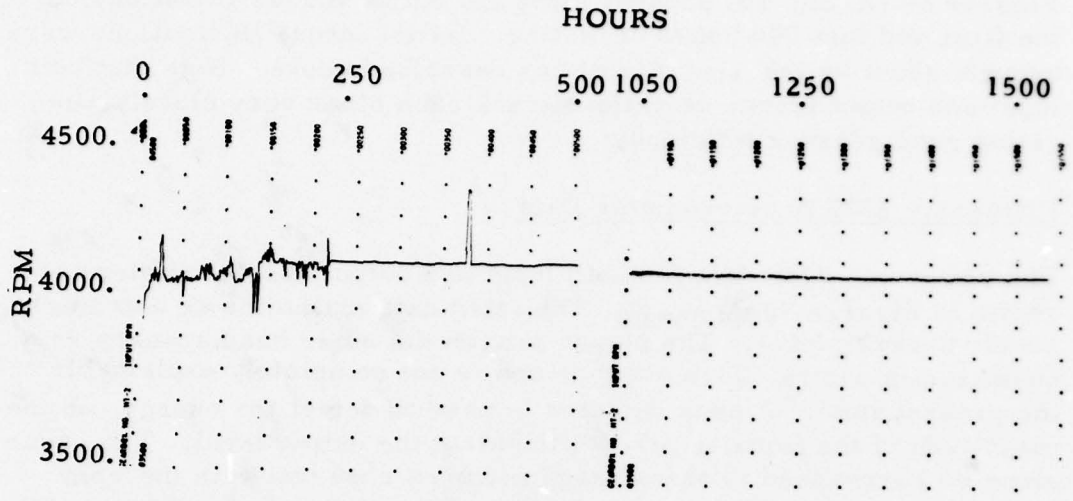

(A) INPUT SHAFT

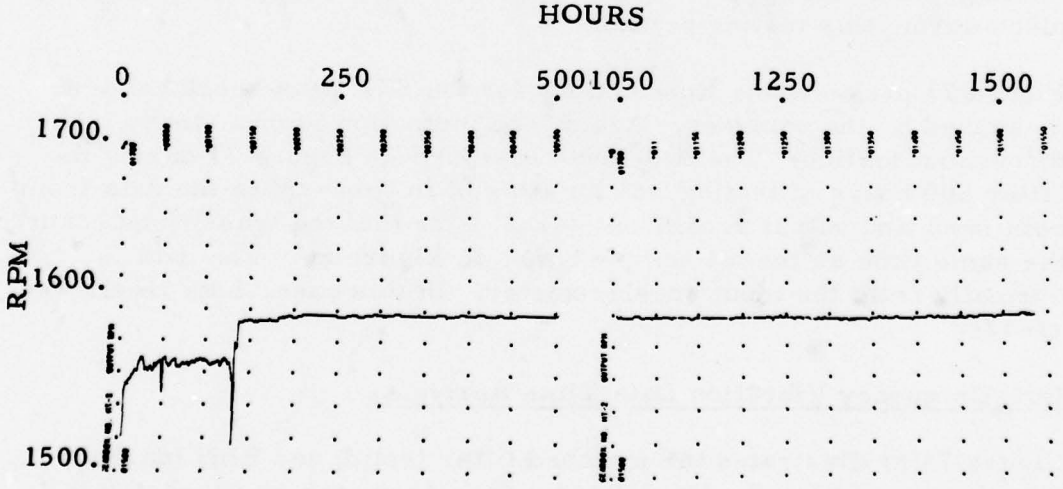

(B) OUTPUT SHAFT

Figure 68. Gearbox HT-2; RPM vs. Test Time.

Figures 69 (A) and (B) present input and output torque variations during the first and last 500 hours of testing. Initial torque fluctuations were brought about by the rpm variations described above. Note that both input and output torque variations track each other very closely, indicating good gearbox efficiency.

Ultrasonic RMS Accelerometer Data

The ultrasonic RMS data for both input and output accelerometers is shown in Figures 70(A) and (B). The input data maintains an extremely steady average level. The output data, on the other hand, appears very quantized in nature. This phenomenon is not completely explainable at the present time. A peak detector is used to detect the energy, so the magnitude of the impulse size will control the output level. The excursions do correspond to transient phenomena observable in the rpm data of Figure 68. The output ultrasonic data is very steady during the last 500 hours of testing, indicating that gearbox operation is extremely invariant during this period.

Shock Pulse Analyzer

The shock profile curves for the input and output shock pulse accelerometers are illustrated in Figures 71 and 72, respectively. Note that the shock profiles are essentially constant over the last 1200 hours of testing, providing supporting evidence that very little wear action took place during this testing period.

Figure 73 presents the time history for the SKF peak shock value as measured by the analyzer. Again, the indication is of a steady level throughout testing. The two-level waveform in Figure 73 during the latter 500 hours of testing was an attempt to time-share the data from both input and output accelerometers. Note that the transitions occur at the same time as the oil sample times in Figure 66. The data is normally from the input accelerometer. In this case, both levels are steady.

Low Frequency Vibration Data Time Analysis

Figure 74(A) illustrates the matched filter (solid) and RMS (dashed) trending curves for the input lateral accelerometer on gearbox HT-2. Figure 74(B) presents the geometric mean (solid) and arithmetic mean (dashed) curves for the same accelerometer. This data is extremely

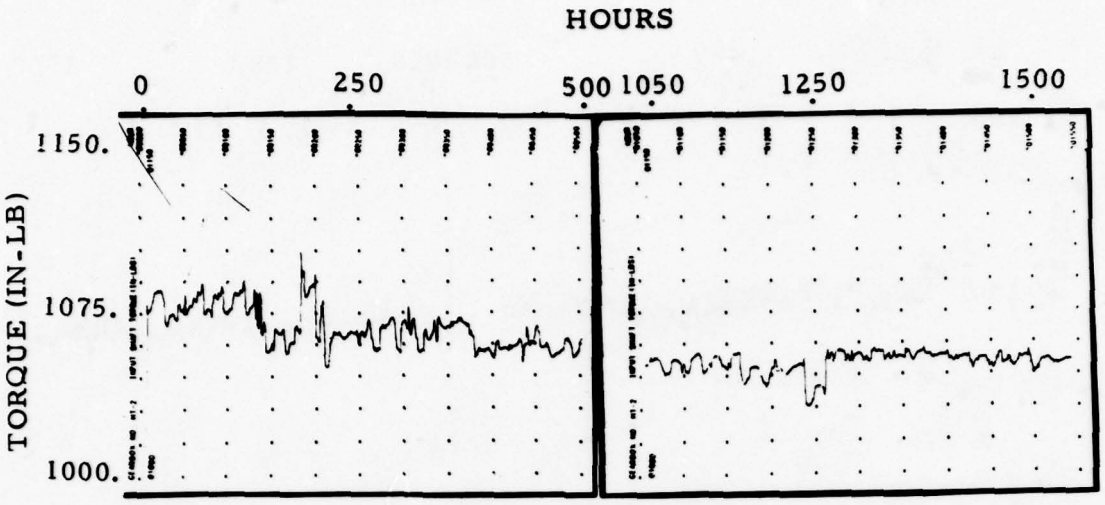

(A) INPUT SHAFT

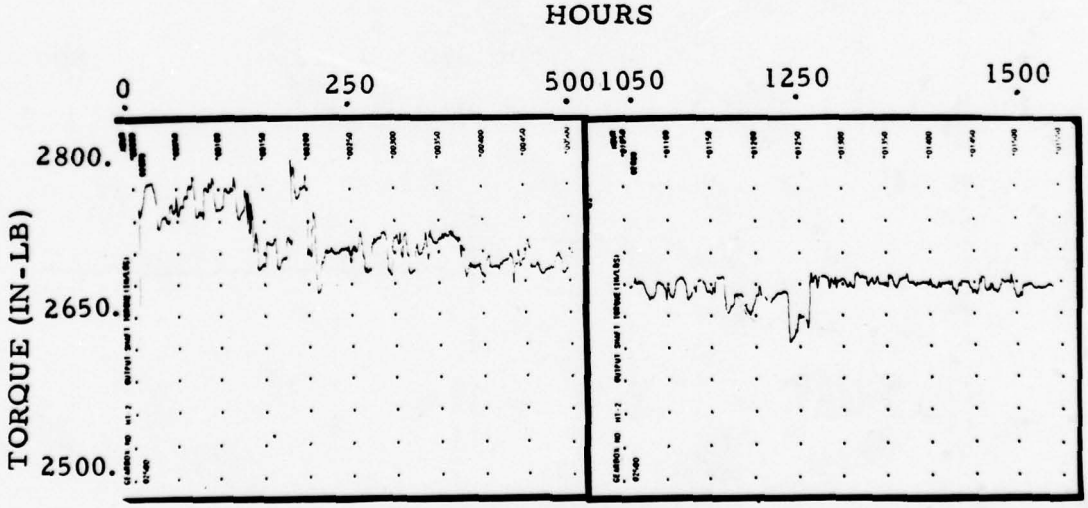

(B) OUTPUT SHAFT

Figure 69. Gearbox HT-2; Torque vs. Test Time.

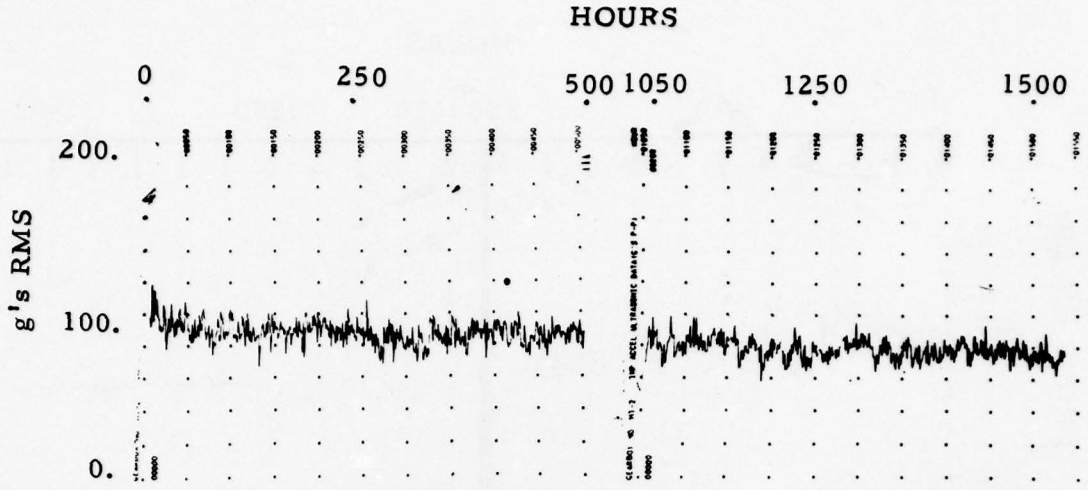

(A) INPUT ACCELEROMETER

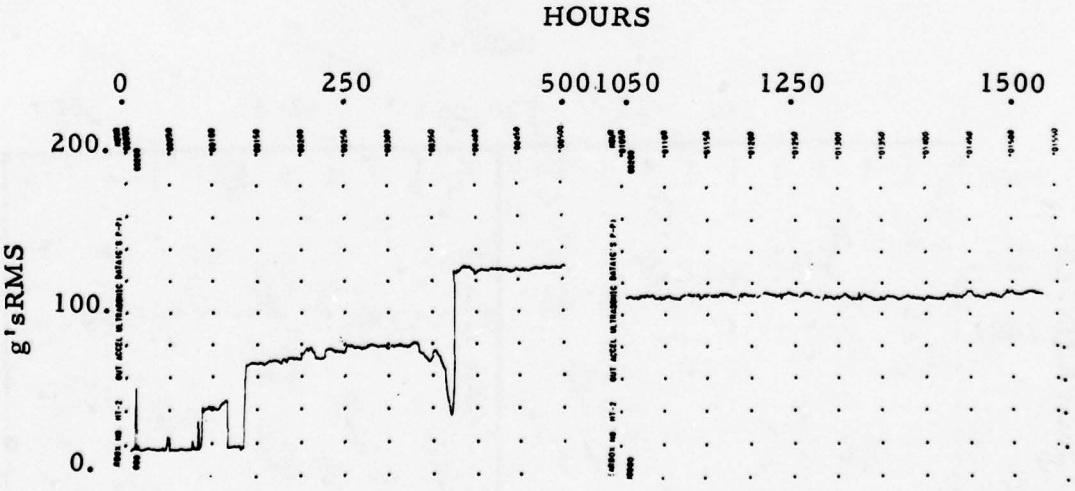

(B) OUTPUT ACCELEROMETER

Figure 70. Gearbox HT-2; Ultrasonic RMS Data.

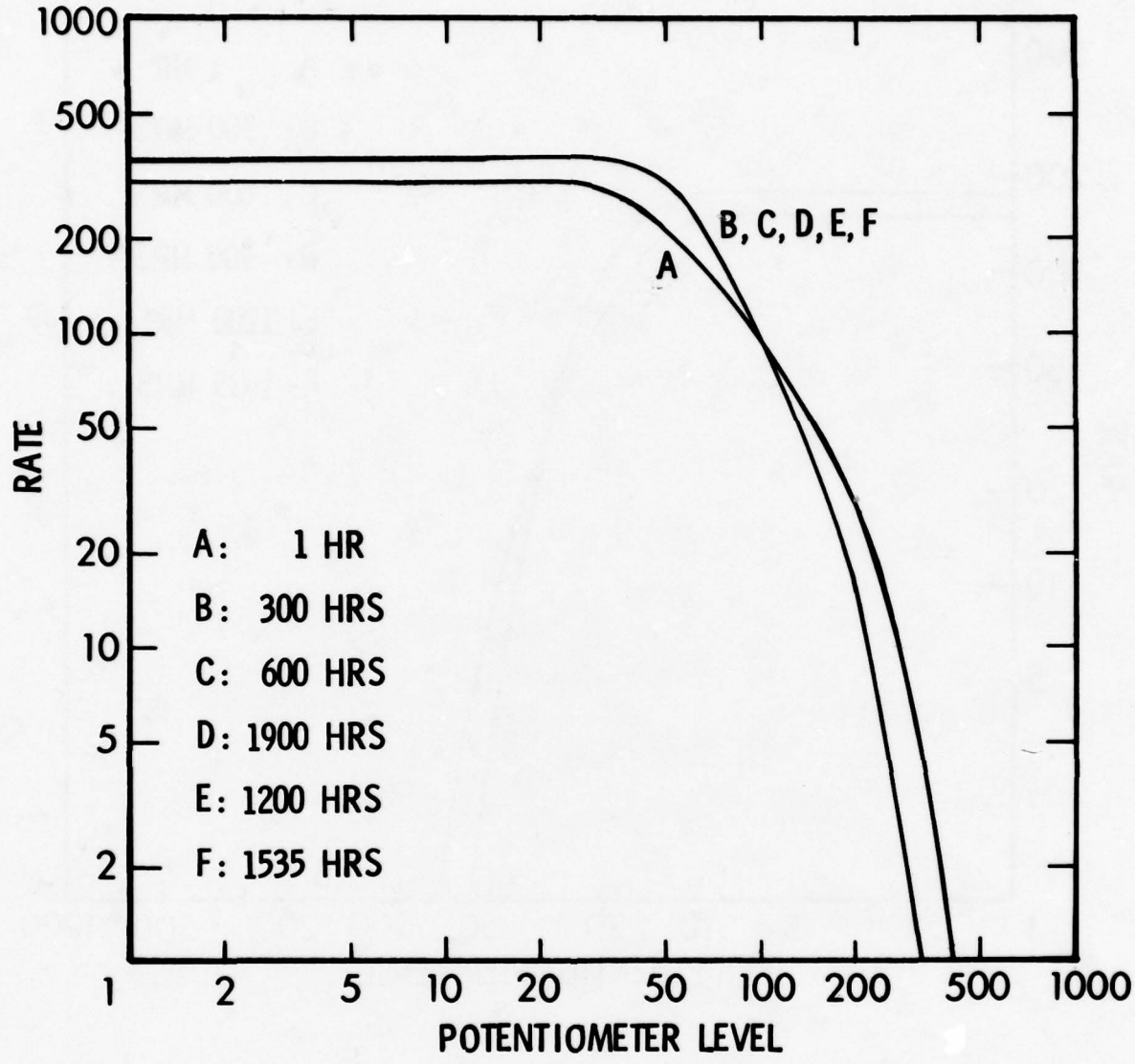

Figure 71. Gearbox HT-2; Shock Profile Curves, Input Accelerometer.

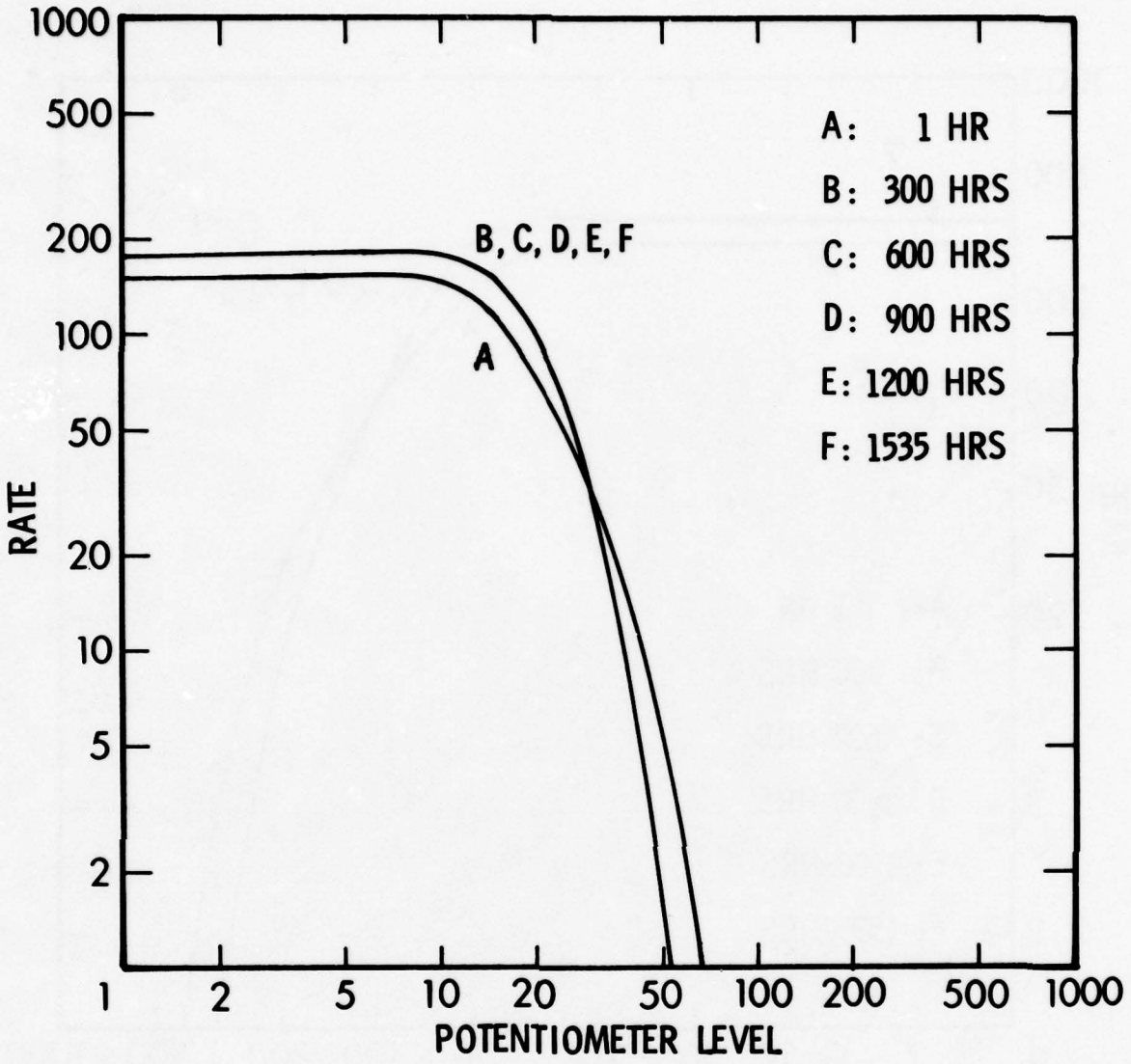

Figure 72. Gearbox HT-2; Shock Profile Curves, Output Accelerometer.

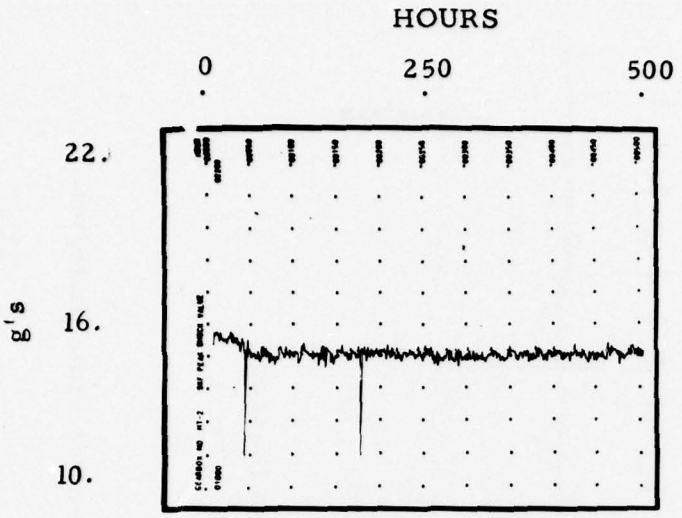

(A) FIRST 500 HOURS

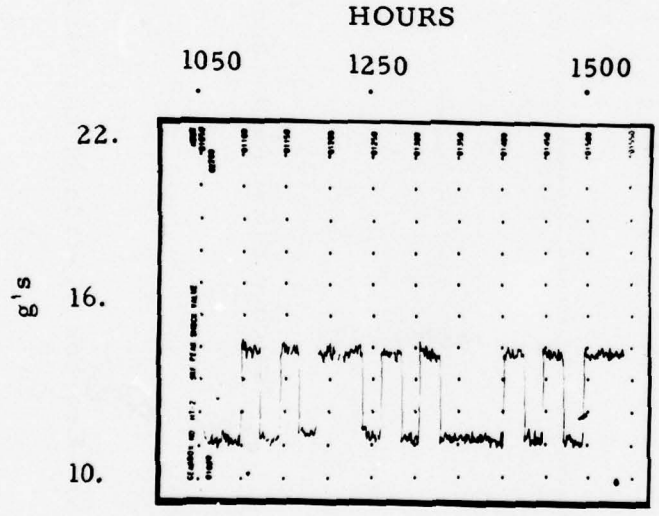

(B) LAST 500 HOURS

Figure 73. Gearbox HT-2; SKF Peak Shock Value.

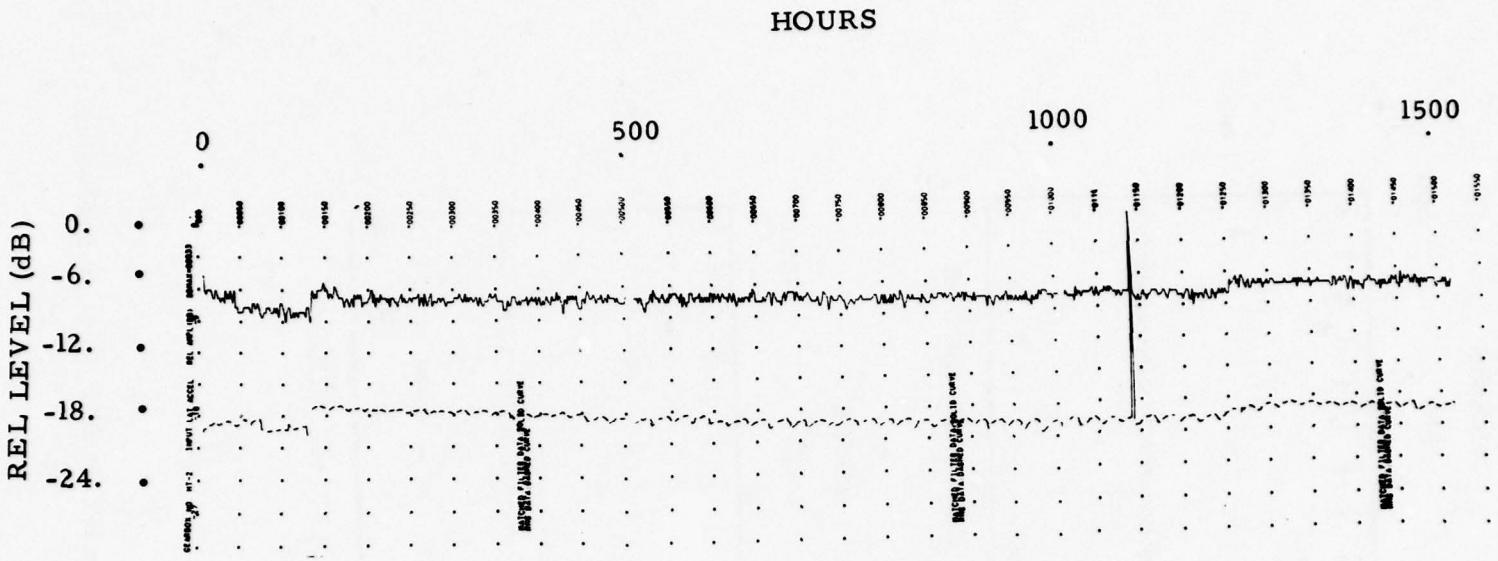

Matched Filter (Solid) and RMS Data (Dashed).

Figure 74 (A). Gearbox HT-2; Input Lateral Accelerometer Time Histories.

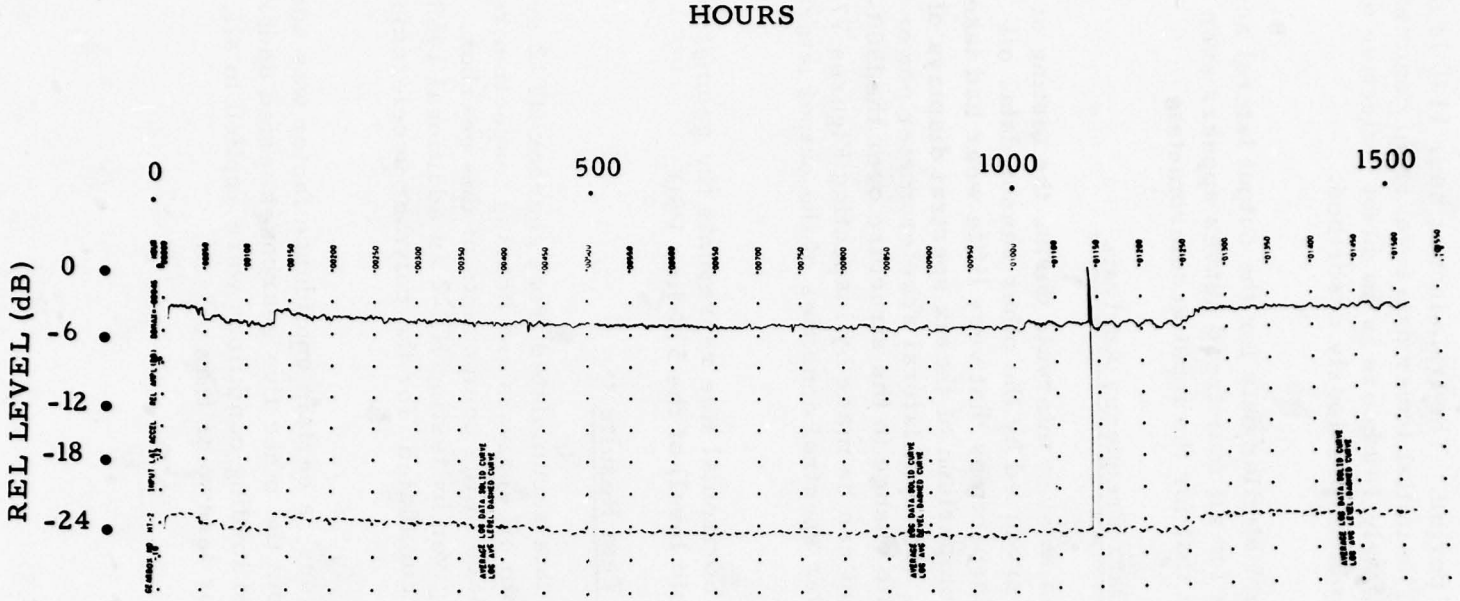

Geometric Mean (Solid) and Arithmetic Mean (Dashed).

Figure 74 (B). Gearbox HT-2; Input Lateral Accelerometer Time Histories.

steady over the entire test period. The transient at hour 1140 is not explainable at this time. The initial lower data level from commencement of testing to approximately 140 hours is no doubt reflective of the test cell mechanical problem previously described.

Figures 75(A) and (B) present similar data for the output lateral accelerometer. The output data for all four trend curves appears even smoother and steadier than that for the input accelerometer.

Low Frequency Vibration Data Frequency Analysis

Spectral presentations taken at even intervals during the testing of HT-3 support the evidence produced by the other sensor data, oil analyses, and mechanical inspections that very little wear had taken place in this gearbox. A comparison of the six spectral displays of Figures 76 (A) through (F), the input lateral accelerometer power spectral density, shows little change in the structure over the 1500-hour period. A similar statement can be made by inspecting Figures 77 (A) through (F). These are power spectral densities of the output lateral accelerometer.

In all the illustrations, the horizontal line represents the geometric mean (or average logarithmic level) of the 512-line PSD.

Summary of HT-2 Gearbox Test Results

The majority of the sensor data accumulated from gearbox HT-2 supports conclusions drawn from oil analysis and bearing inspection reports that only small wear took place in the components of this gearbox. Further substantiation was given by testing HT-2 an additional 1460 hours after this data was accumulated for the polymer accelerometer evaluation.

In addition to these conclusions, a certain confidence factor was added to the test data collected from the other five gearboxes tested under this contract, since identical loading conditions were applied to all, with some producing more or less wear than others.

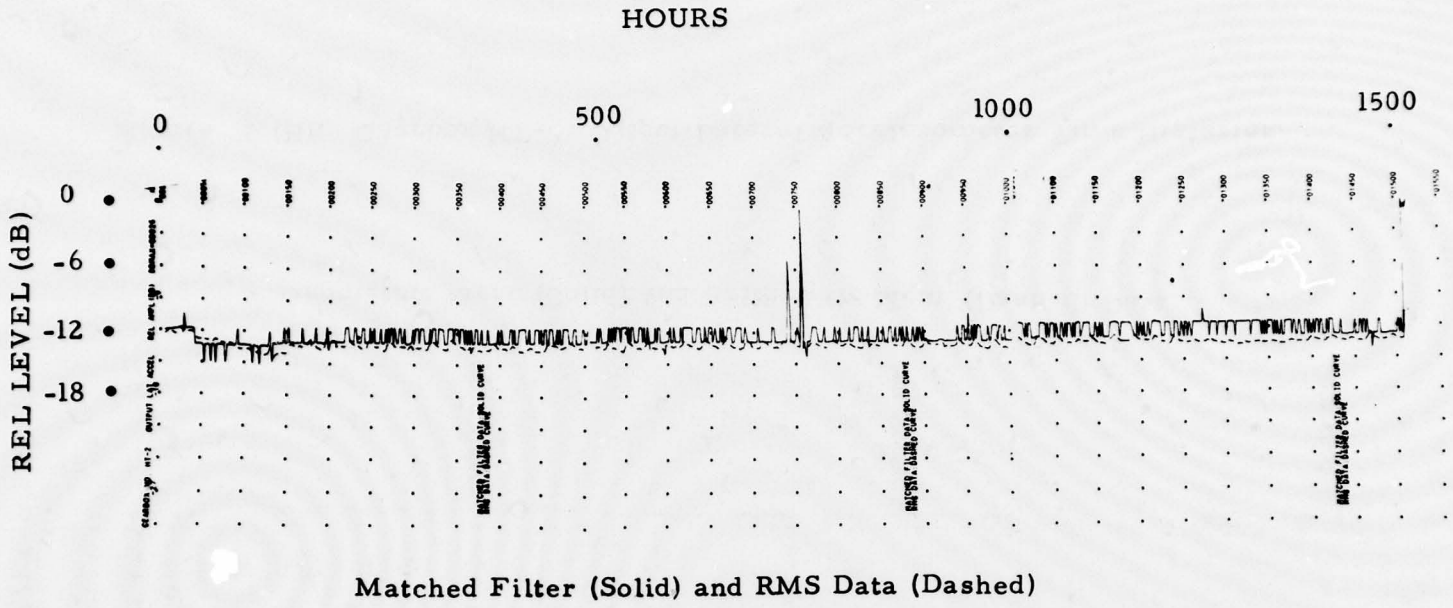

Figure 75 (A). Gearbox HT-2; Output Lateral Accelerometer Time Histories.

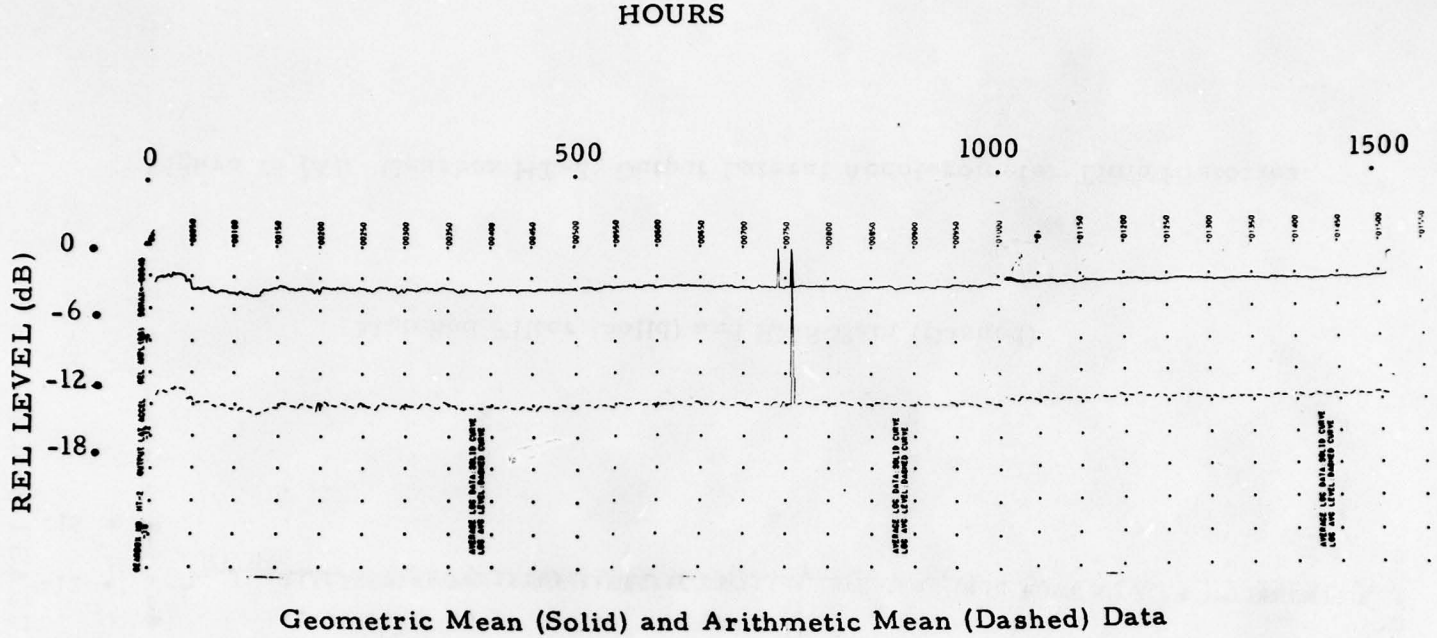

Figure 75 (B). Gearbox HT-2; Output Lateral Accelerometer Time Histories.

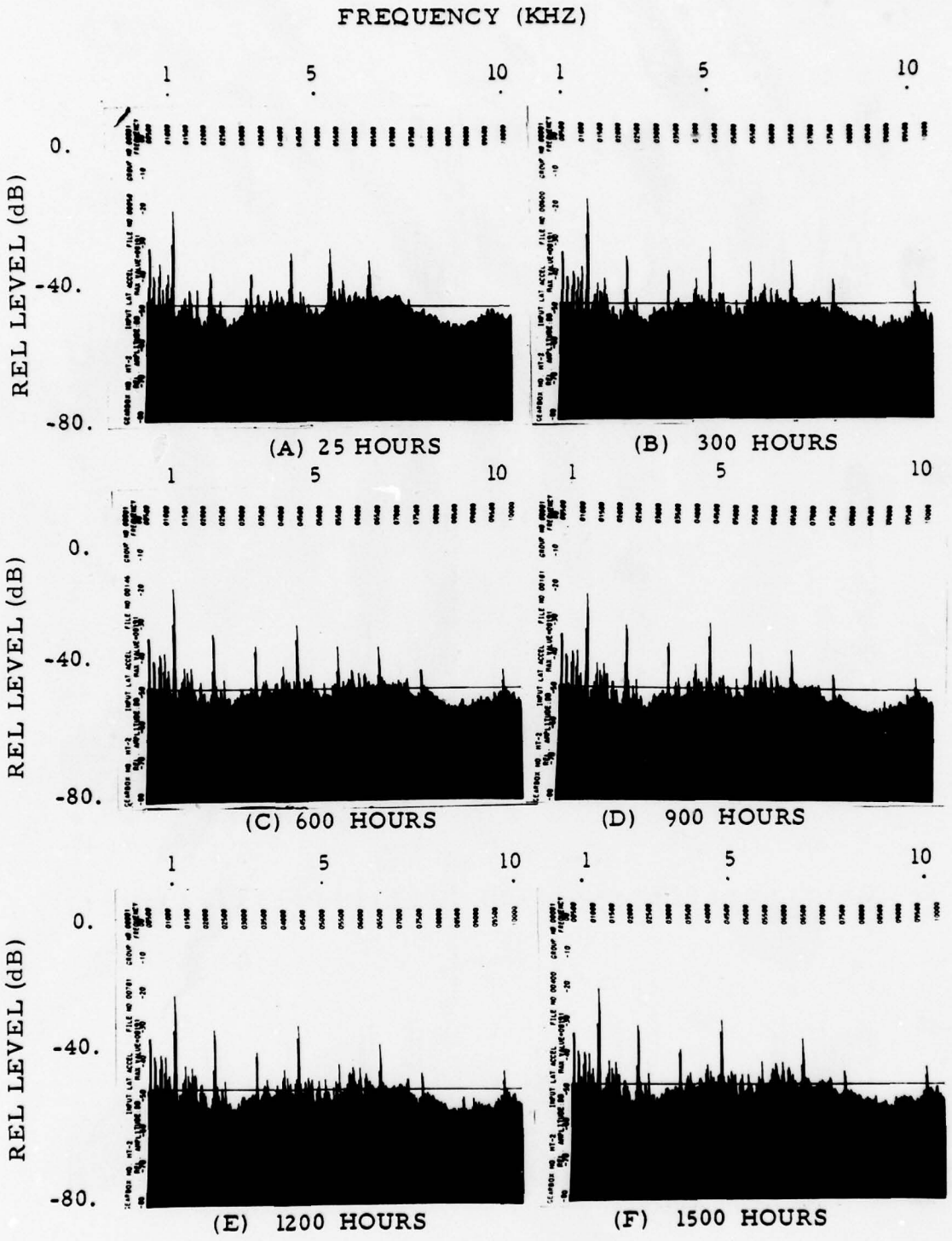

Figure 76. Gearbox HT-2; Input Lateral Accelerometer Power Spectral Density.

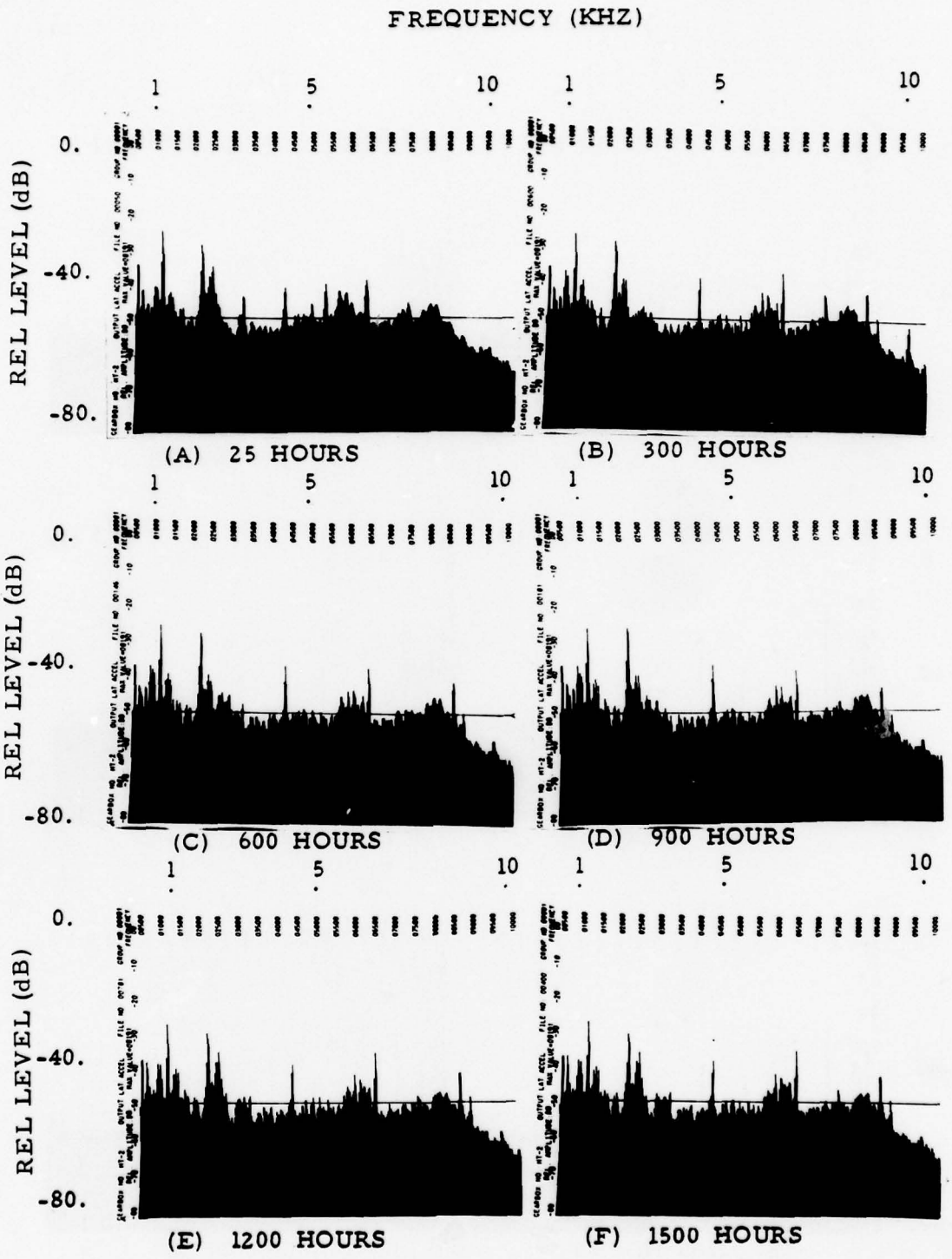

Figure 77. Gearbox HT-2; Output Lateral Accelerometer Power Spectral Density.

HT-3 GEARBOX TESTS

Gearbox HT-3 was the fifth gearbox selected for testing under the present contract. It had two prior overhauls and 1991 hours usage since new. It was removed from service for TBO change, with no apparent defect (Defect Code 803).

There were two phases of testing for this gearbox. Testing was initially terminated with 920 hours accumulated. Since no apparent wear trends were developing, it was decided to remove the gearbox and replace it with gearbox HT-4. This was an attempt to maximize the amount of wear trend data in the available test hours. No intermediate mechanical inspection was made on HT-3. It was kept intact in the event that testing would be resumed at a later date.

Testing was resumed on HT-3 after completion of HT-4 testing. An additional 517 hours of testing were accumulated on this gearbox before an extremely worn No. 4 bearing forced termination of testing.

Mechanical Condition of HT-3 Gearbox (Serial No. B13-5833)

Pre-Test Inspection

During the preliminary mechanical inspection, the ring and pinion gears appeared to be satisfactory, with no scuffing or bad wear pattern. The initial bearing inspection report on HT-3 listed ball bearings 1 and 2 as having moderate wear and ball bearings 3 and 4 as having heavy wear. The roller bearings 5 and 6 were described as in generally good condition.

Post-Test Inspection

Upon removal of the HT-3 gearbox from the test stand, it was observed that the case was full of metal particles. This had been observed in the oil and from the Tedeco chip detector. The initial mechanical inspection indicated that the ring and pinion gears appeared to have excessive, although fairly smooth, wear patterns. Both the No. 1 and No. 2 ball bearing assemblies rotated rather smoothly, with the No. 1 bearing showing the most wear. The No. 3 and No. 4 bearings were excessively worn, with No. 4 bearing exhibiting the noisiest rotation. No. 5 roller bearing was in fair shape, but No. 6 bearing rollers were chipped and pitted badly. The bearing inspection report corroborated that both No. 1 and 2 bearings now had heavy wear and bearings No. 3 and 4 had extreme wear. Very little change in raceway wear depth or radial play was measured.

Spectrometric Oil Analysis (SOA)

Fifty one oil samples were collected for the 1437-hour test period. Thirty one of these samples were taken during the first 920 hours. Figure 78 presents the iron content in the oil (parts per million) versus HT-3 gearbox running time. Only iron content was plotted because of the rather low content of other elements. The only significant iron content occurred during the last 400 hours. In contrast, some of the other test data show wear trends starting to develop as early as the 600th hour of the first test interval. It is not until the last 100 hours of testing that a significant amount of iron was generated. This was also detected by the Tedeco chip detector.

All the oil analyses, particle count, GE oil monitor, and direct-reading ferrograph indicate that the peak iron content occurred at approximately hour 1360. It will be seen later that the accelerometer trending curves also peak approximately at this time.

Temperature Sensors

Figures 80 (A) and (B) present the time history of gearbox HT-3 oil and ambient temperature versus test time. The oil temperature rises gradually during the last 400 hours of testing, actually accelerating its rise during the last 100 hours. Table 3 presents the approximate average oil and ambient temperature during this period. This oil temperature rise approximates the output accelerometer trending curves presented in a later section and correlates very well with the wear process that took place in this gearbox. The fact that ambient temperature does not rise in the same proportion as the oil temperature indicates that the temperature rise is definitely due to increased frictional losses in the gearbox.

RPM and Torque Indicators

Figures 81 (A) and (B) present input and output rpm, respectively, for gearbox HT-3. These stayed very steady at approximately 4160 and 1600 rpm, respectively.

Figures 82 (A) and (B) illustrate the variations in input and output torque, respectively. Although the variation approached 3 percent at times, both

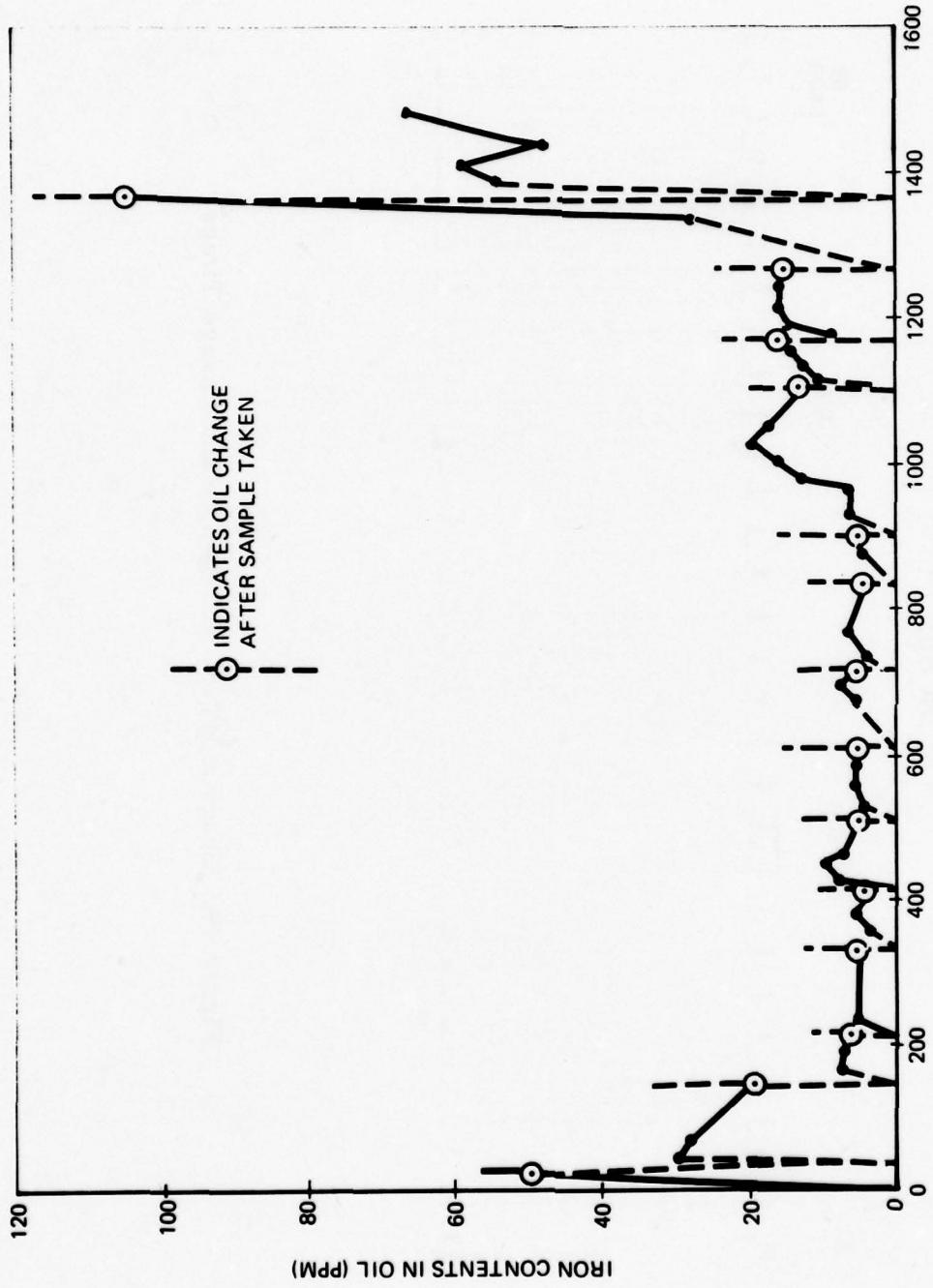

Figure 78. Spectrometric Oil Analysis-Gearbox HT-3.

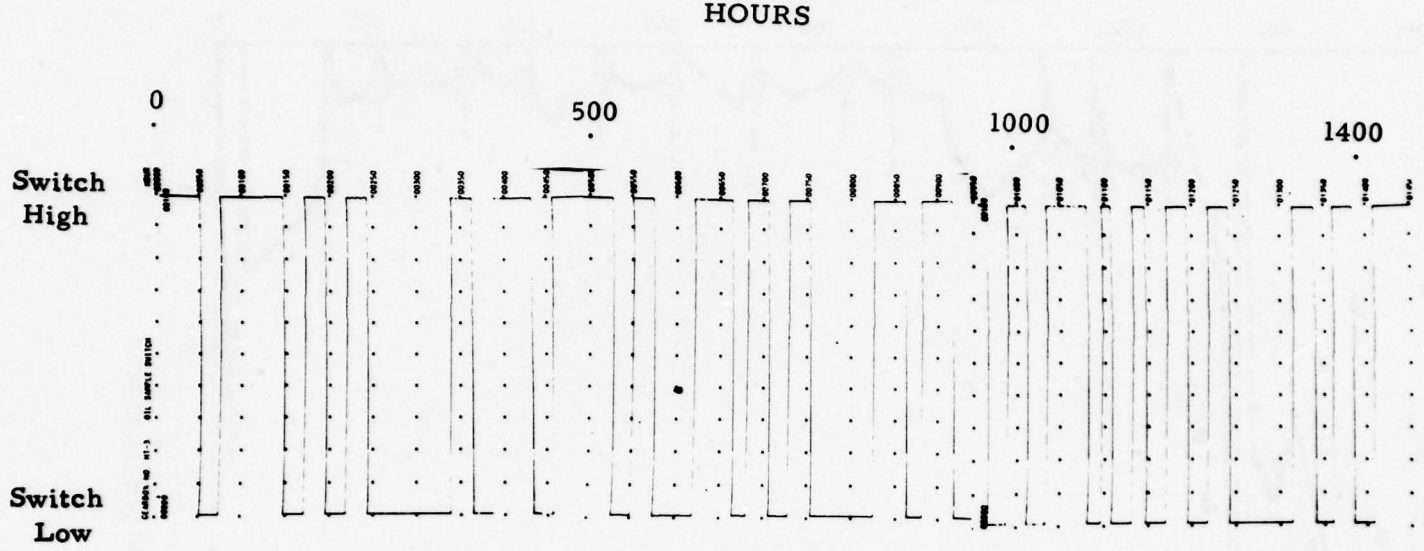

Figure 79. Gearbox HT-3: Oil Sample and Change Times.

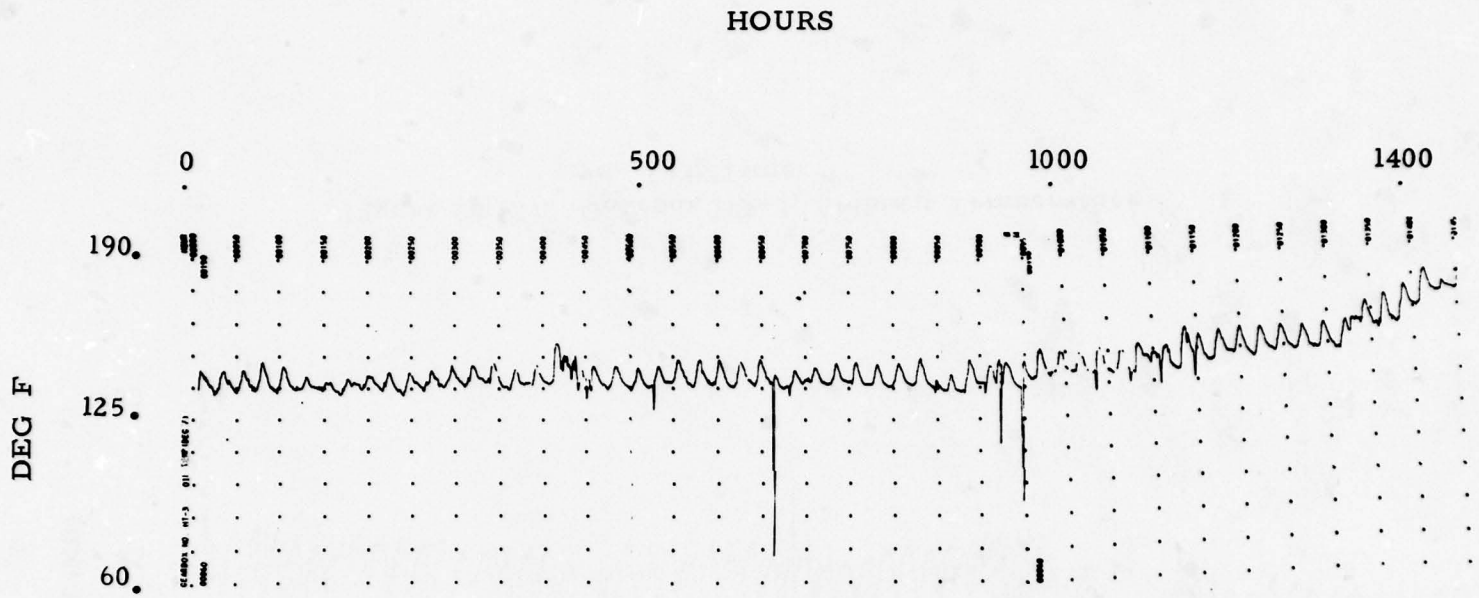

Figure 80 (A). Gearbox HT-3; Oil Temperature vs. Test Time.

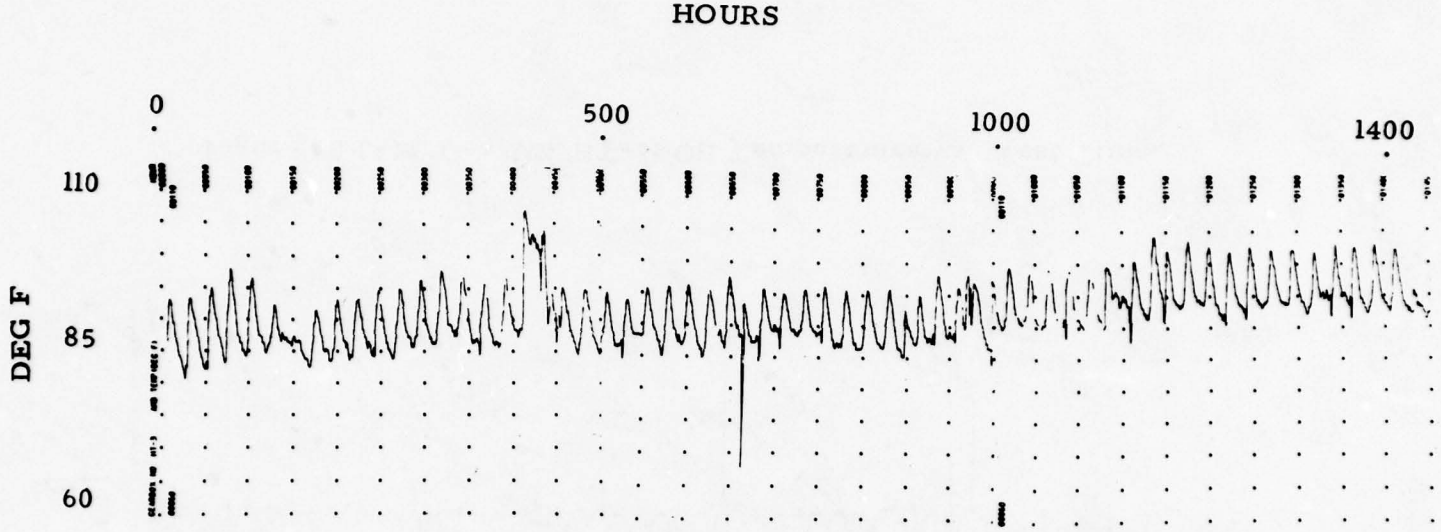

Figure 80 (B). Gearbox HT-3; Ambient Temperature vs. Test Time.

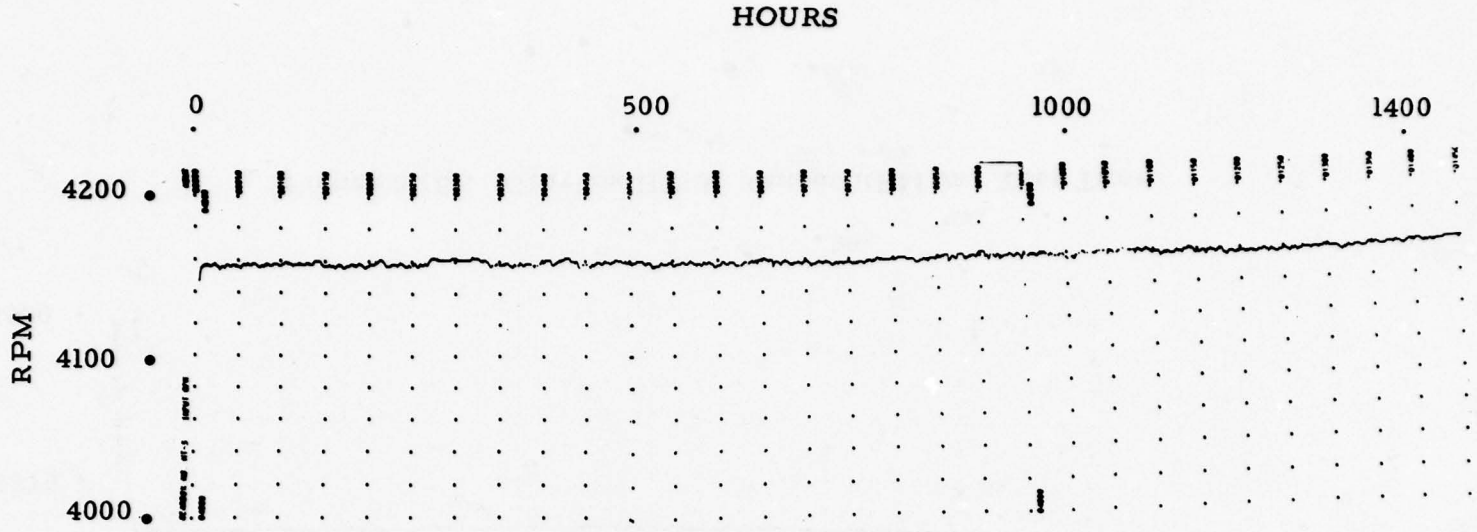

Figure 81 (A). Gearbox HT-3; Input RPM vs. Test Time.

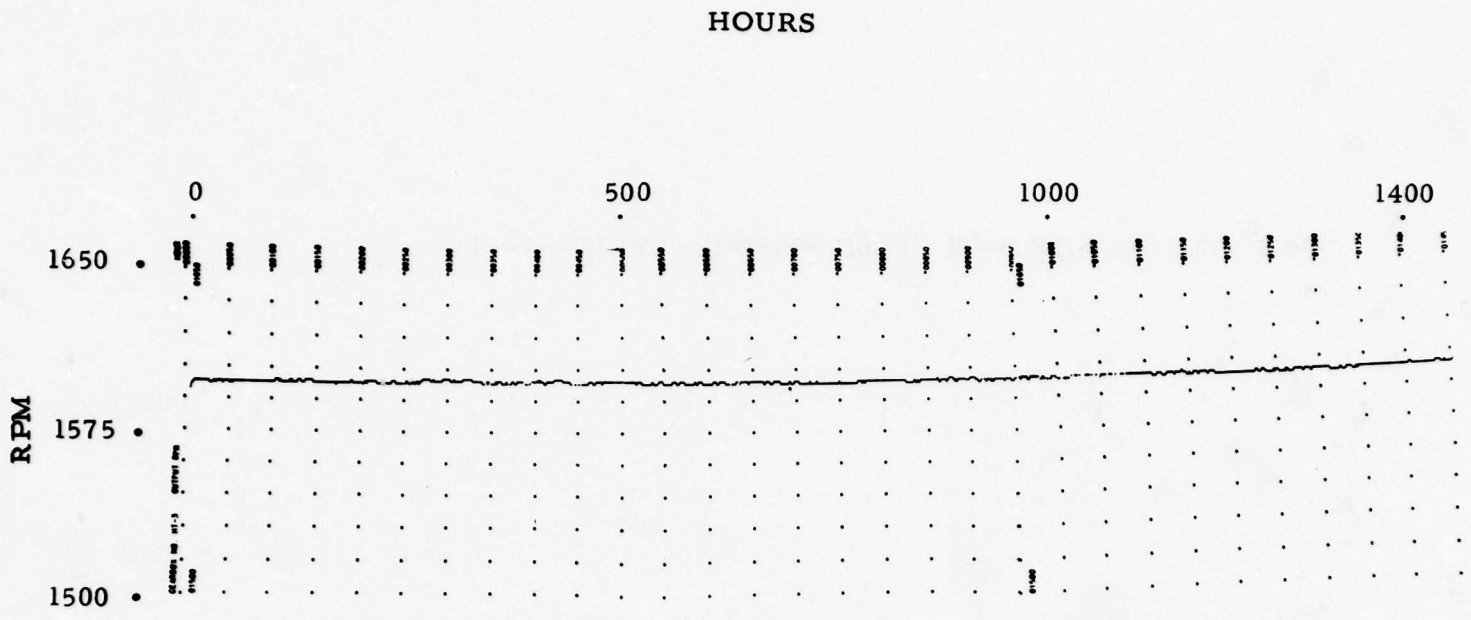

Figure 81(B). Gearbox HT-3; Output RPM vs. Test Time.

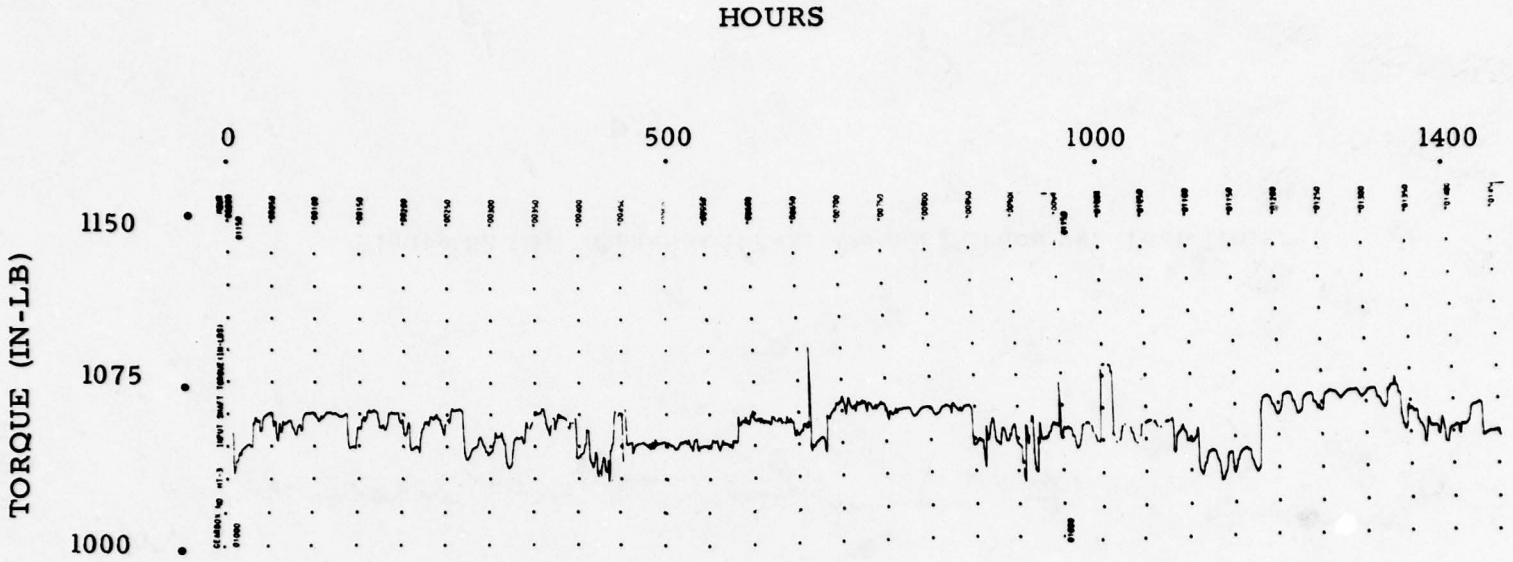

Figure 82 (A). Gearbox HT-3; Input Torque vs. Test Time.

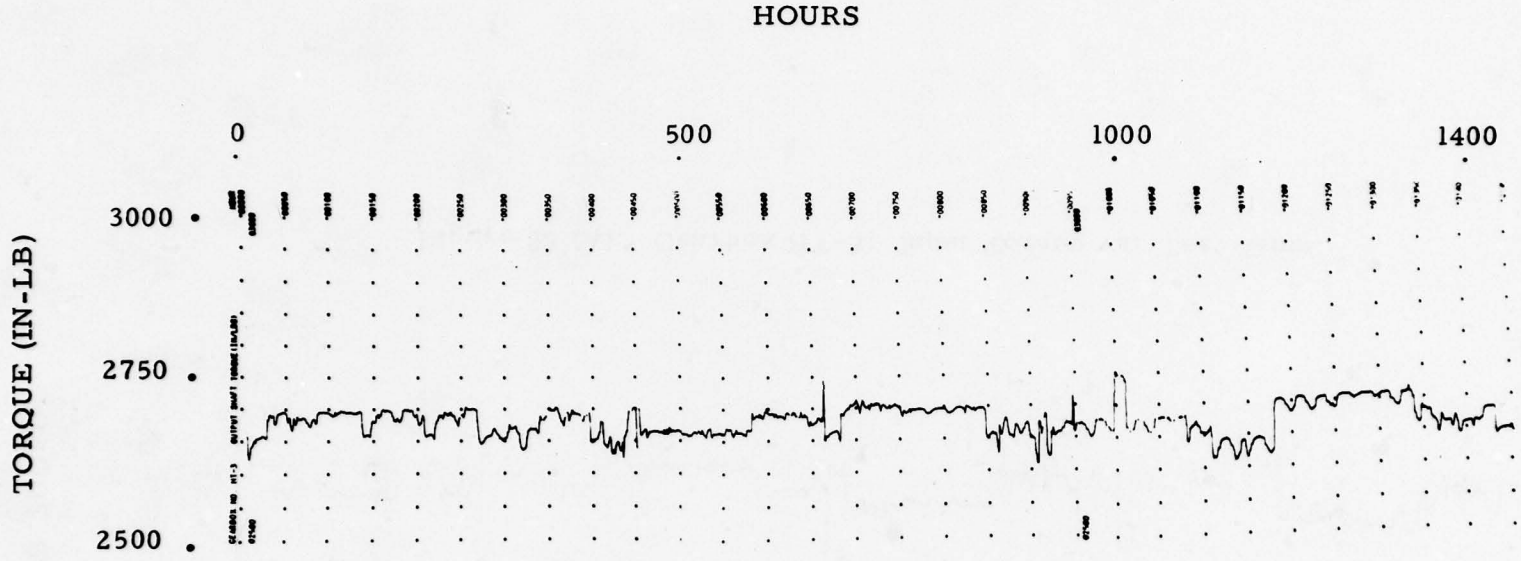

Figure 82 (B). Gearbox HT-3; Output Torque vs. Test Time.

GEARBOX HT-3;
TABLE 3. AVERAGE OIL AND AMBIENT TEMPERATURE VERSUS TEST TIME

Hour	Oil Temp. (Deg. F)	Ambient Temp. (Deg. F)
1000	145	94
1100	150	95
1200	153	98
1300	154	98
1400	171	98

input and output torque varied together. These variations were no doubt due to slightly different settings of the pressure relief valve for the hydraulic portion of the system. This statement is borne out by examining Figure 82(C), which plots gearbox efficiency versus time. Through all these torque variations the gearbox efficiency remained fairly steady at 97 percent.

The tracking of input and output torque indicates that the resultant wear and friction in the gearbox was associated with the output section of the gearbox, since input friction alone should be reflected in only an increase in input torque.

Tedeco Chip Detector

Table 4 presents the cumulative chip detector count versus test time. At 1027 hours, chip activity began at a low level. It was not until the last 70 hours of testing that a large chip count was experienced. This correlates well with the SOAP analysis.

Ultrasonic RMS Accelerometer Data

Figures 83(A) and (B) present the time history of the input and output ultrasonic RMS data. The input data appears to be extremely erratic. There is a correlation, however, with the low frequency data from this same accelerometer. The step increase at hour 1300 appears on both data curves. (See Figure 87 also.) The exact cause of the wild excursions in Figure 83(A) during the earlier testing is undetermined.

The output ultrasonic RMS data is more well-behaved. Looking at Figure 83(B), the sudden step drop in level at hour 950 occurred at the

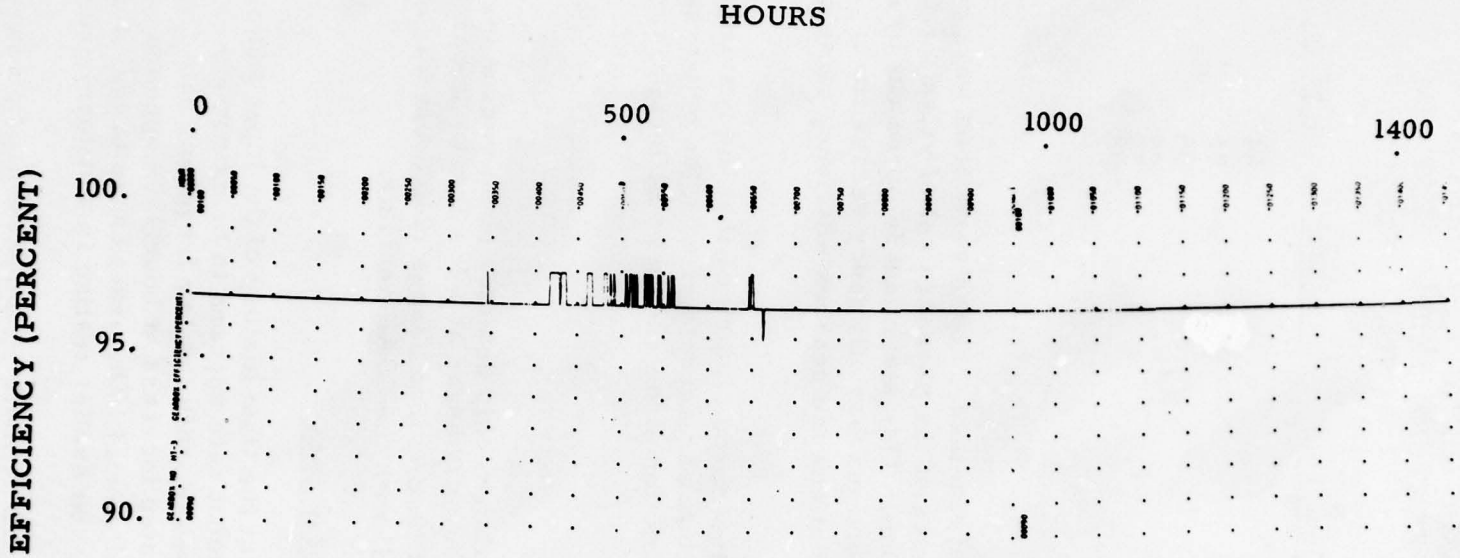

Figure 82 (C). Gearbox HT-3; Gearbox Efficiency vs. Test Time.

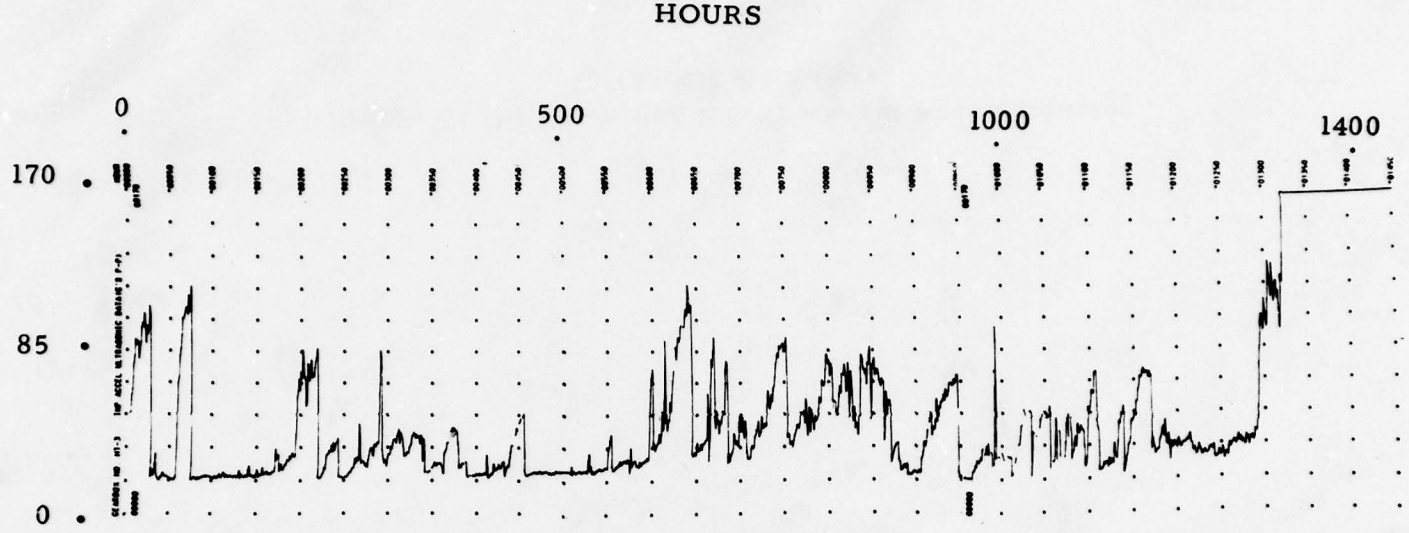

Figure 83 (A). Gearbox HT-3: Input Accelerometer Ultrasonic RMS Data.

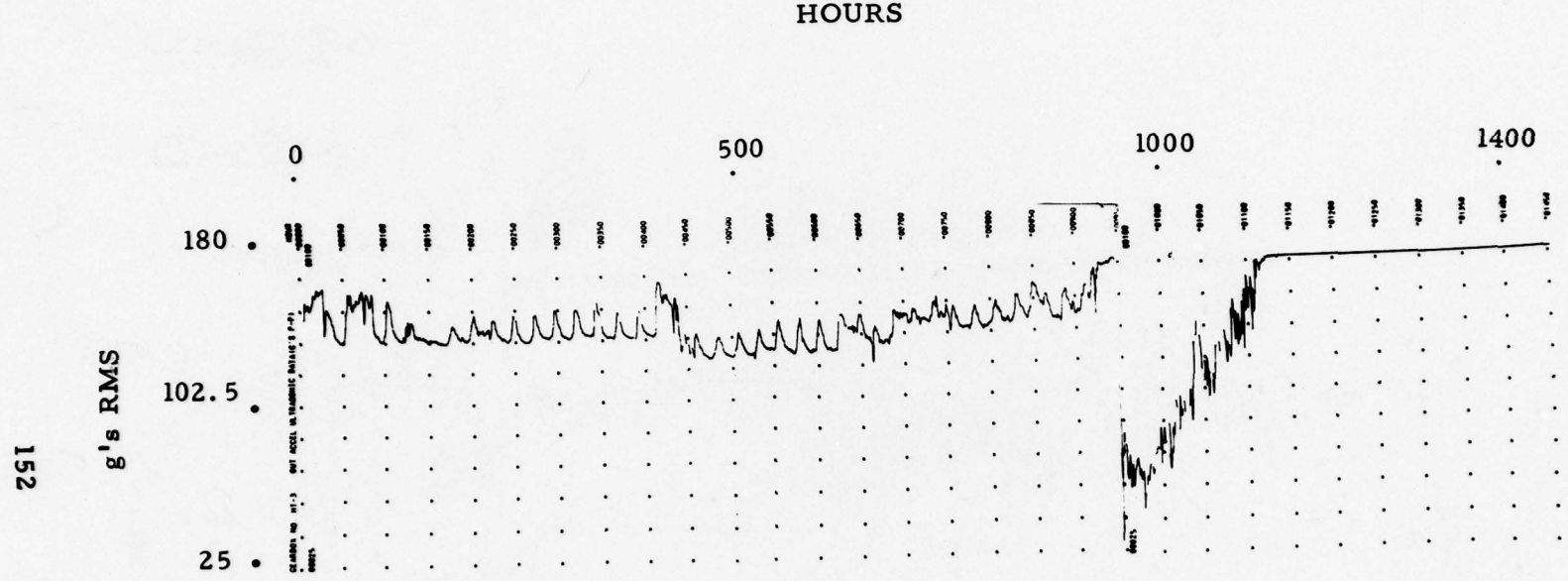

Figure 83 (B). Gearbox HT-3; Output Accelerometer Ultrasonic RMS Data.

TABLE 4. GEARBOX HT-3; TEDECO CHIP DETECTOR BURN-OFFS

Gearbox Running Time (Hrs)	Cumulative Chip Burn-Off Count
100	0
1027	1
1161	3
1193	4
1337	6
1361	1 67 (Loaded with metal particles)
1408	1 68
1432	1 70

interval when testing of gearbox HT-3 was temporarily halted and gearbox HT-4 was tested. It is seen that a trend had already begun prior to this, with the g-level gradually rising about 1-2 dB over a 250-hour period. This is also observable from the various trending curves for the lower frequency energy from the output accelerometer (see Figures 88(A) and (B)). The reason for the new steady state level after test resumption in Figure 83(B) is not certain. However, it did maintain a fairly steady rise from this point on until limiting occurred in the circuitry.

It appears from the output ultrasonic RMS data that a definite wear trend is observable starting at hour 700.

Shock Pulse Analyzer

During the second phase of HT-3 testing, erratic behavior developed in the SKF shock pulse instrumentation. As a result, only shock profile results for the first 1000 hours are available. These curves are plotted in Figures 84 and 85. Very little change in the shock profile measurements was observed during the early testing. As a result, only one curve, representing the average profile, is shown for each accelerometer.

Figure 86 illustrates the SKF peak shock value measured by the output shock accelerometer. Step changes in value at various times are due to inadvertent monitoring of the input accelerometer after measurement of the daily shock profile curves.

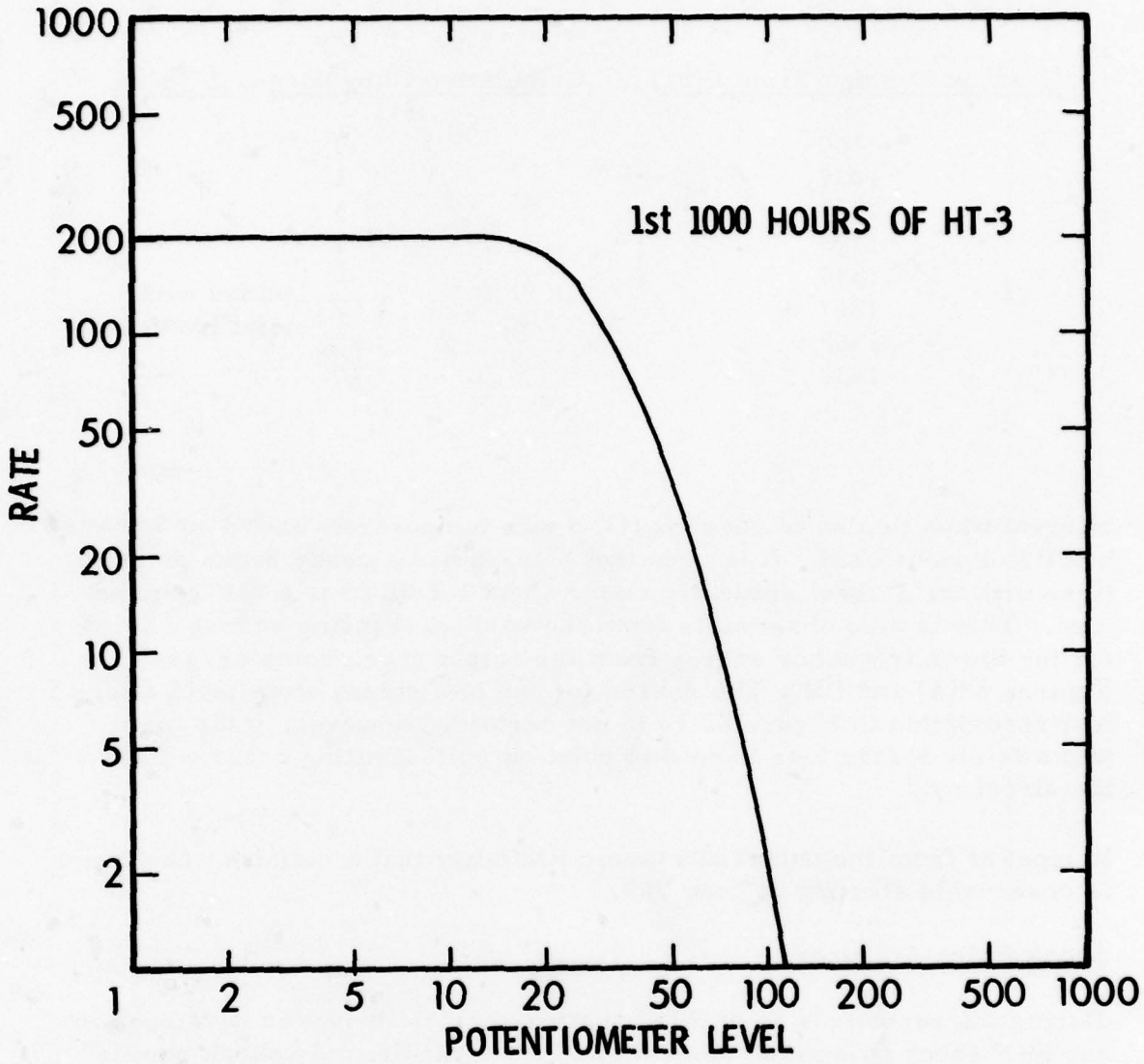

Figure 84. Gearbox HT-3; Shock Profile Curve, Input Accelerometer.

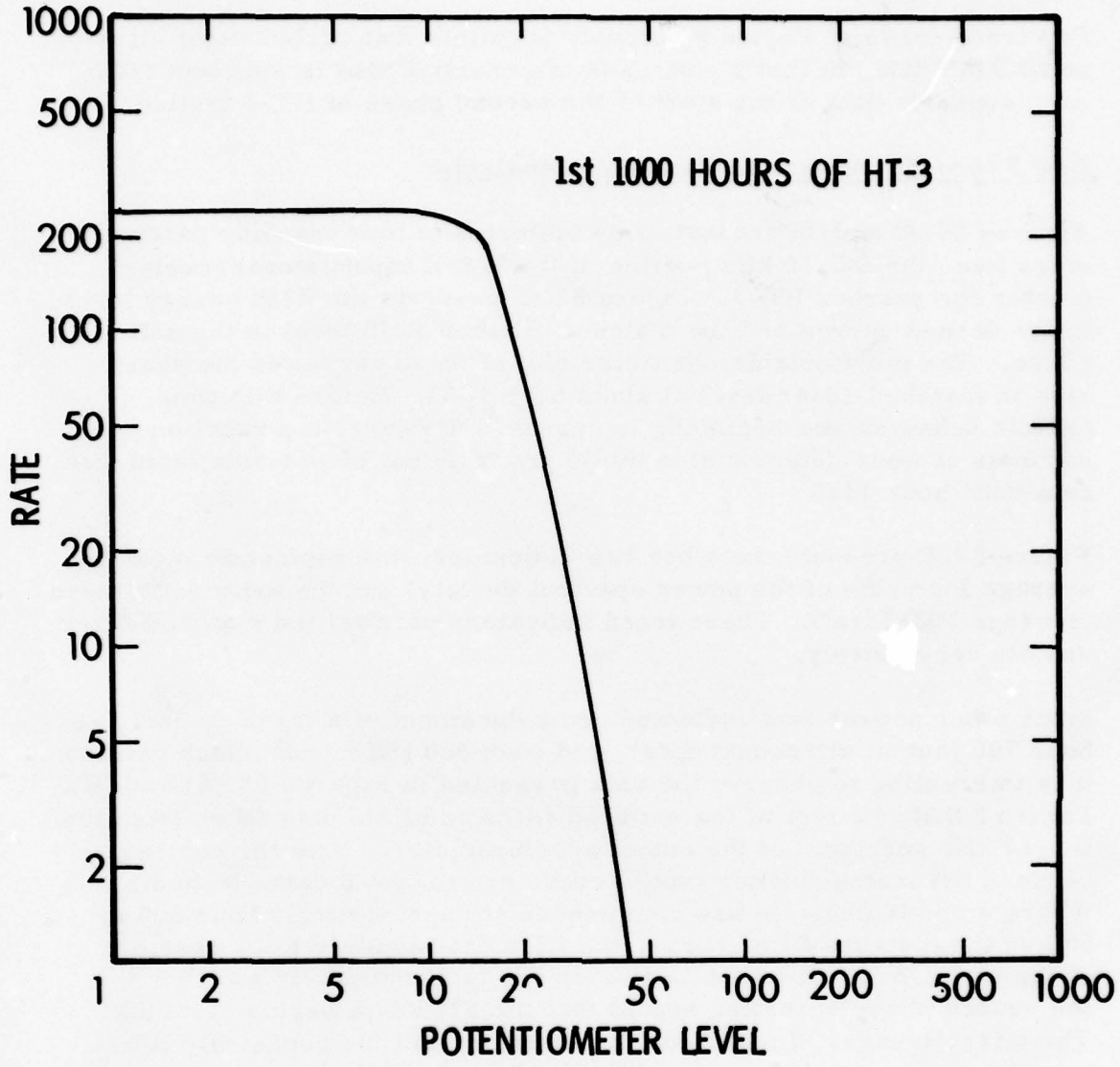

Figure 85. Gearbox HT-3; Shock Profile Curve, Output Accelerometer.

The trend curve of Figure 86 closely parallels that of the output ultrasonic RMS data in that a noticeable exponential rise is apparent from each sensor's data at the start of the second phase of HT-3 testing.

Low Frequency Vibration Data Time Analysis

Figures 87(A) and (B) present time histories of four trending parameters from the DC-10 kHz portion of the B & K input lateral accelerometer for gearbox HT-3. Figure 87(A) presents the RMS energy level in the dashed curve and the matched-filtered RMS level in the solid curve. The most notable characteristic of these curves is the sharp rise in matched-filter level at about hour 1250. Before this time, erratic behavior was beginning to appear. However, a prediction estimate of wear deterioration would probably not be possible from this data until hour 1250.

Figure 87(B) presents the other two indicators: the geometric mean (or average log value of the power spectral density) and the arithmetic mean (average PSD level). These trend indicators parallel the matched-filter results very closely.

Since other sensor data indicated commencement of a trend as early as hour 700 (output ultrasonic data) and hour 960 (SKF peak shock values), it is interesting to observe the data presented in Figures 88 (A) and (B). Figure 88(A) is a plot of the matched-filter and RMS data taken from the DC-10 kHz spectrum of the output accelerometer. Note the contrast between the matched-filter (solid) curve and the RMS data (dashed). Where a continuing rise has commenced at approximately hour 600 or 650 on the matched-filter curve, the RMS data appears to be possibly dropping slightly. It is not until hour 990 (approximately when the second phase of testing began) that the RMS data begins climbing. The attractiveness of matched-filter trending is thus repeatedly illustrated in these gearbox tests. With 1437 hours of total test time on this gearbox, the output matched-filter curve indicated a wear trend at approximately the midpoint of testing, an impressive 700 hours before the test had to be stopped!

The results obtained from geometric mean and arithmetic mean trending are equally impressive. These results are presented in Figure 88(B). Note that the rate of change of these two curves is extremely close. The time when the wear trend appears to start is approximately hour 600. The dynamic range of the complete wear process is approximately 14 dB for the geometric and arithmetic mean curves and 15 dB for the matched-filter curve.

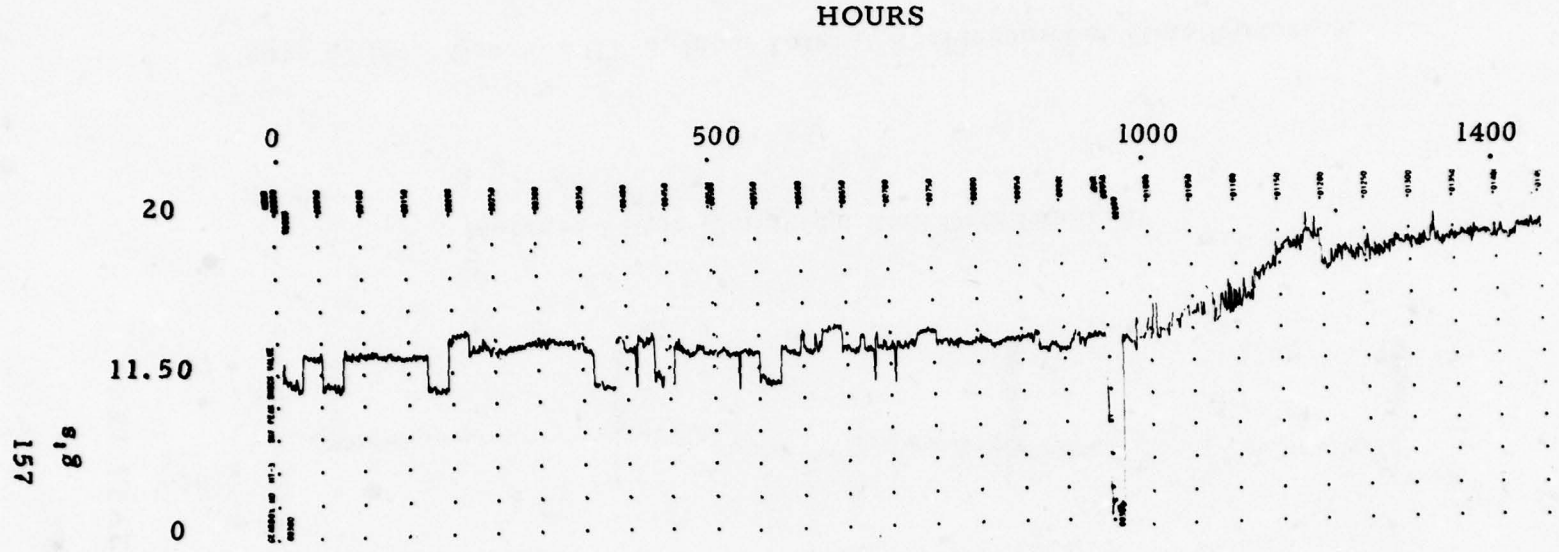

Figure 86. Gearbox HT-3; SKF Peak Shock Value (Output Shock Accelerometer).

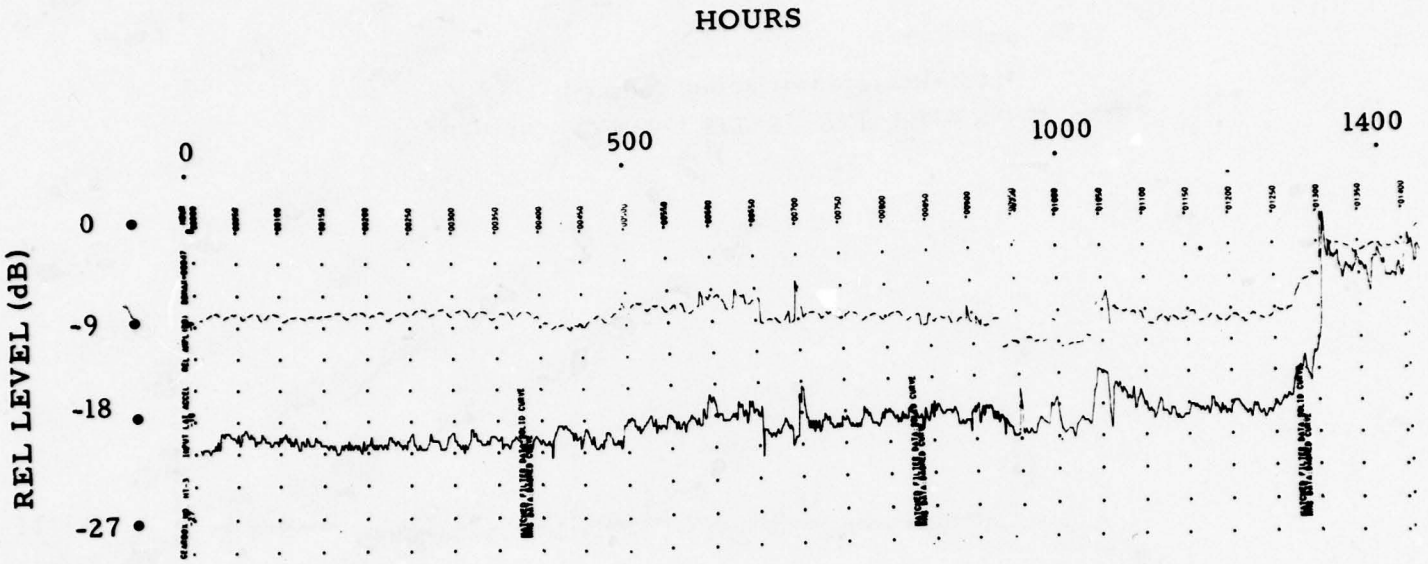

Matched Filter (Solid) and RMS Data (Dashed)

Figure 87 (A). Gearbox HT-3; Input Lateral Accelerometer Time Histories.

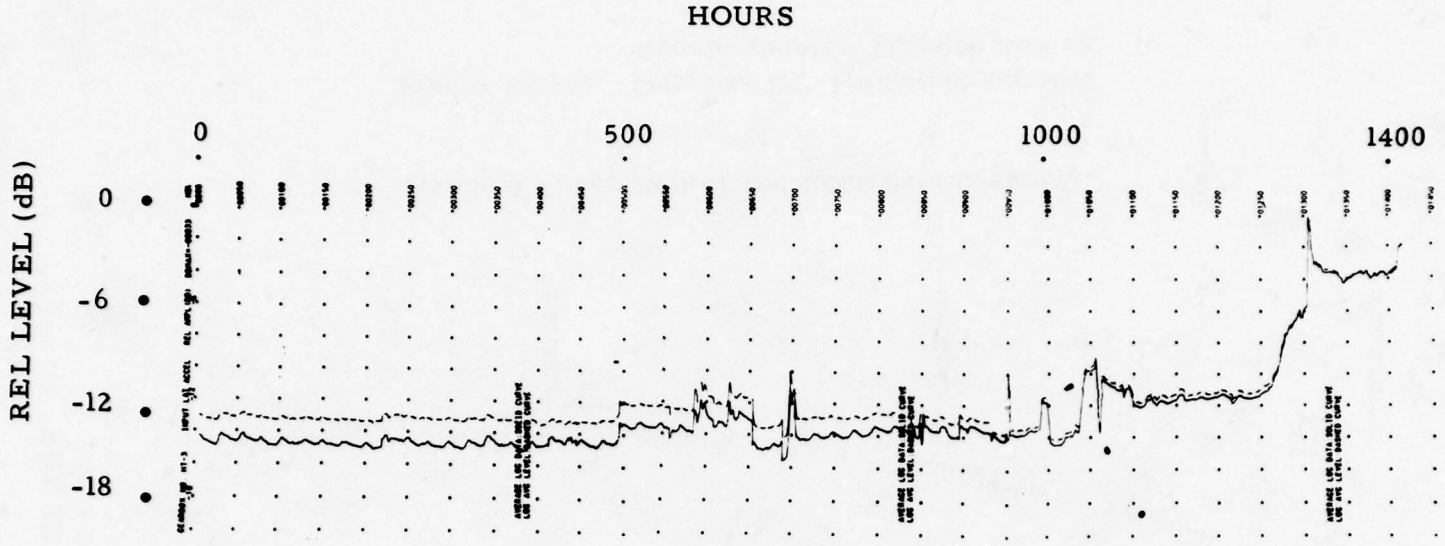

Geometric Mean (Solid) and Arithmetic Mean (Dashed) Data.

Figure 87 (B). Gearbox HT-3; Input Lateral Accelerometer Time Histories.

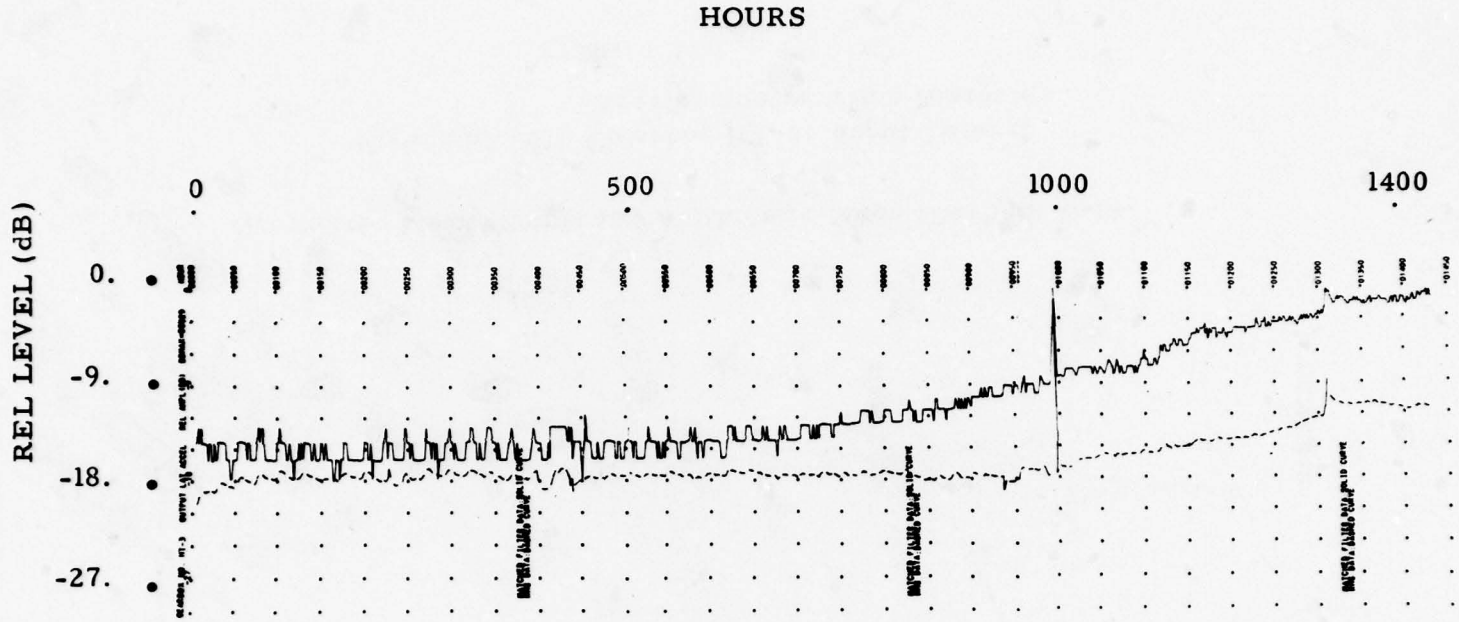

Matched Filter (Solid) and RMS Data (Dashed).

Figure 88 (A). Gearbox HT-3; Output Lateral Accelerometer Time Histories.

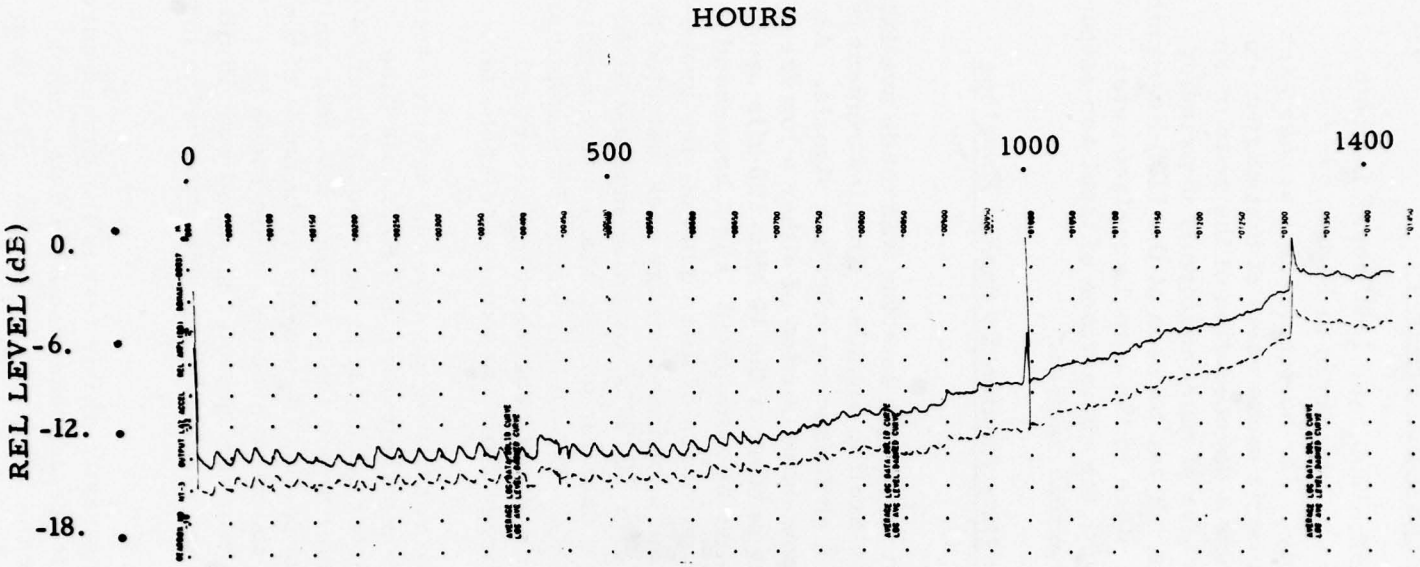

Geometric Mean (Solid) and Arithmetic Mean (Dashed) Data.

Figure 88 (B). Gearbox HT-3; Output Lateral Accelerometer Time Histories.

Low Frequency Vibration Data Frequency Analysis

Power spectral densities at 5, 750, 1150, and 1400 hours for both input and output accelerometers are presented in Figure 89 (A-D) and Figure 90 (A-D), respectively. The horizontal line across each presentation represents the geometric mean value at that particular time. Both presentations show a degeneration of the gear-mesh structure with time and an increase of more uniformly distributed spectral lines as wear increases. It can be seen at the 1150-hour point that more degradation has taken place in the output accelerometer presentation. This correlates with the comparison of input and output trend curves described in the previous section.

Results of B & K Accelerometer Data Applied To Shaker Envelope Detector

Late in this program, the Shaker envelope detector was made available by Fort Eustis for evaluation of vibration signals. This instrument is capable of envelope detection of high frequency vibration signals. As designed, it may examine a narrow-band portion of either a low frequency band from 2-2400 Hz or a portion of the 10 kHz-100 kHz band. In addition, the bandpass filter may be eliminated and a broadband spectrum may be detected. For purposes of this contract, the broadband mode was used, and the same broadband energy peak detected by the ultrasonic RMS detector (20 kHz-100 kHz) was also inputted to the Shaker instrument. The envelope detector output, then, was a replica of any amplitude fluctuations within a DC-10 kHz band. This amplitude modulation energy was then digitized and processed in an identical manner to the raw DC-10 kHz energy from the same accelerometer.

Figures 91 (A) and (B) present the results of the envelope detector trending. Figure 91(A) illustrates the matched-filter and RMS data time history for the output accelerometer. The large step drop at hour 940 occurred when the testing was interrupted for a month. The relatively smooth climb after resumption of testing is impressive because of the dynamic range occurring during the wear process. This range is approximately 18 dB over a 500-hour test period, compared with 15 dB over an 800-hour test period for the matched-filter detection of the low frequency band.

Perhaps an even more interesting result of this test is the dashed curve of Figure 91(A). This represents the unprocessed RMS data, which yields 21 dB dynamic range over the 500-hour test period! This is in vivid contrast to the results obtained from low frequency RMS data. In

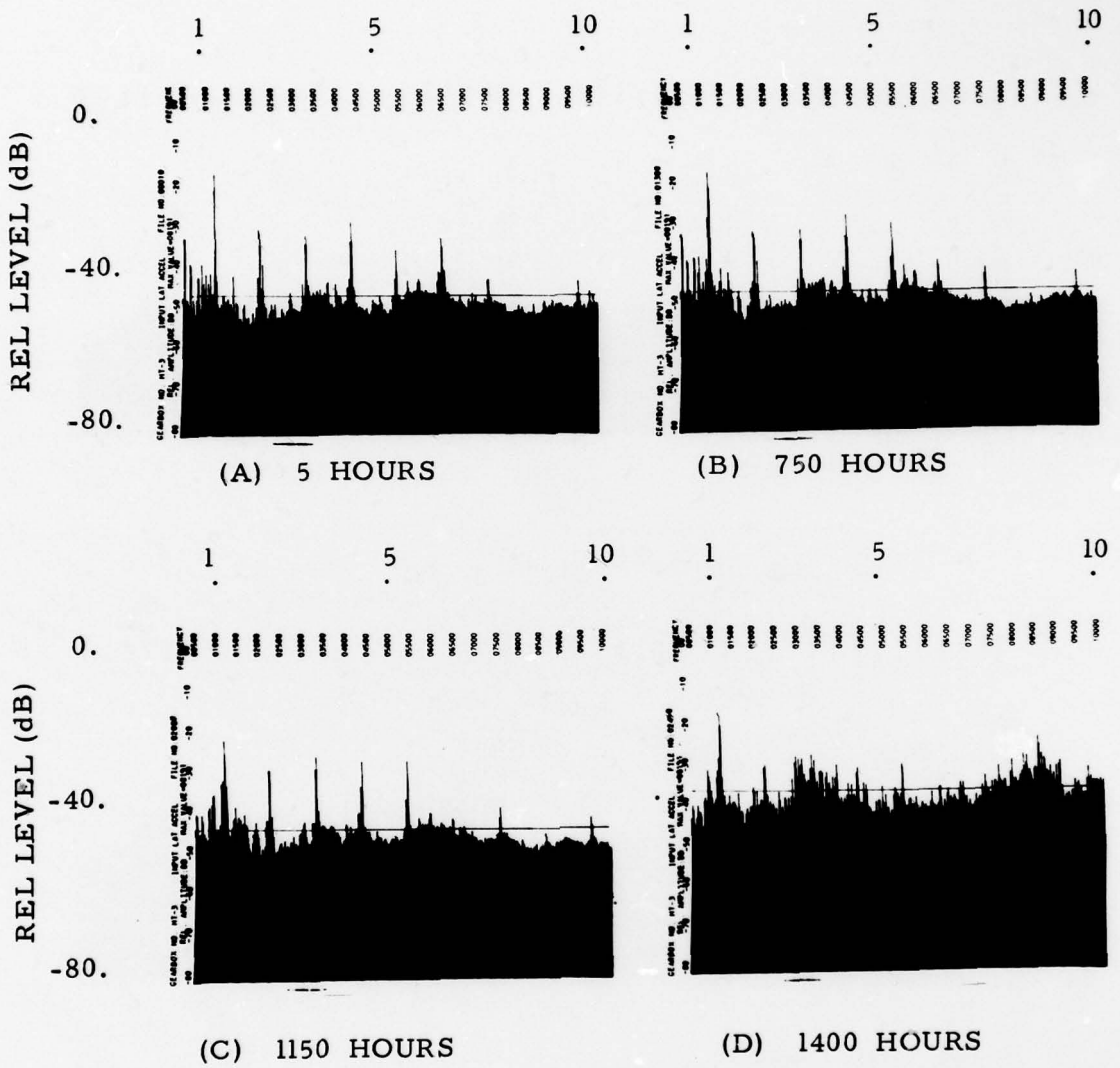

Figure 89. Gearbox HT-3; Input Lateral Accelerometer Power Spectral Density.

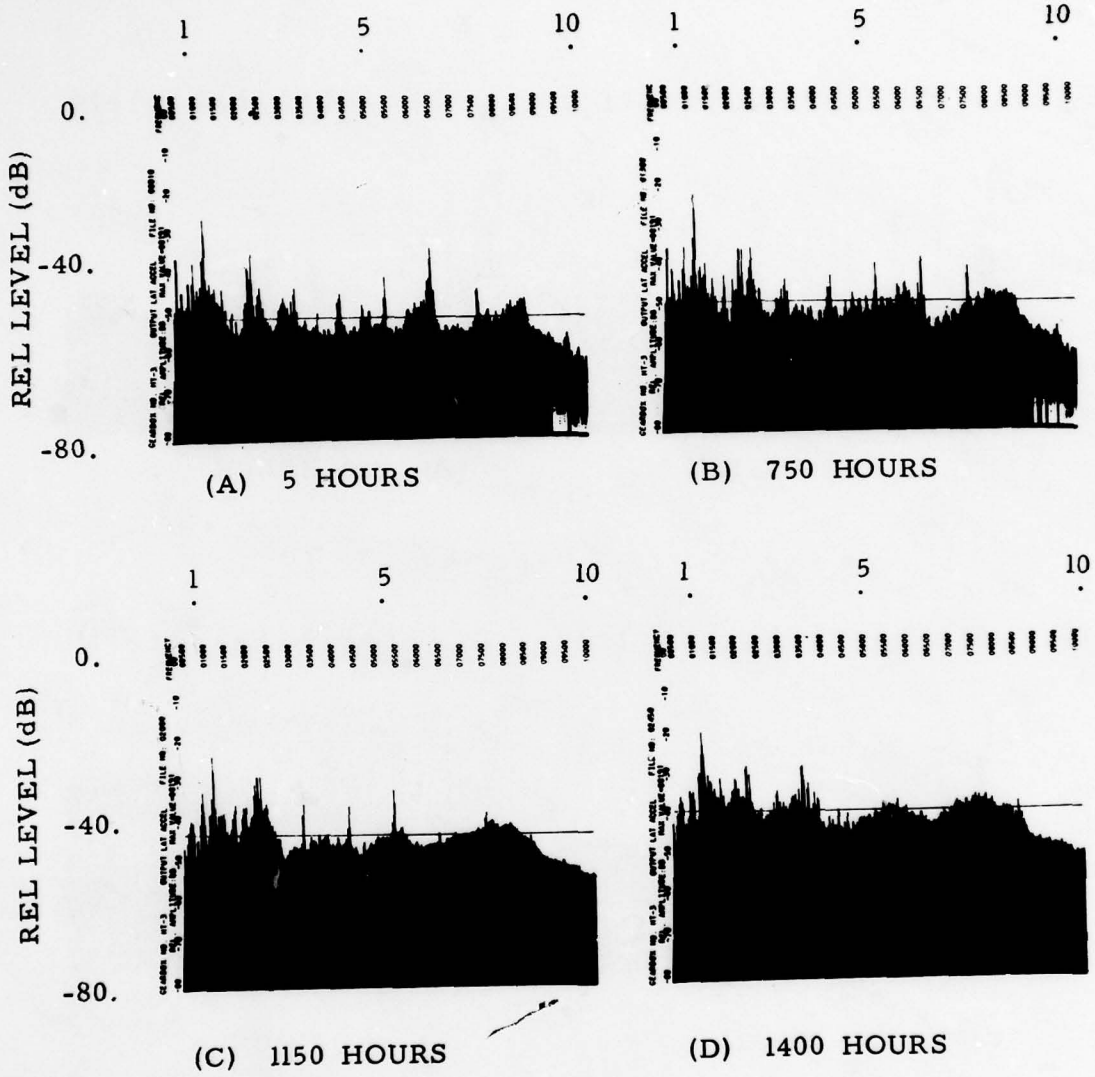

Figure 90. Gearbox HT-3; Output Lateral Accelerometer Power Spectral Density.

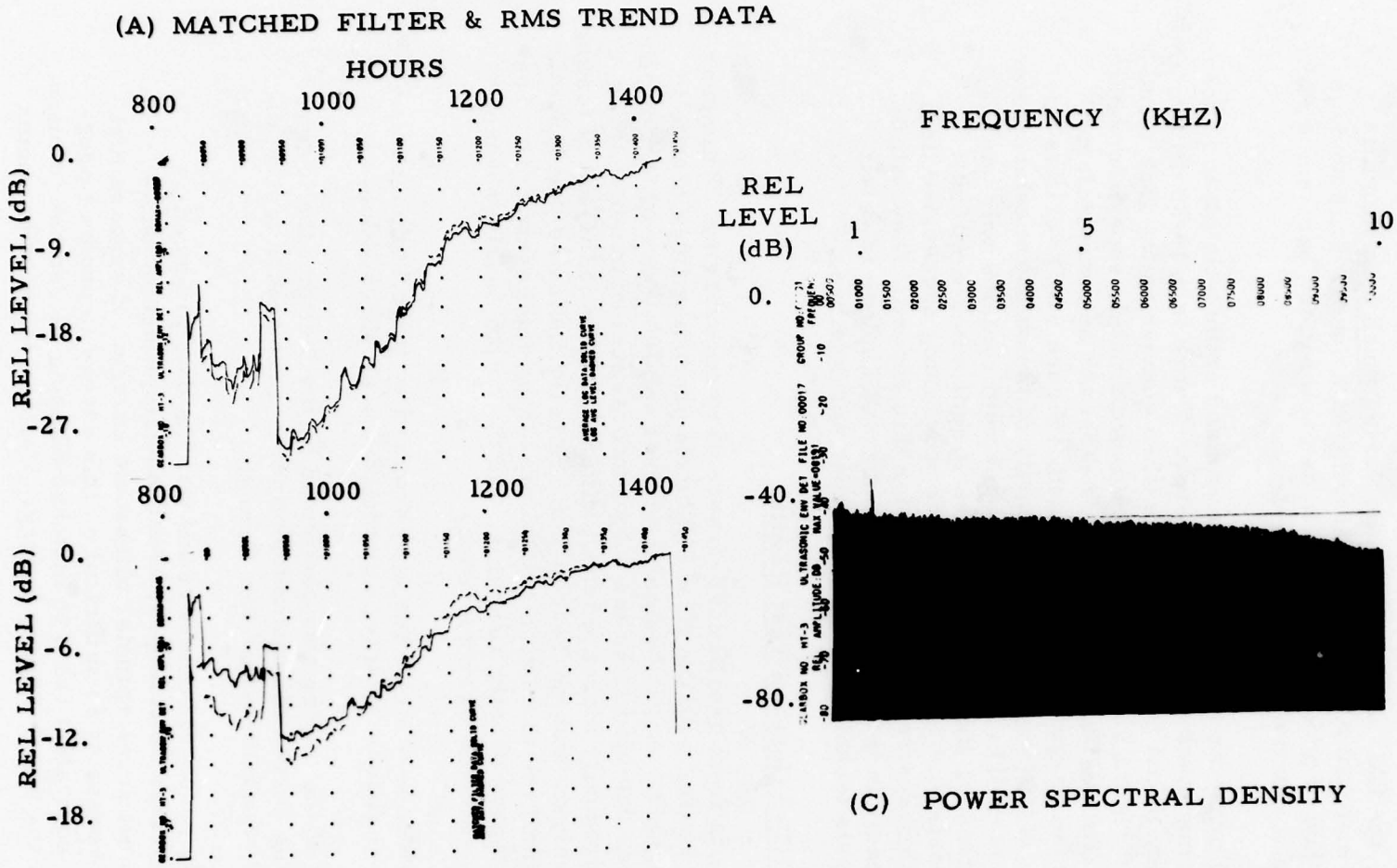

Figure 91. Gearbox HT-3; Output Accelerometer Ultrasonic Envelope Detector.

those cases, the RMS data consistently varied much less than data produced by matched filtering or averaging techniques. It is obvious that this method of processing needs to be explored further, since RMS processing is a relatively simple operation.

Figure 91(B) presents the geometric mean and arithmetic mean processing of this same envelope-detected energy. There is a 19-20 dB dynamic range present. What becomes obvious when comparing the four trending curves of Figure 91 is that they are approximately superimposed on each other. This definitely implies a "near-flat" or near-uniform frequency density across the 10 kHz band. Figure 91(C) verifies this implication. It is a power spectral density of the output accelerometer at the midpoint of HT-3 testing. The spectrum contains only one discrete frequency, the gear-mesh rate at approximately 1000 Hz. Unfortunately, time did not permit processing successive time histories of this spectral presentation for this report. They will be examined closely in the next report, which will explore in detail various analysis techniques using this contract data base.

Summary of HT-3 Gearbox Test Results

The test results from gearbox HT-3 were very encouraging. This gearbox ran 1437 hours, with the first 700 hours producing little change in the sensor signals. At the beginning of the final 700 hours of testing, a wear trend was detected from the output lateral accelerometer. This trend curve gradually increased until within 70 hours of the end of testing, both SOAP analysis and the Tedeco chip detector indicated that large amounts of small metal particles were present in the gearbox oil. The testing was stopped shortly after this, and the output bearings were found to be in extreme wear condition.

Supporting evidence of wear was also supplied by the oil temperature monitor, the ultrasonic energy, and the SKF peak shock value.

The integrity of the testing was confirmed by the fact that the low frequency trending curves maintained continuity even though testing of gearbox HT-3 was interrupted for 1 month.

A significantly encouraging test result was the data produced by the Shaker envelope detecting the broadband amplitude modulation on the output accelerometer ultrasonic energy. It appears that simple RMS processing is sufficient on this energy to produce prognostic data of equivalent value to matched-filtering or geometric mean processing of the low frequency energy. Further exploration seems warranted.

HT-4 GEARBOX TESTS

Gearbox HT-4 was the sixth gearbox selected for testing under the present contract. Although the repair/overhaul record indicated that this gearbox had a total of 588 hours usage since new, it also indicated that it had been used as a test gearbox at Parks College, Cahokia, Illinois, with rejected bearings installed. This was no doubt the case, as our preliminary bearing inspection indicated an extreme wear condition in bearings 3 and 4. These readings were the highest of all bearings in the gearboxes HT-2 through HT-5.

Testing on gearbox HT-4 was terminated because of excessive wear on the No. 1 and No. 2 input duplex bearing pair. A total of 552 hours of testing had been accumulated in a month's span of testing. The RMS level on the B & K input lateral accelerometer had been gradually rising over the test period when, one day, a large number of chip counts were recorded on the Tedeco chip detector. Darker oil and increasing chip counts were observed during the following days. Finally, the RMS level for the input accelerometer had risen more than 15 dB above the level at the start of testing, and the input ultrasonic detector for this accelerometer had reached a level where the A-D converter had begun to limit the data. It was decided that no further useful information could be gained in the test, so the gearbox was removed for mechanical inspection.

Mechanical Condition of HT-4 Gearbox (Serial No. ABC-5688)

Pre-Test Inspection

The preliminary bearing inspection indicated an extreme wear condition in bearings 3 and 4 with noise levels of 23.5 and 21.5 dB, respectively.

Prior to initial disassembly the rotation of the input shaft was stiff and sluggish. The exact cause of this stiffness was not determined. The ring and pinion gear appeared to have acceptable wear patterns.

The other components appeared to be in satisfactory condition.

Post-Test Inspection

During the teardown of the gearbox, it was noted that both shafts turned in a rough manner, especially the input shaft. When the gearbox case was opened, it was discovered that it was loaded with metalized oil with streaks and piles of metal and sludge. All metal particles were very tiny.

The wear pattern on the gear teeth was excessive but surprisingly smooth with very shallow pitting.

The No. 1 bearing assembly was in very bad shape. Both inner and outer races were badly worn and pitted. The inner race and the balls fell out without applied force.

The No. 2 bearing was not in quite as bad shape, but the balls were pitted and the inner race could be pushed out by hand.

The final bearing inspection indicated that most damage had occurred to the input bearings. Bearing 1, after testing, had a raceway wear depth of 56 microns, compared with a "negligible" measurement before testing. This extreme raceway wear after testing was also exhibited by gearboxes BB-4 and BB-5.

Spectrometric Oil Analysis (SOA)

Twenty one oil samples were collected for the 513-hour testing period. In Figure 92, the iron content in this gearbox versus test time is plotted. It is seen that there is approximately a 10:1 increase in iron content of the last sample over the previous samples. This indicates extreme wear in the brass retaining ring on the bearings, which was observable in the post-test inspection.

Temperature Sensors

Both oil temperature (Figure 94 A) and ambient temperature (Figure 94 B) are plotted versus time for the test time duration. The step increase in temperature at approximately hour 270 is attributable to a shutdown of the cooling water used in the test cell hydraulic system. This shutdown lasted approximately 100 hours. The oil temperature during this period rose from a nominal 140°F to approximately 185°F. The corresponding ambient temperature in the gearbox vicinity rose from from a nominal 90° F to approximately 110°F. Because of the relatively high viscosity versus the temperature index of the hydraulic fluid, no appreciable changes in the operating load on the gearbox were experienced.

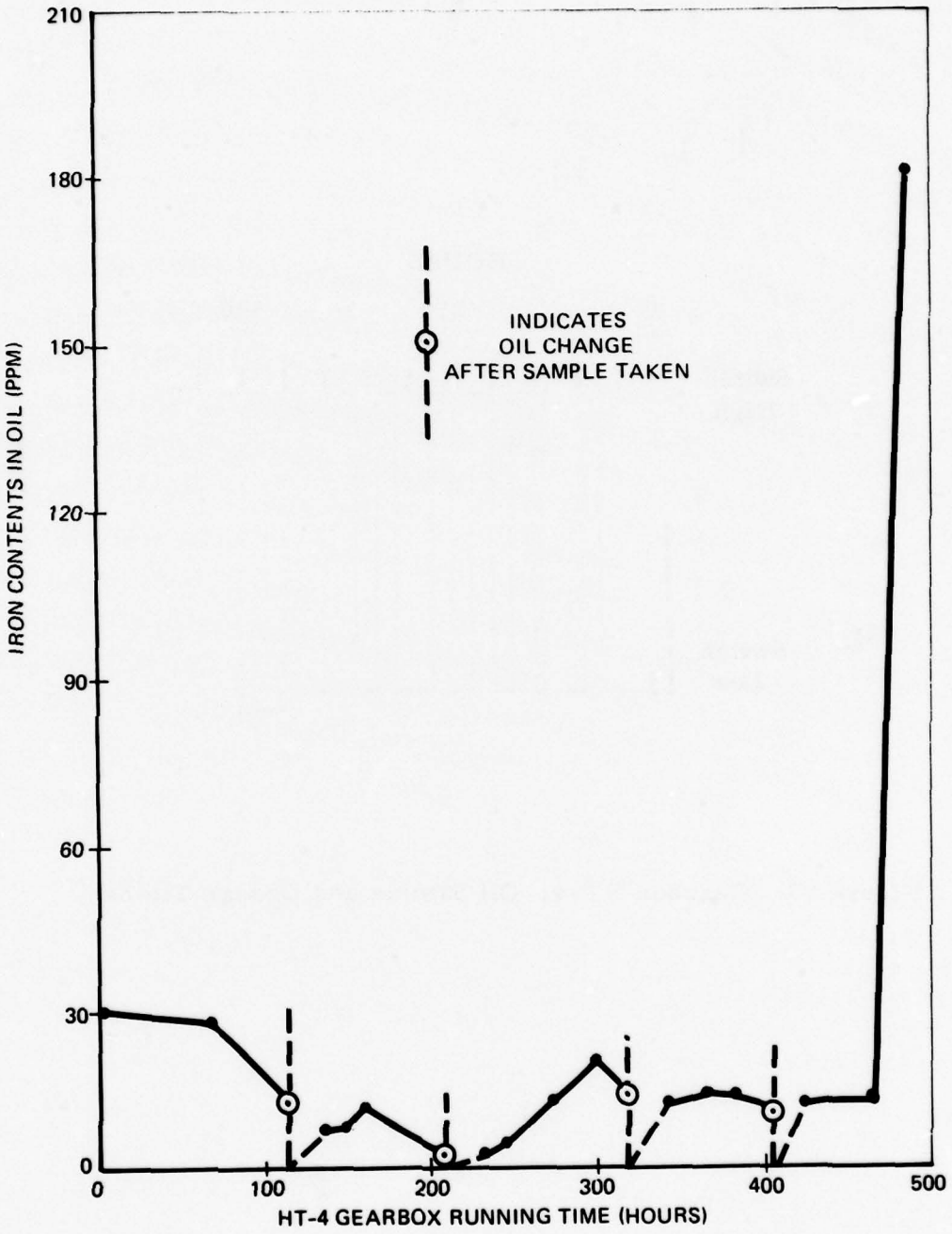

Figure 92. Spectrometric Oil Analysis-Gearbox HT-4.

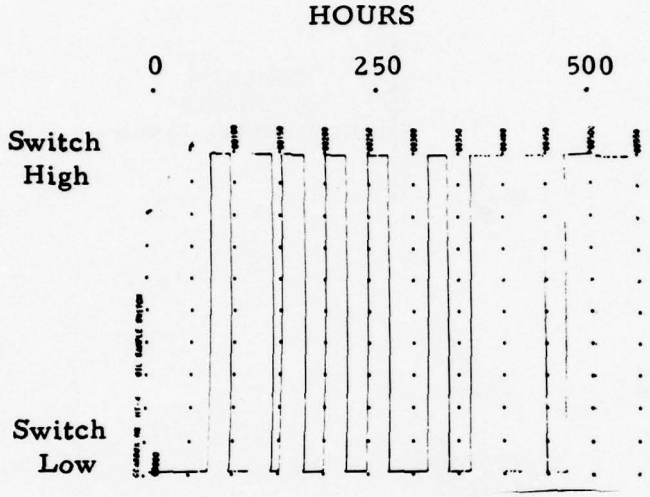

Figure 93. Gearbox HT-4; Oil Sample and Change Times.

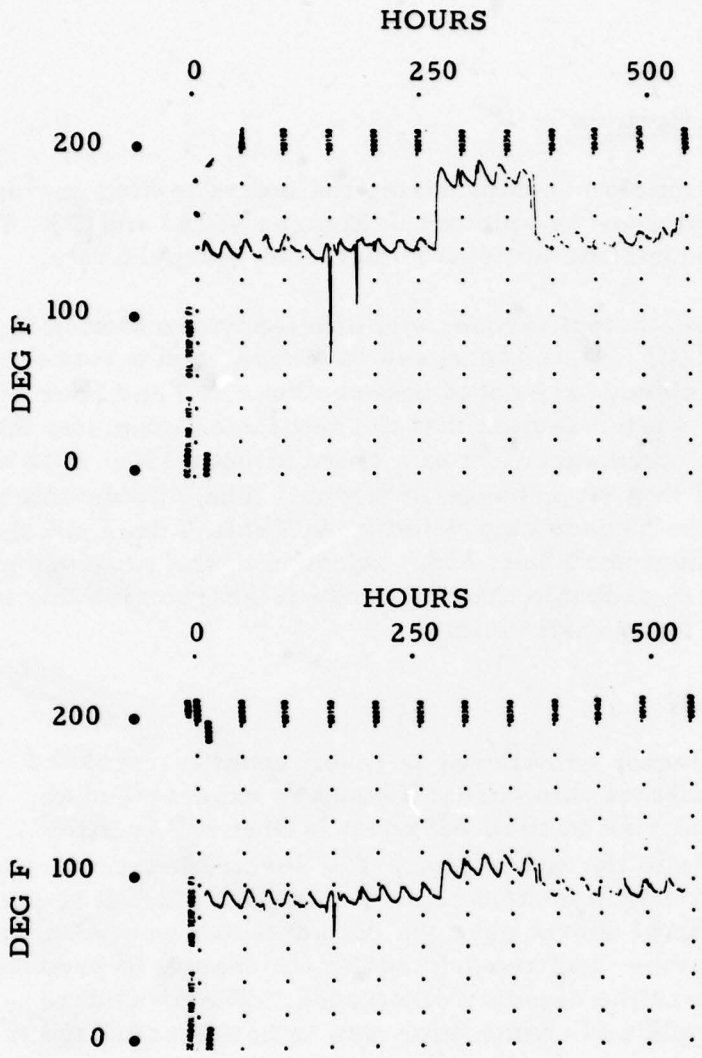

Figure 94. Gearbox HT-4; Oil and Ambient Temperature vs. Test Time.

RPM and Torque Indicators

RPM remained extremely constant during the entire testing period. Both input and output rpm are plotted in Figures 95 (A) and (B). These were maintained at approximately 4160 and 1600, respectively.

Gearbox input torque, output torque, and efficiency are plotted in Figures 96 (A), (B), and (C). A step increase in torque and a corresponding decrease in efficiency are noted between hour 180 and hour 300. It will be observed in a later section that the input accelerometer RMS indicator shows the commencement of a trend at hour 180. It is not certain what caused this step change in torque. The chip detector count recorded by the Tedeco chip detector in Table 5 does not show a significant chip count until hour 365. Because of the subsequent input bearing damage, it is probable that the cause of gearbox loading is associated with the input shaft vicinity.

Tedeco Chip Detector

The Tedeco chip detector cumulative burn-off count is recorded in Table 5. A significant chip burn-off count is experienced at hour 365. A gradual rise in burn-off count is observable after that time, continuing to the end of test. The spectrometric oil analysis indicates a significant iron content increase at hour 272. It is probable that the accumulation of debris near the chip detector was occurring between these two times and reached sufficient density to produce a conductive path across the detector electrodes. The procedure employed at oil sample and change time was to not clean off the detector electrodes.

Ultrasonic RMS Accelerometers Data

Figures 97 (A) and (B) present the RMS levels from the ultrasonic portion of both input and output B & K accelerometers. As noticed on previous gearbox tests, these indicators have a tendency to be erratic at times. It is quite probable that the ultrasonic energy is affected by the oil changes. Figure 97 (A) shows a definite ramp increase in ultrasonic energy beginning at hour 180. This is the hour that increased torque loading was also experienced. The negative-going transient spikes

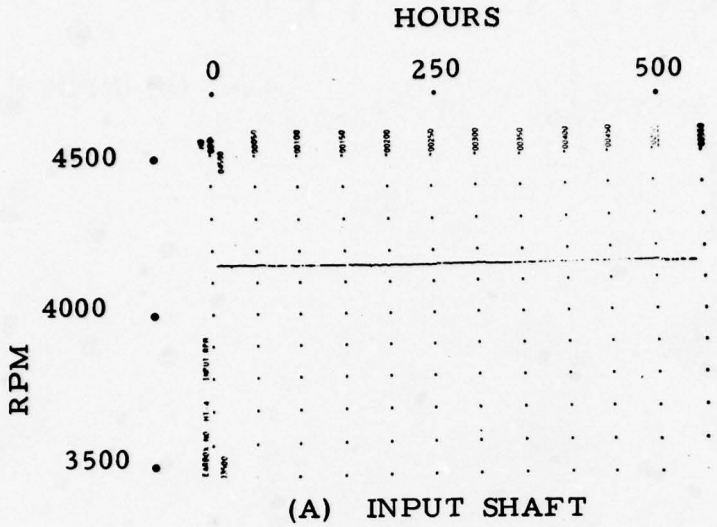

(A) INPUT SHAFT

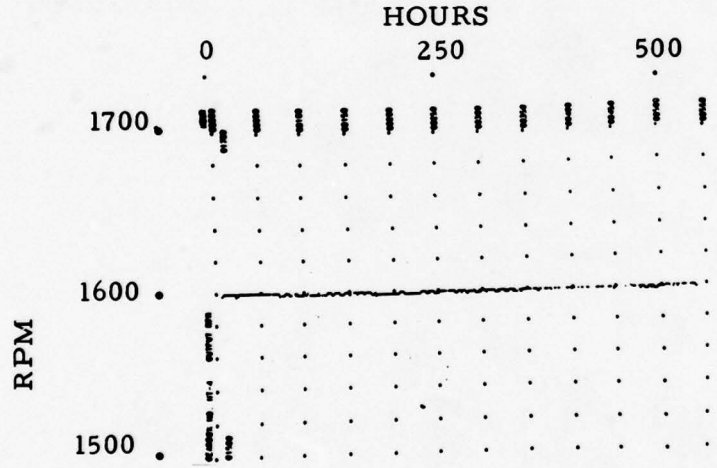

(B) OUTPUT SHAFT

Figure 95. Gearbox HT-4; RPM vs. Test Times.

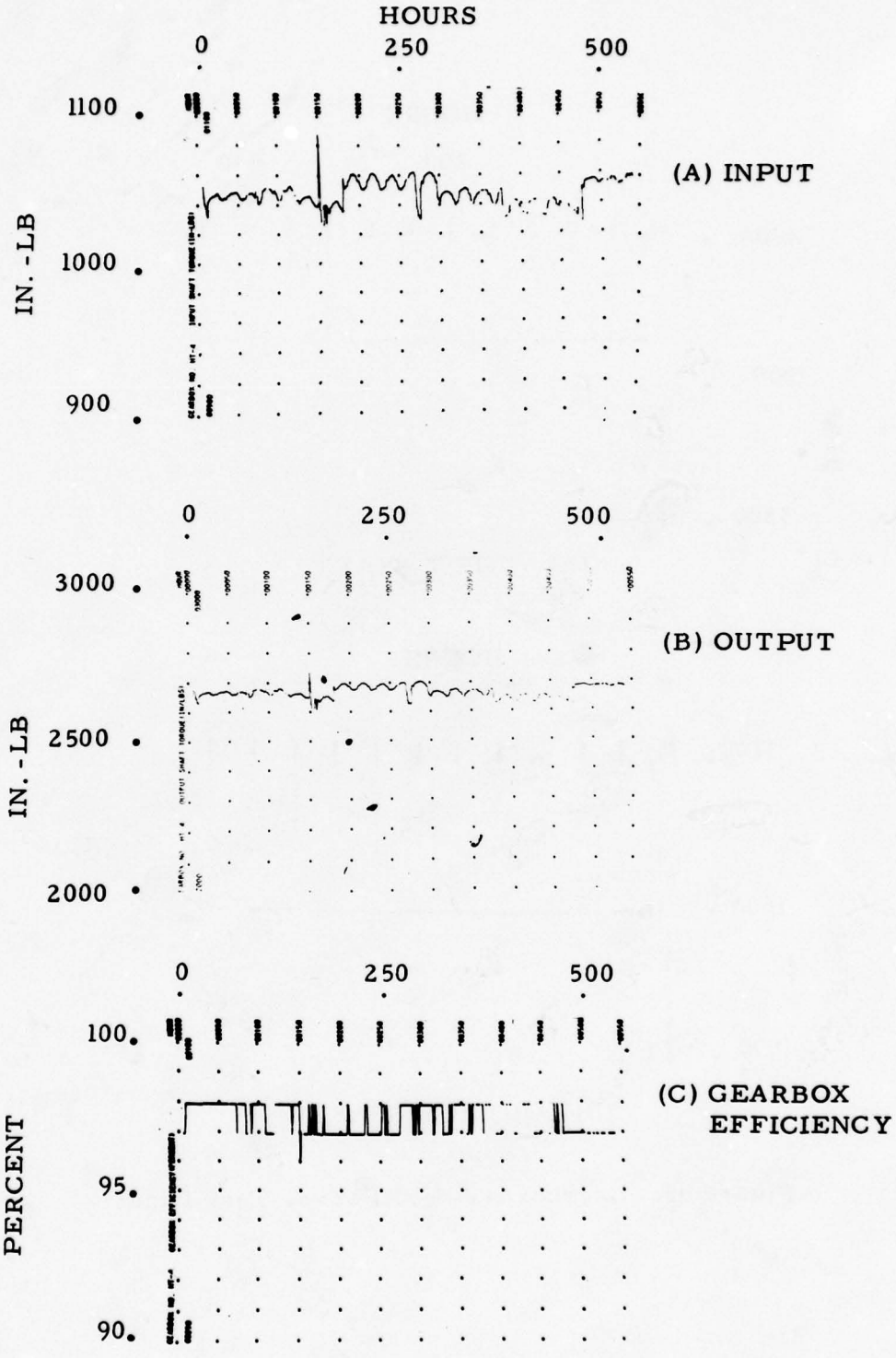

Figure 96. Gearbox HT-4; Torque and Efficiency vs. Test Time.

TABLE 5. GEARBOX HT-4; TEDECO CHIP DETECTOR CUMULATIVE CHIP BURN-OFFS

Gearbox Running Time (Hrs.)	Chip Burn-off Count
67	1
114	1
149	1
181	1
224	1
272	1
341	1
365	33
380	34
403	37
427	49
465	54
489	56
547	81

appear to be at 24-hour intervals and may be associated with oil sampling and changing, since they closely line up with the oil sample excursions of Figure 93.

Figure 97 (B) presents the output accelerometer ultrasonic time history. The step increase at hour 270, decreasing again at hour 300, appears to be riding on a lower level pedestal occurring at the same time that the temperature rise was experienced. The large excursion is difficult to explain. The overall lower pedestal is also observable in the DC-10 kHz portion of the spectrum, as observed in Figure 102, and may be attributable to a change in instrumentation gain.

Shock Pulse Analyzer

Figures 98 and 99 present the shock profile history of both input and output accelerometers for gearbox HT-4. Figure 98 illustrates the degradation of the input bearing. There is very little change over the first 300 hours, but it is seen in curve C that much higher levels of shock are being experienced at shock rates up to 200 pulses per second at hour 513. Figure 99, on the other hand, presents the shock profile history in the vicinity of the output bearing. This series of curves is

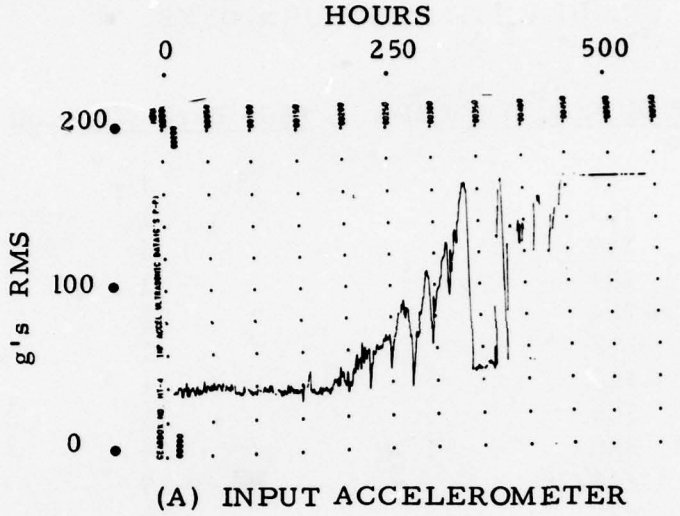

(A) INPUT ACCELEROMETER

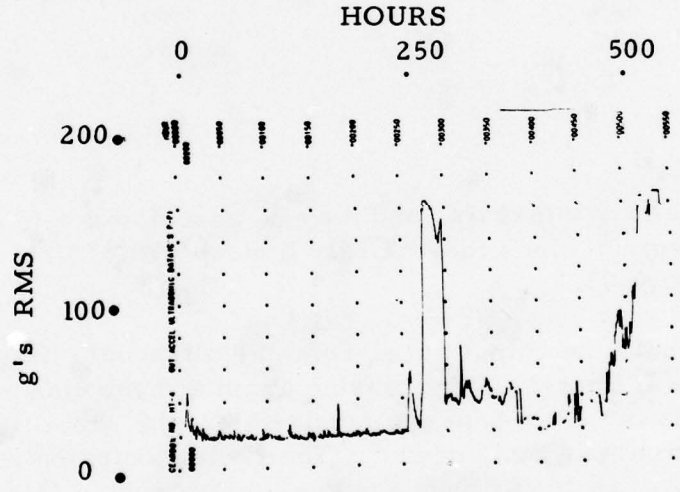

(B) OUTPUT ACCELEROMETER

Figure 97. Gearbox HT-4; Ultrasonic RMS Data.

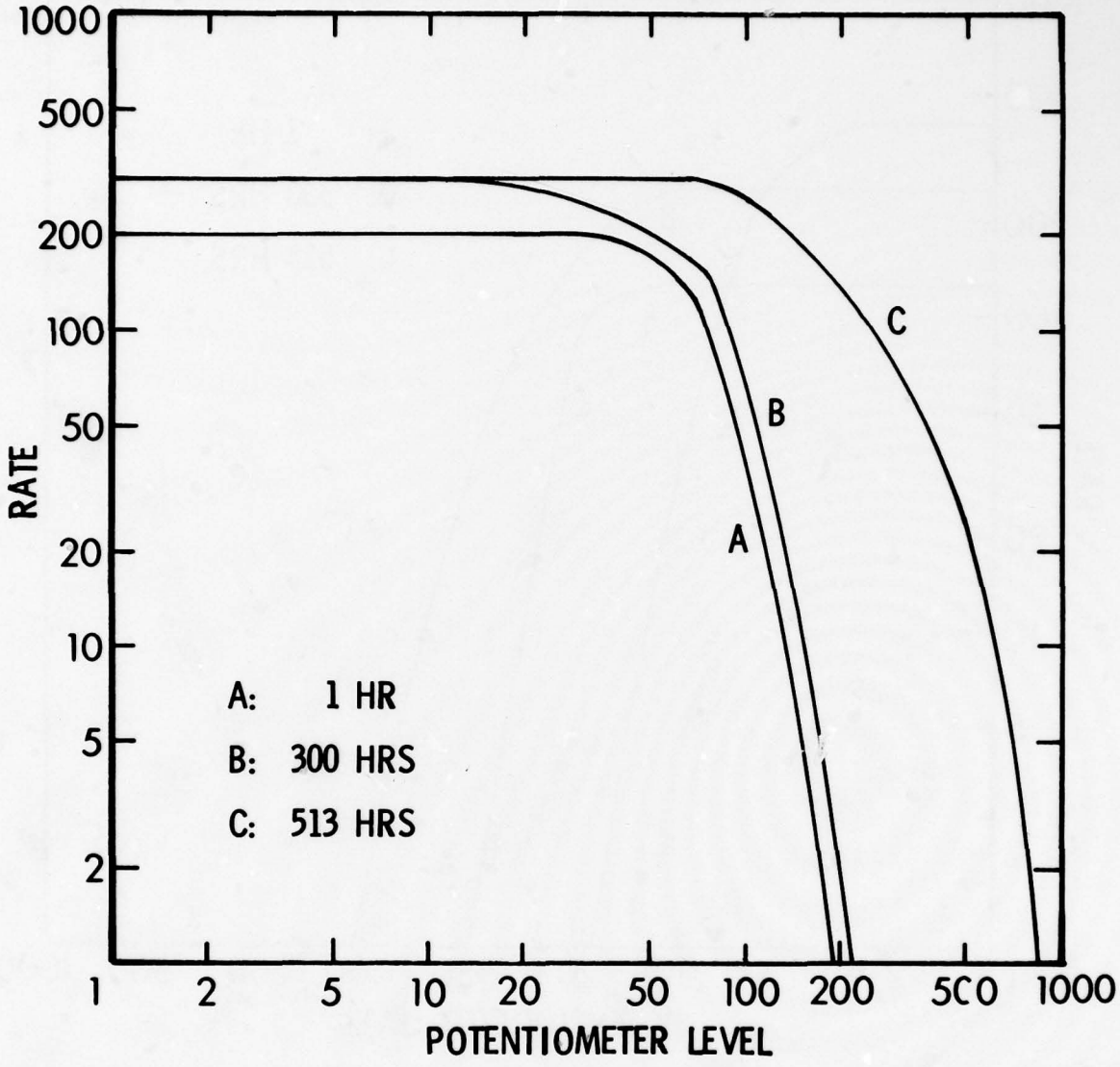

Figure 98. Gearbox HT-4; Shock Profile Curves, Input Accelerometer.

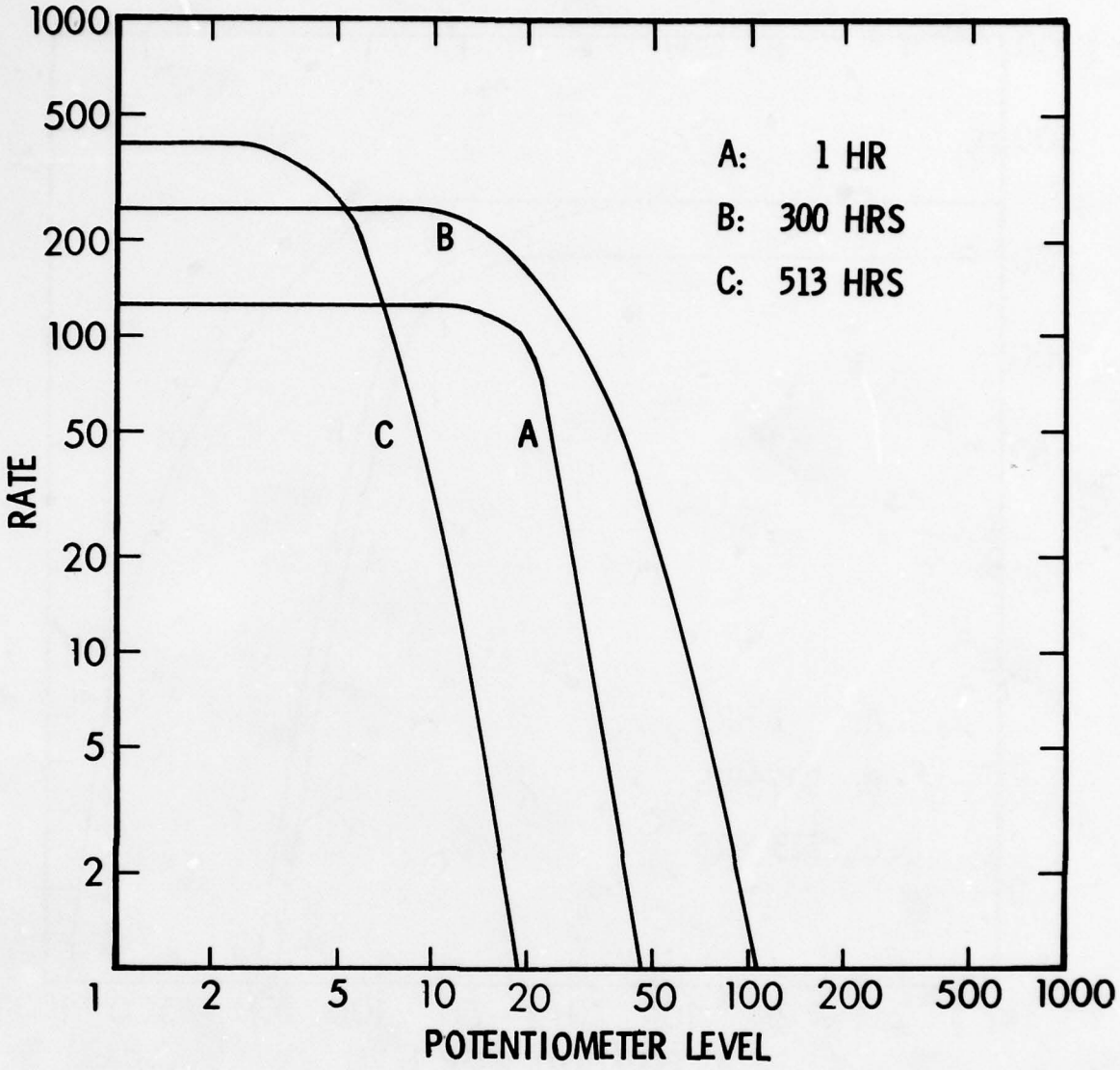

Figure 99. Gearbox HT-4; Shock Profile Curves, Output Accelerometer.

more indicative of foreign matter present in the bearing lubricant.

Figure 100 presents a time history of the SKF peak shock reading for the input accelerometer. The start of increasing shock values appears at approximately hour 270.

Low Frequency Vibration Data Time Analysis

Figures 101(A) and (B) present time histories of four trending parameters on the DC-10 kHz portion of the B & K input lateral accelerometer. Figure 101(A) presents the RMS energy level in the dashed curve and the matched-filtered RMS level in the solid curve. The start of a wear trend occurs somewhere around hour 200. The superiority of the matched-filter indicator over the RMS indicator can be seen by comparing the dynamic ranges: greater than 30 dB for the matched filter versus approximately 15 dB for the RMS indicator. Figure 101(B) presents the other two indicators: the geometric mean (or average of the logarithmic values of 500 spectral lines of the power spectral density versus time) and the arithmetic mean (average of the absolute voltage values of the 500 spectral lines of the PSD). These two indicators, as in previous gearbox tests, appear to be very similar to the matched-filter indicator, although with less dynamic range: approximately 20 dB for the geometric mean and 19 dB for the arithmetic mean. A step reduction in level is observable in all four indicators at hour 150. This appears to be an instrumentation problem (i.e., reduction in signal level) since the effect is not observable in any of the other sensors.

It seems fair to say that a prediction of 300 hours of useful remaining life could be made with the matched-filter indicator monitoring the input accelerometer.

Figure 102 presents the same four indicators monitoring the output accelerometers. It can be seen that the dynamic range of the trend is not as great as for the input accelerometer (i.e., only about 16 dB for the matched filter). It is interesting that the interval when the 40-45° F oil temperature rise occurred is also characterized by a pedestal increase in level from all four output accelerator trend indicators. The relationship is not immediately evident, although it is probably an instrumentation effect (i.e., an increase in amplifier or processing gain versus temperature).

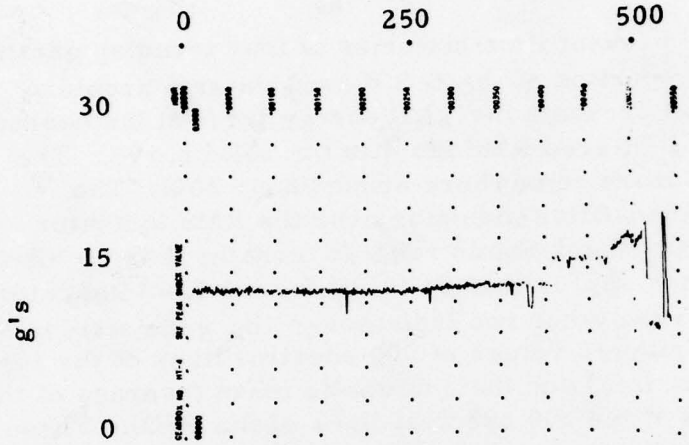

Figure 100. Gearbox HT-4; SKF Peak Shock Value.

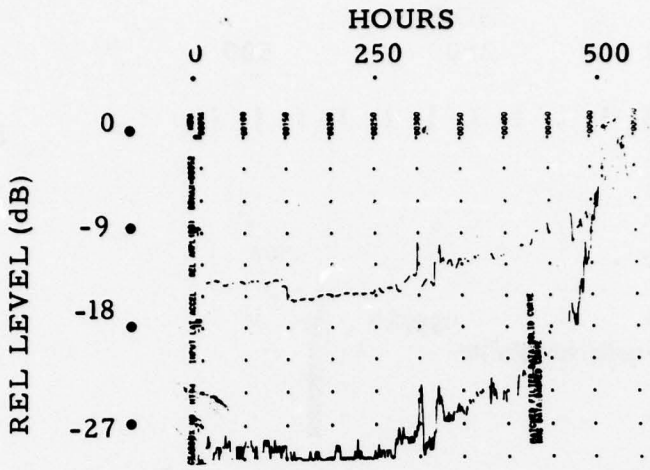

(A) MATCHED FILTER(SOLID) AND RMS DATA (DASHED)

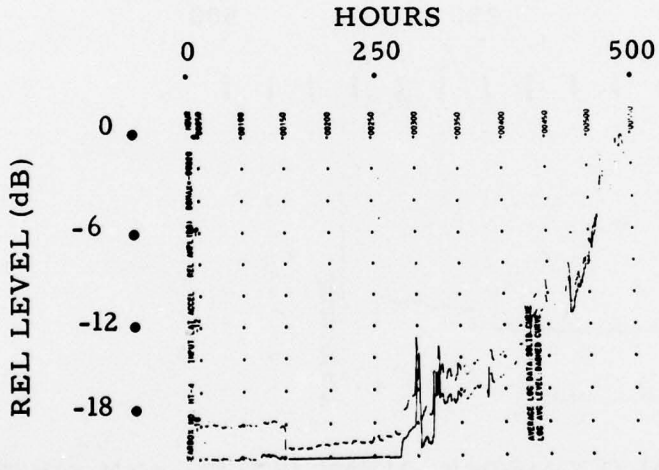

(B) GEOMETRIC MEAN (SOLID) AND ARITHMETIC MEAN (DASHED).

Figure 101. Gearbox HT-4; Input Lateral Accelerometer Trend Parameters.

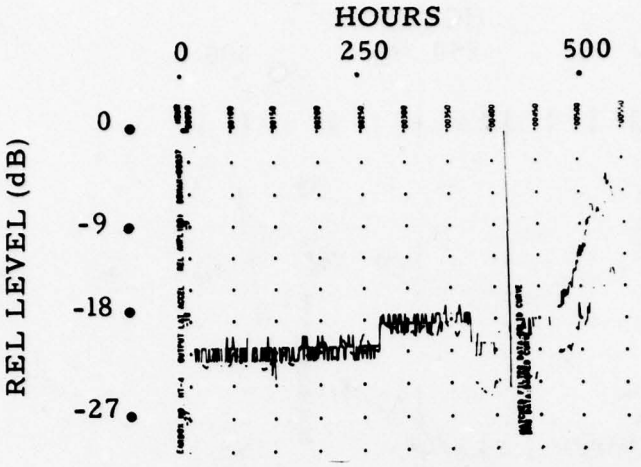

(A) MATCHED FILTER (SOLID) AND RMS DATA (DASHED)

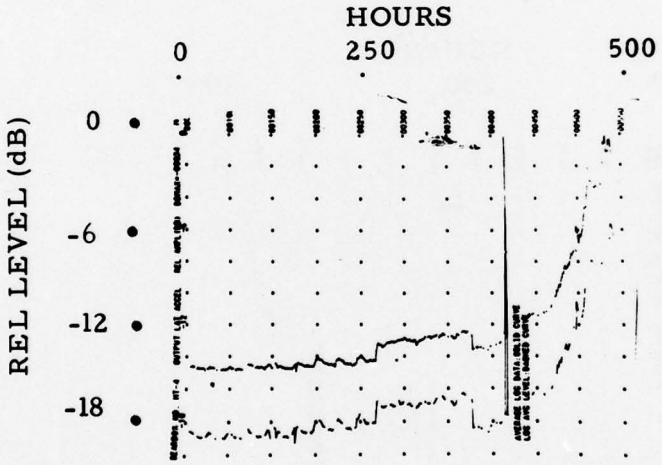

(B) GEOMETRIC MEAN (SOLID) AND ARITHMETIC MEAN (DASHED)

Figure 102. Gearbox HT-4: Output Lateral Accelerometer Trend Parameters.

Low Frequency Vibration Data Frequency Analysis

Power spectral densities at 5, 250, 450, and 500 hours are presented in Figures 103 and 104 for both input and output accelerometers. The horizontal line across each presentation represents the geometric mean value at that particular time. Both Figures 103 and 104 show a degeneration of the gear-mesh structure with time and an increase of more uniformly distributed spectral lines as wear increases. This has consistently appeared in wear patterns for all gearboxes and is the basis for utilizing a large portion of the frequency spectrum as the data base for a wear trend indicator, rather than concentrating on discrete vibration frequencies.

Summary of HT-4 Gearbox Test Results

Gearbox HT-4 was in extreme wear condition prior to testing on this contract, although it was seemingly in better condition than gearboxes BB-4 and BB-5.

The significant result of this test was the relatively smooth trending curve produced by the matched-filter RMS data from the input accelerometer, with the trend developing approximately 300 hours before the culmination of testing.

The ultrasonic RMS data from gearbox HT-4 provided erratic information, as it did in the tests of previous gearboxes.

Both the Tedeco chip detector and the SKF shock meter were useful in correlating the wear produced by testing. The spectrometric oil analysis provided information at about the 272nd hour that the iron level had risen, although the iron content remained fairly constant until hour 489.

It is significant that the matched-filter detection occurred approximately 75-100 hours before the shock meter or chip detector detected significant changes. With this detection level 30 dB below the level finally reached at the end of testing approximately 300 hours later, it appears possible that a reasonably reliable prognosis criterion could be developed.

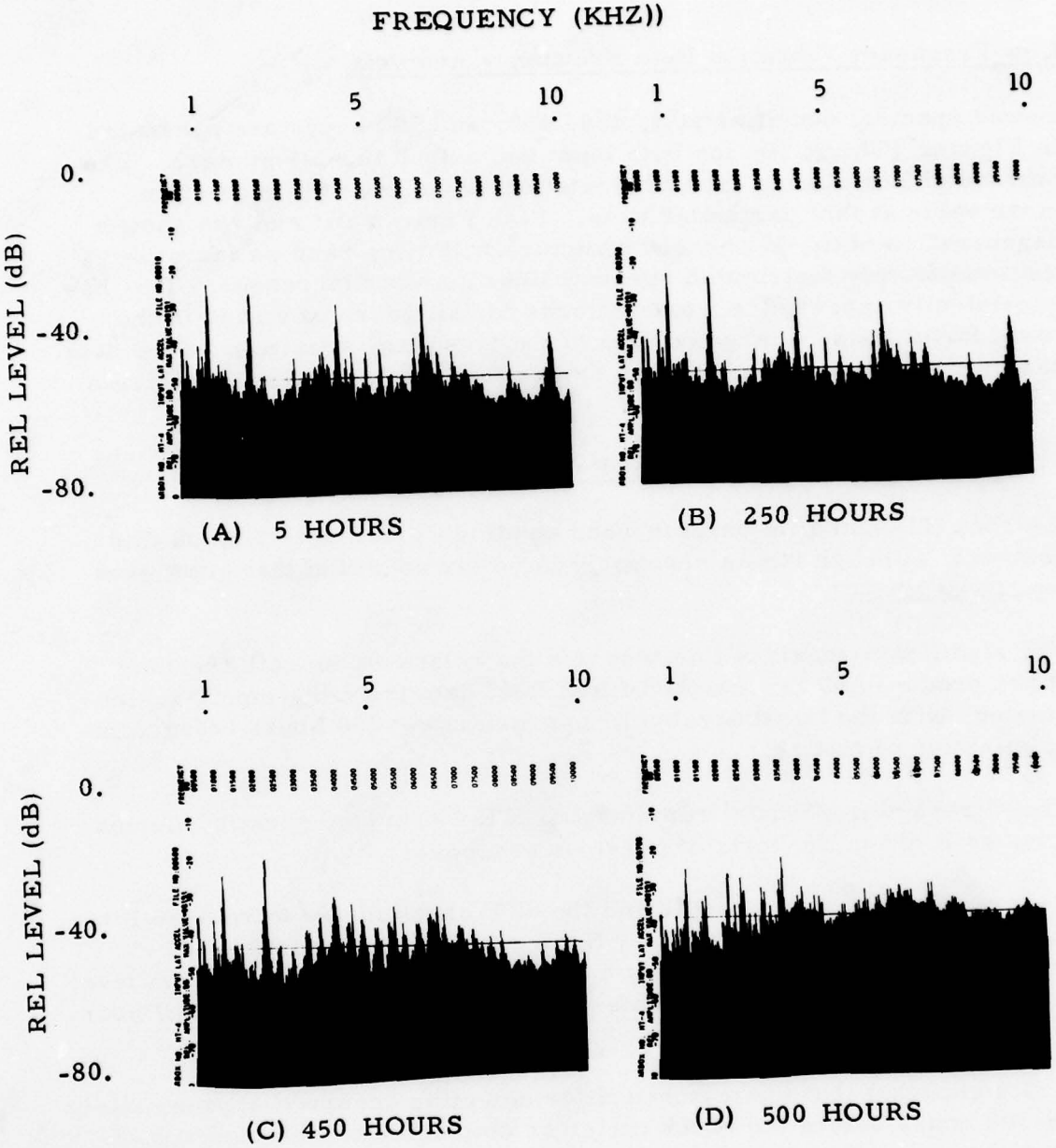

Figure 103. Gearbox HT-4; Input Lateral Accelerometer Power Spectral Density.

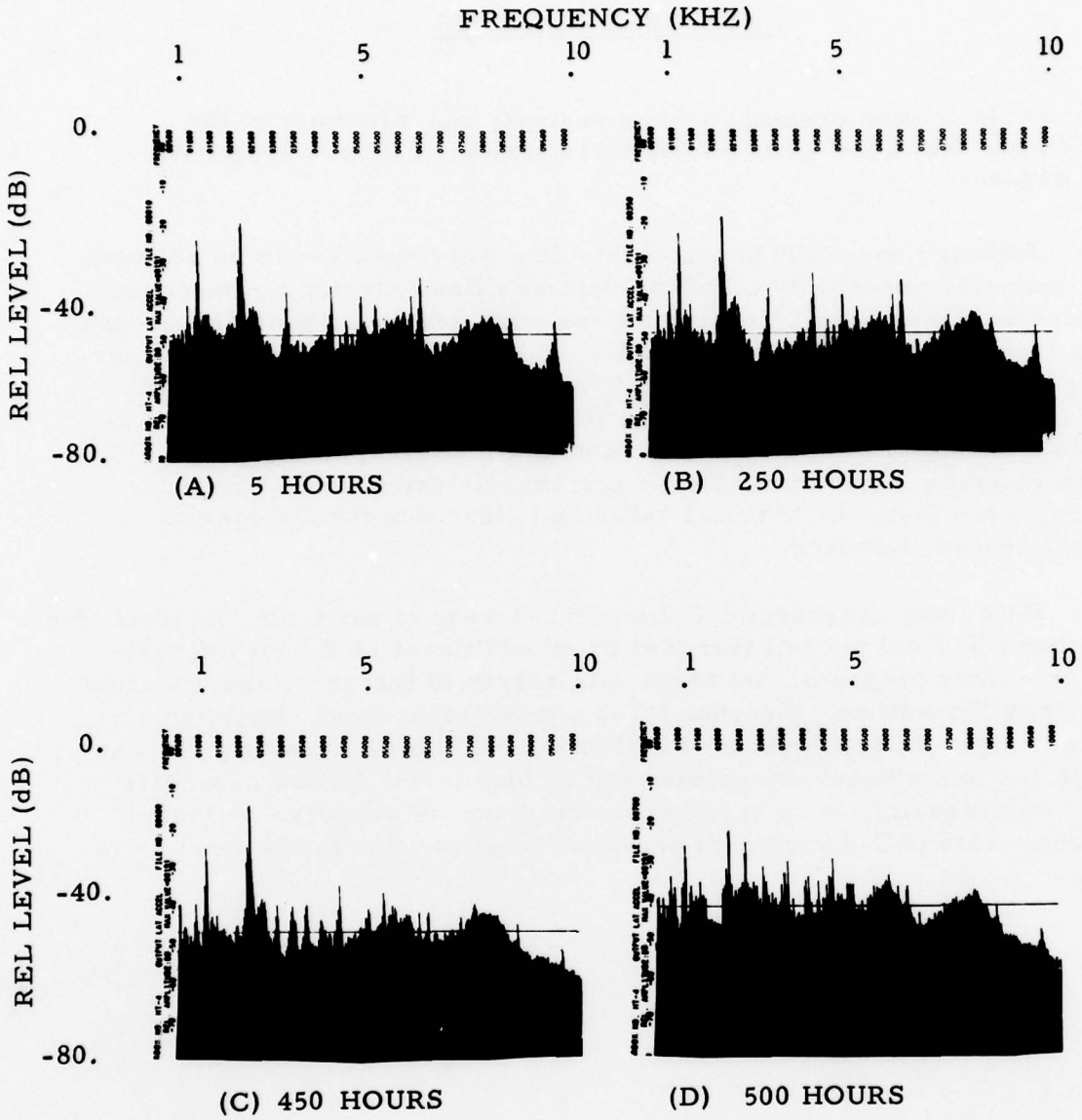

Figure 104. Gearbox HT-4; Output Accelerometer Power Spectral Density.

DATA BASE ANALYSIS

This section presents a brief analysis and summary of the 4712-hour data base collected for investigation of failure prognosis techniques.

Although only 3000 hours of this data were required to be selected for analysis, essentially all of the data was finally tested by the failure prediction algorithms. The algorithms were developed basically around data from four gearboxes: HT-2, HT-3, HT-4, and HT-5. These gearboxes were tested for 1519, 1437, 552, and 596 hours, respectively. The other two gearboxes, BB-4 and BB-5, were actually in a failure mode at the start of test so were of dubious value in optimizing a trend detection algorithm. These gearboxes, tested for 171 and 437 hours, were tested by the final optimized algorithm for the sake of completeness, however.

Data from gearboxes HT-2 and HT-3 were of particular interest. Since gearbox HT-2 did not fail (verified by an additional 1400 hours of testing on a later program), its trend data served to test the trend detection "no-trend" condition. Gearbox HT-3, on the other hand, exhibited "wear" signs during the second half of its 1437 hours of testing. It was subjected to the heaviest analysis since "long term" failure prognosis was, by necessity, to be verified by data from its sensors. All other gearbox tests (HT-2 excluded) produced failures after fairly short term runs.

FREQUENCY ANALYSIS METHODOLOGY

Frequency analysis of the vibration waveforms produced by accelerator sensors mounted on each gearbox is used as the basis of component wear determination under this study effort. In general, the use of frequency domain analysis lends itself quite well to wear evolution perception. For example, continuous or periodic observation of the time-varying sensor waveform reveals very little about small or subtle changes that may be occurring in the dynamic structure of the system under measurement. A small bearing raceway nick or loose particle may be microscopically small, resulting in imperceptible perturbations on the accelerator waveform during early stages of testing. Fourier frequency analysis of this waveform, on the other hand, reclassifies this time-varying voltage into N/2 separate frequency components, where N is the number of consecutive samples of a particular waveform used for a given Fourier transform. The effect, or contribution, of each frequency component is represented by its magnitude relative to the other frequencies in the set.

There are two errors that may result in transforming sampled time data to the frequency domain. An abrupt and finite sampling of a relatively continuous time waveform must be smoothed and weighted to minimize spurious side-lobe structures from forming around bonafide frequency component magnitudes. The Hamming time-weighting of the sample set accomplishes this minimization satisfactorily, as long as the dynamic range of magnitudes considered in the analysis is less than the Hamming suppression factor of 42 dB. That is, no computed frequency magnitude less than 42 dB below the largest recorded magnitude can be considered a valid component.

The second potential source of error is in the interpretation of the frequency magnitude. Because the sampling time is finite, and only a finite number of evenly spaced spectral lines are produced in the transformation, each line is actually representative of a frequency band equal to f_s/N, the sampling frequency divided by the number of samples. In the case of the present contract, this is 19.531 Hz. Consider the gear-mesh-rate frequency of the gearbox: $f_{gm} = \text{rpm} \cdot N_T/60$, where N_T is the rate of successive meshes of consecutive gear teeth in the pinion and ring gears, respectively. Since there are 15 teeth on the pinion gear, which is revolving at approximately 4100 rpm, the gear-mesh rate $f_{gm} = 4100 \times 15/60 = 1025$ Hz. The Fourier analysis produced spectral lines at multiples of 19.531 Hz. Those in the vicinity

of the gear-mesh rate are 1015.625 Hz and 1035.156 Hz. Any energy representative of the fundamental gear-mesh rate will be distributed between these two spectral lines in the ratio

$$K = \frac{1025 - 1015.625}{1035.156 - 1025} = .923 \qquad (4)$$

where K is the ratio of energy at 1035.156 Hz relative to that at 1015.625 Hz. For that reason, any analysis of a particular frequency bin has to be done with caution. Changes in rpm having little or nothing to do with gearbox wear will modify K and affect energy distribution in the frequency bins.

In order to better understand the rationale behind the various trending techniques employed on this contract, it is convenient to consider various time-frequency transform pairs corresponding to a few wear phenomena that occur in rotating machinery.

First of all, the normal condition of a healthy rotating gearbox produces energy at the fundamental and harmonics of the gear-mesh frequency. In addition, shaft force against bearing assemblies produces a lower level periodic energy at a frequency determined by the number of bearings in the assembly and the shaft rpm. In this case, the power spectral density (PSD) of the accelerometer output consists mainly of discrete frequency components at the above-mentioned frequencies.

If a nick or roughness develops in a bearing, it will produce an extremely short duration shock pulse. The rate of occurrence of the pulse train should be more random than periodic during the early stages of rotation, since the ball bearing action will cause the flawed surface to come in contact with the rotating shaft on a rather random basis. Since the PSD of a random pulse train will tend to contain a uniformly distributed frequency spectrum (i.e., the Fourier transform of an impulse is a uniform frequency density of unlimited bandwidth), with the magnitude increasing as the number of pulse occurrences increase, it would seem imperative to "capture" or detect the occurrence of this phenomenon in the processed accelerometer frequency spectrum in order to aid in wear prognosis.

Similarly, abrasions or scarring occurring on certain gear teeth tend to produce a modulation sideband pattern around the gear-mesh fundamental and harmonic frequencies. This occurs because not all teeth are scarred the same amount, thus introducing a lower frequency

modulation. Here again, the tendency is to increase the density of the frequency spectrum, in this case by the generation of a modulation pattern around the normally periodic gear-mesh frequency components.

These phenomena are illustrated in the individual gearbox testing experimental results sections. In all cases where wear and subsequent failure occurred, the PSD history is characterized by an increasing density and density magnitude. For these reasons, the primary trending methods to be described in subsequent sections consider changes in the complete DC-10 kHz spectrum as a function of test time rather than concentration on a single frequency bin. The PSD test histories show that the various wear phenomena manifest themselves by both a "broadening" of the spectral density and a subsequent increase in this broadband energy.

TREND PARAMETER INVESTIGATION

TREND PARAMETER DESCRIPTION

A significant portion of this program's effort was allotted to determination of optimum wear trend parameters that could be extracted from the data collection base. What was needed was a sensitive parameter derived from the 512-point power spectral density array that would indicate, as early as possible, the change from a normal condition. It was necessary that this parameter not only indicate such a departure but maintain its magnitude proportional to the degree of component deterioration at all times.

Twelve parameters were identified and examined; three of these were found to be satisfactory, and one appeared to be the most sensitive to the criteria we had established. The basis for this grading of the parameters was accomplished in stages. First, all parameters were applied to output accelerometer data from HT-3, since it appeared this gearbox experienced a very gradual deterioration and could best evaluate the parameter effectiveness. A sample calculation of each parameter was made at every 24-hour interval of the HT-3 test period. These parameters were then plotted on a common graph and a visual evaluation was made as to which three were superior from the standpoints of (a) early indication of a wear process and (b) total dynamic range of magnitude from "healthy" to "failed" condition. Next, the three highest candidate parameters were calculated from the entire HT-3 output accelerometer data base. This data was then subjected to the trend detection algorithms described in a later section. Finally, a quantitative summary was made of the effectiveness of these three parameters vs. valid trend detection. Included in this summary are assessments of computational complexity of the individual parameters.

Table 6 lists the 12 candidate parameters divided into two classes: Class I consists of 6 parameters that process the entire 10 kHz power spectral density. Class II candidates process only portions of the 10 kHz spectrum.

TABLE 6. TREND PARAMETER CANDIDATES

Class I: Broadband Parameters	Class II: Narrowband Parameters
1. RMS Vibration Level	1. Gear-Mesh MSR vs. Gear-Mesh BW
2. Spectral Correlation	2. Noise MSR vs. Gear-Mesh BW
3. Arithmetic Mean	3. Gear-Mesh MSR vs. Frequency Band
4. Geometric Mean	4. Noise MSR vs. Frequency Band
5. Cepstral Coefficients	5. RMS/Gear-Mesh Energy vs. Gear-Mesh BW
6. Matched-Filter RMS	6. Noise/Gear-Mesh Energy vs. Gear-Mesh BW

First, a description of each of the Class I parameters is presented:

(a) RMS Level

The RMS level represents the total energy in the accelerometer signal. This level may be computed from the power spectral density by the following expression:

$$\text{RMS Level} = \sqrt{\frac{1}{N}\sum_{i=I}^{N} V_i^2} \qquad (5)$$

V_i = amplitude of the ith vibration frequency

N = number of frequency bins (512)

RMS level has long been used as a diagnostic fault indicator. It lacks sensitivity, however, as a prognostic indicator since a large percentage of the accelerometer signal is associated with normal component vibration energy during healthy operation. Because an early detection of wear is desirable, further search for a more optimum parameter was made.

AD-A073 553 NORTHROP RESEARCH AND TECHNOLOGY CENTER PALOS VERDES --ETC F/G 1/3
INVESTIGATION OF ADVANCED PROGNOSTIC ANALYSI S TECHNIQUES.(U)
JUN 79 R C GROVE DAAJ02-77-C-0054

UNCLASSIFIED NRTC78-47R USARTL-TR-79-10 NL

3 OF 3

AD A073563

END

DATE FILMED

10-79

DDC

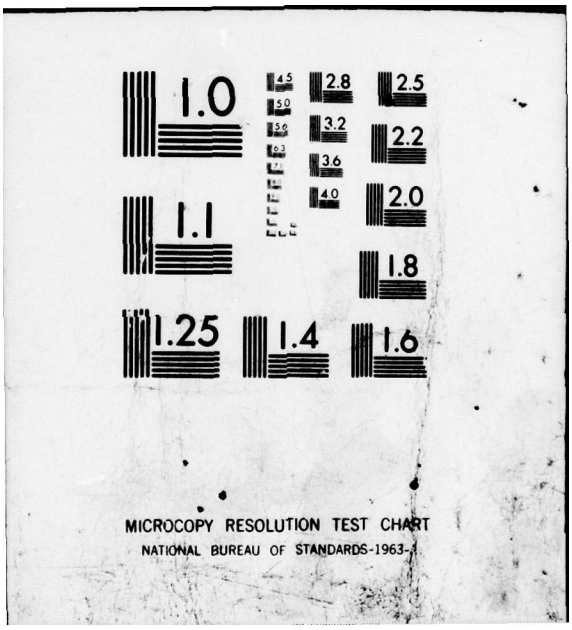
1.0
1.1
1.25
1.4
1.6
1.8
2.0
2.2
2.5
2.8
3.2
3.6
4.0
4.5
5.0
5.6
6.3
MICROCOPY RESOLUTION TEST CHART
NATIONAL BUREAU OF STANDARDS-1963-A

(b) Spectral Correlation[2]

A statistical measure of the "agreement" or "likeness" of two groups of data is the correlation coefficient r, defined as:

$$\text{Correlation Coefficient} = \frac{\text{Covariance between data set X and data set Y}}{\sqrt{(\text{Variance of data set X}) \cdot (\text{Variance of data set Y})}}$$

or

$$r = \frac{\sum_{i=1}^{N} \Delta X_i \Delta Y_i}{\sqrt{\sum_{i=1}^{N} \Delta X_i^2 \cdot \sum_{i=1}^{N} \Delta Y_i^2}} \qquad (6)$$

where $\sum_{i=1}^{N} \Delta X_i^2$ and $\sum_{i=1}^{N} \Delta Y_i^2$

are the sum of squared deviations from the mean value of the data sets X and Y and

$$\sum_{i=1}^{N} \Delta X_i \Delta Y_i$$

are the sum of products of deviations ΔX and ΔY from the means of their respective data sets X and Y.

The value of the coefficient r will fall between the extremes: ±1. " + 1" indicates that X and Y data sets are either identical or at least proportional to each other, i.e., $X_i = KY_i$. A" - 1" indicates that $X_i = -KY_i$. All other sets of conditions can be shown to fall between these extremes.

2. Snedecor, G.W., and Cochran, W.G., "Statistical Methods," Iowa State University Press, 6th Edition, 1967, p. 172.

The time history of power spectral densities can be treated as data sets in the above sense, and the spectral correlation r_s may be examined as a trend parameter. In this case, data set X represents a healthy spectral signature used as a reference set. Data set Y then represents the current power spectral density to be "correlated" against set X.

It will be seen, however, upon examination of the spectral coefficient of the time history of the spectra, that this parameter is not too sensitive to early signs of wear in a component. There are at least two reasons for this: (a) lower level frequency components are not weighted as heavily as higher level, and (b) the parameter is not sensitive to overall spectral energy increases and decreases.

(c) Arithmetic Mean

The arithmetic mean tends to give more significance to the lower level frequency components. Unlike the RMS level, which sums the squared frequency component values, the arithmetic mean averages the magnitudes or equivalent "g" levels of the frequency components. It is computed as follows:

$$\text{Arithmetic Mean} = \frac{1}{N} \sum_{i=1}^{N} V_i \qquad (7)$$

with V_i and N defined above.

(d) Geometric Mean

The geometric mean corresponds to the average logarithmic value of the vibration spectrum. It tends to suppress the influence of large amplitude components. The geometric mean tends to hover close to the average noise level of the spectrum. It is computed as follows:

$$\text{Geometric Mean} = \frac{1}{N} \sum_{i=1}^{N} \log V_i \qquad (8)$$

(e) Cepstral Mean-Squared Ratio

Cepstral smoothing[3] is a technique used with success in speech processing to separate components of the speech waveform to aid in analysis or synthesis of the vocal tract. The vibration waveforms obtained from the gearbox accelerometer signals are very analogous to speech waveforms. The "pitch" component in speech is similar to the gear-mesh component, dominating the energy share of the signal and appearing at the low end of the frequency spectrum. Similarly, the un-voiced sounds are similar to noise produced by bearing wear. Both phenomena are characterized by energy distributed throughout the audio spectrum.

Cepstral smoothing consists of low-pass filtering the Fourier transform of the signal log spectrum. The log spectrum, as observed with the effect of the geometric mean parameter, tends to reduce the dynamic range between the various spectral components. When the Fourier transform is performed on this log spectrum, the resultant data might be thought of as an enhanced autocorrelation function. What is of interest is to determine the degree that the higher order cepstral coefficients change during a wear process. For this reason, various cepstral mean-squared ratios were computed, each one averaging twice as many squared coefficient ratios as the preceding one. The object was to see how this parameter varied, both with time and number of averaged ratios, as a wear trend parameter.

The cepstral mean-squared ratio CR (j) is defined as

$$CR(j) = \frac{1}{N_j} \sum_{i=1}^{N_j} \left[\frac{C_i}{C_{i\,(ref)}} \right]^2 \qquad (9)$$

where $N_j = 2^{j-1}$, $j = 1, 2, \text{---- } 7$

$$\text{and} \sum_{i=1}^{N} C_i = FFT \left(\sum_{i=1}^{N} \log V_i \right) \qquad \text{current spectrum}$$

3. Makhoul, J., "Spectral Analysis of Speech by Linear Prediction," IEEE Transactions on Audio and Electroacoustics, Volume AU-21, June 1973, p. 146.

$$\sum_{i=1}^{N} C_{i\,(Ref)} = FFT\left[\sum_{i=1}^{N} \log V_{i(Ref)}\right] \qquad \text{reference spectrum}$$

The first cepstral coefficient, CR(1) is the ratio of the geometric mean of the current spectrum to the geometric mean of the current spectrum to the geometric mean of the reference spectrum, or

$$CR\,(1) = \left[\frac{C_1}{C_{1\,(Ref)}}\right]^2 = \left[\frac{\frac{1}{N}\sum_{i=1}^{N} \log V_i}{\frac{1}{N}\sum_{i=1}^{N} \log V_{i\,(Ref)}}\right]^2 = \left(\frac{\text{Current G. M}}{\text{Reference G. M.}}\right)^2 \qquad (10)$$

(f) Matched-Filter RMS

Each of the five parameters described above contains features that tend to describe a component wear process time history: The RMS level considers the total energy in the signal, since it is known that vibration energy increases with component wear. The spectral correlation coefficient compares a current vibration spectral signature with a reference level in order to detect differences. The arithmetic mean considers an average "g" or "voltage" level of the signal rather than the average "energy" or "power" level, thus giving higher weight to higher density low level frequency components. The geometric mean improves upon the arithmetic mean by providing exponential weighting to the frequency components, producing a parameter measuring closely the noise floor of the vibration spectra.

The sixth parameter considered – the matched-filter RMS – combines many of the features of the previous parameters. It uses a reference vibration frequency signature similar to the correlation method. Instead of averaging products of reference frequency and current frequency terms, however, it averages the squared ratio of each of these terms. In this way, it is sensitive to overall energy level changes. Also, by averaging frequency component ratios, it

weights each frequency component equally. The matched-filter RMS is defined as

$$\text{Matched-Filter RMS} = \frac{1}{N} \sum_{i=1}^{N} \left[\frac{V_i}{V_{i(REF)}} \right]^2 \qquad (11)$$

where $V_{i(REF)}$ is the ith reference vibration frequency component. V_i and N were previously defined.

RESULTS OF CLASS I PARAMETER EVALUATION

Figures 105 and 106 present time histories of Class I parameters calculated from samples spaced 24 hours apart of HT-3 gearbox output accelerometer PSD data. Figure 105 includes all parameters except the cepstral coefficients. All parameters have been converted to logarithmic (DB) equivalents of their magnitudes. Note that the matched-filter RMS, geometric mean, and arithmetic mean parameters appear to be far superior to the spectral coefficient and RMS level from the standpoint of early detectability of wear. Of these three, the matched-filter RMS has the greater dynamic range, with the geometric mean second.

Figure 106 presents the first three cepstral ratios. Cepstral ratios higher than CR(3) were essentially constant over the test period. Apparently, no new trending information is added by averaging more of the cepstral bandwidth together with the first coefficient. While any one data point may be trendable, such as the first (the geometric mean), it appears that the randomness of the higher cepstral ratios merely produces progressively lower sensitivity vs. bandwidth.

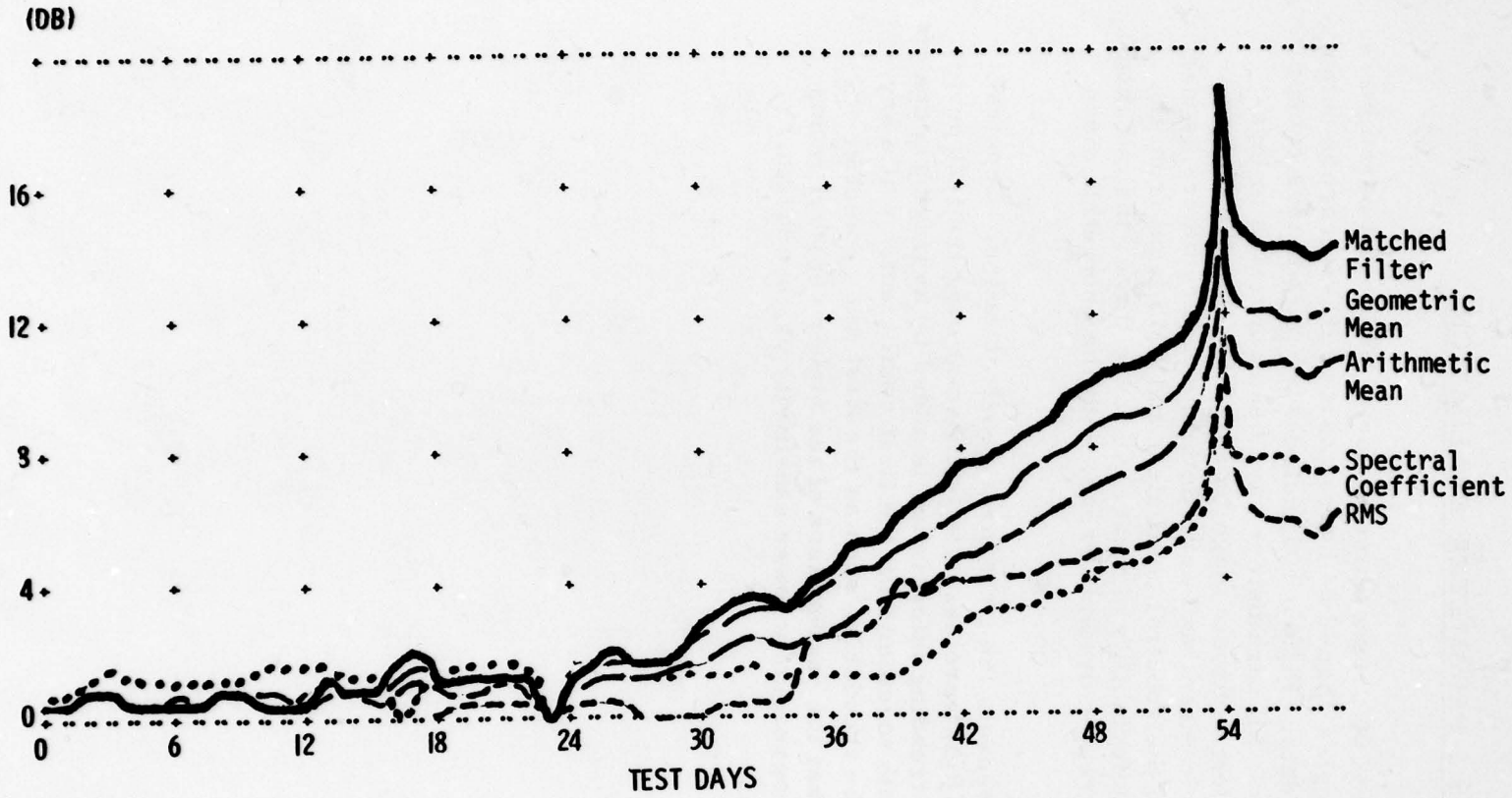

Figure 105. Class I Trend Parameter Comparison.

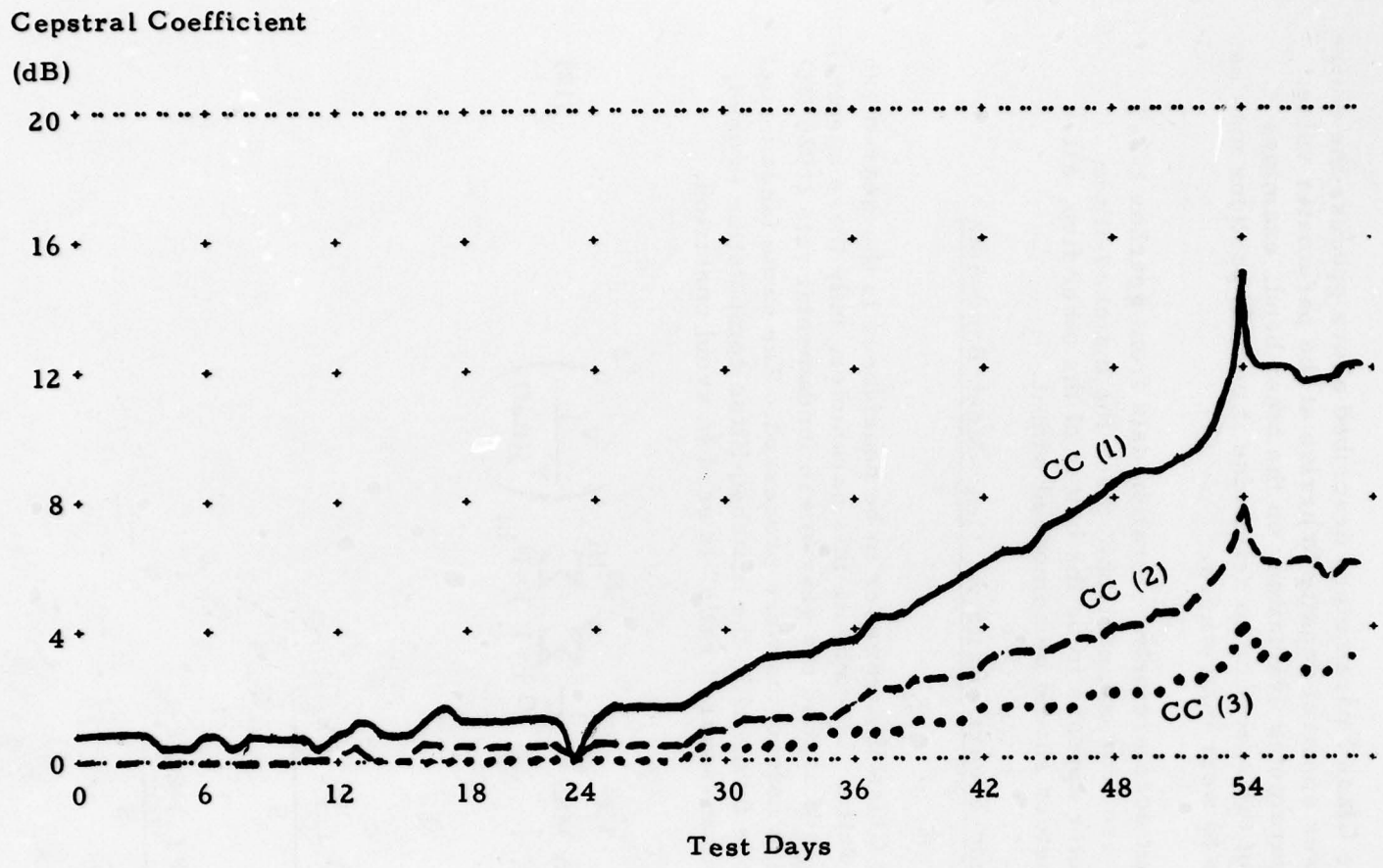

Figure 106. Cepstral Ratio vs. Number of Coefficients.

RESULTS OF CLASS II PARAMETER EVALUATION

All of the Class I parameters described above process the entire DC-10 kHz power spectral density to arrive at the parameter value. This Class II parameter evaluation, on the other hand, examines various parts of the spectrum to determine if certain portions may be more sensitive to wear than others.

The output accelerometer vibration data from gearbox HT-3 has again been used for comparison. Since the matched-filter Class I parameter appears to be the better of the other five, all Class II parameters should be compared with it.

Gear-Mesh Mean-Squared Ratio vs. Gear-Mesh Bandwidth

The first Class II parameter to be considered is the gear-mesh mean-squared ratio. To compute this parameter, only those spectral lines in fixed bands around the gear-mesh fundamental rate (1025 Hz) and its first eight harmonics were processed. The same fundamental computation as is involved in the matched-filter computation is used, but the term "mean-squared ratio" is used to avoid confusion.

$$\text{Gear-mesh MSR} = \frac{1}{N_G} \sum_{i=1}^{9} \sum_{j=N_{Li}}^{N_{Hi}} \left(\frac{V_j}{V_{j(Ref)}} \right)^2 \qquad (12)$$

where

$$N_{Li} = \frac{(i \cdot f_G) - \Delta/2}{S}$$

$$N_{Hi} = \frac{(i - f_G) + \Delta/2}{S}$$

$$N_G = \sum_{i=1}^{9} (N_{Hi} - N_{Li} + 1)$$

f_G = gear-mesh rate (Hz)

Δ = gear-mesh bandwidth (Hz)

S = PSD line spacing (Hz)

V_j and $V_{j\,(Ref)}$ are the magnitudes of the jth frequency components of the current & ref. PSD's.

Figure 107 illustrates this parameter plotted for various bandwidths of the gear-mesh harmonics. At the higher bandwidths, the parameter essentially tracks the broadband matched-filter parameter. At lower bandwidths, the sensitivity becomes less. The conclusion is that this parameter adds no improvement beyond the matched filter.

Noise MSR vs. Gear-Mesh Bandwidth

A noise MSR parameter may be defined for that energy outside the gear-mesh bands. It may be defined in terms of both the matched-filter parameter and the gear-mesh MSR:

$$\text{Noise MSR} = \frac{1}{N - N_G}\left[N \cdot \left(\begin{matrix}\text{Matched} \\ \text{Filter} \\ \text{RMS}\end{matrix}\right) - N_G \cdot \left(\begin{matrix}\text{Gear-mesh} \\ \text{MSR}\end{matrix}\right)\right] \qquad (13)$$

Figure 108 illustrates this parameter plotted for various gear-mesh bandwidths: 32, 64, 128, 256, 512, and 1024 Hz. For the majority of the bandwidths, it resembles both the matched-filter parameter and the gear-mesh MSR. This implies that the wear-trending information is distributed throughout both the gear-mesh and noise bands. The matched

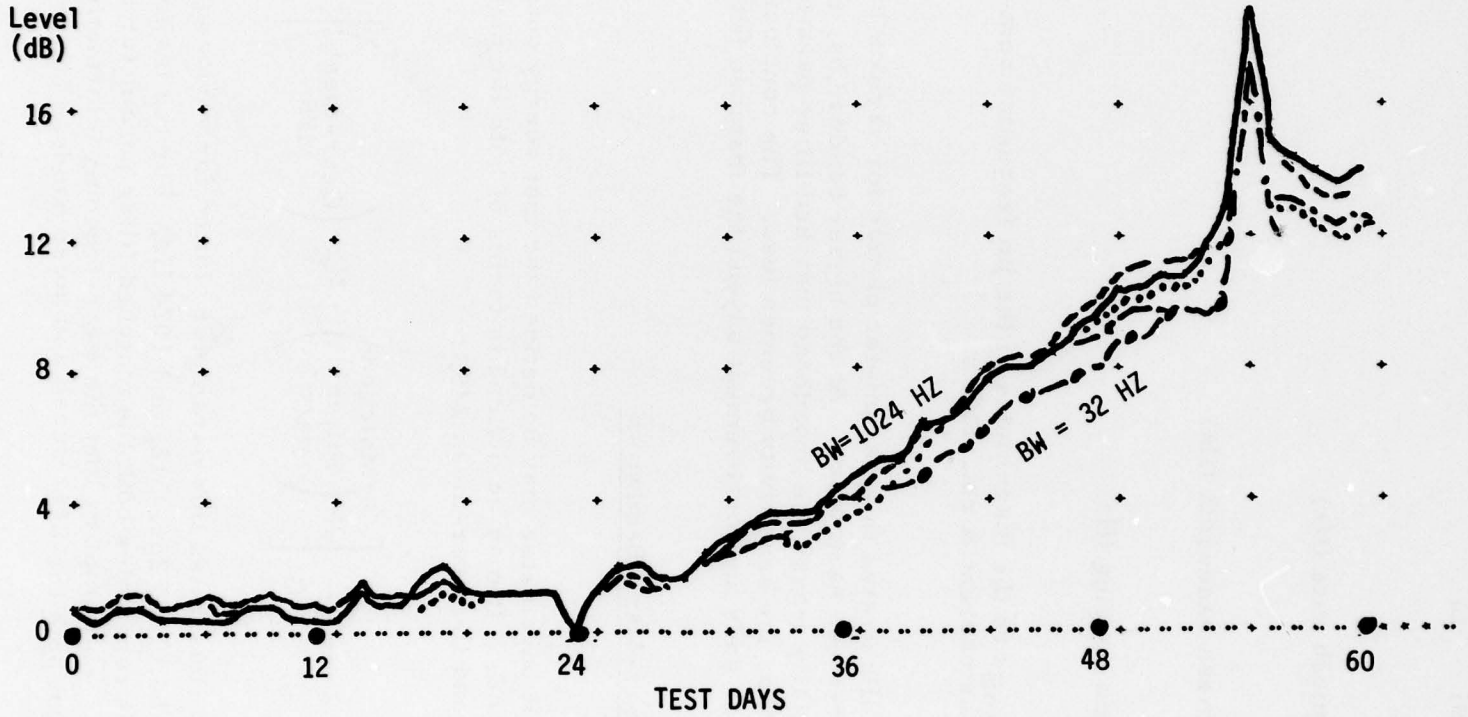

Figure 107. Gear-Mesh Mean-Squared Ratio vs. Gear-Mesh Bandwidth.

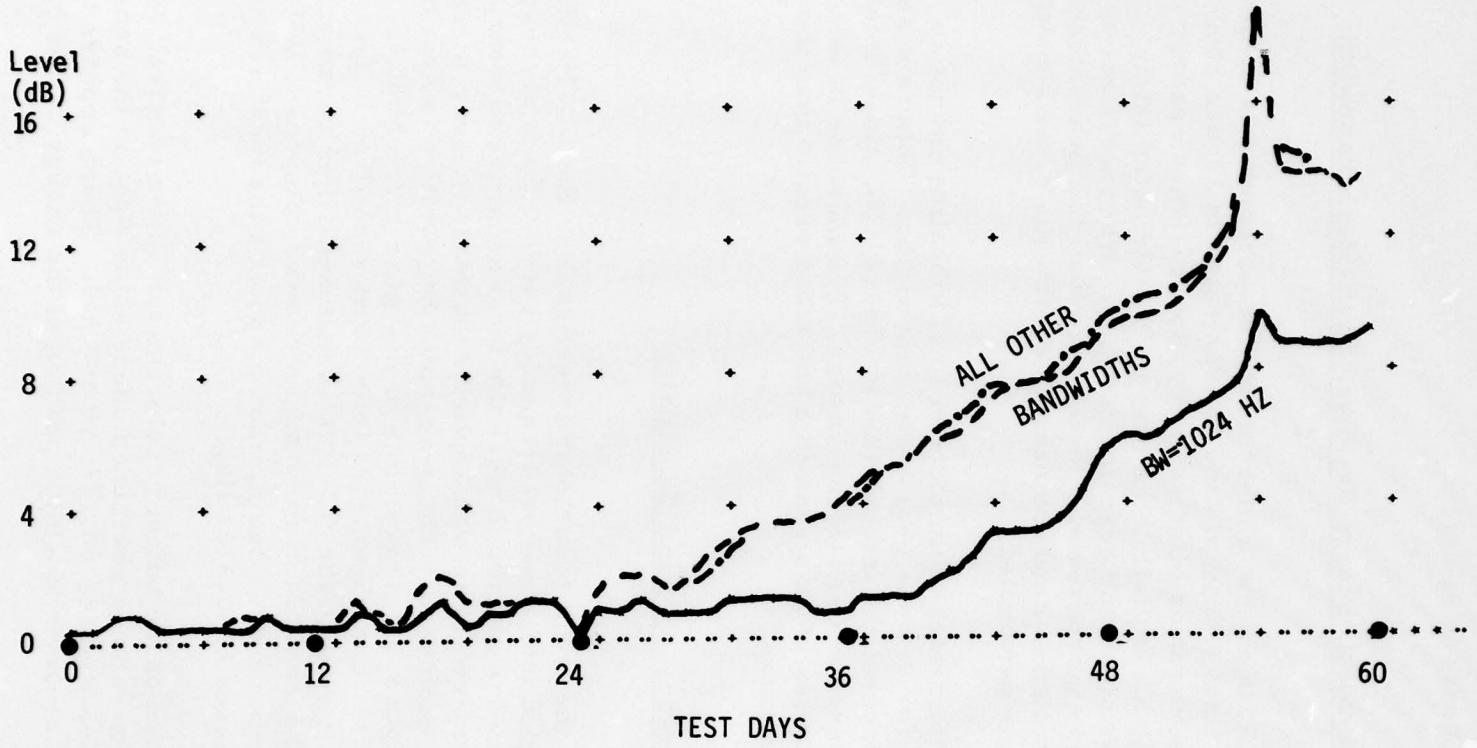

Figure 108. Noise Mean-Squared Ratio vs. Gear-Mesh Bandwidth.

filter parameter, which encompasses the whole band, should therefore be a more sensitive parameter.

Noise Energy/Gear-Mesh Energy Ratio vs. Gear-Mesh Bandwidth

Another verification that a more sensitive parameter is achieved by considering the total vibration band is illustrated in Figure 109. These plots represent ratios of noise energy to gear-mesh energy vs. gear-mesh bandwidth. Initially, the energy is distributed fairly equally between the noise and gear-mesh bands. When wear starts to develop, the noise increases at a faster rate than the gear-mesh energy, but the function is nowhere near as continuous or as sensitive as the matched-filter parameter.

Figure 110 illustrates ratio plots of total vibration energy to gear-mesh energy for various gear-mesh bandwidths. This is essentially another way to represent the information in Figure 109, since Total Energy = Noise Energy + Gear-Mesh Energy. The increase in this ratio as wear increases is less sensitive and more erratic than the matched-filter parameter.

Investigation of Frequency Band Sensitivity

To complete the trend parameter investigation, the DC-10 kHz spectrum was divided into six equal frequency bands. Each of these bands was examined to see which were the most sensitive to wear. First, the mean-squared ratio was applied separately to gear-mesh components within each band. The gear-mesh bandwidth was kept constant at 64 Hz. Figure 111 shows plots of the gear-mesh MSR vs. the six frequency bands. Band 5 appears to be most sensitive, in fact slightly more sensitive than the DC-10 kHz matched-filter parameter. Figure 112 plots the noise MSR (or non-gear-mesh component MSR) within each of the six bands. Again, band 5 appears the most sensitive. This band encompasses 6640-8261 Hz.

An examination of the output accelerometer power spectral density plots for the various gearboxes sheds some light on the sensitivity of band 5. (See Figures 64, 77, 90, and 104.) There appears to be a mechanical resonance causing a peaking of the energy in this band.

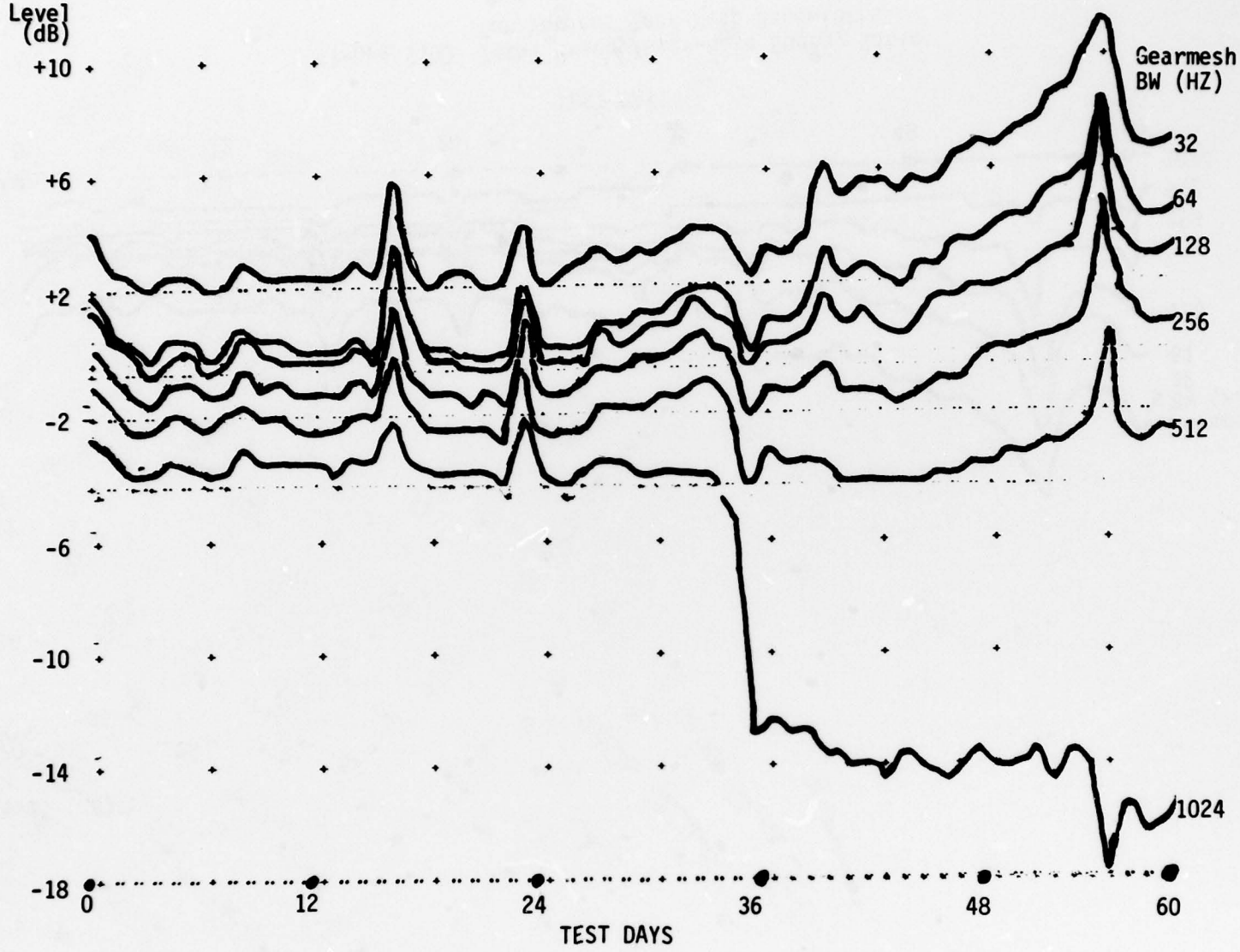

Figure 109. Noise Energy/Gear-Mesh Energy Ratio for Various Gear-Mesh Bandwidths.

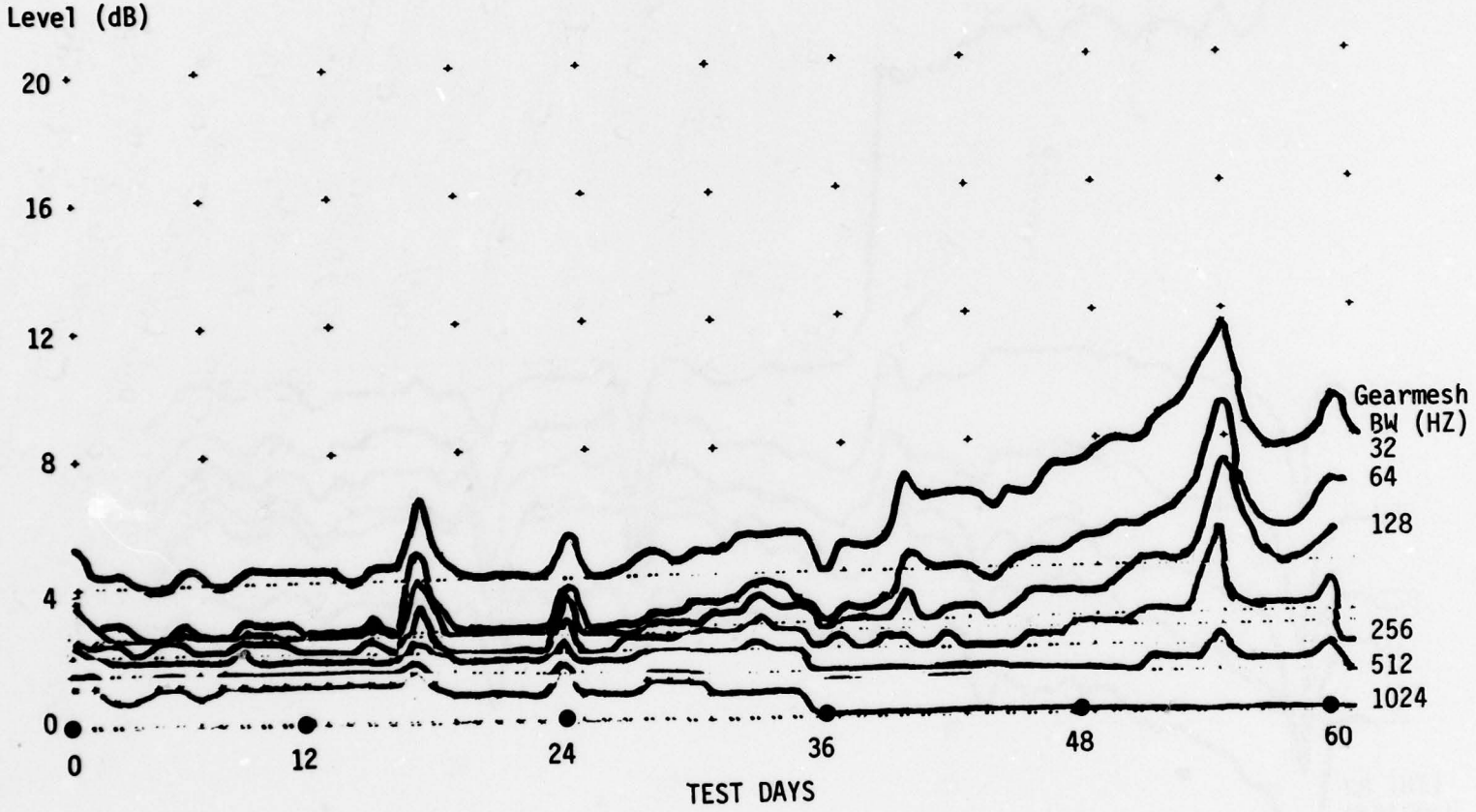

Figure 110. Total Energy/Gear-Mesh Energy Ratio for Various Gear-Mesh Bandwidths.

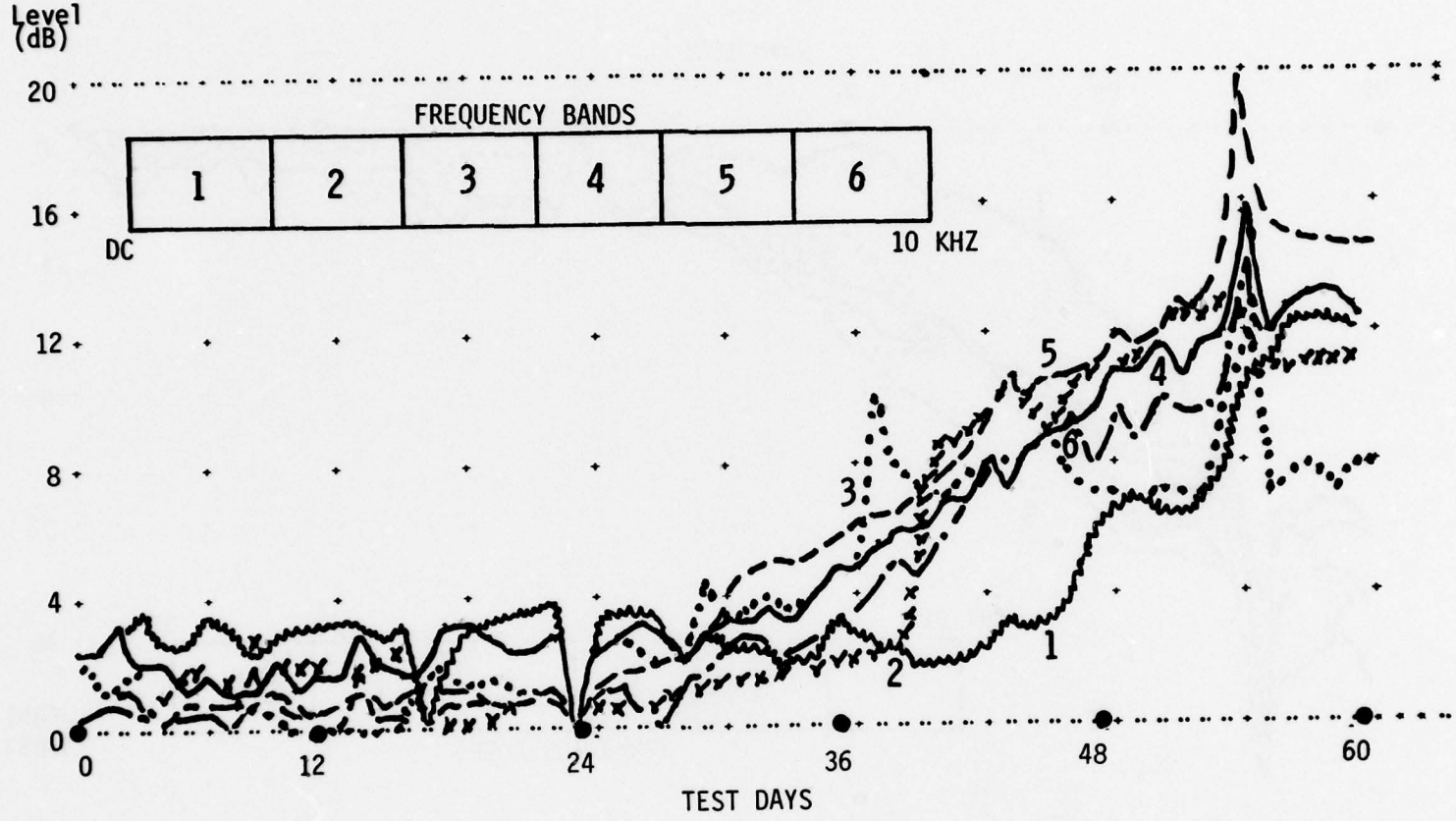

Figure 111. Gear-Mesh Mean-Squared Ratio vs. Frequency Band.

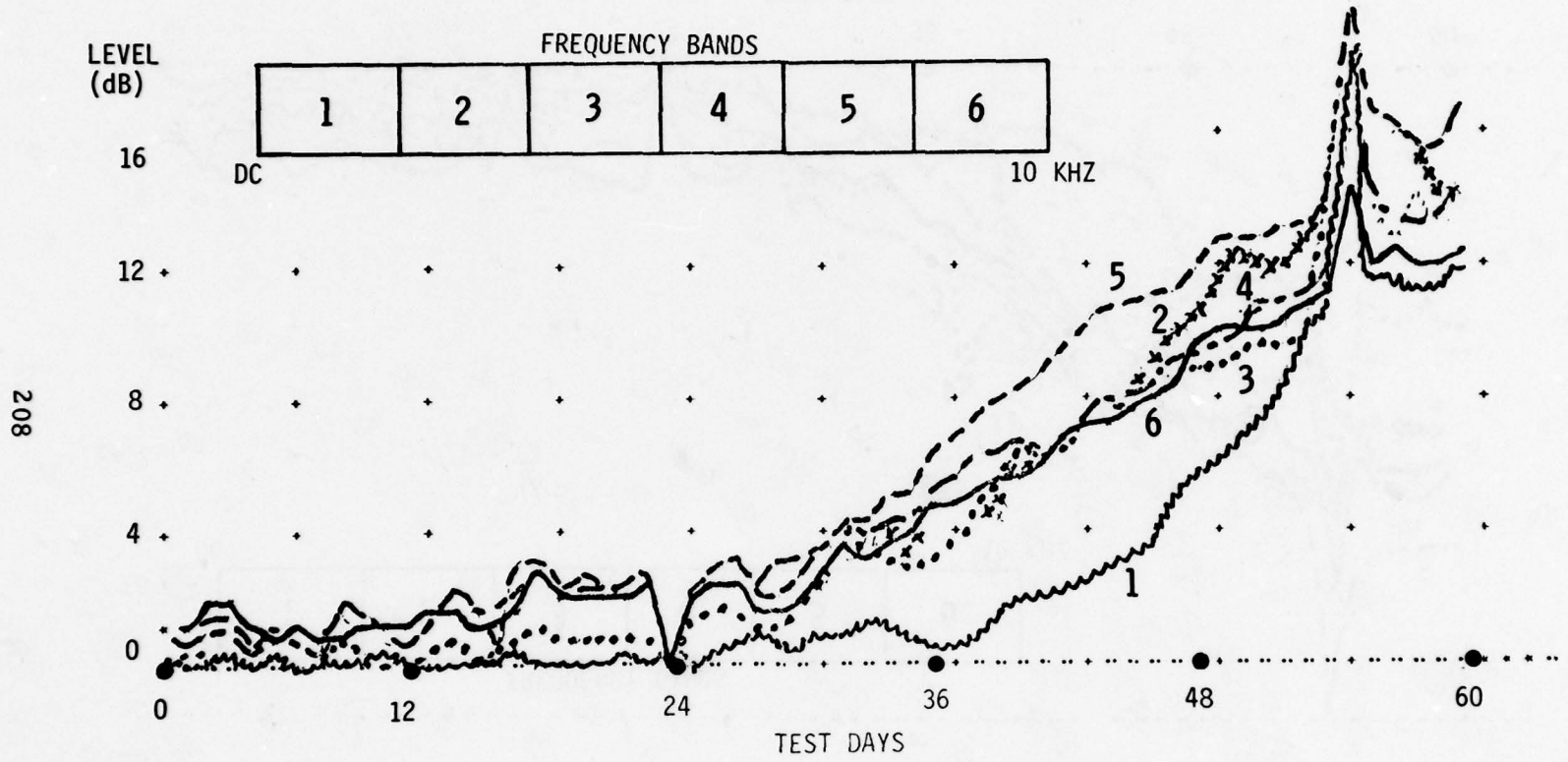

Figure 112. Noise Mean-Squared Ratio vs. Frequency Band.

Observation of the input accelerometer power spectral densities (see Figures 63, 76, 89, and 103) shows no resonance effect.

It would appear that a precautionary approach should be taken toward assuming that band 5 offers the best trend indication. Without an exhaustive search of the entire data base (which was not taken on this contract) it seems safer to rely upon the matched-filter parameter as the better trend parameter for prognostic work.

TREND DETECTION INVESTIGATION

Once a sensitive trend parameter has been established, numerous curve-fitting techniques may be applied to the data to aid in failure prognosis. However, since curve-fitting a straight line introduces no new prognostic information, it is desirable to be able to detect when a departure from a healthy stationary condition occurs. Instrumentation and environmentally introduced noise sometimes mask the commencement of a true wear trend and at other times may introduce false short-term trend indications.

Of the six Class II trend parameters investigated, only one appeared better than the Class I matched-filter parameter. This was the processed MSR data from band 5 of the spectrum. However, due to the questionability of the data because of an accelerometer resonance phenomenon, it appears the more prudent choice would be to investigate the relative trendability and computational complexity of the three highest-rated Class I broadband parameters: (1) matched-filter RMS, (2) geometric mean and (3) arithmetic mean.

To minimize false trend indications, two processes were applied before trend detections to the trend parameters derived from the PSD data. These were (a) step-compensation and (b) 24-hour smoothing. The first process subtracts out any step-discontinuities greater than or equal to 2 dB between consecutive 1-hour samples. The second process performs a 24-sample (hour) moving average of the data. Figure 113 illustrates the flow diagram of the combined data editing algorithm. Each final processed data value thus represents the mean value of the unsmoothed data over the previous 24-hour period, after 2 dB or greater steps have been subtracted.

Many techniques may be used to detect trends: slope computations, inflection point checks, least-squares curve fitting, etc. It is desirable, though, especially if a large amount of equipment is being monitored, to maintain a low computational burden on this phase of monitoring. For this reason, a simple computational algorithm that is sensitive to trend commencement has been used in our failure prognosis effort: the reverse-arrangements technique.[4] What makes

4. Otnes, R.K., and Enochson, L., "Digital Time Series Analysis," Wiley and Sons, 1972, p. 400.

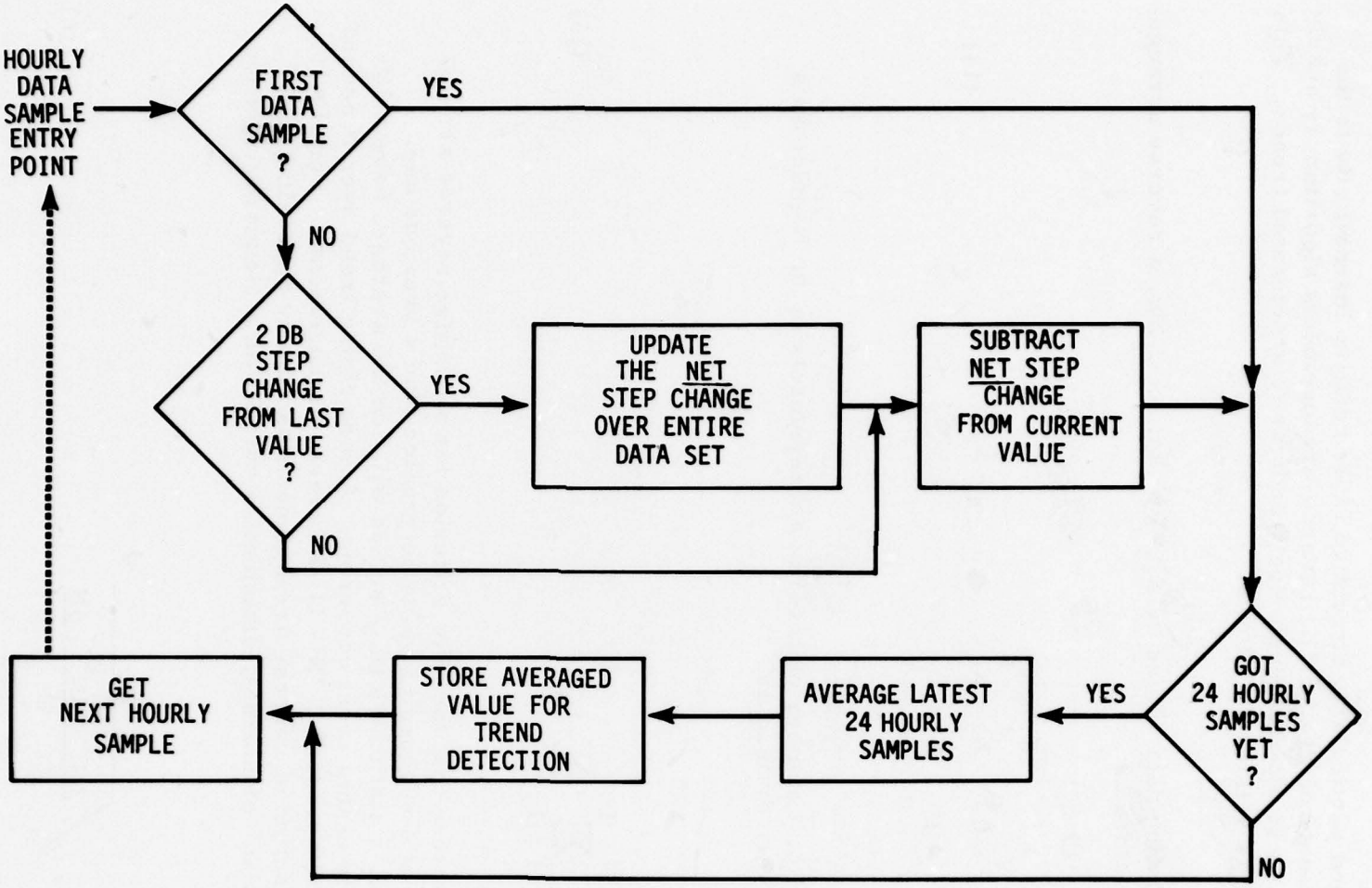

Figure 113. Data Editing Algorithm Flow Diagram.

this method particularly attractive is its relative insensitivity to the rate of change of wear. The reverse-arrangements algorithm is nearly as sensitive to slower developing trends as to accelerated trends. This algorithm is defined as follows:

Denoting data values by X_1, X_2, X_3, ---, X_N, a reverse arrangement is defined as

$$a_{ij} = \begin{cases} +1 & X_j > X_i \\ 0 & X_j = X_i \\ -1 & X_j < X_i \end{cases} \qquad (14)$$

The total number of reverse arrangements in an N-point data record is then defined as

$$A = \sum_{i=1}^{N-1} \sum_{j>i} a_{ij} \qquad (15)$$

It is seen that the only criterion for a positive reverse arrangement is that a succeeding value be greater than a previous one. Therefore, a stationary time series will, on the average, have a 50% probability of this event occurring. A pure rising trend over N record points would produce N (N - 1) /2 reverse arrangements. For $N \geq 10$, the distribution of reverse arrangements is closely approximated by the Gaussian, or normal, distribution curve with a standard deviation of

$$\sigma_A = \sqrt{\frac{2N^3 + 3N^2 - 5N}{18}} \qquad (16)$$

Figures 114 through 115 illustrate various synthesized trends using a 16-point data record. The normalized sum represents the ratio of the summed reverse arrangements to the maximum value of A possible.

Unlike the synthesized data, the gearbox trend data exhibits 24 cyclic variations which could be considered short-term trends. A good example of how 24-hour smoothing of the data eliminates this effect and allows the trend detector to identify true trends is illustrated in Figure 116. Here, displays of approximately 200 hours of HT-3 matched-filter data, both before and after smoothing, are presented, together with their respective reverse-arrangements normalized sums. The smoothed and unsmoothed data is displayed in the (B) and (D) curves, respectively, in Figure 116. Note the cyclic variations in the (D) trace occurring roughly 24 hours apart. The (A) and (C) curves represent the reverse-arrangements trend detector output to each of the data sets. The differences are particularly striking. In the (A) curve, trends have been detected at three points in the data sequence. The first two proved to be false, as they eventually decayed. The third is a valid trend and occurs at roughly the 590th hour. Since the gearbox was finally removed after over 1400 hours of testing, this is a significant detection. However, in the (C) curve, short-term trends are detected and are sufficiently strong to pass the decision threshold located at the 51% point of the vertical scale. These 24-hour cyclic trends are successful in masking the detection of the true wear trend at the 590th hour. The value of smoothing thus becomes very apparent with this example.

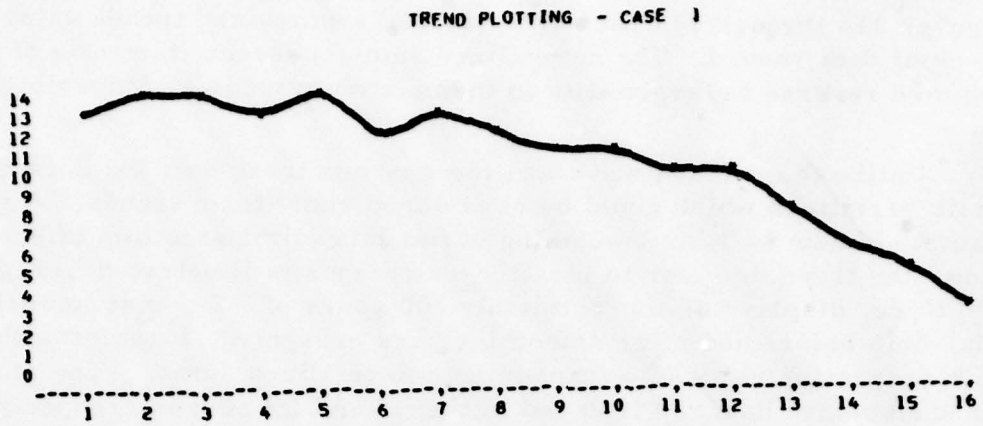

(A) Normalized Sum = -.84

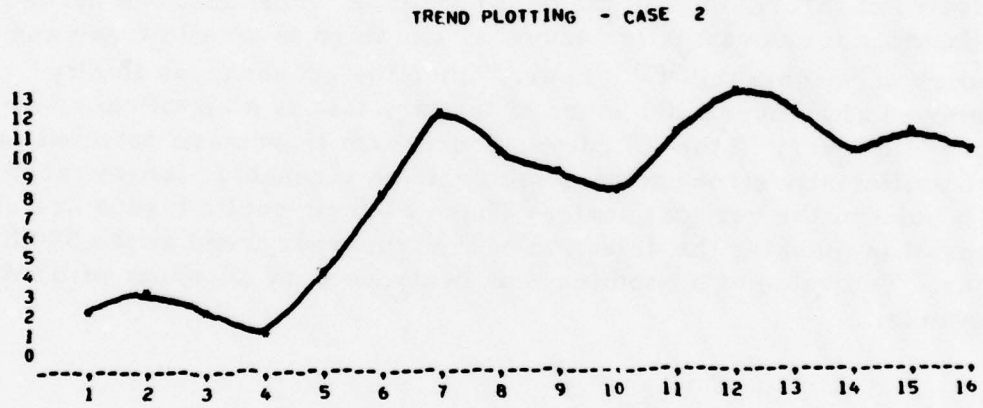

(B) Normalized Sum = +.54

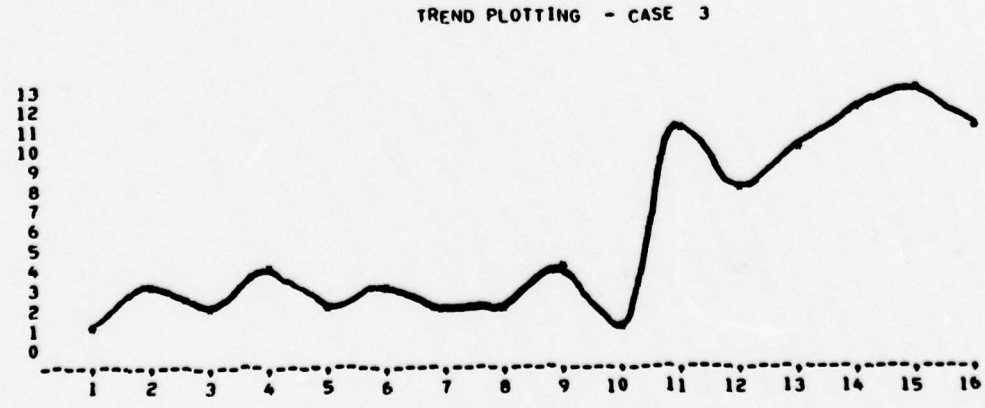

(C) Normalized Sum = +.55

Figure 114. Reverse-Arrangements Scores for Various Waveforms.

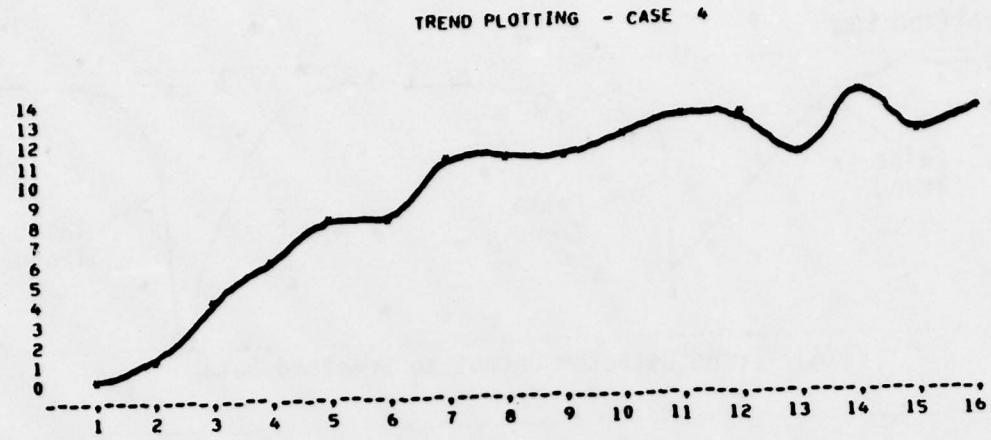

(A) Normalized Sum = +.79

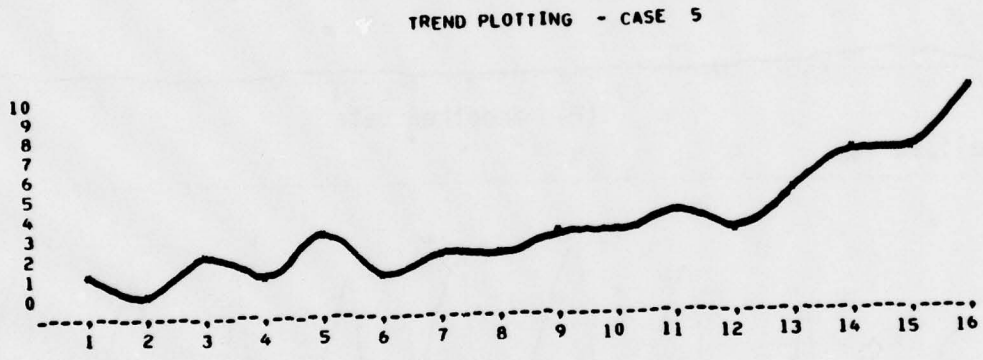

(B) Normalized Sum = +.78

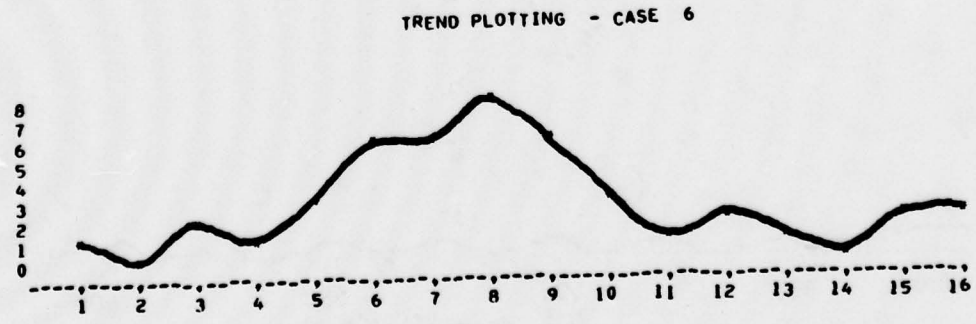

(C) Normalized Sum = -.01

Figure 115. Reverse-Arrangements Scores for Various Waveforms.

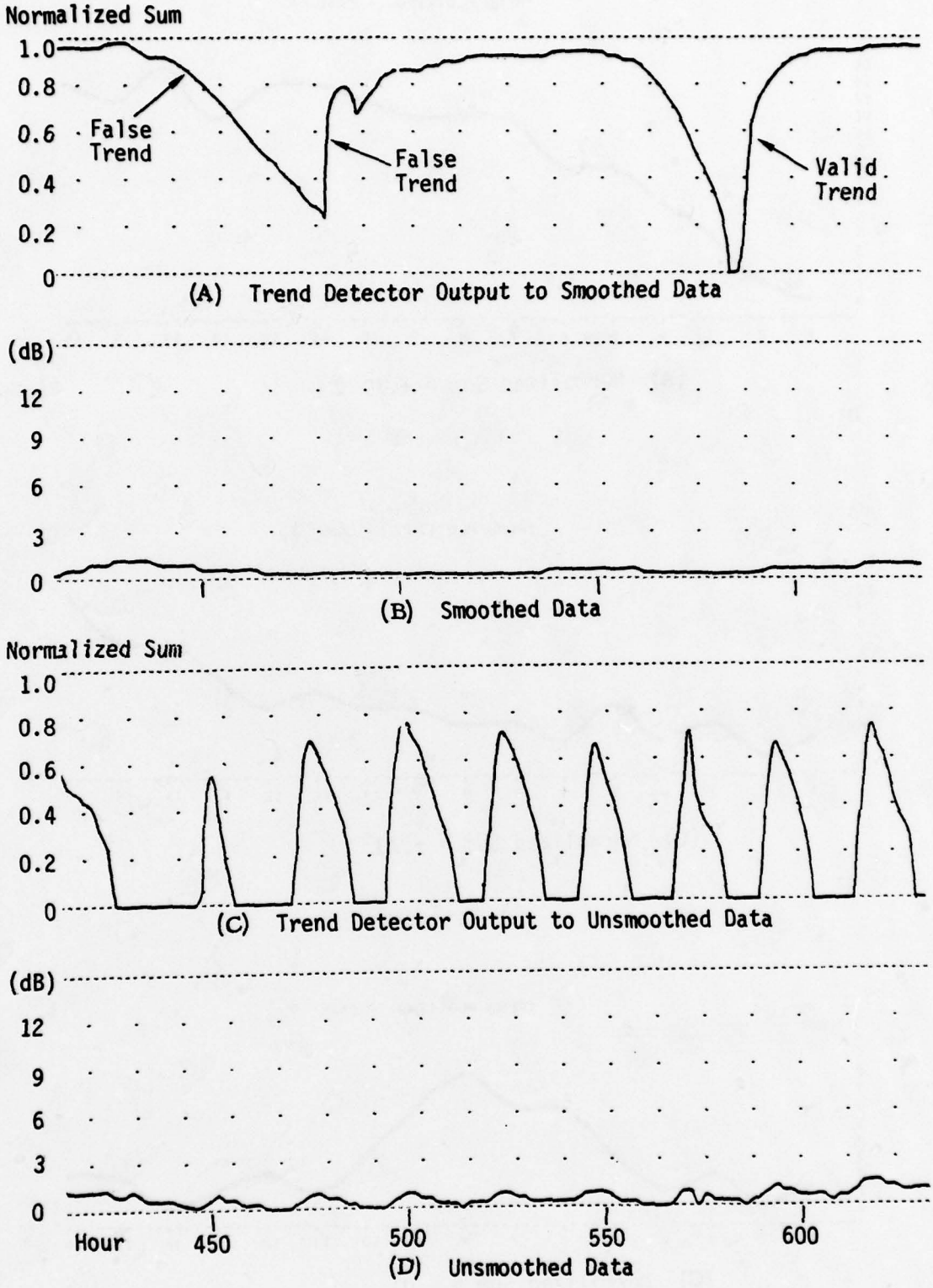

Figure 116. Reverse-Arrangements Trend Detector Applied to HT-3 Matched Filter Output Raw and Smoothed Data.

TREND DETECTION ALGORITHM

In this contractual effort only positive-going trends were considered, since the parameters used on this program increased as the wear process increased. Of major importance in using the reverse-arrangements trend detection method is the establishment of a suitable algorithm that will detect a trend at the earliest possible time and reject the data later if it appears that the trend was not valid. It was decided to do a trend detection continuously on the last 12 hourly samples of the matched-filter parameter. If the trend detector normalized sum exceeded a confidence threshold, the trendable data base was allowed to expand, again testing each hour with the expanded data base. If at any time the normalized sum dropped below the confidence threshold, all but the last 12 hourly samples were discarded and trend detection was then resumed. On the other hand, if no intermediate rejections occurred, the trendable data base was allowed to expand until 96 continuous hours of trendable data were accumulated.

Figure 117 illustrates a flow diagram of the trend detection algorithm. In order to establish a confidence threshold level, the Gaussian properties of the reverse-arrangements algorithm were again examined. It was decided that a 99% confidence level should be the design goal. However, an examination of the probability distribution of reverse-arrangements sums indicates that the ratio of standard deviation of the R. A. score to the maximum possible R. A. score decreases as N, the number of samples, is increased. For this reason, the 99% confidence threshold will also decrease as the data base is expanded, since this level may be calculated from normal or Gaussian distribution tables to be 2.3 σ. Table 7 lists the values of A_{MAX}, σ, σ / A_{MAX}, and the 99% threshold for samples of 12, 24, 48, and 96 consecutive hours.

TABLE 7. REVERSE-ARRANGEMENTS STATISTICS FOR VARIOUS SAMPLE SIZES

No. of Hourly Samples	MAX R. A. Sum A_{MAX}	Standard Deviation	$\frac{\sigma}{A_{MAX}}$	99% Threshold level = $2.3\,\sigma/A_{MAX}$
12	66	14.58	.22	0.51
24	276	40.32	.15	0.34
48	1128	112.51	.10	0.23
96	4560	315.93	.07	0.16

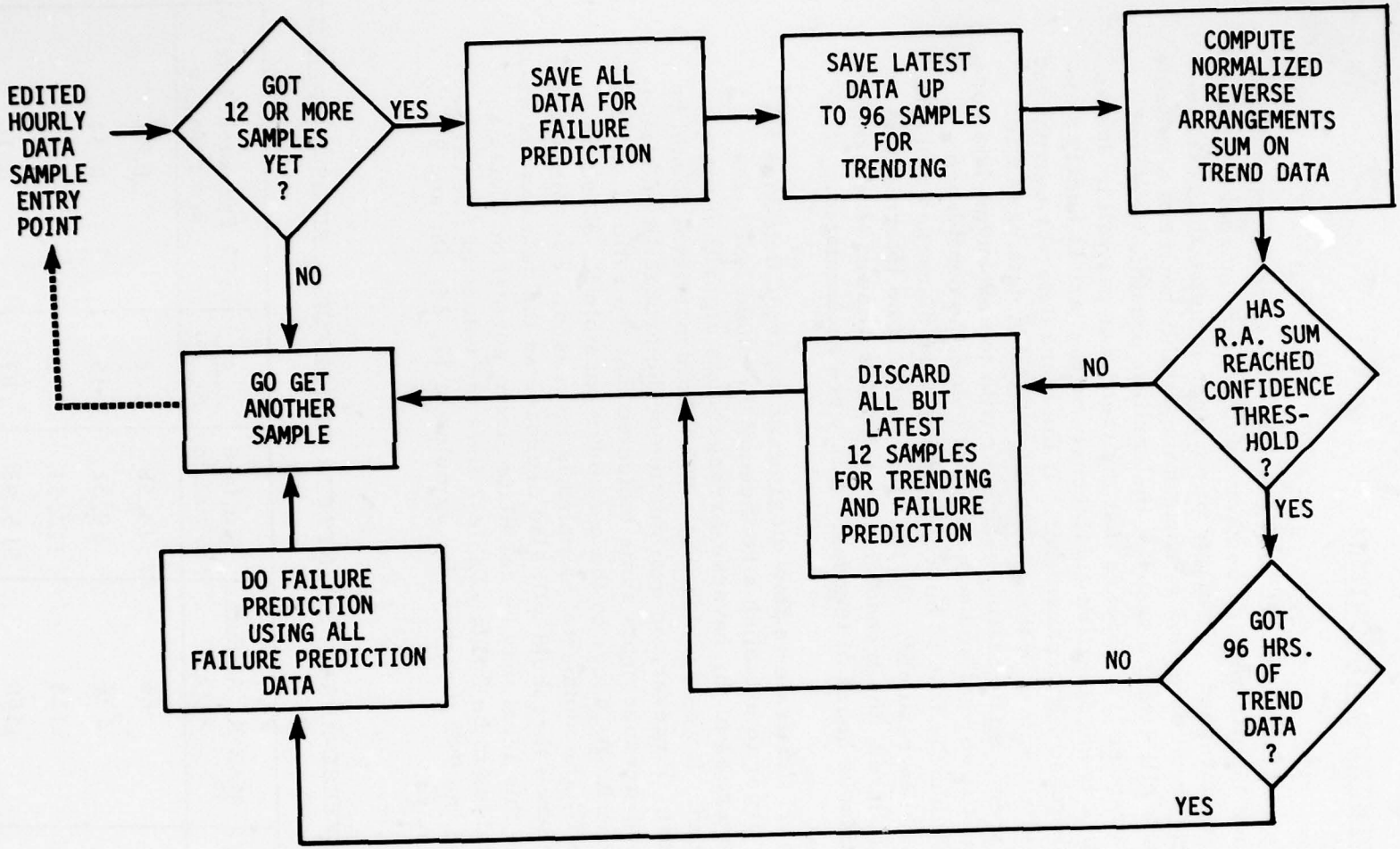

Figure117. Trend Detection Algorithm Flow Diagram.

Figure 118 illustrates a plot of this threshold level vs. number of consecutive hourly data samples tested. At each size data set, the decision to expand the data set or reject all but the latest 12 samples was made on the basis of whether the reverse-arrangements sum exceeded the level indicated in Figure 118. The use of this statistical base for decision making is necessary to prevent the use of questionable trending data for failure predictions.

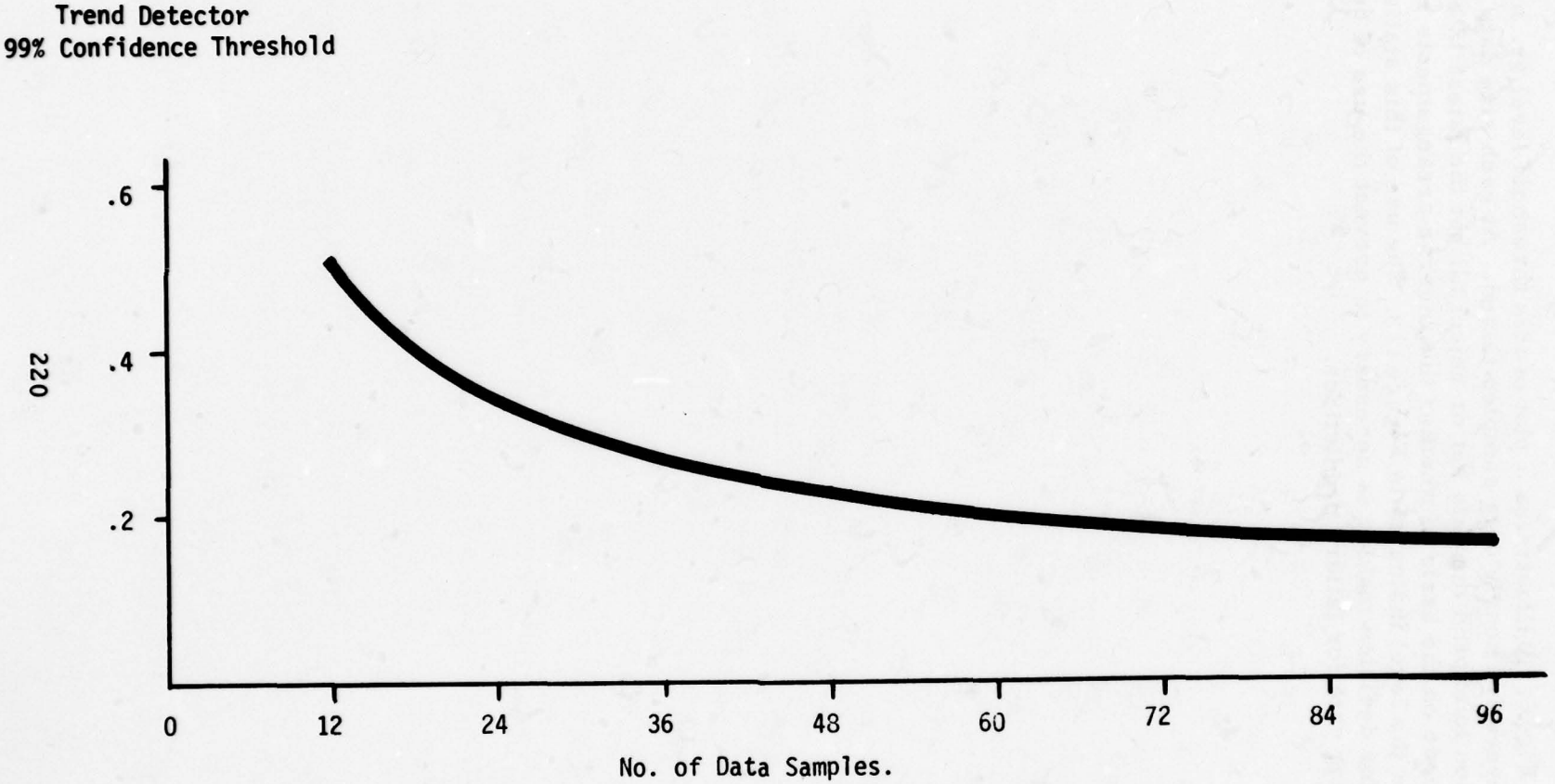

Figure 118. Trend Detection 99% Confidence Threshold vs. No. of Data Samples.

EVALUATION OF MATCHED-FILTER, GEOMETRIC MEAN, AND ARITHMETIC MEAN TREND PARAMETERS USING REVERSE-ARRANGEMENTS TREND DETECTION

The three best Class I trend parameters were selected for a comparative evaluation. The three factors of prime interest are trendability, dynamic range, and ease of computation. Trend dynamic range has already been displayed in Figure 105 and the three Class I parameters having the highest dynamic range and earliest visual commencement of trend are evaluated here. Figures, 119, 120, and 121 illustrate the reverse-arrangements trend detector output and smoothed trend parameter data for the matched-filter, geometric mean, and arithmetic mean trend parameters. Only positive-going trends are displayed. The normalized sum range is 0 to + 1.0. Data from HT-3 output accelerometer was used for the comparison. It is apparent from viewing these trend curves that both the matched-filter and geometric mean parameters detect and sustain the main trend that began at about hour 590. The arithmetic mean parameter detects the commencement of the trend, but at the later plateaus in the data at about the 700th and 850th hours the trend detector output goes much lower than for the other two parameters, indicating that the arithmetic mean trend is unstable.

Figures 122 (A), (B), and (C) illustrate the computational algorithms for these three trend parameters. The arithmetic mean has the simplest computation; the matched filter is the most complex, requiring stored reference PSD data.

Table 8 lists the three parameters and their relative grades on the three factors of trendability, dynamic ranges, and ease of computation. Grading is on a best low score basis on a range of 3. It is seen that both the matched-filter and geometric mean parameters score equally. The matched-filter parameter will be used for failure prediction modeling because it is the leader in two out of three of the categories.

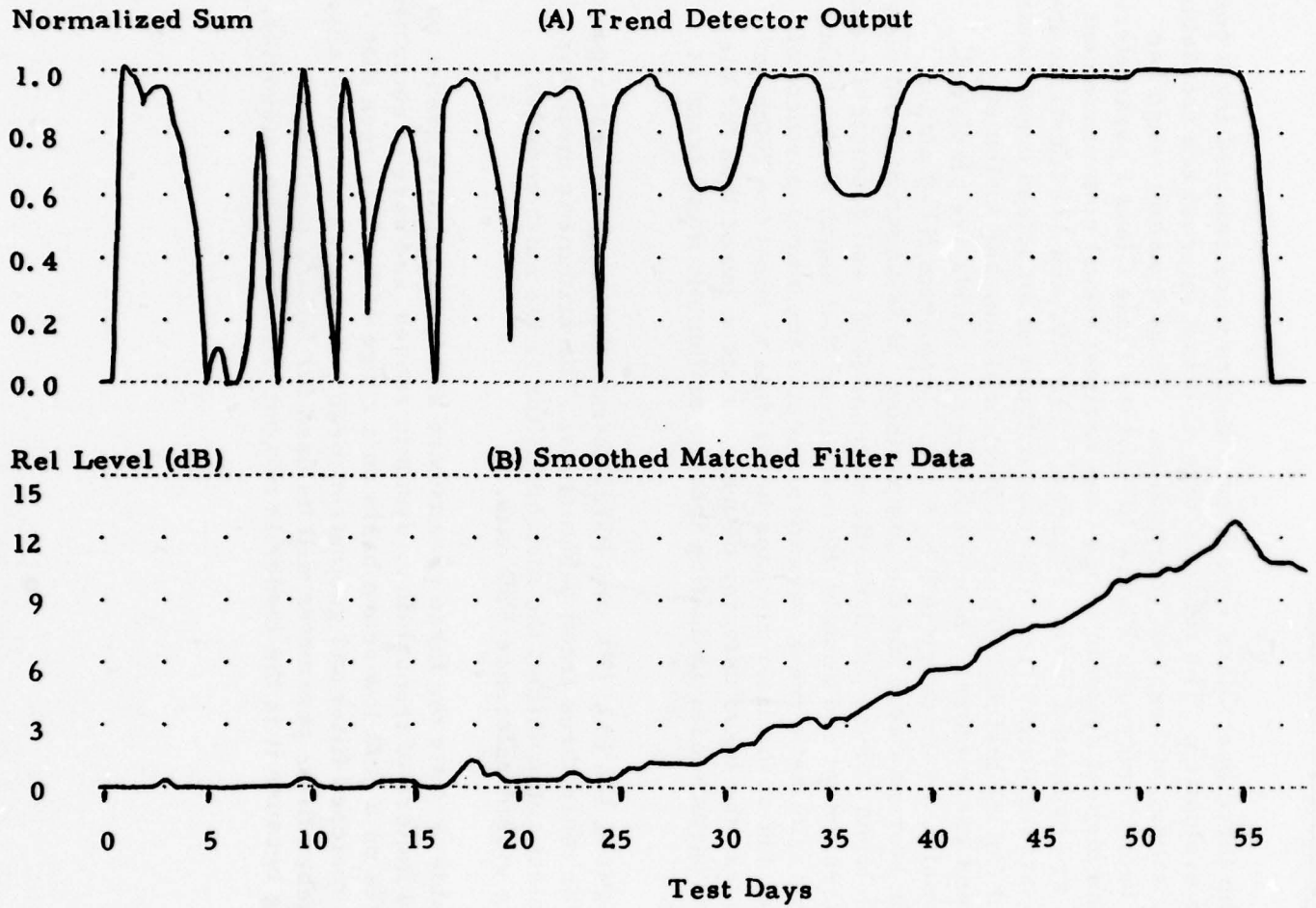

Figure 119. Matched-Filter Data Trend Detection.

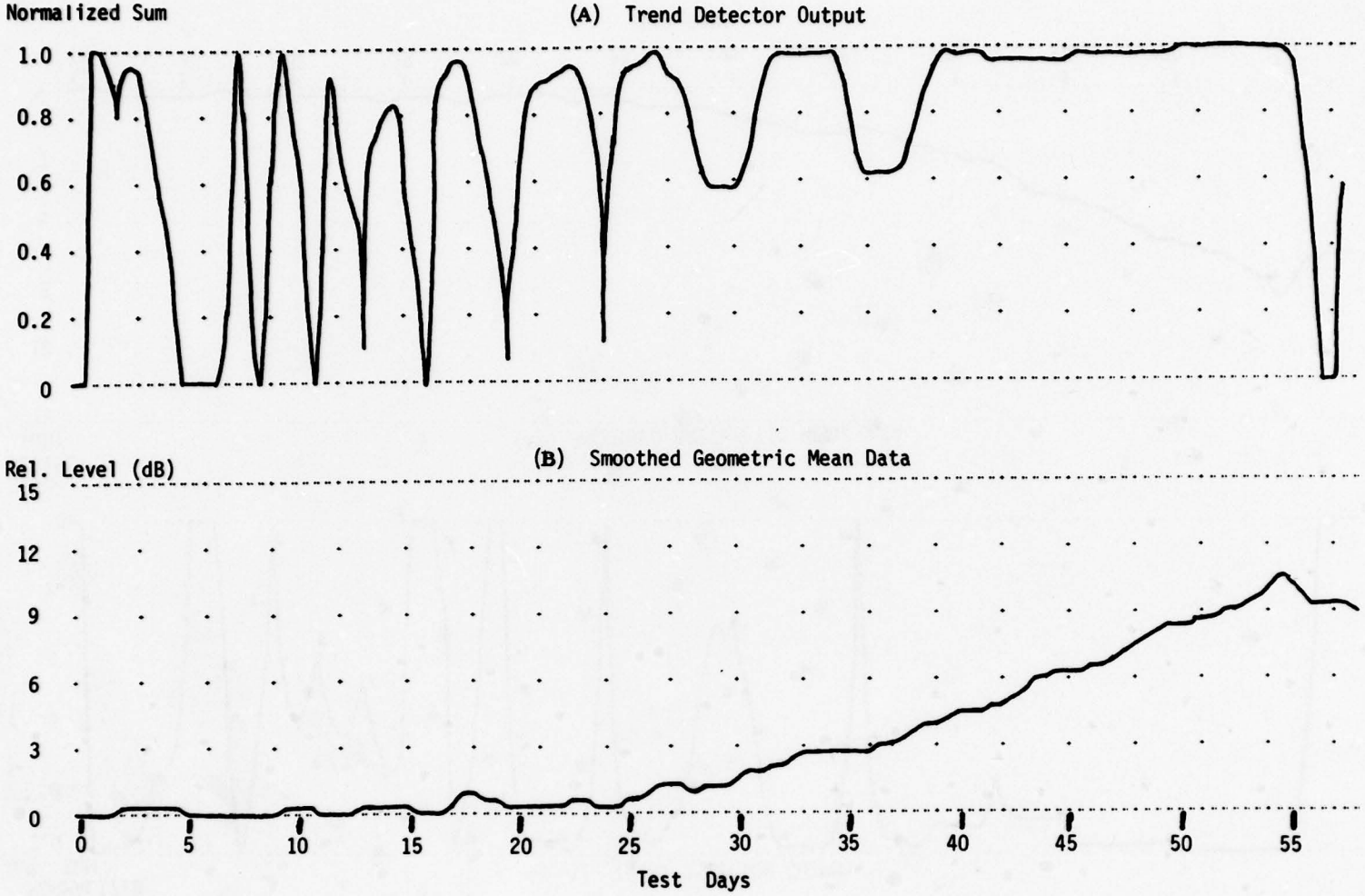

Figure 120. Geometric Mean Data Trend Detection.

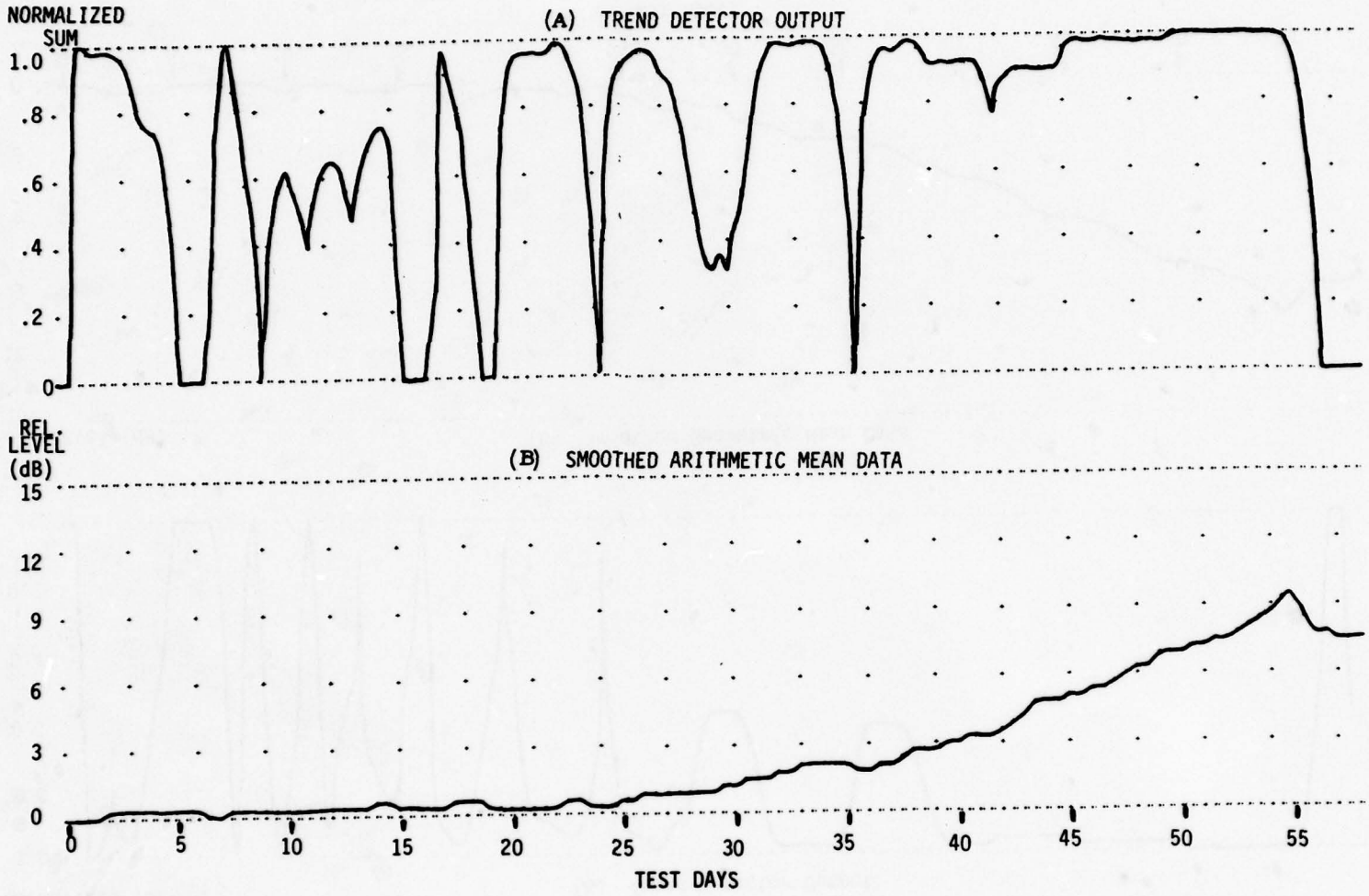

Figure 121. Arithmetic Mean Data Trend Detection.

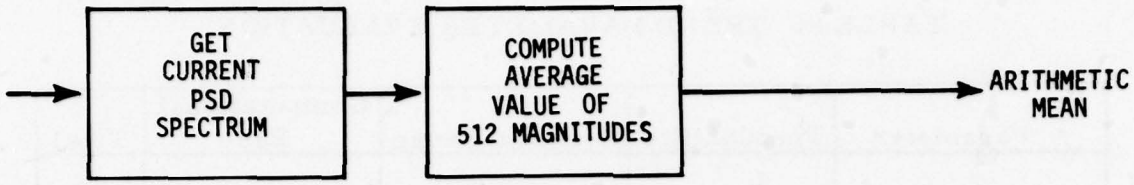

(A) ARITHMETIC MEAN COMPUTATION

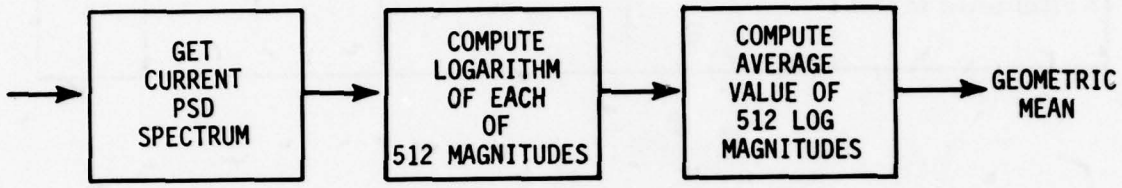

(B) GEOMETRIC MEAN COMPUTATION

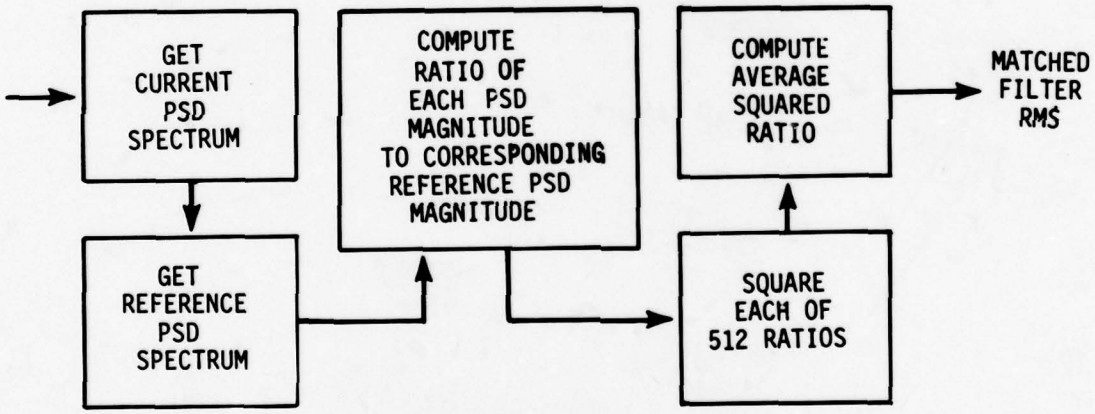

(C) MATCHED FILTER COMPUTATION

Figure 122. Computational Algorithms for Three Trend Parameters.

TABLE 8. TREND PARAMETER EVALUATION

Parameter	Trendability	Dynamic Range	Computational Ease	Total
Matched Filter	1	1	3	5
Geometric Mean	1	2	2	5
Arithmetic Mean	2	3	1	6

WEAR TREND MODELING

METHODOLOGY

Exponential curve-fitting is the method chosen for extrapolating failure predictions using the data collected from the gearbox tests. A fairly valid assumption can be made that the rate of change of a fault or wear in a gearbox component at a particular time is directly proportional to the magnitude or extent of the fault at that time. This concept of exponentially increasing wear is also apparent in statistical life prediction modeling of bearing fatigue life.[5,6]

This assumption of an exponential rise with increasing component wear appears to have been borne out by an examination of the trend parameters of the present data base. All incipient failures were characterized by this quasi-exponential rise in parameter level. Of all the vibration trend parameters considered on this program, the matched-filter processing has proved to be the most sensitive to early detection of failure modes. Consistently through all the individual gearbox tests, matched-filter data was characterized by a higher rate of change in its magnitude. For this reason, this parameter was chosen for exponential curve fitting.

A review of the least-squares theory of exponential curve-fitting is presented in Appendix B.

MATH MODEL EVALUATION

The matched-filter RMS trend parameter was applied to nearly 5000 hours of test data on the six gearboxes, and the trend curves were examined on those gearboxes that failed in an attempt to derive a characterizing mathematical model for the wear process. Figures 123 A, B, and C illustrate three such time histories plotted for output accelerometer data from gearbox HT-3 and input accelerometer data from

5. "Mechanical Component Failure Prognosis Study," AiResearch Manufacturing Company; USAAMRDL-TR-73-26, Eustis Directorate, U.S. Army Air Mobility Research and Development Laboratory, Fort Eustis, Virginia, June 1973, AD 7710 33.

6. Rothbart, H. A., Mechanical Design and Systems Handbook, McGraw-Hill, 1967, p. 13-52.

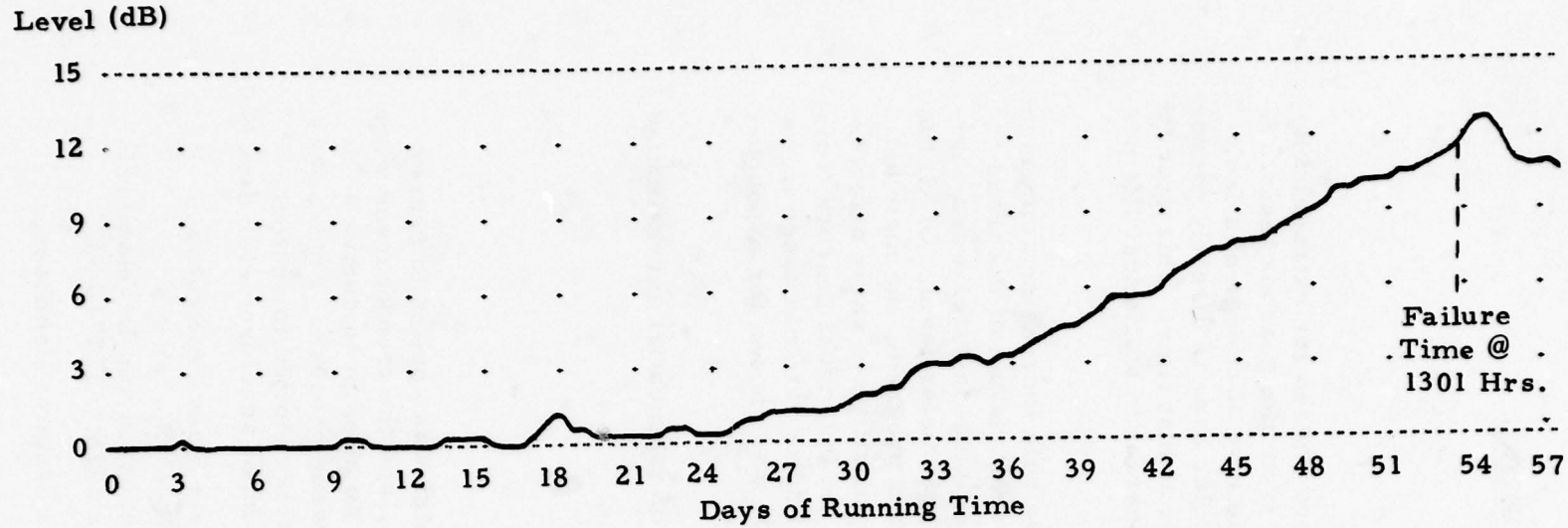

(A) Gearbox HT-3

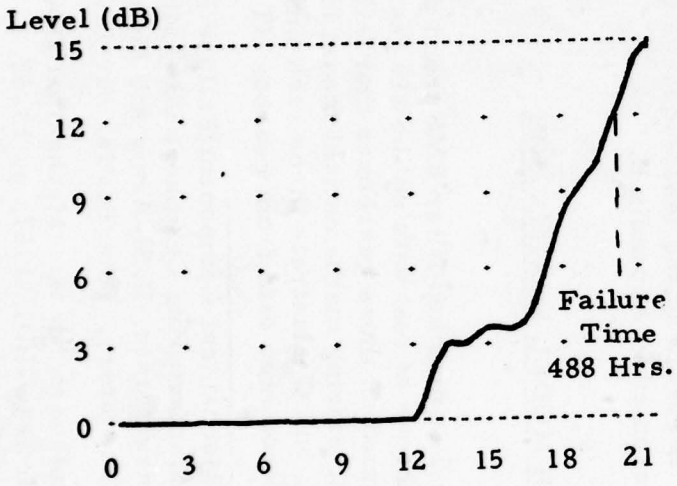

(B) Gearbox HT-4

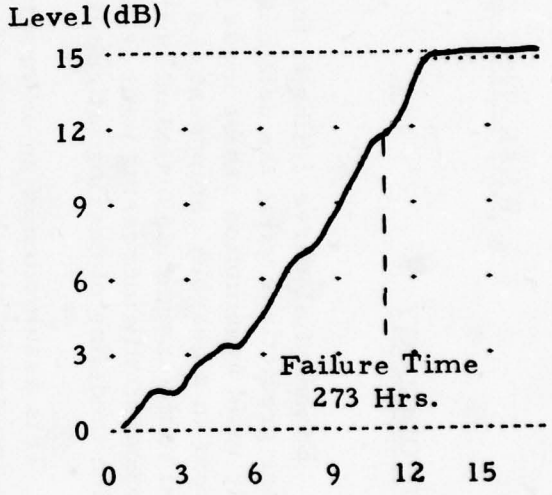

(C) Gearbox BB-5

Figure 123. Smoothed Matched-Filter Data for HT-3, HT-4, and BB-5 Gearboxes.

gearboxes HT-4 and BB-5. The matched-filter parameter is plotted in decibels. The initial matched-filter value is always near zero dB. On the logarithmic scale, the initial wear trend appears to be linear, implying an exponential increase in the matched-filter parameter. As time increases a second order curvature appears. Three different failure prediction models were examined using smoothed matched-filter data from HT-3 output accelerometer. The results of the HT-3 prediction are illustrated in Figure 124. Figure 124(A) illustrates time histories for three different failure prediction methods. Figure 124(B) presents the reverse-arrangements trend detector output for the smoothed data of Figure 124(C).

Key items to observe on Figure 124 are the following: (1) A critical level of 12 dB was chosen as the arbitrary failure time. This level either fell near the peak matched-filter output or in the upper 25% of the dynamic range on all test data. (2) The trend detection algorithm illustrated in Figure 117 was utilized to begin accumulating data for failure predictions. All consecutive hours of data were then accumulated for prediction model curve-fitting, unless the trend detection level fell below the threshold. In the latter case, all but the last 12 hourly samples of the data was discarded, until the trend detector output again rose to the threshold. (3) The first failure predictions were made after accumulating 96 hours of trendable data. The predicted failure time represents an estimate by the prediction model of when the matched-filter data will reach the + 12-dB critical level.

As can be seen in Figure 124(A), three different prediction models are illustrated. The curve labeled "(3)" is obviously the best predictor, and it evolved from attempts at models (1) and (2). A brief description will be given of all three models:

(a) Model 1

This model was an unrestricted second order polynomial least-squares curve fit of the data: $y(t) = B_o + B_1 t + B_2 t^2$

It is seen that after 200 hours have elapsed, this curve begins to converge toward the correct failure time. However, even though the data was rising in a positive fashion up until this time, the rate of change of the data was erratic. In fact, over a good portion of the time the best fit was to an inverted parabola because the data rate of change became lower after the initial trend detection.

It became obvious that restrictions would have to be placed on the second order fit to assure a predictable monotonic rise in the data level.

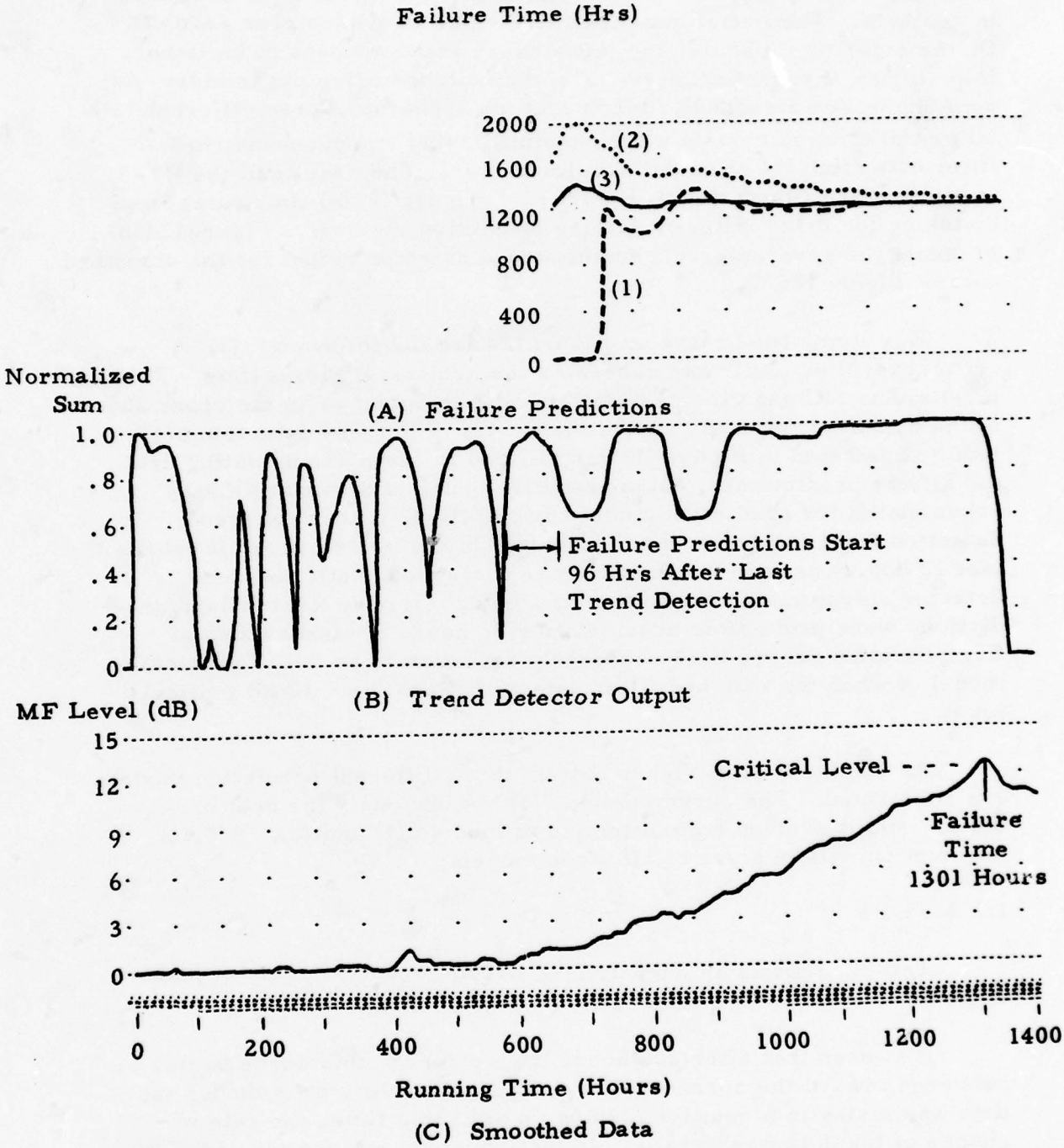

Figure 124. Failure Predictions and Trend Detection Using HT-3 Output Accelerometer Matched-Filter Data.

(b) Model 2

Before attempting to place restrictions on the second order polynomial model, a first order model was examined. Since the data definitely had a positive slope, the first order model would not encounter any of the mathematical difficulties of the second order model, as long as the average rate of change of the data was positive. The first order polynomial model is $y(t) = B_o + B_1 t$.

Again observing Figure 124(A), the first order (dotted curve) predictor is seen to always predict more "useful remaining life" than is actually present. This occurs because the best model for this wear process is more accurately represented by a second order model. Overall, there will be a nearly constant acceleration of the matched-filter parameter, as represented on a dB or logarithmic scale.

(c) Model 3

The restriction that was placed on the second order prediction model to achieve the prediction curve of Model 3 is reasonable, and seems intuitively correct. Defining t_o as the time that the trend is detected, an earlier time, $t_v = t_o - \Delta t$, is assumed to be the time that the trend actually started. Mathematically, t_v is the time that the rate of change of the trend parameter is zero. Figure 125 illustrates how the data is fit to this model. A second order least-squares fit is still used, with the restriction that the first data point occurs at a time Δt later than the vertex of an upward-opening parabola. The mathematical expression for this model is the same as that for Model 1, except that B_2 is restricted to be positive and coefficients B_o and B_1 are related to t_o and Δt, both fixed quantities.

With these underlying assumptions, the following mathematical model was used to predict the time of failure of the component:

$$t_F = t_o - \Delta t + \sqrt{\frac{P_{crit} - P_o}{K}} \qquad (17)$$

where t_F = predicted failure time

t_o = time that trend was detected

Δt = period of undetectable rising trend (fixed)

P_{crit} = value of trend parameter at failure time (fixed)

P_o and K are coefficients of the parabola that best fits the trend data in the least-squares sense. These parameters are graphically depicted in Figure 125 and may be computed by classical least-squares polynomial approximation methods.

Because the third model appeared to be the most realistic for use in failure prediction, it was used for the remainder of the gearbox data base. A flow diagram of the failure prediction algorithm using this model is illustrated in Figure 126.

Various values were used for Δt in curve fits of data from gearboxes HT-3, HT-4, and BB-5. These gearboxes were selected because all three test runs were reasonably long and resulted in gear or bearing failure. A value of Δt = 500 hours appeared to be a reasonable compromise using the limited amount of data. Using lower values of Δt results in failure times that are too low, initially. Likewise, using larger values of Δt results in too high values of predicted failure time during the first 200 hours of predicting.

Table 9 tabulates the results of applying the prediction algorithm (using Δt = 500 hours) to the three gearboxes. It is seen that rapid convergence to the true failure times results after accumulations of 100 - 200 hours of trendable data.

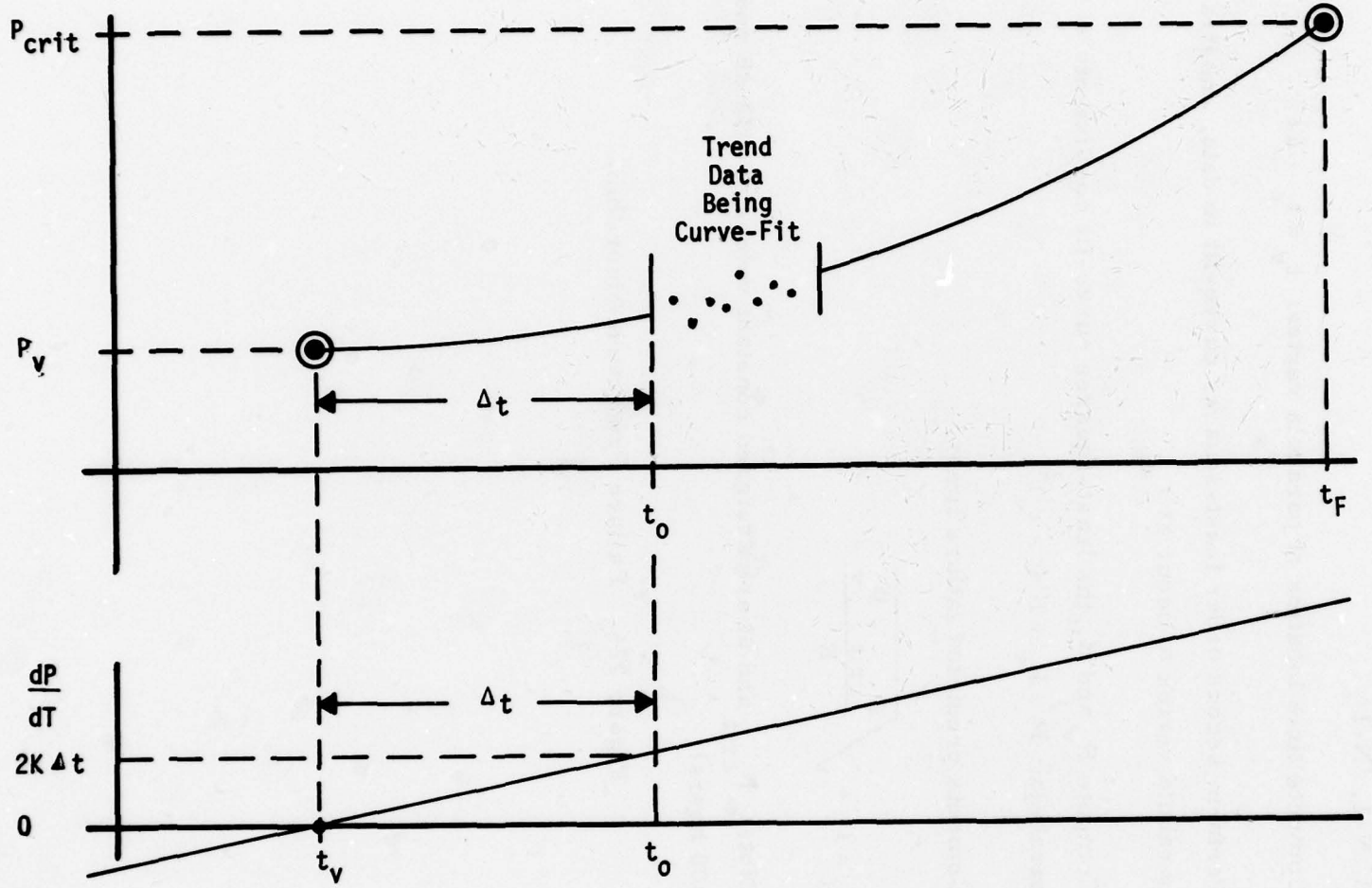

Figure 125. Graphical Depiction of Failure Prediction Model.

1. Gather N failure prediction data pairs: (P_o, t_o), (P_1, t_1), --- (P_{N-1}, t_{N-1})

2. Compute time location of parabola vertex: $t_v = t_o - \Delta t$

3. Perform second order least-squares curve-fit to data, constraining parabola vertex to occur at t_v.

4. Compute P_v and K, the least-squares curve-fit coefficients of the parabola: $P = P_v + K (t - t_v)^2$

5. Compute predicted failure time:

$$t_f = t_v + \sqrt{\frac{P_{crit} - P_v}{K}}$$

(Note: P_{crit} and Δt are assigned constant values of + 12 dB and 500 hours)

Figure 126. Failure Prediction Algorithm.

TABLE 9. FAILURE TIME PREDICTIONS FOR THREE GEARBOXES MADE AT 100, 150, AND 200 HOURS AFTER TREND DETECTION.

	Time (Hours)		
	Gearbox HT-3	Gearbox BB-5	Gearbox HT-4
Trend Detection Hour, t_o	590	24	175
Actual Failure Hour, t_F	1301	273	488
Time of Prediction:			
t_o + 100 Hours	1398	359	1070
t_o + 150 Hours	1438	335	519
t_o + 200 Hours	1324	309	487

APPLICATION OF TEST CELL DATA TO SMOOTHING, DETECTION, AND PREDICTION ALGORITHMS

CRITERIA FOR SENSOR DATA SELECTION

It became obvious during the testing phase of this program that signs of wear were being detected in differing degrees from the input and output shaft accelerometers. This becomes clear when we consider that one of these two accelerometers will be physically closer to the center of wear intensity. If one were to decide to select the better of the two locations for a single sensor condition monitor, it would be a very difficult choice and one that was not made in our analysis. Rather, certain criteria were established whenever a decision was made whether or not to make a failure prediction based on the data from a particular accelerometer data base. Three criteria were established as follows:

(1) Both sensor data outputs were processed in parallel (trend parameter computation, compensation, smoothing, trend detection).

(2) Whenever either sensor had collected 96 hours of trendable data, the question was asked: Is its latest trend parameter level greater than + 0.5 dB? If not, the trend is probably a very weak one and the resultant failure prediction will probably have questionable accuracy. Therefore, keep trending but make no failure predictions yet.

(3) However, if the parameter level was greater than + 0.5 dB a check was made to determine if data from the other accelerometer had passed criterion No. 2 above. If it had, the trend parameter levels from the two data bases were compared. That data base having the highest trend parameter level was then selected for failure prediction computation.

If only one of the data bases passes criteria 2 and 3, it is the obvious choice for basing failure predictions. However, if at any hourly sample the other data base proves superior in the criteria 2 and 3 tests, then failure predictions will be based upon its data.

These data selection decision criteria are illustrated in flowchart form in Figure 127.

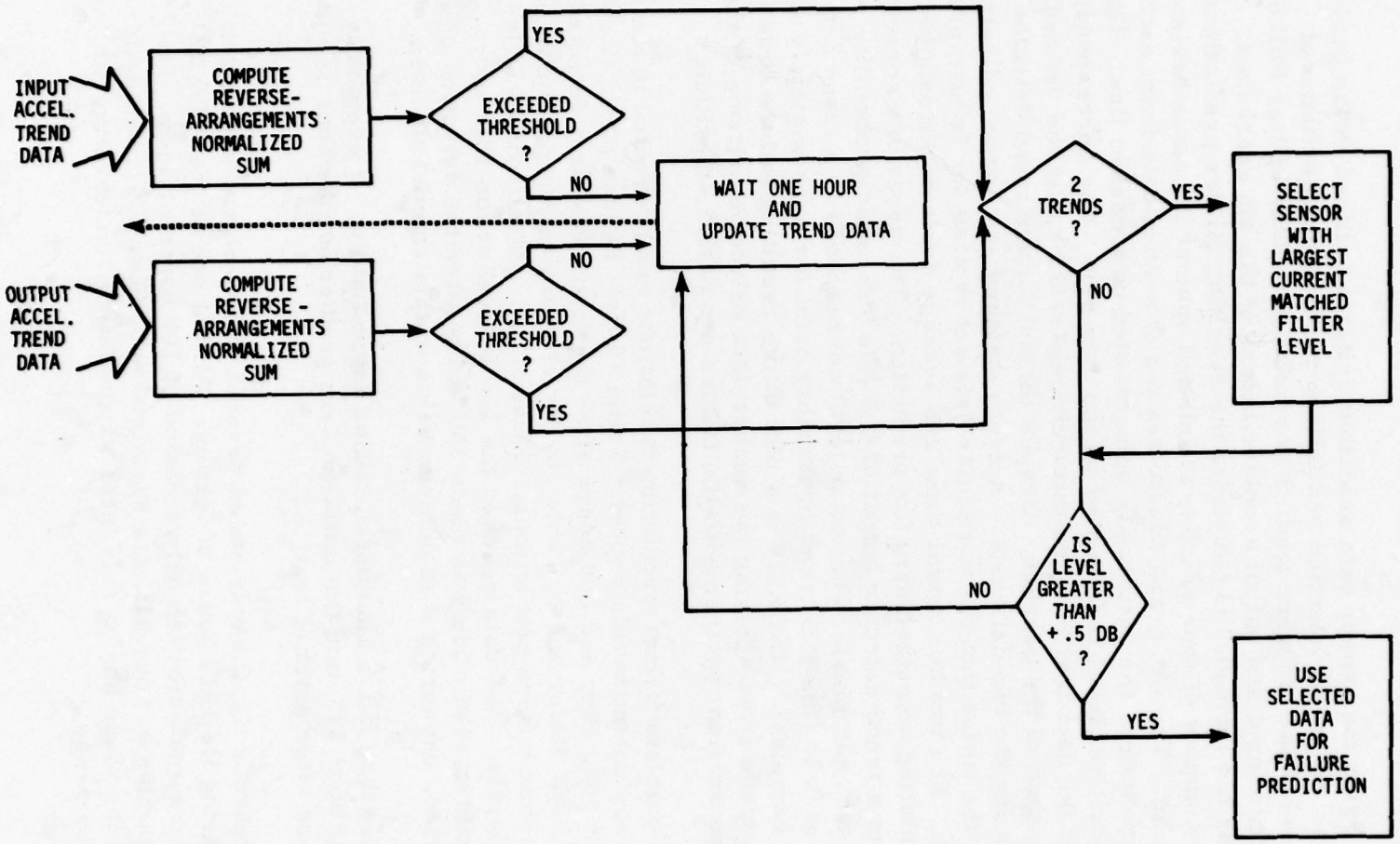

Figure 127. Sensor Data Selection Flowchart.

FAILURE PREDICTION RESULTS

Using the sensor data selection criteria outlined in the previous section, the trend detection and failure prediction algorithms of Figures 117 and 126 were applied to smoothed matched-filter PSD data from both input and output accelerometers of the six gearboxes. Figures 128 through 133 illustrate the resulting failure predictions. Each figure consists of four graphs, all plotted against the same horizontal time axis. The (A) graph illustrates the smoothed data from each accelerometer, the output data being plotted on a dashed line. The 12-dB critical level is indicated on the data plot. The corresponding time of the data that reaches this critical level first is the defined failure time of the gearbox. Graphs (B) and (C) are trend detector outputs for the two data sets. A cross-hatched shading is indicated during the times that the particular data set is used for failure prediction. The two horizontal lines are average decision thresholds for accumulating smoothed data for prediction. The upper one corresponds to a trend detector output of 0.5 (the 99% trend probability point for 12 data samples). The lower level corresponds to a trend detector output of 0.25 (the 99% trend probability point for approximately 48 hourly samples). Graph (D) is a plot of the resulting failure time prediction made from applying the sensor data selection criteria of the previous section together with the failure prediction algorithm.

Complete failure prediction tabulations are presented in the software supplement to this report. Table 10 lists failure prediction times made at 100, 150, and 200 hours after the trend was first detected, where applicable. Referring to Table 10, let us examine the results of each of the gearbox failure predictions. First of all, gearbox BB-4 failed almost immediately. The data reached the 12-dB level at the 88th hour. The first failure prediction was made 100 hours after the detection of a trend at hour 24, rendering it of dubious value in this anomalous case.

Gearbox BB-5 also began failing immediately. It eventually failed at hour 273, and the initial failure prediction was hour 359 made 124 hours after start of test.

Gearbox HT-2 experienced several "false-alarm" trend detections during its 1519 hours of testing. All but one of these "false" trends was sustained for only a period of 100 hours or less. The trend starting at hour 915 was sustained until hour 1272, and failure predictions made during this interval are fairly conservative (in the 3000-hour range).

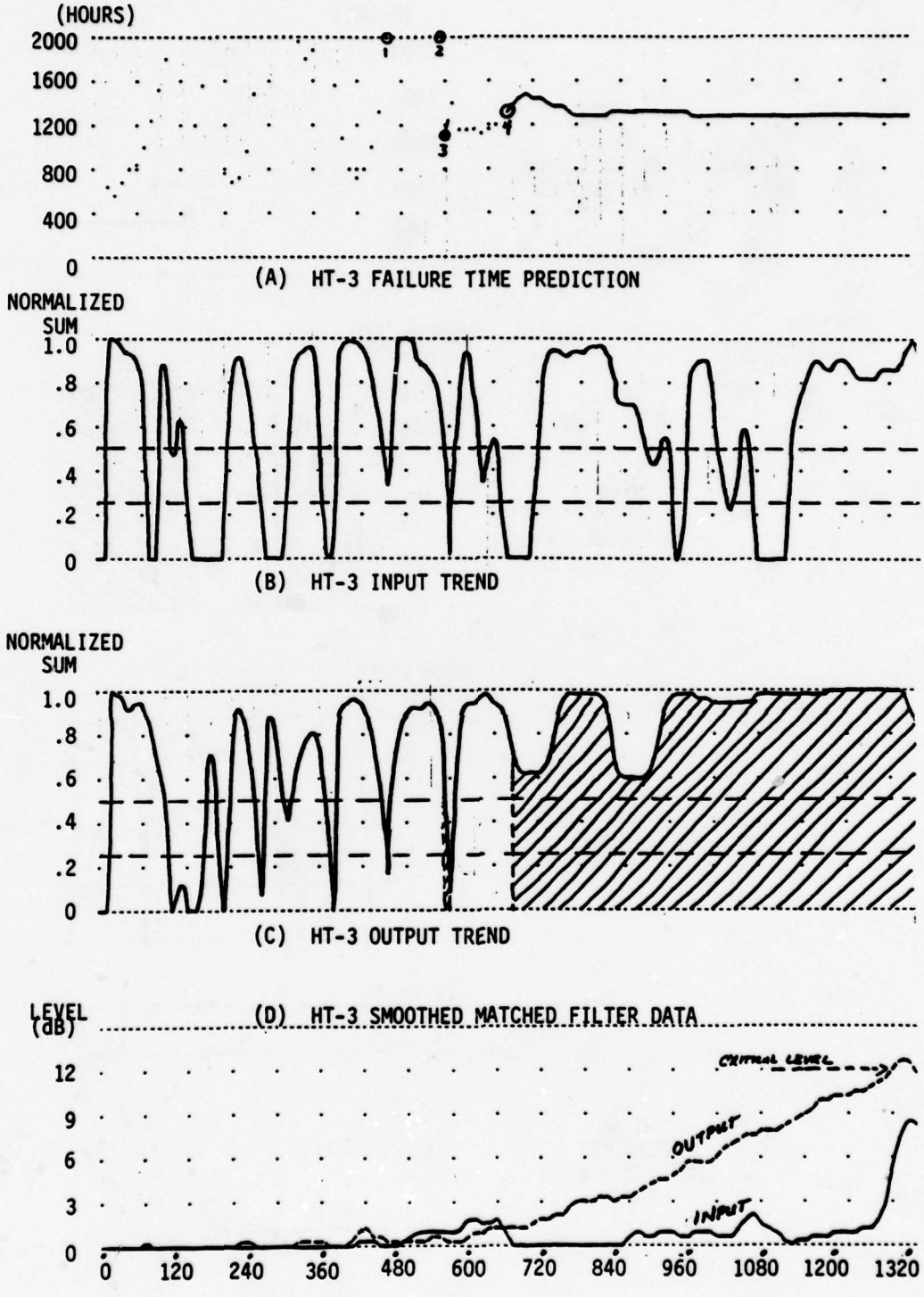

Figure 128. Failure Prediction Time History for Gearbox HT-3.

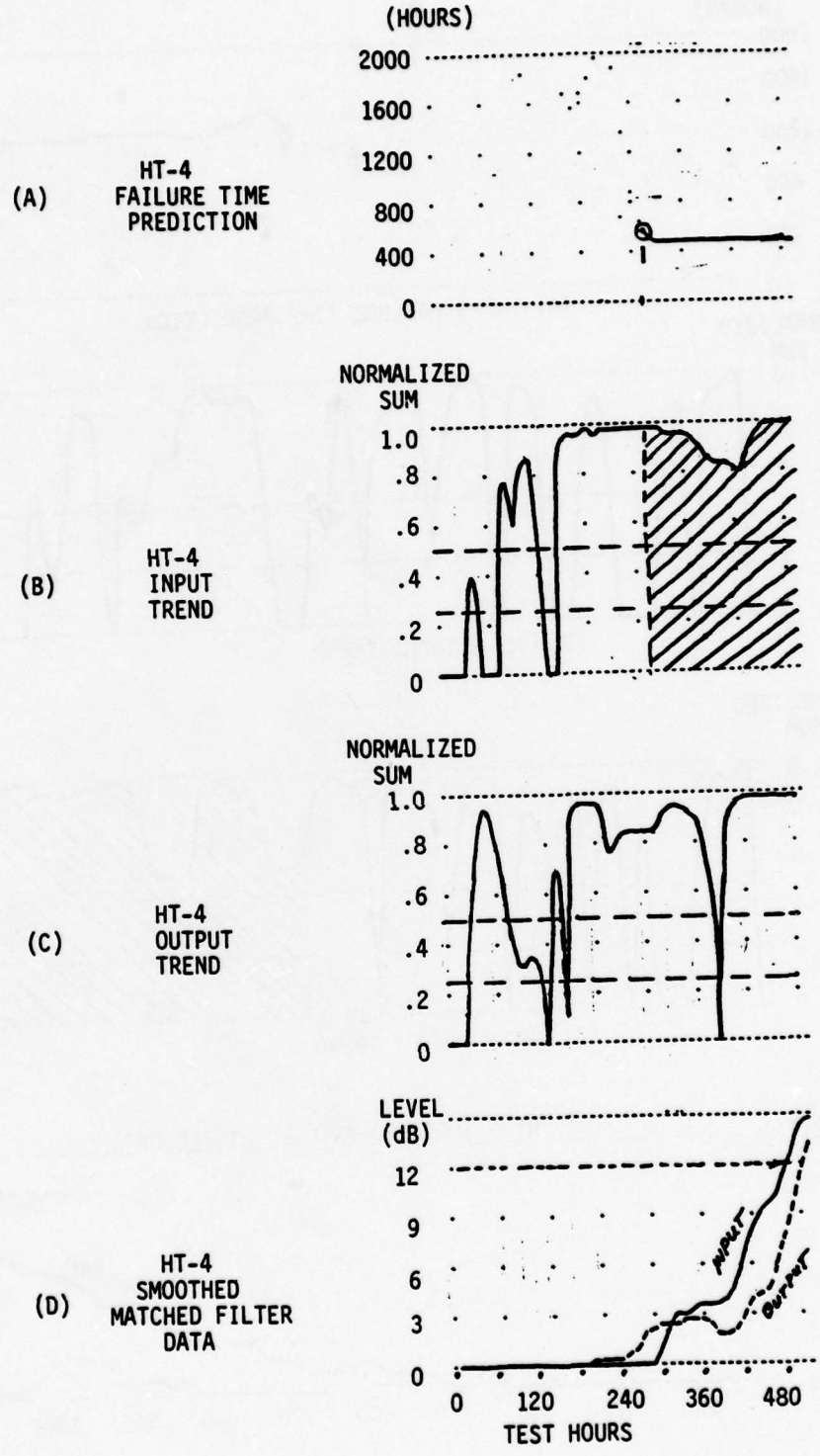

Figure 129. Failure Prediction Time History for Gearbox HT-4.

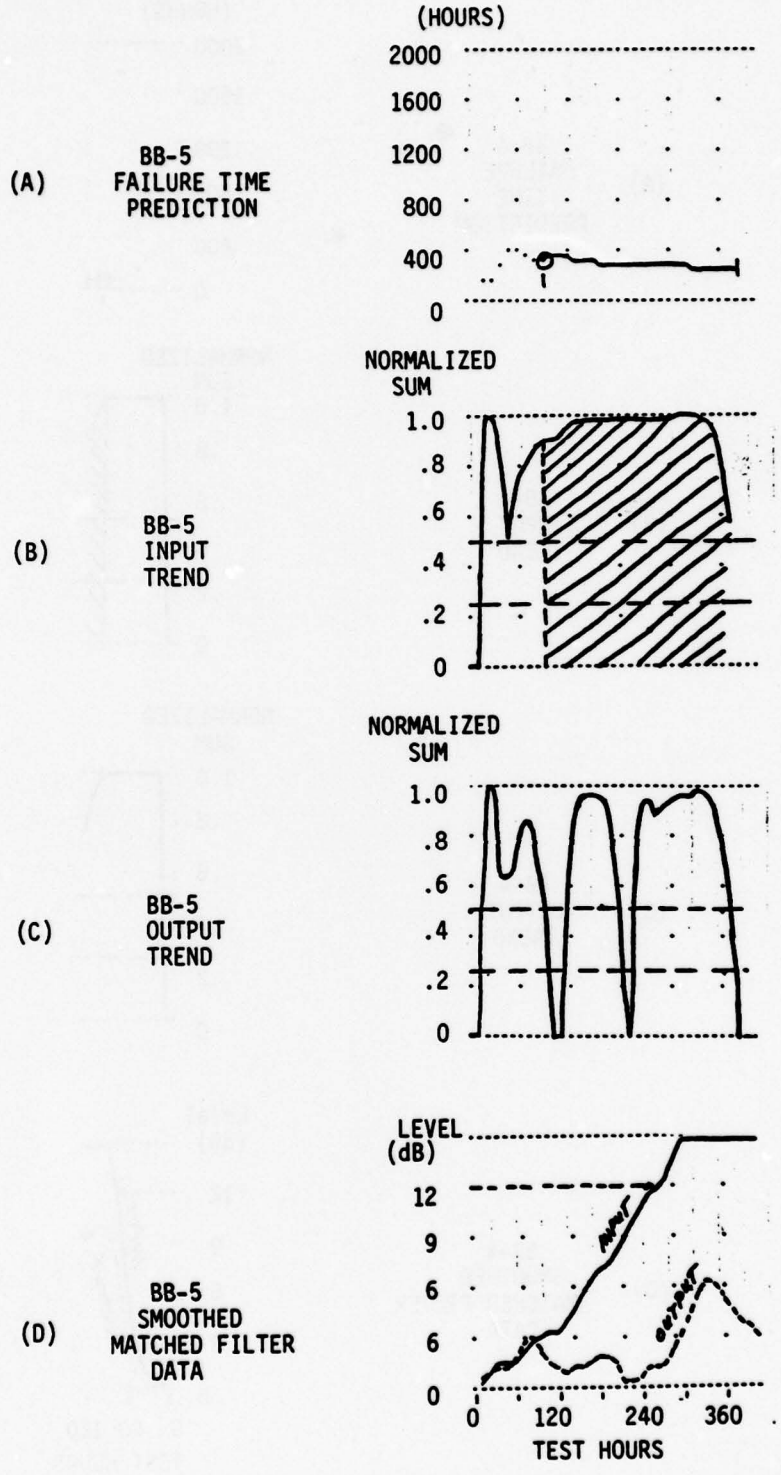

Figure 130. Failure Prediction Time History for Gearbox BB-5.

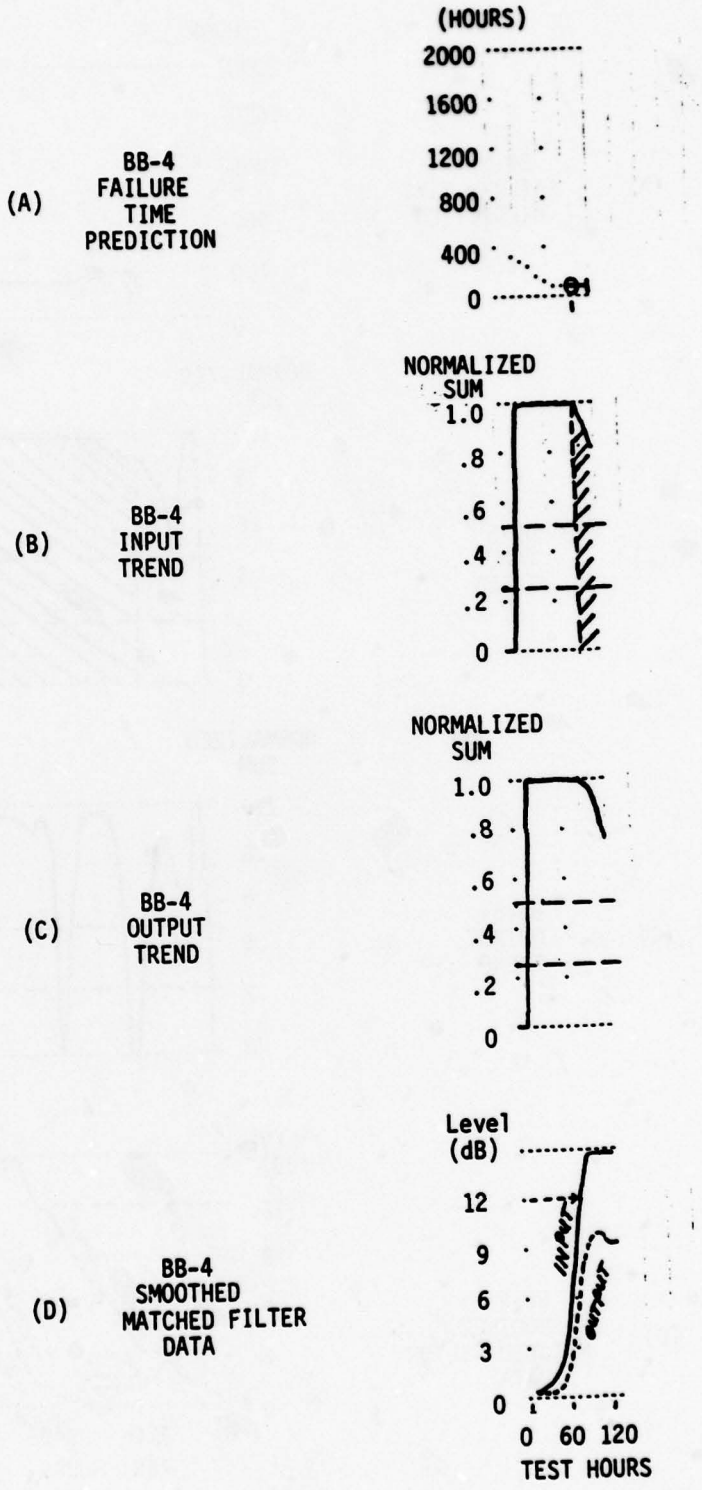

Figure 131. Failure Prediction Time History for Gearbox BB-4.

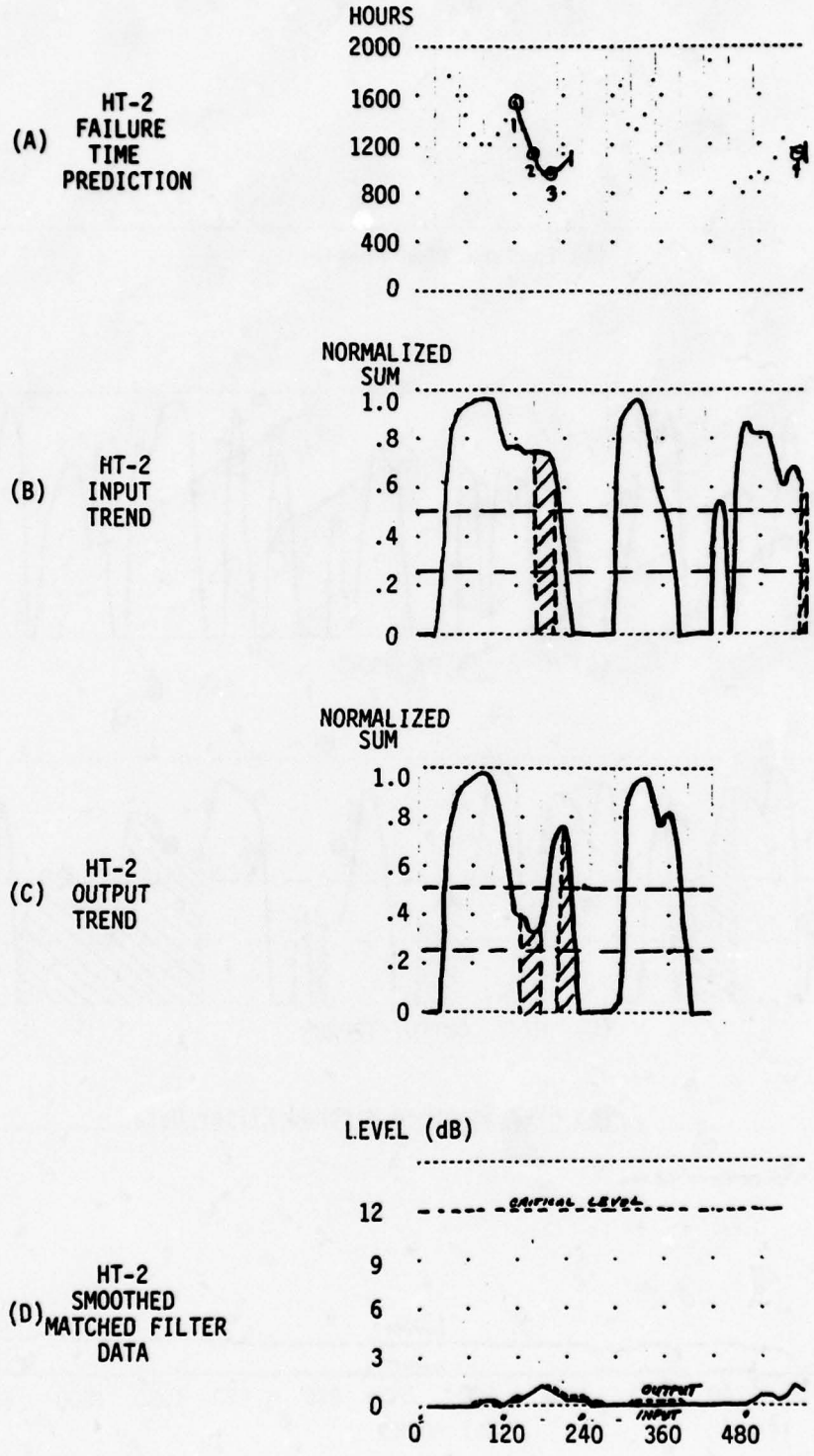

Figure 132. Failure Prediction Time History for Gearbox HT-5.

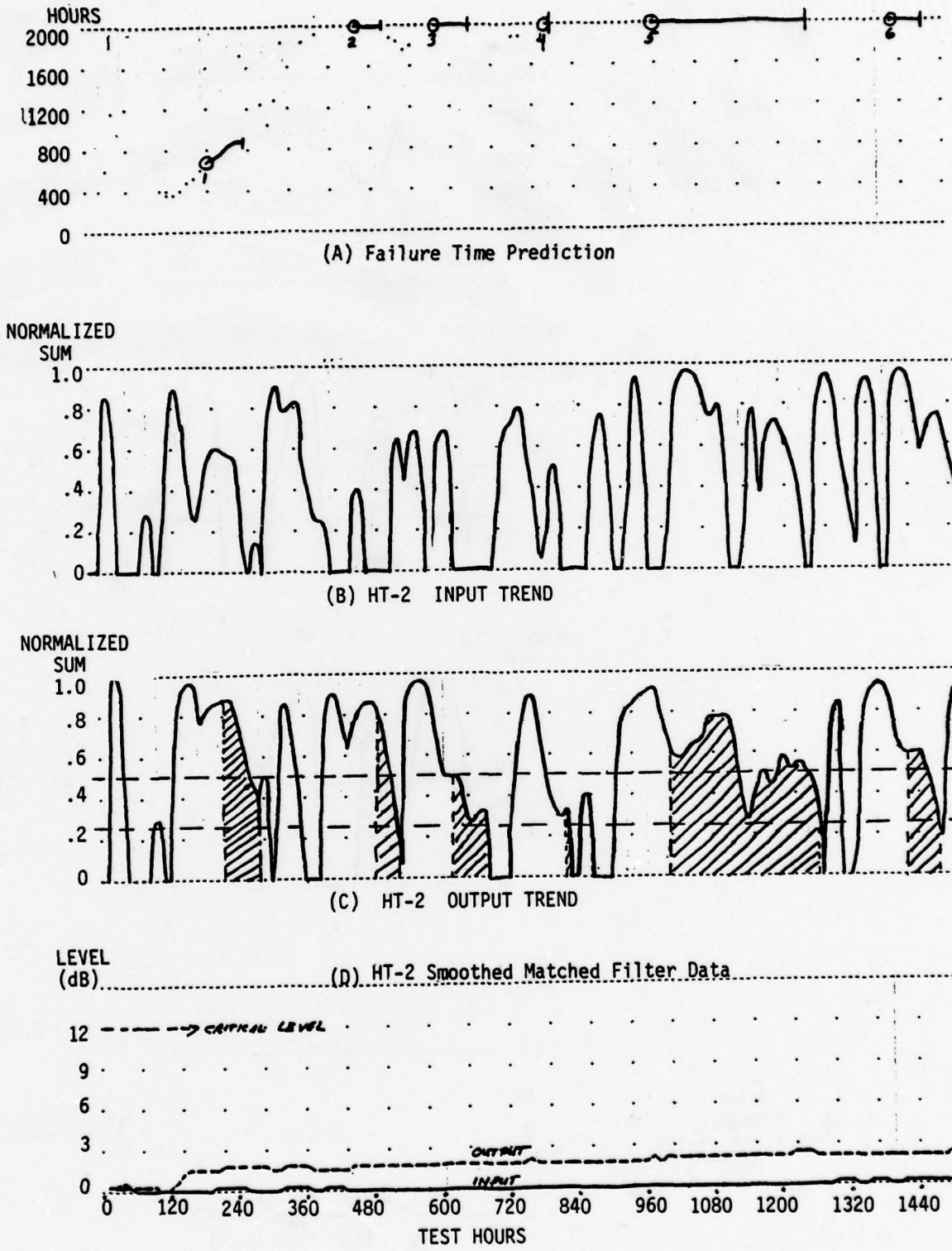

Figure 133. Failure Prediction Time History for Gearbox HT-2.

TABLE 10. GEARBOX FAILURE PREDICTION TIMES MADE AT 100, 150, AND 200 HOURS AFTER TREND DETECTION

GEARBOX NO.	BB4	BB5	HT-2						HT-3			HT-4	HT-5	
TREND NO.	1	1	1	2	3	4	5	6	1	2	3	1	1	2
TREND DETECTION HR (t_o)	24	24	134	392	535	734	915	1338	391	484	590	175	61	473
ACTUAL FAILURE HOUR	88	273	NO FAILURE						1301			488	Test Cell Failure at 596 Hours	
TIME OF PREDICTION	FAILURE PREDICTION TIMES													
t_o + 100 HOURS	107	359	727	2079	2818	--	2951	4100	--	--	1398	1070	1372	1153
t_o + 150 HOURS	--	335	--	--	--	--	3162	--	--	--	1438	519	1017	--
t_o + 200 HOURS	--	309	--	--	--	--	3438	--	--	--	1324	487	--	--

Gearbox HT-3 failure predictions relied entirely on the output accelerometer data and were most impressive. After " false " trend detections at hours 391 and 484, a valid trend was detected at the 590th hour. Subsequent failure predictions made at hours 690, 740, and 790 were extremely close to the actual failure hour of 1301.

Gearbox HT-4 data experienced a wear trend detection at the 175th hour of test. This trend, fairly weak at first, was sustained throughout the remainder of test and resulted in extremely close failure predictions after 150 hours of trend data collection.

Gearbox HT-5 test was terminated 596 hours after its start due to a test cell failure. Two trends were detected, however, during this test period. The initial trend was detected at the start of test (61st hour) and was sustained for less than 200 hours. Another trend was detected near the end of the test period. All failure prediction times were greater than 1000 hours. Since the test was terminated prematurely, no conclusions can be drawn from these predictions other than to note that the mechanical inspections after the test revealed that bearing wear was developing.

SUMMARY

Because of the wide variety in the initial conditions and the testing times of the individual gearboxes, it might be well to summarize the failure prediction results from a different perspective. Since the information that is most coveted by operations and maintenance groups is the useful remaining life of the component, the prediction data of Table 10 has been rearranged in Table 11 to present gearbox predicted remaining life versus the actual remaining life in the component, still defined as the time that the trend parameter reached the 12-dB level. Three categories can be defined to encompass all tested gearboxes on this program: (a) Gearboxes that were in a failure mode at the start of the test -- this inclues BB-4 and BB-5. Since BB-4 failed before a prediction could be made according to the algorithm, it will not be included in this synopsis. (b) Gearboxes that failed during the test -- this includes HT-3 and HT-4. (c) Gearboxes that did not fail during testing - - this includes HT-2 and HT-5.

Table 11 shows that all prediction errors are less than 150 hours, with the exception of two: (a) false "healthy" prediction for HT-4 that was quickly updated 50 hours later and (b) a false "failing prediction for HT-2 that also was quickly abandoned. The predictions of HT-3 condition are particularly impressive, since fairly accurate predictions were made approximately 600 hours in advance of failure.

It should be stated that considerably more collected data should be subjected to the prediction algorithms before any definitive or statistical judgments can be made on these techniques. Also, the defined failure time corresponding to a 12-dB matched filter level may not be the best operational criteria. Useful remaining life may be considerably shorter than the defined failure time utilized in the investigation, when operational standards are applied. This definition has, however, provided a stringent test for the predicition algorithms, and the overall results, from a failure prognosis viewpoint, are promising.

TABLE 11. PREDICTED VS. ACTUAL REMAINING GEARBOX LIFE

CATEGORY	GEARBOX	ACTUAL REMAINING LIFE (HOURS)	PREDICTED REMAINING LIFE (HOURS)	PREDICTION ERROR (HOURS)
Gearbox in Failure Mode at Start of Test	BB-5	149	235	86
		99	161	62
		49	85	36
Gearbox Experienced Failure During Test	HT-3	611	708	97
		561	698	137
		511	534	23
	HT-4	213	795	582
		163	194	31
		113	112	1
No Gearbox Failure Experienced During Test	HT-2	> 1285	493	> 792
		> 1027	1587	Not Applicable
		> 884	2183	"
		> 504	1936	"
		> 454	2097	"
		> 404	2323	"
		> 81	2662	"
	HT-5	> 435	1211	Not Applicable
		> 385	806	"
		> 23	580	"

CONCLUSIONS

1. Data Base Integrity

A strong data base has been collected on this program for analyzing the prognosis problem. The set of gearboxes exhibited a good "spread" with regard to (a) variety of initial wear condition, (b) longevity of test time, and (c) final failure mode.

The use of the lower mass B & K model 4344 accelerometers on the program greatly contributed to a higher data base integrity. Since the frequency response of the accelerometer was flat to 50 kHz, useful ultrasonic data was collected in addition to the energy from the lower DC-10 kHz band.

The addition of a 14-bit analog-digital converter for sensor data digitization allowed greater dynamic range to be achieved (nearly 80 dB), which in turn aided early wear trends in being detected by the more sensitive trend parameters, notably, matched filtering and geometric mean processing.

The use of a 1024 point fast Fourier transform for data processing allowed finer frequency resolution (< 20 kHz), which permitted a truer representation of the energy frequency distribution in the vibration signals.

2. Applicability of Test Data to Long Term Failure Prediction

Though most of the gearbox test runs (BB-4, BB-5, HT-4, and HT-5) were less than 700 hours duration due to varying degrees of pre-test wear caused by flight operation, two gearboxes (HT-2 and HT-3) were tested over 1400 hours each.

The test results from gearbox HT-3 were very encouraging. This gearbox ran 1437 hours, with the first 700 hours producing little change in the sensor signals. At the beginning of the final 700 hours of testing, both SOAP analysis and the Tedeco Chip Detector indicated that large amounts of small metal particles were present in the gearbox oil. Supporting evidence of wear was also supplied by the oil temperature monitor, the ultrasonic energy, and the SKF peak shock value.

Gearbox HT-2 ran a total of 1519 hours with no signs of impending failure indicated by either the computer-collected data or physically observable data. This was subsequently verified by using HT-2 gearbox in a test evaluation of polymer-film accelerometers (a separate report-addition to this contract). An additional 1460 hours of testing were accumulated on that evaluation with still no signs of failure!

From the standpoint of component wear prognosis, the testing of HT-2 served to verify that the sensors used were valid trend indicators because of the correlation between "steady" data and the post-mechanical inspection and later testing of this gearbox.

3. Processed Ultrasonic Energy as an Aid to Failure Prognosis

Another significantly encouraging result during the testing of gearbox HT-3 was the data produced by envelope-detecting broadband 10 kHz-wide amplitude modulation on the output accelerometer ultrasonic spectrum (20 kHz - 50 kHz). This was accomplished using the Shaker Envelope Detector supplied by Ft. Eustis near the end of the testing. It appears that simple RMS processing is sufficient on this energy to produce prognostic data of equivalent value to matched filtering or geometric mean processing of the low frequency energy. Since this processing was only performed during the latter half of the HT-3 test, further examination of this technique seems necessary and desirable.

Unfortunately, peak detection of the ultrasonic signals did not produce consistent results. The trend data was very erratic during most gearbox tests, especially the peak-detected output ultrasonic energy. Step discontinuities were present and have not been fully accounted for.

4. Sensitivity of Sensor Placement to Trend Detection

Another relevant observation in this series of tests has been a definite correlation between accelerometer placement and the localized vicinity of the fault. A review of the individual gearbox tests will bear out the fact that the sensor (either input or output lateral accelerometer) located furthest from the region of intense wear activity exhibited a slower response time to this failure mode initiation than the sensor closest to the wear action. In many cases, considerable hours elapsed

before the more distant sensor began a noticeable trend. For this reason, the matched-filter data from the sensor closest to the physical location of highest determined damage was utilized for failure prognosis. This has resulted in a fairly balanced examination of both input and output sensor response, since three of the failures (BB-4, BB-5, and HT-4) were due to damage to input bearings or gears, two (HT-3 and HT-5) occurred in the output region, and the sixth (HT-2) test produced no failure after 1500 hours of testing.

5. Temperature Sensors

The ambient air and gearbox oil temperature sensors were useful on some, but not all, of the gearbox wear trends. On gearbox HT-3, during the final hours of testing an observable rise in temperature was noted as metal chip generation accelerated. Good temperature data correlation was obtained with the following mechanical problems that occurred during test cell operation: pulley belt slippage, cooling water shutdown, and addition of cooling fans.

6. RPM and Torque Sensors

For the most part, rpm remained steady throughout the testing. During a period when pulley belt slippage was occurring, the rpm sensors provided information to shut down the test cell. The addition of the two torque sensors allowed continuous monitoring of gearbox loading and efficiency. This feature was not in use until after the test cell failure occurred during the testing of gearbox HT-5. The collected torque data provided many insights as to when wear processes were occurring as step or gradual changes in gearbox torque and efficiency were observed during various phases of the testing.

7. Oil Analysis

The oil analysis provided by the Army's oil analysis group at ARADMAC was useful in correlating wear information obtained from other sensors. While the oil analysis does not appear to be the earliest detector of wear, it serves as a detector of failure and is useful in determining causes and location of the wear regions.

8. Shock Pulse Analyzer

The shock pulse analyzer also provided corroborating data to the B & K accelerometer data. The shock profiles, however, exhibited quite a degree of erratic behavior whenever oil samples were taken or when the oil was changed. For this reason the shock profiles shown in this report represent the condition before an oil sample or oil change was initiated.

9. Documentation of Bearing Wear

The pre-and post-test bearing inspection reports, in conjunction with the SEM bearing photographs, were useful in corroborating information obtained from oil analysis and other sensor data. Particularly on gearbox HT-2, which ran for over 1500 hours without signs of failure from other sensors, the bearing reports indicated that little problem would be encountered in continuing to test this gearbox. As in the previous program, it was not possible to obtain any quantitative information (only visual) on gear wear.

10. Tedeco Chip Detector

This instrument was made available during testing of the last two gearboxes: HT-3 and HT-4. Its information correlated well with the oil analysis; but like the oil analysis, it does not appear to be the earliest detector of the commencement of a failure mode.

11. Vibration Trend Parameters

Of the twelve trend parameters investigated, three were finally selected as best characterizing the vibration energy spectrum by a single meaningful number to indicate the current wear condition of the gearbox. These were (a) matched-filter RMS level, (b) geometric mean level, and (c) arithmetic mean level. The matched-filter parameter is the most sensitive of the three, but also requires more computational complexity than the other two. Because of its sensitivity and trendability, it was chosen for failure prediction modeling.

12. Trend Detection

The reverse-arrangements trend detection algorithm was selected for use in this analysis effort. It is extremely sensitive to detection of trends and requires a low computational burden. Its trend decision levels are not arbitrary, but have a statistical foundation, since the probability of the trend data being random and stationary has a near-Gaussian distribution.

The problem of verifying that a data trend corresponds to a valid wear trend requires a sufficient waiting period. For the present analysis, 96 hours of sustained trend detection was utilized. This proved to be adequate for all but a few exceptions. In a practical application, it may well be that various levels of information are weighed together: number of trends, length of unsustained trends, trend parameter level, etc.

13. Wear Trend Modeling

Three math models were investigated as possible wear trend models.

An upward-constrained second order exponential mathematical model was finally chosen to extrapolate failure prediction information from the trendable data. This decision had a twofold basis: (a) all incipient gearbox failures were characterized by a quasi-exponential positive rise in parameter level, and (b) a fairly valid assumption can be made that the rate of change of a fault or wear in a rotating machinery component at a particular time is directly proportional to the magnitude or extent of the fault at that time. Mathematically, this implies an exponential trajectory. The second-order term introduces an increased severity factor if the test time has been sufficiently long.

14. Application of the Test Cell Data to Trend Detection and Failure Prediction Algorithms

In spite of a wide variety of initial wear conditions associated with the six gearboxes, all failure predictions made at least 150 hours after a detected and sustained wear trend were within 150 hours of the defined failure time. In the case of those gearboxes that did not fail, unsustained trends longer than 150 hours were detected, and corresponding failure prediction times were consistent with the test results in that they were substantially longer than the individual gearbox test time.

There may be a better criterion for failure time than the time corresponding to the 12-dB trend parameter level. The component useful remaining life may be considerably shorter than the defined failure time when operational standards are applied. However, this definition has provided a stringent test for the failure prediction algorithm, and the overall results are encouraging.

RECOMMENDATIONS

Further experimental work in this emerging field of failure prognosis is encouraged. From the perspective of this analysis effort, research effort in the following three areas is recommended:

a) Application of the algorithms to other rotating machinery components tested under similar controlled conditions.

b) Application of the algorithms to on-line equipment using existing ground instrumentation.

c) Development of a portable processing unit to monitor operational equipment.

REFERENCES

1. Houser, Donald R., et. al., VIBRATION SIGNAL ANALYSIS TECHNIQUE, Ohio State University Research Foundation; USAAMRDL Technical Report 73-101, Eustis Directorate, U.S. Army Air Mobility Research and Development Laboratory, Fort Eustis, Virginia, December 1973, AD776397, p. 78.

2. Snedecor, G.W., and Cochran, W.G., "Statistical Methods," Iowa State University Press, 6th Edition, 1967, p. 172.

3. Makhoul, J., "Spectral Analysis of Speech by Linear Prediction," IEEE Transactions on Audio and Electroacoustics, Volume AU-21, June 1973, p. 146.

4. Otnes, R.K., and Enochson, L., "Digital Time Series Analysis," Wiley and Sons, 1972, p. 400.

5. "Mechanical Component Failure Prognosis Study," AiResearch Manufacturing Company; USAAMRDL-TR-73-26, Eustis Directorate, U.S. Army Air Mobility Research and Development Laboratory, Fort Eustis, Virginia, June 1973, AD 7710 33.

6. Rothbart, H. A., Mechanical Design and Systems Handbook, McGraw-Hill, 1967, p. 13-52.

APPENDIX A

SOFTWARE DATA COLLECTION SUBROUTINE FLOW DIAGRAMS

Data Collection Subroutines

Three of the data collection subroutines illustrated in Figure 20 from the main body of this report are expanded here because they significantly bear the brunt of the data processing accomplished in the gearbox testing. The software for each of these subroutines was developed in the Lockheed Electronics "MAC-JR" assembly language to provide a higher processing speed, thus allowing more statistically significant data to be collected.

Figure A-1 is a flow diagram of the subroutine DCMEAS that collects and averages an ensemble of 128 groups of data from each addressed DC channel. Each group contains 1024 samples of data from that particular sensor, resulting in 128,000 samples of data being collected, averaged, and stored in approximately 15 seconds.

Figure A-2 illustrates the operations performed in obtaining a power spectral density of each vibration channel. In this subroutine SFFT, 128 separate fast Fourier transform operations are performed. The RMS value of each computed frequency bin value is determined by squaring and accumulating real and imaginary frequency bin values and performing a double-precision square root on each accumulated sum. Included in the subroutine is a branch to another data collection subroutine: RTADC, illustrated in Figure A-3. This subroutine is similar to DCMEAS (Figure A-1) except that it collects only one group of 1024 vibration channel samples for each FFT process. Each vibration channel power spectral density computation, which represents a statistical ensemble of 128 individual fast Fourier transforms, is accomplished (collection, computation, and tape storage) in approximately 2 1/2 minutes.

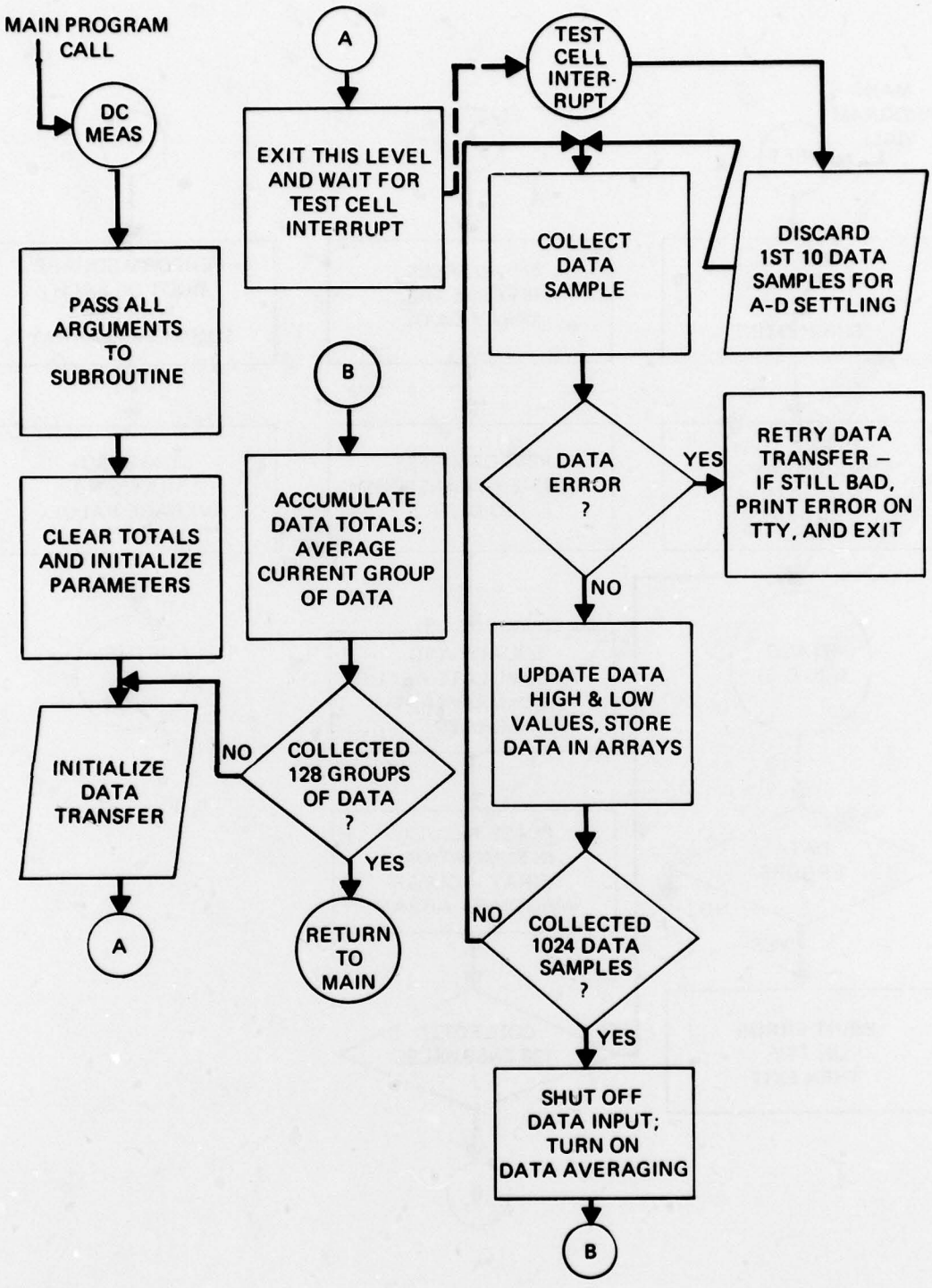

Figure A-1. A-D Converted and Averaged DC Data Collection Subroutine.

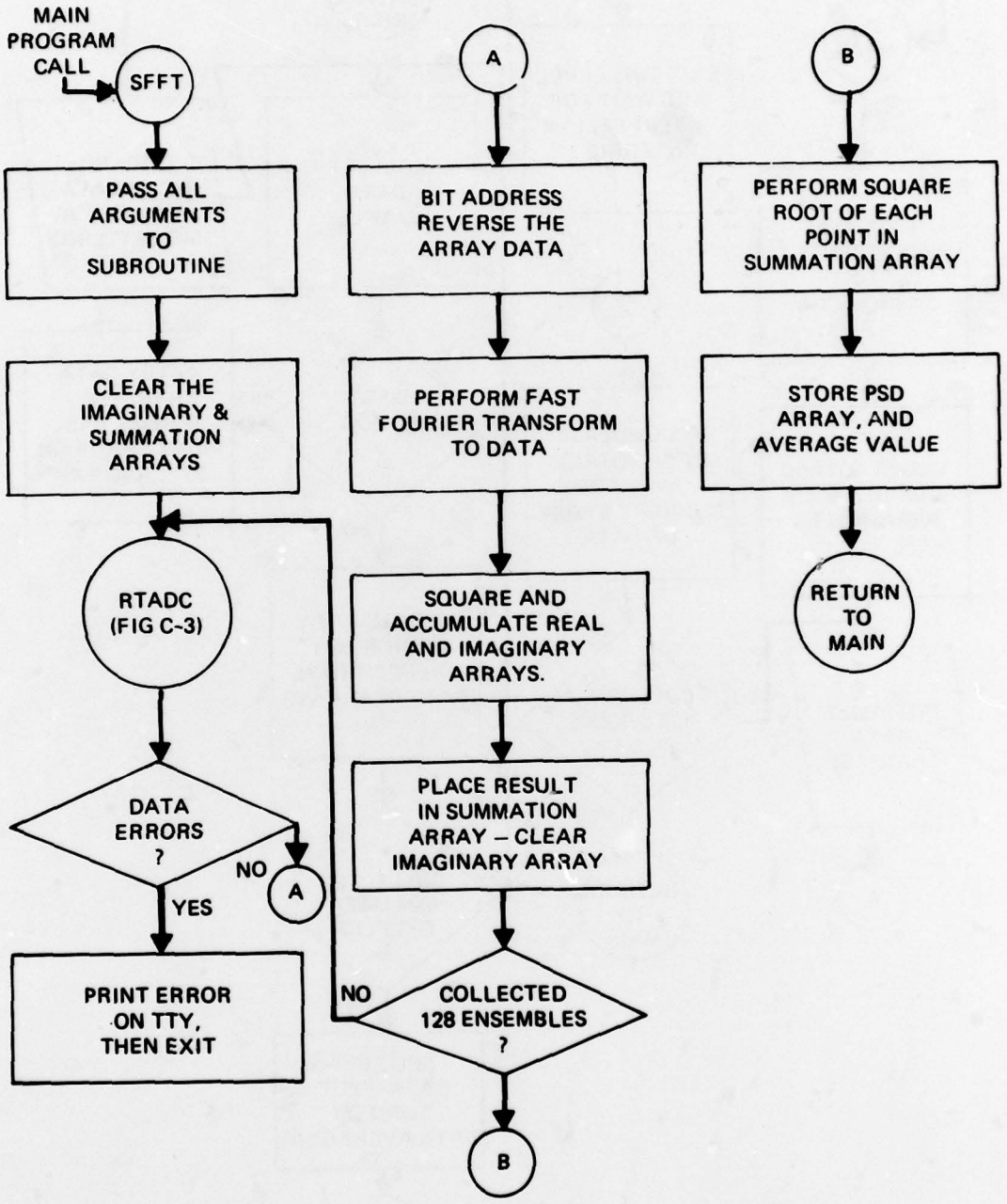

Figure A-2. Sorted FFT Subroutine.

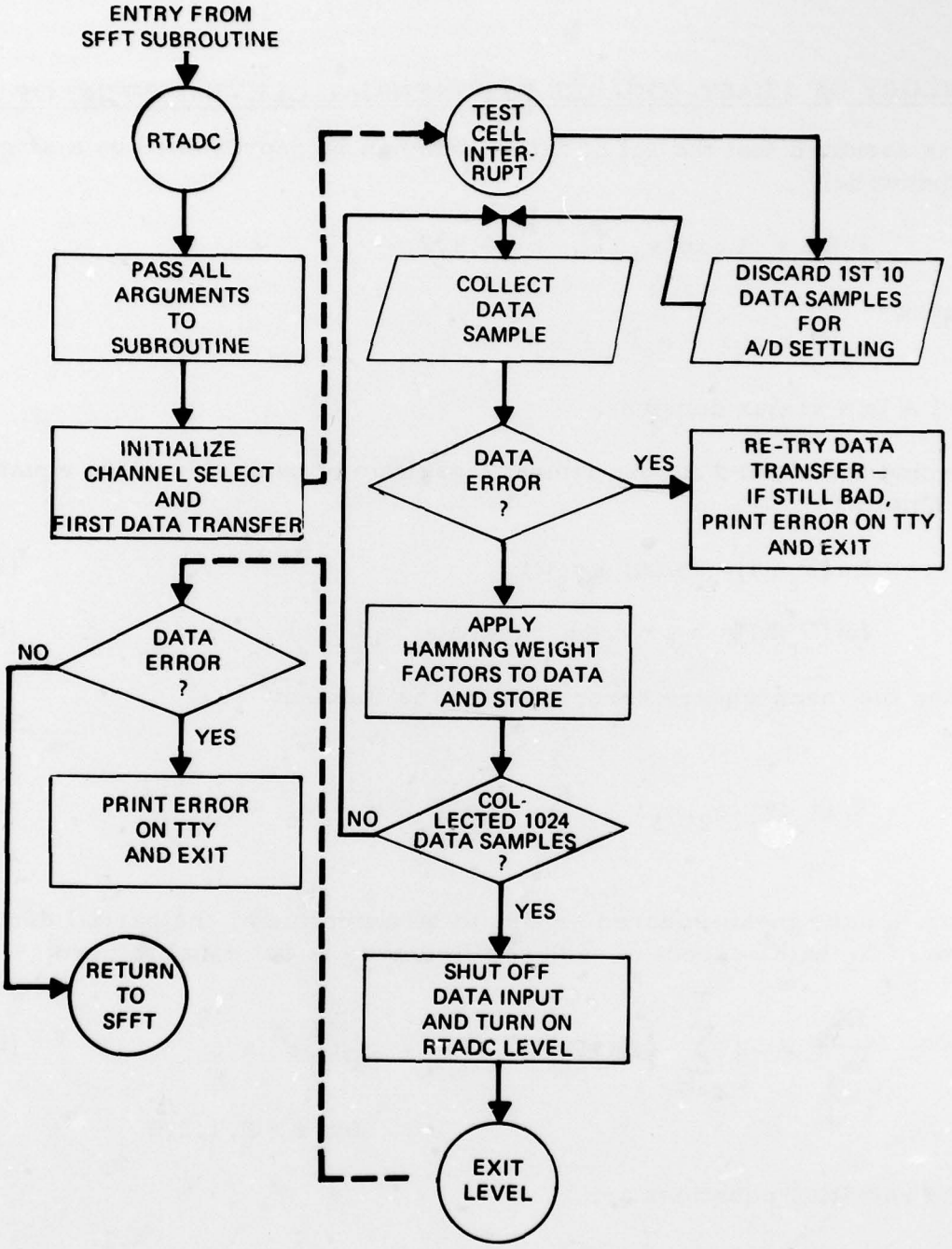

Figure A-3. A-D Converted, Hamming-Weighted Vibration Data Collection Subroutine.

APPENDIX B

THEORY OF LEAST-SQUARES EXPONENTIAL CURVE-FITTING OF DATA

It is assumed that the set of data points can be represented by a single exponential

$$P_t(k) = A \exp[y_3(t)], \quad t = 0, 1, 2, ---, T \tag{B1}$$

where

$$y_3(t) = a_1 t + a_2 t^2 + a_3 t^3$$

and A is a scalar constant.

To find the a's and A, the natural logarithm of each side of the equation is obtained:

$$\mathrm{Ln}[P_t(k)] = \mathrm{Ln}(A) + y_3(t) \tag{B2}$$

or $$\mathrm{Ln}[P_t(k)] = a_o + y_3(t), \quad \text{where } a_o = \mathrm{Ln}(A) \tag{B2a}$$

Then the mean-square error criterion is formed:

$$X_k(a_o, a_1, a_2, a_3) = \sum_{t=0}^{T} \left\{ \mathrm{Ln}[P_t(k)] - a_o - y_3(t) \right\}^2 \tag{B3}$$

For X_k, the mean-squared error, to be a minimum, the partial derivative of X_k with respect to each coefficient a_ℓ is set equal to zero;

$$\frac{\partial X_k}{\partial a_\ell} = -2 \sum_{t=0}^{T} \left\{ \mathrm{Ln}[P_t(k)] - a_0 - y_3(t) \right\} t^\ell = 0 \tag{B4}$$

$$\text{for } \ell = 0, 1, 2, 3$$

The resulting equations are

$$\sum_{t=0}^{T} \mathrm{Ln}[P_t(k)] t^\ell = a_o \sum_{t=0}^{T} t^\ell + a_1 \sum_{t=0}^{T} t^{\ell+1} + a_2 \sum_{t=0}^{T} t^{\ell+2} + a_3 \sum_{t=0}^{T} t^{\ell+3} \tag{B5}$$

$$\text{for } \ell = 0, 1, 2, 3$$

This represents four equations (ℓ's) in four unknowns (a's) which can be solved for the unknown coefficients: a_ℓ.

3923-79